

# Sheffield Hallam University

*Thermotropic and lyotropic mesophases formed by some lithium soaps.*

HARRISON, William James.

Available from the Sheffield Hallam University Research Archive (SHURA) at:

<http://shura.shu.ac.uk/19760/>

## A Sheffield Hallam University thesis

This thesis is protected by copyright which belongs to the author.

The content must not be changed in any way or sold commercially in any format or medium without the formal permission of the author.

When referring to this work, full bibliographic details including the author, title, awarding institution and date of the thesis must be given.

Please visit <http://shura.shu.ac.uk/19760/> and <http://shura.shu.ac.uk/information.html> for further details about copyright and re-use permissions.

SHEFFIELD CITY  
POLYTECHNIC LIBRARY  
POND STREET  
SHEFFIELD S1 1WB

TELEPEN

100249199 1



**Sheffield City Polytechnic Library**

**REFERENCE ONLY**

ProQuest Number: 10697062

All rights reserved

INFORMATION TO ALL USERS

The quality of this reproduction is dependent upon the quality of the copy submitted.

In the unlikely event that the author did not send a complete manuscript and there are missing pages, these will be noted. Also, if material had to be removed, a note will indicate the deletion.



ProQuest 10697062

Published by ProQuest LLC (2017). Copyright of the Dissertation is held by the Author.

All rights reserved.

This work is protected against unauthorized copying under Title 17, United States Code  
Microform Edition © ProQuest LLC.

ProQuest LLC.  
789 East Eisenhower Parkway  
P.O. Box 1346  
Ann Arbor, MI 48106 – 1346

THERMOTROPIC AND LYOTROPIC MESOPHASES

FORMED BY SOME LITHIUM SOAPS

by

WILLIAM JAMES HARRISON, BSc

A Thesis submitted to the Council for National Academic Awards in partial fulfilment of the requirements for the degree of Doctor of Philosophy.

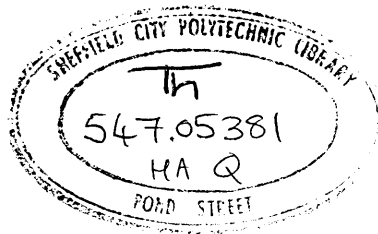
Sponsoring Establishment :

Sheffield City Polytechnic : Department of Chemistry

Collaborating Establishment :

Unilever Research, Port Sunlight Laboratory

December 1988



## ACKNOWLEDGEMENTS

The author wishes to express to the following people his gratitude for their contributions to this effort.

- \* Dr M P McDonald (Sheffield City Polytechnic) for his guidance, discussions and advice throughout the course of this work.
- \* Professor G J T Tiddy (Unilever Research, Port Sunlight Laboratory) for his advice, support, friendship and many stimulating discussions.
- \* The SERC and Unilever Research (Port Sunlight Laboratory) for a CASE award.
- \* Unilever Research (Port Sunlight Laboratory) for eight months' funding and for the use of their facilities. In particular to Jeff Rockliffe for his practical help with NMR spectroscopy measurements and to Mark Flanagan and Phil Smith for their help with the x-ray diffraction experiments.
- \* His fellow students, too many to be named, whose friendship will always be remembered. They know who they are.
- \* Ann Wilson for the excellent typing.
- \* His parents, Mr and Mrs W Harrison, for their patience, understanding and financial support.

## ABSTRACT

### Thermotropic and Lyotropic Mesophases formed by some Lithium Soaps

William James Harrison : December 1988

The thermotropic polymorphism of anhydrous lithium stearate (n-octadecanoate,  $\text{LiC}_{18}$ ), lithium oleate (cis-9-octadecenoate) and an unusual semi-crystalline lithium phenylstearate (LiPS) soap mixture composed of 12 positional isomers, was studied using differential scanning calorimetry (DSC) and polarizing microscopy (plus x-ray diffraction and  $^7\text{Li}$  NMR spectroscopy for the latter). Each soap exhibited a characteristic stepwise melting behaviour. In contrast to the oleate, both  $\text{LiC}_{18}$  and LiPS formed high temperature liquid crystal phases (lamellar and reversed hexagonal structures respectively) directly preceding their amorphous melts.

The phase behaviour of  $\text{LiC}_{18}$  in the hydrocarbon solvents n-hexadecane and squalane and that of LiPS in 1-phenylheptane was investigated using DSC and microscopic and macroscopic observations in polarized light (plus x-ray diffraction and  $^7\text{Li}$  NMR spectroscopy for the latter). Phase diagrams were constructed. The phase behaviour of each system was critically dependent upon the thermotropic polymorphism of the solvent-free soap itself. At high temperatures two distinct mesophases were formed in the LiPS-1-phenylheptane system; a solvent-swollen reversed hexagonal mesophase at low solvent concentrations and a novel reversed micellar nematic mesophase at higher solvent concentrations. No mesophase formation was observed, however, in the  $\text{LiC}_{18}$ -hydrocarbon systems.

The phase behaviour of LiPS with  $^2\text{H}_2\text{O}$  was investigated (using the experimental techniques employed for the 1-phenylheptane system plus  $^2\text{H}$  NMR spectroscopy) and a phase diagram constructed. LiPS was shown to form a single homogeneous lamellar mesophase on addition of  $^2\text{H}_2\text{O}$  at room temperature with a broad composition and temperature range of stability.

# CONTENTS

	<u>Page No.</u>
Ch. 1 : <u>Introduction</u>	1
1.1 The Thermotropic Polymorphism and Mesomorphism of Fatty Acid Soaps .. .. .	2
1.1.1 Short-Chain Monovalent Soaps .. ..	3
1.1.2 Long-Chain Soaps .. .. .	5
1.1.2.1 Phase Structures of the Alkali Metal Soaps .. .. .	6
1.1.2.2 Lithium Soaps .. .. .	10
1.1.2.3 Phase Structures of the Alkaline Earth Soaps .. .. .	12
1.1.2.4 Discrepancies in Phase Behaviour ..	14
1.1.2.5 Unsaturated Soaps .. .. .	15
1.1.3 Anionic Amphiphiles of Low Crystallizing Tendency .. .. .	15
1.2 Binary Solutions of Anionic Amphiphiles in Non-Polar Organic Solvents .. .. .	17
1.2.1 Solubility and Micellization .. ..	17

1.2.1.1	Long-Chain Metal Soaps of Groups I and II .. .. .	17
1.2.1.2	Divalent Heavy Metal Soaps .. .. .	19
1.2.1.3	Aluminium Soaps .. .. .	20
1.2.1.4	Anionic Amphiphiles of Low Crystallizing Tendency .. .. .	21
1.2.2	Lyotropic Mesophase Formation in Anionic Amphiphile - Non-Polar Solvent Systems .. .. .	21
1.2.2.1	Long-Chain Sodium Soaps .. .. .	22
1.2.2.2	Long-Chain Lithium Soaps .. .. .	25
1.2.2.3	Effect of Added Water .. .. .	27
1.2.2.4	Anionic Amphiphiles of Low Crystallizing Tendency .. .. .	29
1.2.3	Solution Behaviour in Dilute Alkali Metal and Alkaline Earth Phenylstearate-Benzene Systems .. .. .	30
1.2.3.1	The Isomeric Nature of Phenylstearic Acid .. .. .	31
1.2.3.2	Solubility of Soap Mixtures .. .. .	32
1.2.3.3	Solution Structure of the Phenylstearate Soaps in Benzene .. .. .	35

1.3	Lyotropic Mesophase Formation in Anionic Amphiphile-Water Systems .. .. .	39
1.3.1	Long-Chain Alkali Metal Soaps .. ..	39
1.3.1.1	Sodium Laurate .. .. .	39
1.3.1.2	Potassium, Rubidium and Caesium Soaps .. .. .	43
1.3.1.3	Lithium Soaps .. .. .	44
1.3.2	Other Anionic Amphiphiles .. .. .	45
1.3.2.1	Aerosol OT .. .. .	45
1.3.2.2	Sodium 4-(1'-heptylnonyl) benzenesulphonate .. .. .	47
1.3.2.3	Lithium 4-trans-n-pentyl cyclo- hexanoate .. .. .	49
1.4	Proposed Programme of Work .. .. .	50
Ch. 2	<u>Experimental</u>	53
2.1	Materials and Methods of Preparation .. .. .	53
2.1.1	Lithium Stearate .. .. .	53
2.1.2	Lithium Oleate .. .. .	54
2.1.3	Phenylstearic Acid .. .. .	54

2.1.3.1	Phenylstearic Acid						
	Characterization	..	..	..	..	..	56
2.1.4	Lithium Phenylstearate	..	..	..	..		61
2.1.5	Soap-Solvent Samples	..	..	..	..		63
2.2	Instrumental Techniques	..	..	..			68
2.2.1	Polarizing Microscopy	..	..	..	..		68
2.2.1.1	Introduction	..	..	..	..	..	68
2.2.1.2	Experimental Method	..	..	..	..		69
2.2.2	Macroscopic Visual Observations	..					71
2.2.3	Differential Scanning Calorimetry	..					72
2.2.3.1	Introduction	..	..	..	..	..	72
2.2.3.2	Principles	..	..	..	..	..	72
2.2.3.3	Experimental Method	..	..	..	..		73
2.2.4	X-ray Diffraction	..	..	..	..	..	78
2.2.4.1	Introduction	..	..	..	..	..	78
2.2.4.2	The Lamellar Phase	..	..	..	..		80
	Determination of the Structure						
	Parameters	..	..	..	..	..	81

2.2.4.3	The Hexagonal Phase .. .. .	82
	Determination of the Structure	
	Parameters .. .. .	83
2.2.4.4	Experimental Method .. .. .	84
2.2.5	Nuclear Magnetic Resonance	
	Spectroscopy .. .. .	86
2.2.5.1	Introduction .. .. .	86
2.2.5.2	Theory of Quadrupole Splitting .. ..	87
	Macroscopically Aligned Samples ..	88
	Powder Samples .. .. .	90
	Effect of Mesophase Structure .. ..	92
2.2.5.3	Experimental Method .. .. .	93
Ch. 3 : <u>The Thermotropic Behaviour of</u>		
	<u>Anhydrous Lithium Soaps</u>	97
3.1	Lithium Stearate .. .. .	97
3.1.1	Differential Scanning Calorimetry ..	97
3.1.2	Polarizing Microscopy and	
	Macroscopic Visual Observations ..	108
3.1.3	Discussion .. .. .	111
3.2	Lithium Oleate .. .. .	122
3.2.1	Differential Scanning Calorimetry ..	122

3.2.2	Polarizing Microscopy .. .. .	126
3.2.3	Discussion .. .. .	127
3.3	Lithium and Sodium Phenylstearates ..	134
3.3.1	Differential Scanning Calorimetry ..	134
3.3.2	Polarizing Microscopy .. .. .	140
3.3.3	$^7\text{Li}$ and $^{23}\text{Na}$ NMR Spectroscopy .. ..	143
3.3.4	X-Ray Diffraction .. .. .	149
3.3.5	Discussion .. .. .	158
Ch. 4 : <u>The Phase Behaviour of Anhydrous</u> <u>Lithium Soap-Hydrocarbon Systems</u>		164
4.1	The Lithium Stearate-n-Hexadecane and Lithium Stearate-Squalane Systems .. .. .	164
4.1.1	Differential Scanning Calorimetry ..	164
4.1.1.1	The Lithium Stearate-n-Hexadecane System .. .. .	170
4.1.1.2	The Lithium Stearate-Squalane System .. .. .	173
4.1.2	Macroscopic Visual Observations and Polarizing Microscopy .. .. .	174
4.1.3	The Equilibrium Phase Diagrams .. ..	176

4.1.4	Discussion .. .. .	179
4.2	The Lithium Phenylstearate- Hydrocarbon Systems .. .. .	187
4.2.1	The Lithium Phenylstearate- 1-Phenylheptane System .. .. .	187
4.2.1.1	Differential Scanning Calorimetry ..	188
4.2.1.2	Polarizing Microscopy and Macroscopic Visual Observations ..	195
4.2.1.3	X-Ray Diffraction .. .. .	205
4.2.1.4	<sup>7</sup> Li NMR Spectroscopy .. .. .	214
4.2.1.5	The Equilibrium Phase Diagram .. ..	232
4.2.2	The Lithium Phenylstearate-Benzene and Toluene Systems .. .. .	234
4.2.3	The Lithium Phenylstearate- Non-Aromatic Hydrocarbon Systems ..	238
4.2.4	Discussion .. .. .	241
Ch. 5 :	<u>The Lithium Phenylstearate-Water System</u>	250
5.1	Polarizing Microscopy and Macroscopic Visual Observations ..	251
5.1.1	Microscopy Penetration Experiment ..	251
5.1.2	Macroscopic Observations .. .. .	254

5.1.3	Microscopic Observations .. .. .	256
5.2	Differential Scanning Calorimetry ..	261
5.2.1	Above Room Temperature .. .. .	261
5.2.2	Below Room Temperature .. .. .	267
5.3	X-Ray Diffraction .. .. .	273
5.3.1	At Room Temperature .. .. .	273
5.3.2	Mechanism of Water Uptake .. .. .	278
5.3.3	Above Room Temperature .. .. .	285
5.4	NMR Spectroscopy .. .. .	287
5.4.1	$^2\text{H}$ NMR .. .. .	287
5.4.1.1	At Room Temperature .. .. .	287
5.4.1.2	Above Room Temperature .. .. .	295
5.4.2	$^7\text{Li}$ NMR .. .. .	301
5.4.2.1	At Room Temperature .. .. .	301
5.4.2.2	Above Room Temperature .. .. .	311
5.4.2.3	Below Room Temperature .. .. .	318
5.5	The Equilibrium Phase Diagram .. ..	322
5.6	Discussion .. .. .	324
Ch. 6	: <u>Summary of Results</u>	332
	<u>References</u>	336

## CHAPTER ONE : INTRODUCTION

Liquid crystals, or mesophases, represent a number of different states of matter in which the degrees of molecular order lie intermediate between the almost perfect long-range positional and orientational order found in solid crystals and the statistical long-range disorder found in ordinary isotropic amorphous liquids and gases.

The alkali metal salts of long-chain carboxylic acids (fatty acid soaps) are among the most well-known class of amphiphilic compounds capable of forming these intermediate states of matter both on heating [1,2,3] and on the addition of a solvent, most commonly water [2-10]. These thermodynamically stable phases are known as thermotropic and lyotropic mesophases respectively.

Amphiphilic mesophases may be regarded as based not on structural arrangements of individual molecules but on the arrangement of multi-molecular units termed "aggregates" or "micelles". Their formation depends on two broadly separable sets of interactions [2,7,8]; short-range intramicellar interactions determining the micellar shape (spherical, cylindrical, disc or sheet-like) and size and the long-range inter-micellar interactions, determining the mutual orientation of the micelles.

## 1.1 The Thermotropic Polymorphism and Mesomorphism of Fatty Acid Soaps

Unlike the corresponding acids, the fatty acid soaps can undergo a process of complex stepwise melting involving one or more intermediate phases between the crystalline solid and the isotropic liquid [1,2,3]. The number and structures of these intermediate phases depend upon both the cation and the hydrocarbon chain length [11].

For the majority of alkali metal soaps (Na, K, Rb, Cs), it has been established that conventional melting, from the crystalline solid to the isotropic liquid, only occurs when the number of carbon atoms in the hydrocarbon chain ( $n_C$ ) is small, less than or equal to three [12,13]. For greater chain lengths (Na and K,  $n_C = 4$ ; Rb,  $n_C = 5$ ; Cs,  $n_C = 6$ ), the soaps also pass through a "melting" transition,  $T_f$ , resulting in the formation of turbid, anisotropic liquid crystals which only melt to isotropic liquids at remarkably higher temperatures, denoted  $T_{c1}$ , the clearing point [14-17].

However, for the lithium n-carboxylates ( $n_C$ , 1-11) the systematic differential scanning calorimetry (DSC) studies of Ferloni et al [13,17,18] and the x-ray diffraction work of Gallot and Skoulios [19] have established that conventional melting occurs with up to 11 carbon atoms in the hydrocarbon chain. No thermotropic liquid crystalline mesophases have been observed for these lithium soaps.

### 1.1.1 Short-Chain Monovalent Soaps

To date, the only thermotropic mesophases formed by short-chain alkyl carboxylates to have been studied in depth are those of sodium [20-33]. Ubbelohde et al carried out extensive studies into the thermodynamic and transport properties of the mesophases of sodium n-butyrate (n-butanoate) and sodium isovalerate (3-methylbutanoate), [20-27]. Phase transition temperatures and their corresponding enthalpies and entropies were measured [12,14,20] and the temperature dependence of molar volume [11], specific electrical conductivity [12,20,26], magnetic susceptibility [25] and viscosity [21,24] was determined over the range of mesophase stability. Their x-ray diffraction studies suggested that the randomly oriented liquid crystal domains consisted of "sandwich-type" bilayers stabilized by electrostatic forces [22]. Polarized microscopy experiments carried out by Bonekamp et al [33] supported these findings, showing that both sodium n-butyrate and sodium isovalerate form smectic A type liquid crystalline structures ("neat" or "lamellar" mesophases).

The dynamic properties of the short-chain sodium carboxylates have been investigated in more detail only in recent NMR studies [28-32]. Proton and sodium-23 NMR data, including the measurement of quadrupole coupling constants and spin-lattice relaxation times, were obtained for the mesophase of several branched and straight, short-chain sodium soaps. These results, along with previous polarized microscopy

data [33], showed that the mesophase properties, such as quadrupole coupling constant, domain size and range of mesophase stability, changed drastically when the alkyl chains were branched. Soaps such as sodium 2-methylbutyrate and sodium isobutyrate (2-methylpropanoate) are known not to form thermotropic mesophases [12,34]. These results have been explained in terms of a model for the arrangement of the polar groups in the smectic A mesophase of all short-chain sodium soaps [32]. This model is based upon an ionic double layer with interdigitated polar groups as opposed to the sandwich-type structure proposed by Ubbelohde et al [22].

A study of the melting mechanisms of alkali metal n-carboxylates containing up to 6 carbon atoms has indicated that the choice of cation for a particular carboxylate also significantly influences the temperature range of stability of the mesophase [14]. In the case of the short-chain lithium n-carboxylates, no stable liquid crystal phases were observed.

DSC studies of the alkali metal n-carboxylates with up to 12 carbon atoms [Ferloni et al, 13, 15-18, 35], the polarized microscope work of Baum et al [36] and the

x-ray diffraction studies of Skoulios and co-workers [11] represent a comparison between the thermal behaviours of the short and longer chain Group I soaps. In particular, they show the variation with chain length of the isotropic melt to neat mesophase transition (not observed for the lithium soaps) and the transition from the neat phase to ordered semi-crystalline "plastic" and crystalline phases. The formation of intermediate semi-crystalline phases is only observed for the longer chain homologues (for lithium soaps  $n_c \geq 12$ , [18,19]); see Section 1.1.2.1.

### 1.1.2 Long-Chain Soaps

Research into the thermotropic polymorphism and mesomorphism of long-chain metal soaps (where  $n_c > 12$ ) extends over many years. Early reports of this complex thermal behaviour were made by Vorländer in 1910 [34], and in 1938 Lawrence reported the existence of temperatures at which a number of long-chain metal soaps became "plastic" before reaching their melting points [37]. These investigations were extended by McBain and Vold in the 1930's and 1940's as part of their studies on alkali metal soap-water systems [38-46].

The application of differential thermal analysis (DTA) to the study of this stepwise melting was first attempted by Vold [47] on several sodium soaps (even-numbered homologues between  $C_{12}$  and  $C_{18}$ ). Subsequently, many workers have reported DTA and DSC studies of long-chain soaps of the alkali metals [47-66], the alkaline earth

metals [65, 67-70], main-group heavy metals such as lead [70,71,72] and aluminium [70,74] and a number of divalent transition metals [70,73,75-78].

Other physical techniques used to study the polymorphism of these soaps include, polarized microscopy [36], dilatometry [43,62,63,79-81], infrared spectroscopy [82-90], NMR spectroscopy (measurements of line-width and second moment [91-103] and proton spin-lattice relaxation times [103-106]) and x-ray diffraction [11,19,48,49,53,66,68,107-125].

#### 1.1.2.1 Phase Structures of the Alkali Metal Soaps

The structures of the phases occurring during the course of fusion of the long-chain alkali metal soaps have been examined extensively by Skoulios and co-workers using x-ray diffraction [11, 19, 111-117]. A number of these structures have only been established with reasonable assurance whilst others have been corroborated by NMR spectroscopy [91-106], dilatometry [80] and polarized microscopy [36].

At room temperature, the alkali metal soaps form lamellar crystalline phases (denoted LC by Skoulios and co-workers). In these structures the soap molecules are packed in a three-dimensional lattice in which the polar groups and the hydrocarbon chains form alternating double layers [11]. The hydrocarbon chains are fully extended and inclined with respect to the end group planes [11].

As the temperature is raised, the paraffin chain zones of the lamellae commence to melt, resulting in the formation of individual, apparently semi-crystalline ribbon or disc phases (also commonly referred to in the literature as "plastic" [54], or "subwaxy", "waxy", "superwaxy" and "subneat" phases [47]). The number and structure of these intermediate phases depend upon both the cation and the hydrocarbon chain length.

For the soaps of lithium and sodium (the even-numbered homologues from  $C_{12} - C_{22}$  and  $C_{12} - C_{18}$  respectively), ribbon structures are formed. These structures are thought to consist of sets of parallel ribbons, indefinite in length and packed in a two-dimensional rectangular centred lattice, denoted BR [19, 111-114], see FIG. 1.

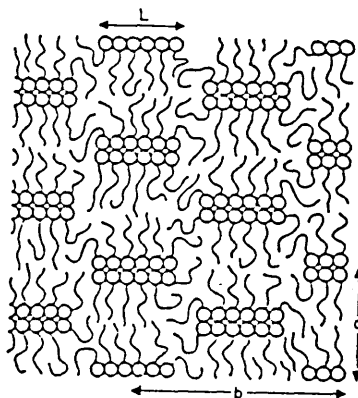


FIG. 1 : Structure of the two-dimensional rectangular-centred lattice of the ribbon phase ; cross-section of the ribbons [112]

For the potassium soaps (even-numbered homologues from  $C_{16}$  to  $C_{22}$ ) the ribbons are arranged in a two-dimensional oblique lattice [114,115,116]. The ribbon phases are thought to contain the polar groups in a quasi-crystalline type of organization dispersed in a liquid matrix comprised of the fully disordered hydrocarbon chains. The breadth of the ribbons is determined by the equilibrium between the thermal agitation of the hydrocarbon chains and the cohesion of the polar groups. For potassium myristate (n-tetradecanoate) and for the soaps of rubidium (even-numbered homologues from  $C_{16}$  to  $C_{20}$ , [117]) semi-crystalline disc phases are formed. Here the parallel discs are arranged on a face-centred orthorhombic lattice. The discs are the loci of the polar groups which are separated by the disordered hydrocarbon chains. In the disc phases of the  $C_{18}$ ,  $C_{20}$  and  $C_{22}$  soaps of caesium [11], the discs are located in parallel and equidistant planes but their lateral correlations appear to be loose.

For a given soap, the breadth of the ribbons and the size of the discs decrease discontinuously with a rise in temperature, each decrease corresponding to a sharp phase transition. The ribbons are thought to become more symmetrical with each decrease in breadth and as a consequence the lattices of the successive ribbon phases, whether rectangular or oblique, tend towards two-dimensional hexagonal in the higher temperature phases.

According to Skoulios and co-workers, the lamellar bilayer phase (smectic A or neat soap), is formed on rise of temperature by all the long-chain alkali metal soaps, except those of lithium, as the phase immediately preceding the amorphous melt [11]. The transition from a ribbon or disc phase to the lamellar mesophase is therefore thought to be accompanied by fusion of the polar group region.

FIG. 2 shows the succession of phases occurring during the fusion of several long-chain lithium soaps as determined by Gallot and Skoulios [19].

C <sub>10</sub> Li	C <sub>12</sub> Li	C <sub>14</sub> Li	C <sub>16</sub> Li	C <sub>18</sub> Li
LC 1	LC 1	LC 1	LC 1	LC 1
—39—	—67—	—87—	—102—	—122—
LC 2	LC 2	LC 2	LC 2	LC 2
—238—	BR { 229 239 }	BR { 210 231 239 }	BR { 190 211 223 }	BR { 190 215 229 }
F	F	F	F	F

LC, lamellar crystalline

BR, ribbons in a two-dimensional rectangular lattice

F, amorphous melt.

FIG. 2 : Phase structures occurring during the fusion of long-chain lithium soaps [19].

A recent study by Busico et al [126] attempted to explain the complicated polymorphism and mesomorphism of these anionic soaps using a simple electrostatic model. They have concluded that the stepwise melting behaviour results from a balance between the tendency of the ionic end groups to segregate in layers for electrostatic reasons, and that of the alkyl chains to break these layers in order to gain complete conformational freedom. They have suggested that other factors play only minor roles and have excluded any contribution of long-range electrostatic interactions between adjacent ionic layers as suggested by Duruz and Ubbelohde for the short-chain sodium soaps [22].

#### 1.1.2.2 Lithium Soaps

The thermotropic polymorphism of the long-chain lithium soaps [54], despite being somewhat less complicated than the corresponding sodium analogues [55, 112], has not been fully resolved. The work of Franzosini [54] contains a brief review of the thermal behaviour of the  $\text{LiC}_{14}$ ,  $\text{LiC}_{16}$  and  $\text{LiC}_{18}$  soaps in which largely conflicting data from different laboratories is presented.

Lithium palmitate (n-hexadecanoate), in particular, has been the subject of detailed thermodynamic and structural investigations [19,36,46,48,54,62,65,66,80]. Most studies have detected two main phase transitions in the temperature ranges 101-111°C (an intercrystalline transition) and 222-231°C (considered to be the final melt to isotropic

liquid). Discrepancies exist, however, concerning the number and nature of the intermediate phases.

In a variable temperature, x-ray diffraction investigation, Gallot and Skoulios postulated the existence of two semi-crystalline ribbon structures, stable between 190°C and 223°C [19]. The polarized microscopy observations of Baum et al supported these findings [36].

Vold, Funakoshi and Vold, however, employing DSC, x-ray diffraction and polarized microscopy found no evidence for such "waxy", ribbon phases but reported the existence of a "viscous, doubly-refracting fluid mesophase, with hexagonally close-packed chains" which was stable between 208°C and 222°C, the isotropic melt [66].

More recently, the results of Busico et al [48] stand in direct contrast to those of Vold et al [66]. They proposed the existence of a single intermediate ribbon phase stable between 209°C and 231°C which "melted" to form a smectic mesophase, not previously reported in the literature (denoted smectic II), and stable up to at least 300°C. Unlike the high temperature smectic "neat" mesophases formed by all the anhydrous alkali metal soaps except lithium (optically turbid and birefringent with regular bilayer stacking), the smectic II mesophase is considered to be a less well-organized structure showing irregularities in the x-ray long spacing. It is optically clear and

non-birefringent. This property is attributed to the reduced dimensions of the smectic domains. Smectic II mesophases have also been reported by Busico et al for the "melts" of the n-alkylammonium chlorides [130] and lithium 16-hydroxyhexadecanoate [49]. To date, however, no reports of such mesophases have been made by other workers.

#### 1.1.2.3 Phase Structures of the Alkaline Earth Soaps

The long-chain soaps of divalent metals,  $(RCO.O)_2M$ , like those of the alkali metals, show stepwise melting with a series of sharp transitions between distinct phases [67-78]. The thermotropic phases formed by the alkaline earth metal soaps (plus those of cadmium and zinc) have been studied in detail by Spegt and Skoulios who were able to propose various structures which were consistent with their x-ray investigations [118-120, 123-125]. A number of these structures (originally interpreted in terms of discs for the soaps of calcium [120] and strontium [123]) have been the subject of extensive revision (the "structure elements" were later interpreted in terms of finite sized rod-structures [122]) but still cannot be regarded as definite. The structures of the high temperature hexagonal liquid crystal phases, however, have been established with reasonable assurance.

Unlike the alkali metal soaps, a number of these divalent metal soaps form two-dimensional hexagonal mesophases ("middle" type soap phases) of the reversed type preceding the isotropic melt (denoted  $H_2$  or  $M_2$ ), see FIG. 3.

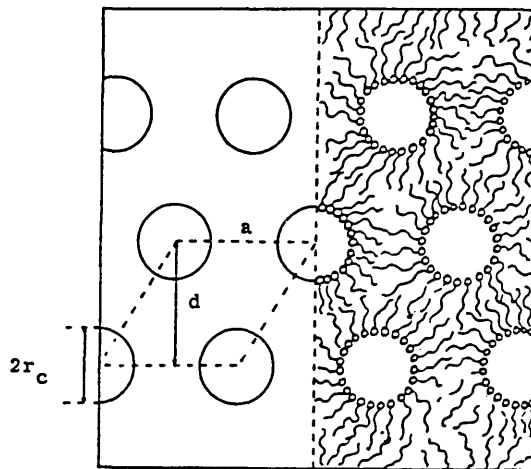


FIG. 3 : Structure of the two-dimensional reversed  
hexagonal mesophase (refer to Section 2.2.4.3)

This structure is made up of parallel rod micelles of indefinite length which are arranged in a two-dimensional hexagonal array. The polar groups form the central core of the rods whilst the hydrocarbon chains extend radially from them forming the continuous medium between the rods. Whereas the x-ray measurements indicate that the hydrocarbon chains are in a disordered state, it is less clear whether the polar groups are in a "crystalline" state or fused as in the high temperature lamellar mesophases of the alkali metal soaps [123].

The soaps of magnesium and cadmium each give two hexagonal mesophases which apparently differ in possessing modified arrangements of the polar groups, the higher temperature arrangement being slightly less compact [118,124]. The anhydrous soaps of calcium and strontium form only one hexagonal phase. For the soaps of barium and strontium, a high temperature body-centred cubic

mesophase, whose structure is based upon rods of finite length, has also been proposed [121,123].

#### 1.1.2.4 Discrepancies in Phase Behaviour

Despite the varied and extensive investigations into the thermal behaviour of the long-chain soaps, discrepancies exist in the literature as to the temperatures and in some cases even the number and nature of the transitions involved [54]. Careful study of the literature of soap phases suggests that most of the major discrepancies are not due to impurities or experimental imprecision, but arise from failure to maintain equilibrium, or confusion of one phase with another (especially when more than one mesomorphic phase exists [81]), or the ability of one technique to detect a given transition which cannot be detected by another. Ripmeester and Dunell [58] have also demonstrated in a DSC study of the alkali metal stearates ( $n_c = 18$ ) that the thermal history of the sample prior to analysis had a significant influence on the results obtained. Similarly Trzebowski [60] has reported three different DTA thermograms for samples of sodium stearate obtained by different drying methods. Such results might be expected since x-ray studies carried out on the long-chain soaps of sodium and calcium have shown the possibility of their existence in a number of different stable hydrated modifications at room temperature [68,69,127-129]. Drying soaps at elevated temperatures may also lead to the formation of additional metastable phases.

#### 1.1.2.5 Unsaturated Soaps

By introducing non-linear chains into the soap molecule, it is possible to form liquid crystal phases at reduced temperatures. (This reduction in temperature may not always occur for short branched-chain soaps [131,132].) The effect of unsaturation in the chain, however, has not been systematically studied. Sodium oleate (cis-9-octadecenoate) undergoes a similar number of thermotropic transitions to sodium stearate (n-octadecanoate), although the range of temperatures is lowered by approximately 20°C [52]. In addition to the lamellar phase exhibited by sodium stearate, sodium oleate is reported as forming two further mesophases at lower temperatures (between 119.5°C and 174.5°C) with face-centred cubic structures [52]. Such phase structures are not formed by the monovalent saturated soaps.

#### 1.1.3 Anionic Amphiphiles of Low Crystallizing Tendency

Anionic soaps and surfactants in which the lipophilic groups are of a non-compact branched type frequently do not crystallize and the pure, anhydrous salts exist as mesophases, apparently of the fused type, at room temperature [123,133-136]. The hydrocarbon groups, on account of their branched character, do not themselves crystallize; further, on account of their relatively large cross-section they prevent sufficiently close lateral approach of the polar groups for their crystallization to occur.

FIG. 4 shows the structural formula of the branched-chain surfactant Aerosol OT (sodium di-2-ethylhexylsulphosuccinate) which has been reported to exist as a reversed hexagonal mesophase in the anhydrous state at room temperature [134]. This mesomorphic phase is also produced by both 1-methyl and 1-ethyl branching in the hexyl chain [134]. The straight-chain isomers, however, sodium di-n-hexylsulphosuccinate and sodium di-n-octylsulphosuccinate, crystallize readily [134].

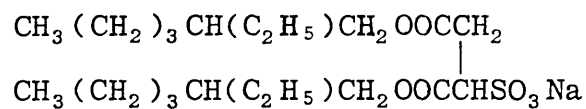


FIG. 4 : Sodium di-2-ethylhexylsulphosuccinate  
(Aerosol OT)

## 1.2 Binary Solutions of Anionic Amphiphiles in Non-Polar Organic Solvents

### 1.2.1 Solubility and Micellization

Although most of the published literature on micelle formation concerns aqueous systems, the literature on micelle formation in organic solvents extends over many years [37, 137-140].

Whilst the aggregation of surfactants in aqueous solution leads to the formation of micelles with the polar head groups situated at the surfactant-water interface [5], a similar aggregation can occur in non-polar solvents to form "reversed" or "inverted" micellar structures [140]. Here the polar head groups are contained within the micellar core, surrounded and shielded by the lipophilic paraffin chains of the surfactant molecules which extend into the continuous medium. The aggregation numbers and micellar shape in nonaqueous systems are closely dependent upon a number of factors such as surfactant type and concentration, the nature of the solvent employed, the presence of water or other polar additives and the temperature of the system [140].

#### 1.2.1.1 Long-Chain Metal Soaps of Groups I and II

At room temperature, the crystalline alkali metal and alkaline earth long-chain fatty acid soaps show very little solubility in hydrocarbons due to their very strong

polar bonding [51,59,141-143]. The solubility increases rapidly over a temperature range which depends both on the soap and the solvent but more critically on the soap. When heated, the anhydrous soaps undergo a process of complex stepwise melting in which first the hydrocarbon chains and then the polar groups undergo progressive disordering (see Sections 1.1.2.1 and 1.1.2.3). Over the intermediate temperature ranges, hydrocarbons can be dissolved in limited amounts in the disordered hydrocarbon regions of the soap while the polar groups largely retain their crystalline order [123,144,145]. In cases where the solvent-free soap undergoes a thermotropic transition to a liquid crystal phase, complete solubility of the soap has been observed in non-polar solvents at temperatures above this phase transition. For example, it has been reported that magnesium laurate (n-dodecanoate) forms small reversed spherical micelles with an aggregation number of 13 at a concentration of 0.02 M in boiling toluene (110.6°C) [150]. Spegt and Skoulios [118] have shown, using x-ray diffraction, that solvent-free magnesium stearate (n-octadecanoate) undergoes a transition from a crystalline state to a reversed hexagonal mesophase at 109°C. No data was presented for the phase behaviour of magnesium laurate although a similar transition temperature would be expected for this homologue by comparison to the very similar phase behaviours observed for calcium laurate and calcium stearate [120].

### 1.2.1.2 Divalent Heavy Metal Soaps

Similar sudden increases in solubility, at a "critical solution temperature", have been observed for a number of divalent heavy metal soaps in non-polar organic solvents. For example, Nelson and Pink [150] have shown that, at concentrations of 0.02 M in boiling toluene, the laurates of copper and zinc form small reversed spherical micelles with aggregation numbers of 8 and 5-6 respectively. The laurates of cadmium and lead, however, were insoluble at this temperature.

The solubility behaviour of the heavy metal soaps has been compared to that of aqueous soap systems at the Krafft point [146]. Murray and Hartley [152] have explained the Krafft point in aqueous soap systems as the temperature at which the solubility of the crystalline soap reaches the critical micelle concentration, c.m.c. At temperatures higher than the Krafft point, the crystalline phase, therefore, cannot exist in equilibrium with micelles. The same explanation is applicable in principle to sudden increases in solubility observed for the divalent heavy metal soaps in low polarity solvents. It should be noted, however, that this critical increase in solubility may, in certain cases, result from a thermotropic phase transition associated with the anhydrous soap to the isotropic liquid phase, which is likely to have a greater solubility than the c.m.c. for the micellar form. Both copper laurate and zinc laurate have been reported to undergo crystalline to isotropic liquid phase transitions

at 112.1°C and 133.8°C respectively [73]. The temperature of this transition would probably be lowered by the presence of the solvent.

A review of the properties of organic solutions of heavy metal soaps has been given by Pilpel [138].

#### 1.2.1.3 Aluminium Soaps

Aluminium soaps exhibit quite a different behaviour from the soaps of divalent metals. Generally, aluminium soaps are mono- or disoaps and possess one or two free hydroxyl groups [138]; aggregation in organic solvents is determined by intermolecular bonds involving the free hydroxyls [153,154]. The high viscosities observed with aluminium soaps suggest the existence of high molecular weight filamentous aggregates, postulated by some to be linear polymers [155]. Debye's diffraction and viscosity measurements, however, suggested that aluminium soaps form elongated micelles, 40 Å in diameter and 200 to 1500 Å in length [156]. Additives can promote or reduce the degree of hydrogen bonding and thereby render these soaps more or less viscous [157-159].

Similar polymer-like solution behaviour has been reported recently for a cobalt hydroxy monooleate soap in apolar solvents (0.5 - 2.0% w/v), [160]. The results indicated an open-type mechanism for the soap association process, involving OH-bridging between the cobalt atoms, to produce viscous solutions of long polymer soap chains

in both benzene and heptane. The presence of small amounts of additives, such as acetylacetone, pyridine and dimethylsulphoxide, greatly reduced the solution viscosity, even to the same level as the solvent itself.

#### 1.2.1.4 Anionic Amphiphiles of Low Crystallizing Tendency

The study of ionic amphiphiles of low crystallizing tendency, the so-called "oil-soluble soaps" has been made in a wide variety of organic solvents [140].

Association micelles of the reversed type have been observed at room temperatures in various organic media with, for example, the alkali metal dialkyl sulphosuccinic esters or "Aerosols" [161-165], the alkyl aryl sulphonates [166-174] and the aryl stearates [175-180].

The solution behaviour of the arylstearates in non-polar organic solvents is of special interest and will be considered in detail in Section 1.2.3.

#### 1.2.2 Lyotropic Mesophase Formation in Anionic Amphiphile - Non-Polar Solvent Systems

Most of the factors governing the formation and stability of liquid crystal phases occurring in surfactant-water systems, such as electrostatic interactions, surfactant head group hydration, steric repulsions and alkyl chain conformations, have been extensively investigated and are qualitatively understood [2-10]. In contrast to the ready formation of aqueous mesophases, however, anhydrous liquid crystalline phases in organic solvents are rarely encountered.

Few fundamental studies have been made of concentrated binary surfactant-hydrocarbon mixtures [51,59,61,134,144, 181-199] in spite of their widespread use in industry and their special relevance to the field of soap-thickened lubricating greases [60,141,142,183-185,190]. In many cases, the results of such phase studies do not present a consistent picture.

#### 1.2.2.1 Long-Chain Sodium Soaps

Smith and McBain [186] used visual observations in polarized light to study the phase behaviour of sodium stearate (n-octadecanoate; hereafter denoted  $\text{NaC}_{18}$ ) with various aromatic, naphthenic and paraffinic solvents of low molecular weight. They presented binary phase diagrams for the systems  $\text{NaC}_{18}$ -toluene and  $\text{NaC}_{18}$ -cyclohexane based on these observations. Their results indicated that there was little interaction between the soap and solvent below approximately  $90^\circ\text{C}$ , but at higher temperatures they showed the existence of two liquid crystalline "phase islands" occurring at very similar composition ranges for both solvent systems. The phase observed at higher  $\text{NaC}_{18}$  concentrations (between approximately 55% and 85% by weight  $\text{NaC}_{18}$ ) was described as a "white, waxy, liquid-crystalline phase" and was stable to temperatures greater than  $288^\circ\text{C}$ , the melting point of the pure solvent-free soap. The second phase island, observed between approximately 20% and 45% by weight  $\text{NaC}_{18}$ , was described as a "golden, liquid-crystalline phase" and was stable to approximately  $250^\circ\text{C}$ .

Similar phase behaviour was also observed for  $\text{NaC}_{18}$  with o, m and p-xylene, ethylbenzene, cumene, benzene, isooctane and n-heptane.

The structures of the liquid crystal phases observed for the  $\text{NaC}_{18}$ -cyclohexane system by Smith and McBain [186] were later determined by Skoulios [144] using x-ray diffraction methods. The phase observed at higher  $\text{NaC}_{18}$  concentrations was considered to be a solvent-swollen, semi-crystalline phase of the pure anhydrous soap, having a two-dimensional, rectangular-centred ribbon structure (see Section 1.1.2.1). The "golden, liquid crystalline phase" observed at lower  $\text{NaC}_{18}$  concentrations was identified as a lamellar mesophase with a solvent-swollen bilayer structure.

The  $\text{NaC}_{18}$ -cetane (n-hexadecane) system studied by Doscher and Vold [187], using polarized microscopy, was found to be very different in character to the  $\text{NaC}_{18}$ -hydrocarbon systems of Smith and McBain [186]. One feature common to each system, however, was the observation of phase islands, although they too differed considerably both in size and location on the respective phase diagrams. Doscher and Vold designated the high  $\text{NaC}_{18}$  concentration phase island in the cetane system as a "superwaxy" phase by analogy to the high temperature phase observed for the pure solvent-free soap [47]. The second, much smaller phase island, at intermediate soap concentrations was labelled non-aqueous "middle" soap by analogy to mesophases observed in

aqueous sodium soap systems [38-44]. The structure of this non-aqueous middle phase, however, was described as being a smectic rather than a hexagonal liquid crystal [186].

Further studies on the  $\text{NaC}_{18}$ -cetane system carried out by Stross and Abrams [59,188] produced substantially different results from those of Doscher and Vold [187]. A phase diagram was constructed, using carefully prepared and rigorously dried  $\text{NaC}_{18}$  and cetane, by means of DTA supplemented by visual and microscopic observations in polarized light. The phase diagram indicated no appreciable interaction between the soap and solvent below approximately  $140^\circ\text{C}$ . At higher temperatures, the transition temperatures of the anhydrous soap were depressed by the addition of the solvent, the depression being constant over most of the concentration range studied. No phase islands of the type ascribed to the  $\text{NaC}_{18}$ -cetane system by Doscher and Vold [187], nor those described by Smith and McBain [186] were observed, all phases being continuous with ones occurring in the solvent-free soap. Stross and Abrams [59,188] stated that a possible reason for the discrepancy between their findings and those of Doscher and Vold [187] might lie in the failure of the latter to exclude all traces of water from the system.

#### 1.2.2.2 Long-Chain Lithium Soaps

The disagreement concerning the phase behaviour of sodium stearate with cetane [59,187,188] may be compared to a similar case involving the lithium stearate ( $\text{LiC}_{18}$ )-cetane system [51, 195].

The phase diagram for this system (and also for the  $\text{LiC}_{18}$ -decalin system) reported by Vold and Vold [195] (based on DTA results supported by visual observations in polarized light) showed a phase island labelled non-aqueous "middle" soap by analogy to a similar phase observed for the corresponding  $\text{NaC}_{18}$  system [187], see FIG. 5. The middle soap of  $\text{LiC}_{18}$  was described as liquid crystalline, consisting of "sheet-like aggregates of clusters of commonly oriented soap and solvent molecules", and was shown to be bound by the waxy and isotropic solution phases. It was stated that this phase was not produced by direct incorporation of solvent into any form of the solvent-free soap.

The experimental observations of Cox and McGlynn [51] on the  $\text{LiC}_{18}$ -cetane system, however, clearly indicated that their liquid crystalline phase had the same character as the Vold and Vold middle soap [195], but that the phase was continuous with a previously unreported high temperature, liquid crystal phase of the pure solvent-free soap, and persisted to as low a soap concentration as measured. There was no evidence of any phase island, see FIG. 6.

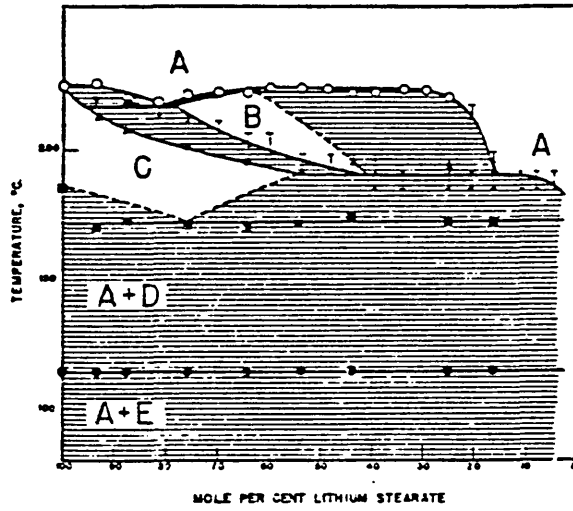


FIG. 5 : A phase diagram for the system lithium stearate - cetane [195]

A, isotropic liquid; B, non-aqueous middle soap; C, waxy lithium stearate; D, crystalline lithium stearate I; E, crystalline lithium stearate II.

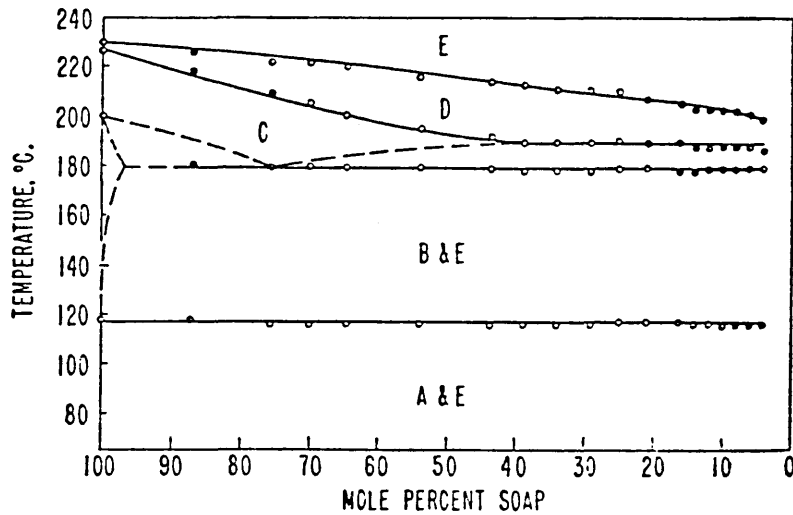


FIG. 6 : A phase diagram for the system lithium stearate - cetane [51]

A, crystalline lithium stearate II; B, crystalline lithium stearate I; C, waxy phase; D, liquid-crystal phase; E, isotropic solution

Similar results were obtained by Cox [196] in a DTA study of several  $\text{LiC}_{18}$ -high molecular weight mineral oil systems. In each of the systems, the number and nature of the phases found was remarkably similar, each soap-containing phase being continuous with a phase of the solvent-free soap. The phase diagrams were remarkably similar to the  $\text{LiC}_{18}$ -cetane system [51]. A correlation was found between the equilibrium phase change temperatures of the waxy-liquid crystal transitions and the molecular weight of the hydrocarbons, and a new structure was postulated for the liquid crystal phase based on long, chain-like aggregates of soap molecules. Similar phase diagrams for  $\text{LiC}_{18}$ -oil systems have subsequently been reported by Vold et al [197] and Uzu [61].

#### 1.2.2.3 Effect of Added Water

Attempts have been made to understand the role played by water in soap-hydrocarbon systems [189-192].

Vold and Philipson [189] studied the system  $\text{NaC}_{18}$ -cetane-water and represented their visual observations in terms of a partial phase diagram. Attempts were made to relate the changes in observed phase behaviour (sample appearance and properties) to the changes in the nature of the solvent.

Similarly, Smith [190] studied the effects of water, and additives such as methanol and lauric acid, (n-dodecanoic acid), on the phase behaviour of  $\text{NaC}_{18}$  in toluene and cyclohexane. These additives were found to

significantly lower the liquid crystal to isotropic solution phase boundary in the two systems. Less than 1 wt % of water was required to produce remarkable deviations from the phase behaviour of the pure anhydrous systems.

Doscher and Davis [192] in a similar study, used a dielectric absorption method to determine the minimum quantities of water which were required to produce significant changes in phase transition temperatures for the  $\text{NaC}_{18}$ -cetane system.

X-ray diffraction studies of the systems calcium stearate-cetane [194] and calcium stearate monohydrate-cetane [193], carried out by Vold et al, showed that the presence of water tended to increase the stability of the systems of  $\text{CaC}_{18}$  and cetane due to its effect on the colloidal structure of the gel formed at room temperature (size, shape and manner and degree of association of the aggregates formed) rather than its reaction to form the monohydrate.

It should be noted that the strictly anhydrous solutions of surfactants in non-polar organic solvents, to which most of Section 1.2 refers, can only be maintained in a dry atmosphere. When exposed to atmospheric humidity, such solutions will take up or "solubilize" moisture until in equilibrium with their surroundings at the particular water vapour pressure and temperature. With a surfactant solution in a hydrophilic organic solvent, the uptake of water will be partly due to the hygroscopicity

of the solvent itself. With solutions in hydrocarbons the water will be solubilized by the surfactant micelles and will modify their properties considerably [140].

#### 1.2.2.4 Anionic Amphiphiles of Low Crystallizing Tendency

Very little information is available on the mesomorphic behaviour of the ionic amphiphiles of low-crystallizing tendency in concentrated hydrocarbon systems. It has been shown, however, that Aerosol OT, which itself exists as a reversed hexagonal mesophase at room temperature, can only take up small amounts of hydrocarbon solvents before passing into viscous, highly concentrated isotropic solutions [134,198,199].

Balmbra and Clunie [134] have shown that Aerosol OT can take up approximately 18 wt % of toluene at room temperature before passing into the isotropic liquid phase. Similar results were obtained by Rosenfeld and Frank [199] for Aerosol OT in a number of n-aliphatic hydrocarbons; see FIG. 7. This shows the variation of the liquid crystal to isotropic liquid transition temperature with composition for the Aerosol OT - n-dodecane system.

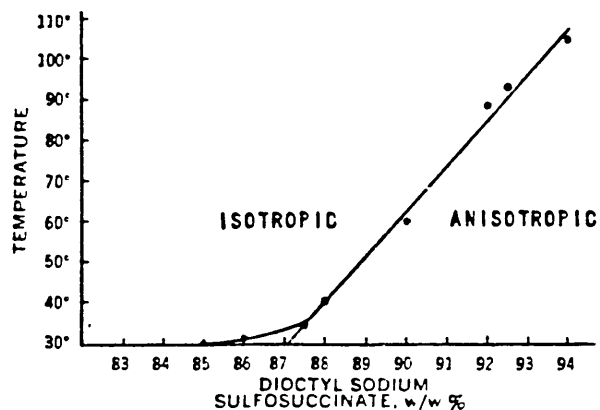


FIG. 7 : The variation of the anisotropic (liquid crystal) to isotropic transition temperature with composition for the Aerosol OT - n-dodecane system [199]

The findings of Rosenfeld and Frank [199] are supported by the small-angle x-ray diffraction results obtained by Siegel [198] for Aerosol OT (6% to 75% by weight) in n-dodecane at room temperature. The experimental scattering curves suggested the existence of a reversed isotropic micellar solution over the entire concentration range studied.

### 1.2.3 Solution Behaviour in Dilute Alkali Metal and Alkaline Earth Phenylstearate-Benzene Systems

Whereas the crystalline Group I and Group II metal n-carboxylates are essentially insoluble in hydrocarbons at room temperature (see Section 1.2.1.1), the corresponding salts of phenylstearic (phenyloctadecanoic) acid have been reported to be soluble in benzene at room temperature.

### 1.2.3.1 The Isomeric Nature of Phenylstearic Acid

Phenylstearic acid obtained by the Friedel-Crafts reaction of oleic acid (cis-9-octadecenoic acid) with benzene, has in the past been considered as primarily the 10-phenylstearic acid [200], a mixture of approximately equal parts of the 9 and 10 isomers [201], or, if hydride shifts of the intermediate carbonium ions is extensive, a mixture of several isomers in which the 17-phenyl isomer is thought to predominate [202]. More recent investigations by Smith and co-workers [203-205] showed, by gas liquid chromatography of the alkyl aryl ketones obtained by chromic acid oxidation, that the phenylstearic acid is in fact a complex mixture of 12 positional isomers with substitution at the C6 to C17 positions on the fatty acid chain (see TABLE 1).

Substitution of the phenyl group was shown to predominate at the C9 and C10 positions (the position of the original double bond in oleic acid) and at other positions near to the middle of the chain. Substitution at positions lower than C6 are thought not to occur because of the "repelling action" of the carboxyl group.

A re-investigation of this work in our laboratories [206-208] has produced similar results to those of Smith and coworkers (see TABLE 1).

<u>Positional Isomer (Carbon No on Fatty Acid Chain)</u>	<u>Mole % of Isomer</u>	
	<u>Ref [205]</u>	<u>Ref [206]</u>
17	6.1	3.3
16	3.6	1.8
15	4.7	2.9
14	7.5	5.3
13	8.9	7.4
12	10.7	9.3
11	12.8	12.3
10	16.5	18.4
9	14.7	18.7
8	8.5	11.5
7	3.9	6.8
6	2.0	2.8

TABLE 1 : Distribution of isomeric phenylstearic acids obtained by the Friedel-Crafts reaction of oleic acid with benzene

#### 1.2.3.2 Solubility of Soap Mixtures

The relatively high solubility of the alkali metal and alkaline earth phenylstearates in benzene at room temperature may be explained by the findings of Kissa [143,209] who has reported extensive data on the solubility of crystalline lithium salts of aliphatic and alicyclic acids in n-heptane, isooctane and benzene at 27°C. Kissa found the pure crystalline salts, whether straight-chain, branched or alicyclic, to have low solubilities at this temperature (less than  $10^{-4}$  mol dm<sup>-3</sup>),

the straight-chain salts being least soluble [143]. He also showed, however, that the solubility of mixtures of alkali metal carboxylates, featuring a branched aliphatic chain or an alkyl substituted alicyclic ring, in hydrocarbon solvents exceeded by far the sum of the individual solubilities [209]. For a mixture of nine branched-chain lithium carboxylates in isooctane at 27°C, the solubility was increased to 400 times the sum of their individual solubilities. The salts of isomeric mixed acids from commercial intermediates had solubilities as much as 1000 times that of some of the pure single salts of which they were composed.

The differences in solubility behaviour of the pure crystalline salts and of mixtures of the same pure salts can be explained by considering the different free energies of the solid phases involved in the surfactant-solvent system. Straight-chain aliphatic radicals can pack closely in the crystal allowing strong dispersion force interactions between the methylene groups of the chain [210]. The standard free energy decrease for such a molecule on passing from hydrocarbon solution into the crystal would be relatively large and the solubility accordingly small. Mixing straight-chain salts causes only a minor decrease in the amount of interaction between chains, so mixtures of straight-chain salts show no enhanced solubility. In the reversed, non-aqueous micelle the hydrocarbon chains of the surfactant must be in rather intimate contact with the disordered solvent molecules, rather

than adlinedated to each other as in the crystal, so the standard free energy change for micelle formation is less than that for crystal formation. Consequently, the micellar phase is unstable with respect to the crystal until the temperature of the system approaches the "melting point" of the soap, when there is usually a sharp transition to unlimited solubility. When, on the other hand, the carboxylate molecules are branched, the molecules cannot pack so closely in the crystal and there is less dispersion force interaction between chains. Mixing different branched-chain species results in a further decrease in packing efficiency and an increase in entropy in the solid phase. This further minimizes the free energy of solid formation and increases the equilibrium solubility. As the complexity and heterogeneity of the molecules in the solid carboxylate phase are increased, a point is reached at which the mixture is in equilibrium with a higher concentration of dissolved species than is required for the formation of micelles. The solid phase then passes over completely to the more favourable "mixed micellar" state unless the system is below the critical solution temperature, in which case a solvent-swollen "solid" phase equilibrates with the micellar solution, ie there is limited micellar solubility.

### 1.2.3.3 Solution Structure of the Phenylstearate Soaps in Benzene

The dilute anhydrous solutions of the alkali metal and alkaline earth phenylstearate soaps in benzene (approximately 1 - 2.5%), unlike the oil-soluble sulphonates [171], are shear-birefringent, highly viscous and slightly non-Newtonian in flow [178,179]. For such systems, it has been postulated that the soap molecules are organized into extensive linear structures. Similar polymeric chain structures have recently been suggested for a cobalt hydroxy monooleate soap (0.5 - 2.0% w/v) in both benzene and heptane [160].

The basic structure for the alkali metal phenylstearate micelles in anhydrous benzene solutions is considered to be the co-ordinately bonded single chain of alternating cations and anions [180], see FIG. 8. Some additional

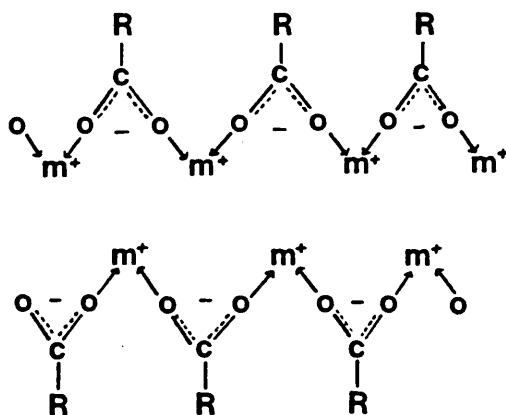


FIG. 8 : Proposed configuration for the alkali metal phenylstearate soap micelles in dilute, anhydrous benzene solutions [180]

decrease in the free energy of the system is believed to occur if portions of such chains are juxtaposed by coiling or folding, or by parallel alignment as indicated schematically in FIG. 8. This chain structure allows full resonance of the carboxylate group even when the coordination effect leads to something less than full ionic character of the soap. The full equivalence of the two carboxylate oxygens has been deduced from infrared studies [211]. Infrared spectra also show that the strength of the C-O linkage, as revealed by the  $\omega_2$  carboxylate ion band in the 1500-1600  $\text{cm}^{-1}$  region, is linearly linked to the Pauling electronegativity of the alkali cation present [212]. This points to some specific interaction between the metal and the carboxylate ions, as might arise if coordination occurred but which would not be expected if the soaps were fully ionic. Since the properties of the carboxyl group are constant for the different alkali metal soaps, the strength of the coordination bonds should increase with increasing charge of the metal ion and decrease with increasing size of the metal ion. This trend was, in fact, observed by Honig and Singleterry [179] who found that lithium phenylstearate of 0.9% concentration in benzene forms a highly viscous solution whereas the caesium soap even at 2.65% concentration gives a solution only slightly more viscous than pure benzene.

A different, but related, coordinated structure has been proposed for the alkaline earth phenylstearate micelles in anhydrous benzene solutions [180]. This structure

assigns a coordination number of 4 to each alkaline earth cation and makes each a member of two eight-membered rings which might be expected to enhance the stability of the system as with chelation.

The rheological behaviour of the alkali metal and alkaline earth phenylstearates in benzene is profoundly affected by the addition of small amounts of certain polar additives [179]. These additives are thought to cause a breakdown of the coordinately-linked micellar structure to smaller aggregates by competing with the soap carboxyl oxygens for coordination with the metal ion. The effectiveness of the additive in producing this breakdown and resultant decrease in viscosity of the system was found to decrease in the order; phenylstearic acid, water, phenol and ethanol. The relative efficiency of these additives is probably a reflection of the partition of the additives between the solution and the micelles. The unusual resistance of the strongly coordinated lithium carboxylate chain to breakdown was demonstrated by the fact that ten times as much water or phenylstearic acid was required to decrease the viscosity of the lithium soap than was required for the sodium or potassium soaps. A combination of viscometric and fluorescence depolarization data indicated that the small micelles formed in the presence of suitable amounts of water are prolate spheroids (rods) having axial ratios of 4 to 1 or less and containing from twenty to forty phenylstearate radicals [179,180]. Since these results

support cylindrical micelles, it is also possible that similar, but much longer, cylindrical structures may exist in the viscous anhydrous solutions.

In the alkali metal phenylstearate-benzene solutions, further addition of bifunctional groups, such as water or glycol, caused a secondary aggregation to a highly elastic, viscous system [178-180]. This secondary aggregation is believed to result from micellar interactions, occurring by bridging between the polar cores of the micelles through hydrogen bonding by one or more water or glycol molecules, to form a cross-linked or three-dimensional, elastic but shear-sensitive structure. Similar secondary aggregation effects have been observed on addition of water to 1% solutions of aluminium disoaps in benzene [213]. The alkaline earth phenylstearates, however, did not exhibit this phenomenon. When sufficient water had been added, however, all of the phenylstearates studied (with the exception of lithium) separated from benzene solutions [179,180]. Addition of approximately 2 moles of water per equivalent of soap to the magnesium or calcium phenylstearate-benzene solutions, or 4 to 5 moles of water per mole of soap to the alkali metal soap solutions (except lithium) caused precipitation. Under controlled conditions, highly birefringent soap-rich phases were observed to separate at the onset of precipitation.

## 1.3 Lyotropic Mesophase Formation in Anionic Amphiphile-Water Systems

### 1.3.1 Long-Chain Alkali Metal Soaps

The fatty acid soaps were amongst the earliest surfactants subjected to systematic investigation, particularly by McBain and co-workers who reported the binary phase diagrams for many long-chain sodium and potassium *soap-water* systems [38-45]. The same basic diagrams, with minor variations due to differences in soap chain length and anhydrous thermotropic behaviour, are characteristic of all these systems [55].

#### 1.3.1.1 Sodium Laurate

FIG. 9 shows the composite phase diagram for the sodium laurate-water system, as first defined by McBain and Lee [44] and later modified by the x-ray studies of Luzzati and co-workers [214,215] and the more recent detailed calorimetry work of Madelmont and Perron [55, 216-219]. The vertical axis at zero percent water shows the thermotropic phase transitions exhibited by the anhydrous soap on heating (see Section 1.1.2); the horizontal axis shows the changes and development of new phases as a function of water content.

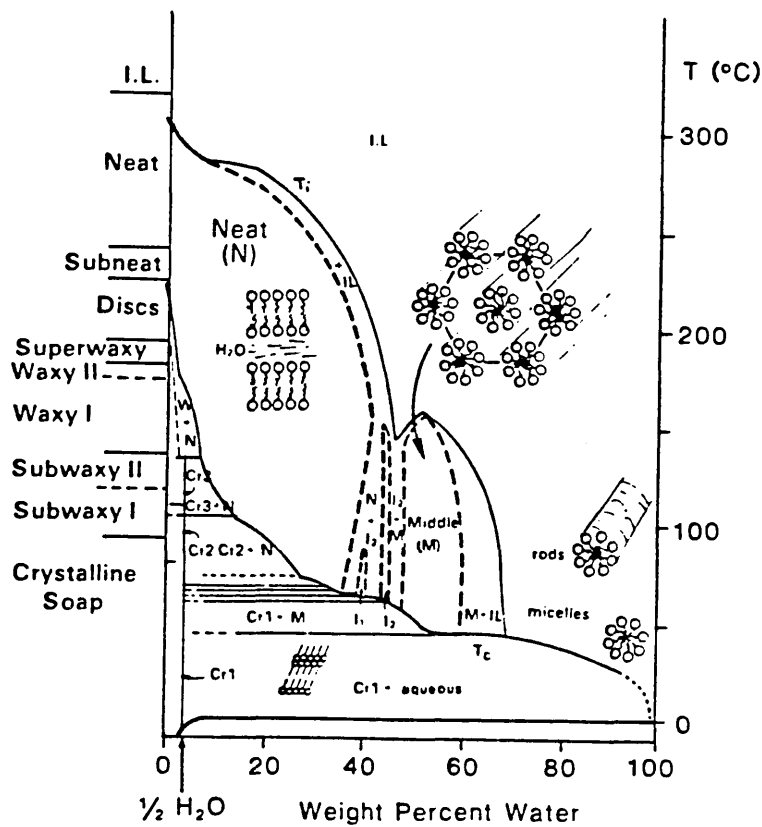


FIG. 9 : Composite phase diagram for the sodium laurate-water system [3]

Each of the crystalline (Cr1, Cr2 and Cr3) and semi-crystalline (subwaxy, waxy, superwaxy etc.) phases of the anhydrous soap, up to the subneat phase, can incorporate only a very small amount of water, less than one-half a molecule of water per molecule of soap. There is evidence in the long-chain sodium soaps of a hemihydrate crystalline form that can apparently have three polymorphic forms, although the precise structure of these has not been determined [55].

The neat, or lamellar, phase that occurs at higher temperatures can incorporate up to 40% by weight of water in its bilayer structure. The presence of water has the marked effect of decreasing the temperature at which this phase can form, from 241°C in the anhydrous state to about 70°C with a water content of approximately 35 wt %.

The line that defines the temperature-composition boundary for lamellar phase formation forms part of the  $T_c$  line.

The  $T_c$  line may, with certain qualifications, be regarded as representing the curve which shows the depression of the melting point of the soap by water. For compositions at temperatures higher than those indicated by this line, the solid crystal lattice has been entirely broken down resulting in liquid or liquid crystalline systems. Below the  $T_c$  line the soap retains, at least in part, its crystalline order.

At higher water concentrations, a second single-phase region labelled "middle" soap is formed. This liquid crystal phase is characterized by a hexagonal I type structure in which the soap molecules pack in parallel rod micelles of indefinite length which are arranged in a two-dimensional hexagonal array. The core of these rods is made up of the disordered soap hydrocarbon chains, whilst the exterior surface contains the polar groups which interact with the water.

Compositions between the neat and middle mesophases were originally thought by McBain [44] to consist of a two-phase region (neat + middle). Luzzati and co-workers [214,215], however, suggested the existence of two "intermediate" hexagonal type structures in this region for the C<sub>14</sub>, C<sub>16</sub> and C<sub>18</sub> sodium soaps. The presence of two intermediate phases (denoted "I<sub>1</sub>" and "I<sub>2</sub>") was also suggested by Madelmont and Perron for the sodium laurate and sodium myristate-water systems [55, 216-221]. Recent NMR investigations (<sup>2</sup>H and <sup>23</sup>Na), supported by polarized microscopy [222], are in agreement with the findings of Madelmont and Perron. These results have indicated that the "I<sub>2</sub>" phase has a deformed hexagonal structure (denoted H<sub>1d</sub>) containing rod micelles on a slightly distorted hexagonal lattice [214,215,274]. The second intermediate phase "I<sub>1</sub>" was thought to be an additional lamellar structure made up of very thin bilayers [222]. It was suggested that within the "I<sub>1</sub>" phase, there was a hydrogen-bonded water network linking the bilayers. Both intermediate phases exist over rather narrow ranges of composition, showing that their formation depends upon a critical balance of interactions. Polarized microscopy has also been used to investigate the occurrence of these intermediate phases in other even-numbered C<sub>8</sub> to C<sub>18</sub> sodium and potassium n-alkanoate-water systems [222].

As the temperature of the system is increased, a point is reached corresponding to each soap-water composition where

the increased thermal agitation brings about a breakdown of the extended long-range order existing in the liquid crystalline phases and an isotropic micellar solution is produced. The  $T_i$  line on the phase diagram thus indicates the variation in the temperature of breakdown of long-range liquid crystalline order with change in composition.

On increasing the water content further to approximately 70% by weight, a clear, mobile, isotropic solution is formed that is made up of rod-shaped micelles at the higher soap concentrations, or of almost spherical micelles at very low soap concentrations which are in equilibrium with soap monomers at the c.m.c.

The region below the  $T_c$  line contains a number of two-phase zones in which one of the crystalline hemihydrate phases (Cr1, Cr2 and Cr3) is in equilibrium with a second phase (neat, middle or micellar).

#### 1.3.1.2 Potassium, Rubidium and Caesium Soaps

The phase behaviour of the long-chain potassium, rubidium and caesium soaps with water is similar to that displayed by the corresponding sodium soaps [45,116,214,215,222-224]. Differences are observed, however, due to; the different thermotropic behaviours of the anhydrous soaps [2], a lowering of the  $T_c$  lines with increasing atomic number of the cation, and the formation of thermodynamically stable "gel" phases at temperatures below the  $T_c$  lines. The "gel" phase consists of single layers of parallel, interdigitated soap molecules in which the hydrocarbon chains are stiff

and fully extended whilst the polar and aqueous regions are thought to be fluid [225-229].

### 1.3.1.3 Lithium Soaps

The long-chain lithium soaps, like those of the divalent metals, are quite insoluble in water, their  $T_c$ 's and Krafft points being above  $100^\circ\text{C}$ . [316] Consequently few systematic phase studies of these soaps have been reported. FIG. 10, however, shows the binary phase diagram for the system lithium palmitate-water as determined by Vold in 1943 based solely on visual observations [46]. The general features of this diagram

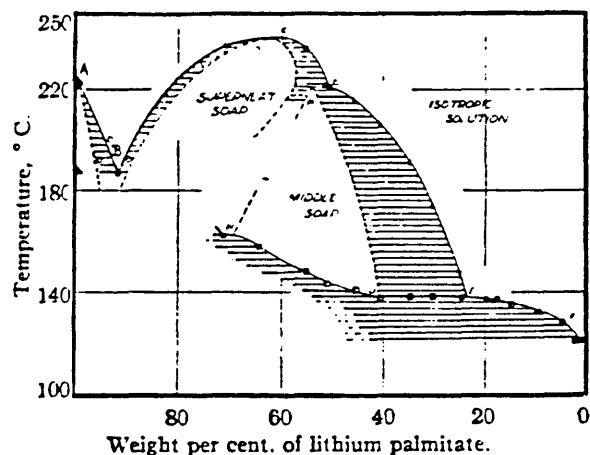


FIG. 10 : The phase diagram for the lithium palmitate-water system [46]

are similar to those for the sodium palmitate-water system as determined by McBain et al [38]; the most noticeable differences being the much higher temperatures of the  $T_c$  line and the greater temperature and composition stability of the liquid crystalline middle soap phase.

### 1.3.2 Other Anionic Amphiphiles

#### 1.3.2.1 Aerosol OT (Sodium di-2-ethylhexylsulphosuccinate)

A number of branched-chain soaps and surfactants have been reported which exist as mesophases in the anhydrous state at room temperature (see Section 1.1.3). On addition of water, these amphiphiles give rise to isotropic liquid or hydrated liquid crystal phases at room temperature according to surfactant concentration [ref 2, p 252].

The binary phase diagram for the branched-chain surfactant Aerosol OT (sodium di-2-ethylhexylsulphosuccinate) with water is shown in FIG. 11.

Aerosol OT in the anhydrous state exists as a reversed middle type mesophase,  $M_2$  (reversed hexagonal structure), [134]. Water can be solubilized (up to 16% by weight) without any modification of the phase, but with an increase in the dimensions of the rod-like aggregates [231]. On further addition of water, this phase is initially converted to a reversed viscous isotropic phase,  $V_2$  (reversed cubic structure) which on dilution gives rise to a neat or lamellar phase, G (bilayer structure) with a considerable temperature-composition range of stability. As the concentration of water is increased past approximately 90% by weight, a narrow two-phase region consisting of the neat phase + isotropic micellar solution is formed before the system finally passes into the isotropic micellar phase at approximately 1.3 wt % Aerosol OT [248].

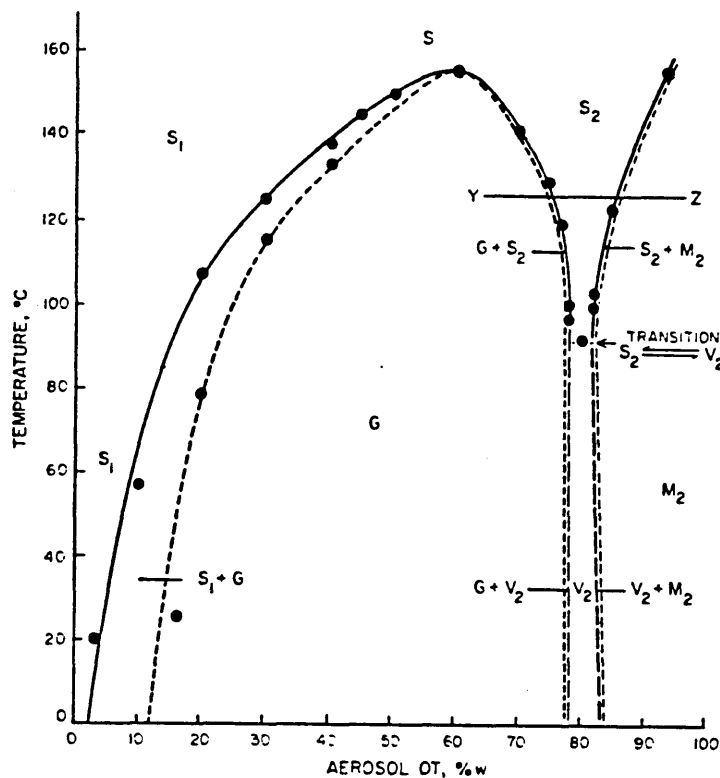


FIG. 11 : Phase diagram for the Aerosol OT-water system [231]. The boundaries indicated by broken lines are tentative.

S ( $S_1$ ,  $S_2$ ) - mobile isotropic phase; G - neat phase;  $M_2$  - reversed middle phase;  $V_2$  - reversed viscous isotropic phase.

However, in contrast to the mesomorphic phase sequence exhibited by Aerosol OT, Balmbra and Clunie [134] have reported that the crystalline sodium di-n-alkyl sulphosuccinates (where the alkyl chain has 4,6 or 8 carbon atoms) form only neat phases on addition of water.

The aqueous phase behaviour of the divalent calcium and magnesium di-2-ethylhexylsulphosuccinates have been

investigated recently by Khan et al [232] and the results compared to the corresponding sodium system (Aerosol OT). In all three systems, the sequence of homogeneous phases with increasing surfactant concentration was; isotropic solution, lamellar, cubic and reversed hexagonal liquid crystalline phases. The  $\text{Ca}^{2+}$  and  $\text{Mg}^{2+}$  systems gave very similar phase diagrams which differed considerably in two respects from the sodium system phase diagram. Firstly, the aqueous solubility was found to be lower by orders of magnitude with the divalent counterions. Secondly, the lamellar phase was observed to swell and incorporate water to a much greater extent with  $\text{Na}^+$  than with  $\text{Ca}^{2+}$  and  $\text{Mg}^{2+}$  resulting in the formation of much larger two-phase regions (lamellar + isotropic solution) for the divalent counterion systems. These results were explained qualitatively by suggesting that the valency of the counterions drastically influenced the long-range electrostatic interactions [233] leading to different aggregate stability conditions.

#### 1.3.2.2 Sodium 4-(1'-heptylnonyl)benzenesulphonate

In recent studies, Miller and co-workers [234-239] have shown that the aqueous phase behaviour of the double-chain surfactant, sodium 4-(1'-heptylnonyl)benzenesulphonate (SHBS), differs considerably from that of the branched double-chain surfactant, sodium di-2-ethylhexylsulphosuccinate (Aerosol OT).

Their results have shown that SHBS is only slightly soluble in water; the solubility limit being 0.06 wt % SHBS at 25°C. Below this concentration, the isotropic SHBS solution formed is not micellar, although conductance measurements [240] and sodium-23 NMR chemical shift and line-width data [239] indicated weak concentration dependent aggregation. There is convincing evidence, from both surface tension [241,242] and conductance data [243], that Aerosol OT forms micelles at surfactant concentrations greater than  $2.5 \times 10^{-3}$  M in water ( $\sim 1.1$  wt %) at 20°C. At still higher Aerosol OT concentrations, liquid-crystalline phases appear (see Section 1.3.2.1). Many other double-chain sulphosuccinates also micellize [241,242]. The behaviour of another homologous series, the dialkanoyl phosphatidylcholines (lecithins), depends upon the lipophilic group chain length; short-chain homologues micellize whilst in higher homologues a lamellar phase boundary is reached before micellization occurs [244-247].

For the SHBS-water system, no evidence of a Krafft boundary was observed, the solubility limit only increasing from 0.06 wt % SHBS at 25°C at 0.7 wt % SHBS at 90°C [234]. At concentrations between the solubility limit and approximately 75 wt % SHBS, the phase behaviour from 20°C to 90°C was dominated by a broad biphasic region consisting of a hydrated lamellar phase in equilibrium with the dilute isotropic SHBS solution [234,237,238]. This biphasic region is extremely broad compared to the corresponding

two-phase region in the Aerosol OT-water system [248]. Above approximately 75 wt % SHBS, a single hydrated lamellar mesophase is formed; the reversed cubic and hexagonal mesophases found in the Aerosol OT system appear to be absent. The precise position of the phase boundary between the lamellar mesophase and the anhydrous solid SHBS was not determined.

Although very little information is available on the straight-chain analogues of Aerosol OT, a number of these compounds (where the alkyl chain has 4, 6 or 8 carbon atoms), like SHBS, have been reported to form only lamellar mesophases upon hydration [134].

#### 1.3.2.3 Lithium 4-trans-n-pentyl cyclohexanoate

Unlike the long-chain lithium n-carboxylates, which have Krafft points above 100°C, the lithium salt of 4-trans-n-pentyl cyclohexanoic acid (Li 5CH) has been observed using polarized microscopy to produce a succession of mesophases on contact with water at room temperature [249]. These phases have been identified as a lyotropic nematic phase, a hexagonal phase and a possible rectangular phase, with decreasing water content. Similar mesophases (plus additional lamellar phases) were observed for other alkali metal salts of this acid [249].

For the Li 5CH-water system, the lyotropic nematic mesophase was observed at room temperature for a sample containing 32.15 wt % Li 5CH, and was identified by its low viscosity and characteristic microscopic schlieren

texture. The occurrence of such a phase in a binary amphiphile-water system is rare [250-253, 310]. Most phases of this type reported to date contain three or four components, often including long-chain alcohols and electrolytes [254, 310].

The structure and properties of lyotropic nematic mesophases will be discussed in Section 4.2.

#### 1.4 Proposed Programme of Work

The principal aim of these investigations is to study the phase behaviour of surfactants in non-polar hydrocarbon media with the objective of determining mesophase structures and the factors governing their occurrence.

The first system to be studied will be that of a typical crystalline straight-chain soap, lithium stearate (n-octadecanoate) with the hydrocarbon solvent cetane (n-hexadecane). This system has been chosen in an attempt to resolve the inconsistent character of two previously published phase diagrams [51, 195], see Section 1.2.2.2.

Since the nature of the hydrocarbon solvent has been shown to affect mesophase formation [61, 196], the effects of a branched-chain solvent such as squalane (2,6,10,15,19,23-hexamethyltetracosane) with lithium stearate will also be investigated.

The presence of small amounts of water has been shown to significantly influence the phase behaviour of soap-

hydrocarbon systems, see Section 1.2.2.3. Great care will therefore be taken to prepare and maintain the soap in a pure anhydrous state. One advantage of studying the crystalline long-chain lithium soaps is that, unlike their sodium and calcium analogues [68,69,127-129], they do not form hydrates and are only slightly hygroscopic [48,51,66].

A further important consideration is the thermotropic behaviour of the solvent-free soap. It has been suggested that this may influence the soap solubility and mesophase formation in hydrocarbon solvents [51,59], see Sections 1.2.2.1 and 1.2.2.2. In the case of lithium stearate [54] (and other long-chain lithium soaps, see Section 1.1.2.2) discrepancies exist in the literature as to the temperatures, and in some cases, the number and nature of the phase transitions involved on heating from the crystalline solid to the amorphous liquid. The thermotropic phase behaviour of lithium stearate will therefore be carefully re-investigated and the results compared to those already available in the literature [54].

As a direct comparison with lithium stearate, the lyotropic and thermotropic phase behaviour of a branched-chain stearate, lithium phenylstearate will be investigated. Benzene and toluene have been chosen for preliminary solution studies in order to extend the work of Honig and Singleterry [178-180], see Section 1.2.3.3. Because of the high volatilities of these solvents, problems may be encountered when studying these systems at elevated temperatures. 1-Phenylheptane (boiling point, 233°C) will

therefore be used for more detailed phase studies. The effects of other non-polar hydrocarbon solvents will also be considered briefly.

The long straight-chain lithium soaps, such as lithium stearate, have been reported to be quite insoluble in water, their T.c.'s and Krafft points being above 100°C, see Section 1.3.1.3. No data is available in the literature, however, for the aqueous phase behaviour of lithium phenylstearate. This will therefore be investigated.

Finally, to help explain possible differences in the lyotropic and thermotropic behaviours of the lithium stearate and phenylstearate soaps (due to differences in the chemical structure of the lipophilic chains) a brief study of the unsaturated soap, lithium oleate (cis-9-octadecenoate) may be carried out.

Preliminary studies will make use of visual and microscopic observations in polarized light and differential scanning calorimetry to identify thermotropic and lyotropic mesophase formation and to establish the soap-solvent phase diagrams. Further development of the work will include the use of variable temperature small-angle x-ray diffraction and pulsed NMR methods to provide structural information on the soap mesophases encountered.

## CHAPTER TWO : EXPERIMENTAL

### 2.1 Materials and Methods of Preparation

#### 2.1.1 Lithium Stearate

Lithium stearate was prepared from methods outlined by Cox and McGlynn [51] and Vold et al [66].

Specially pure stearic acid, supplied by BDH Chemicals Ltd (minimum assay, GLC, 99%, m.p. 68-71°C), was further purified by two recrystallizations from 2-butanone to yield the acid with a melting point of 69.2-69.3°C (as determined by differential scanning calorimetry). A warm solution of the acid in absolute ethanol was neutralized to a phenolphthalein end point by addition of a carbonate-free, 50% aqueous ethanol solution of lithium hydroxide monohydrate (BDH Chemicals Ltd, minimum assay 99.5%). The precipitated soap was stirred for approximately 20 minutes, filtered, washed with cold ethanol and acetone and air-dried. Samples of the soap were then recrystallized twice from either absolute ethanol to yield white crystals of lath-like habit or from a 50% by volume ethanol/water mixture to yield lustrous white hexagonal platelike crystals. Drying was accomplished by heating the soap to 110°C in vacuo over phosphorus pentoxide for approximately 48 hours. This procedure was repeated periodically to maintain the lithium stearate in an anhydrous condition. When not in use, the dried soap was stored in vacuo over phosphorus pentoxide.

### 2.1.2 Lithium Oleate

Lithium oleate was prepared by the method employed by Curat and Perron for the preparation of the sodium analogue [52].

Pure oleic acid, supplied by the Sigma London Chemical Co Ltd (approximately 99% purity and used without further treatment), was neutralized to a phenolphthalein end point in warm absolute ethanol using a solution of lithium ethoxide (prepared by dissolving lithium metal in absolute ethanol under nitrogen). The crystallized soap, obtained by cooling the solution to approximately 5°C overnight, was re-dissolved in warm absolute ethanol and filtered to remove traces of lithium carbonate. After a further low temperature crystallization from absolute ethanol the pure soap, obtained as a fine white powder, was washed with anhydrous acetone. Drying was accomplished by the method outlined for lithium stearate.

### 2.1.3 Phenylstearic Acid

Phenylstearic acid was prepared by the Friedel-Crafts reaction of oleic acid (cis-9-octadecenoic acid) with an excess of benzene using aluminium chloride as the catalyst under anhydrous conditions [200,255].

Commercial oleic acid, supplied by BDH Biochemicals, 92% minimum assay (200g, 0.71 mol based on 100% oleic acid), was dissolved in sodium dried benzene (401g, 5.13 mol). To this was carefully added finely powdered anhydrous aluminium chloride (105g, 0.79 mol), producing a vigorous reaction with the evolution of hydrogen chloride.

When this reaction had moderated, the mixture was slowly heated to 80°C and refluxed with stirring until hydrogen chloride was no longer evolved (approximately 7 hours). The resulting mixture was then added to 20% w/w HCl (600 mls) and the excess benzene removed by steam distillation. The dark-brown viscous oil recovered was added to diethyl ether (300 mls) and the combined organic phases washed twice with dilute HCl (2M, 300 mls). Subsequent removal of the ether from the organic layer gave the crude acid product (typical yield, 244g). This was purified by three distillations under reduced pressure to give three major fractions :

- (i) A creamy-yellow low-melting solid fraction was obtained as a forerunner of the phenylstearic acid, between approximately 110° and 210°C at 0.15 mm Hg (typical yield, 33g). This was thought to consist of saturated fatty acids which had been present as impurities in the oleic acid [200] and the possible products of side reactions [255].
- (ii) The phenylstearic acid fraction.
- (iii) A viscous red-brown still residue.

The purest phenylstearic acid fraction, obtained as a very pale yellow oil at room temperature, was collected between 212° and 217°C at 0.05 to 0.10 mm Hg (typical yield 66g, 28.1%; based on a minimum pure oleic acid content of 92%).

Micro-analysis (performed by Elemental Micro-analysis Ltd, Beauworthy, Devon, UK) gave the following results for the purest acid fraction:

Calculated for  $C_{24}H_{40}O_2$ ; C, 79.94% H, 11.18%

Found for  $C_{24}H_{40}O_2$ ; C, 80.02% H, 11.19%

The purity of acid fractions obtained from subsequent preparations was checked by comparing the refractive index, M.P., I.R. and N.M.R. ( $^1H$  and  $^{13}C$ ) with those of the purest acid fraction above (see Section 2.1.3.1). Absolute purity and types of impurity play very important roles in governing the type, transition temperature and range of mesophase formation. A further check on purity was therefore made by comparing the temperatures and enthalpies of the phase transitions observed on heating the anhydrous lithium salts of the different acid fractions from room temperature to the isotropic melt, with those obtained for the lithium salt of the purest acid fraction (see Section 3.3.1.1).

#### 2.1.3.1 Phenylstearic Acid Characterization

##### (i) Gas Liquid Chromatography.

Analysis of the purest acid fraction in our laboratories [206] by GLC of the alkyl aryl ketones obtained by chromic acid oxidation of the acid, has shown it to be a complex mixture of 12 positional isomers with substitution at the C6 to C17 positions on the fatty acid chain.

These results compare favourably with those obtained by Smith et al [203-205] using the same methods (see TABLE 1, p 32).

(ii) Refractive Index (Abbé),  $n_D^{20} = 1.4900$

Nicolet and de Milt [200] reported a value of  $n_D^{20} = 1.4905$  for their purest phenylstearic acid fraction collected at 250°C/4 mm Hg.

(iii) Melting Point

The DSC thermogram, obtained at a heating rate of 5°C min<sup>-1</sup>, showed a complex low-temperature melting process for the isomeric phenylstearic acid mixture (see FIG. 12). A number of endotherms were observed below room temperature, the most pronounced being observed at -57.3°C. The total enthalpy for the unresolved melting transitions, integrated over the temperature range -75°C to 25°C, was approximately 27 J g<sup>-1</sup>, 9.7 KJ mol<sup>-1</sup>. By comparison, pure crystalline stearic acid melts at 68.8°C with an enthalpy of fusion of 198.7 J g<sup>-1</sup>, 56.6 KJ mol<sup>-1</sup> [288].

(iv) The Infrared Spectrum of the acid was obtained as a thin-film between sodium chloride plates using a Pye-Unicam SP3-100 spectrophotometer (see FIG.13). The following major absorption bands have been assigned [212]:

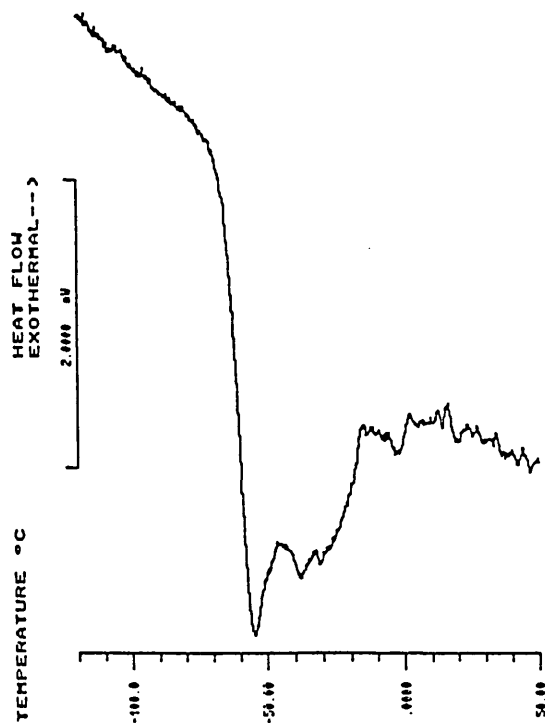


FIG. 12 : DSC thermogram showing the complex, low temperature melting of phenylstearic acid (mixture of 12 positional isomers)

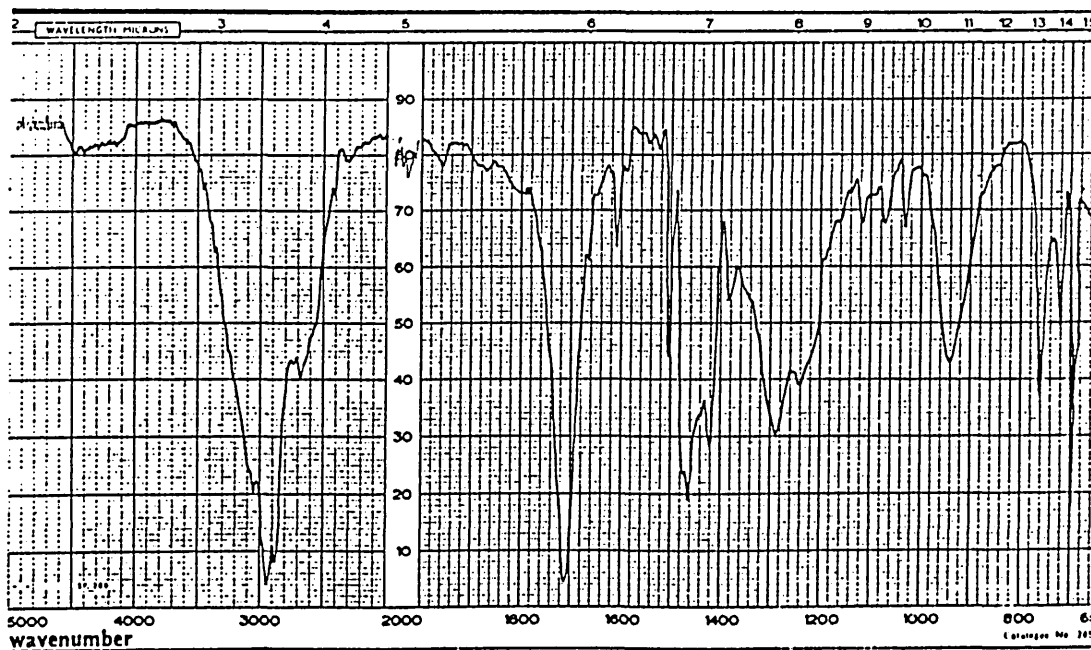


FIG. 13 : Infrared spectrum of phenylstearic acid obtained as a liquid film

<u>Wavenumber, cm<sup>-1</sup></u>	<u>Intensity</u>	<u>Assignment</u>
3300 to 2500	s	OH stretch
3040	w	Aromatic CH str.
2930	s	Aliphatic CH str.
2875	s	Aliphatic CH str.
1710	s	C=O str.
1600	m	Aromatic C=C str.
1490	m	Aromatic C=C str.
1280	s	C-O str.
1235	s	C-O str.
935	s	OH bend
760	s	Aromatic CH b.
720	s	Aliphatic CH <sub>2</sub> rocking
700	s	Aromatic CH b.

The letters s, m and w denoting peak intensities correspond to strong, medium and weak respectively.

(v) The Nuclear Magnetic Resonance spectra (<sup>1</sup>H and <sup>13</sup>C broad-band proton decoupled) of the acid were obtained in CDCl<sub>3</sub> with tetramethylsilane (TMS) as the internal reference using a Bruker WP 80 SY spectrometer (see FIGS. 14 and 15 respectively). The letters m and s in parenthesis correspond to observed multiplets and singlets respectively. In recording the <sup>13</sup>C NMR spectrum (0-200 ppm) a "J-modulation" mode was employed. In this mode CH and CH<sub>3</sub> carbon atoms exhibit peaks with negative intensities whilst C and CH<sub>2</sub> carbons exhibit peaks with positive intensities.

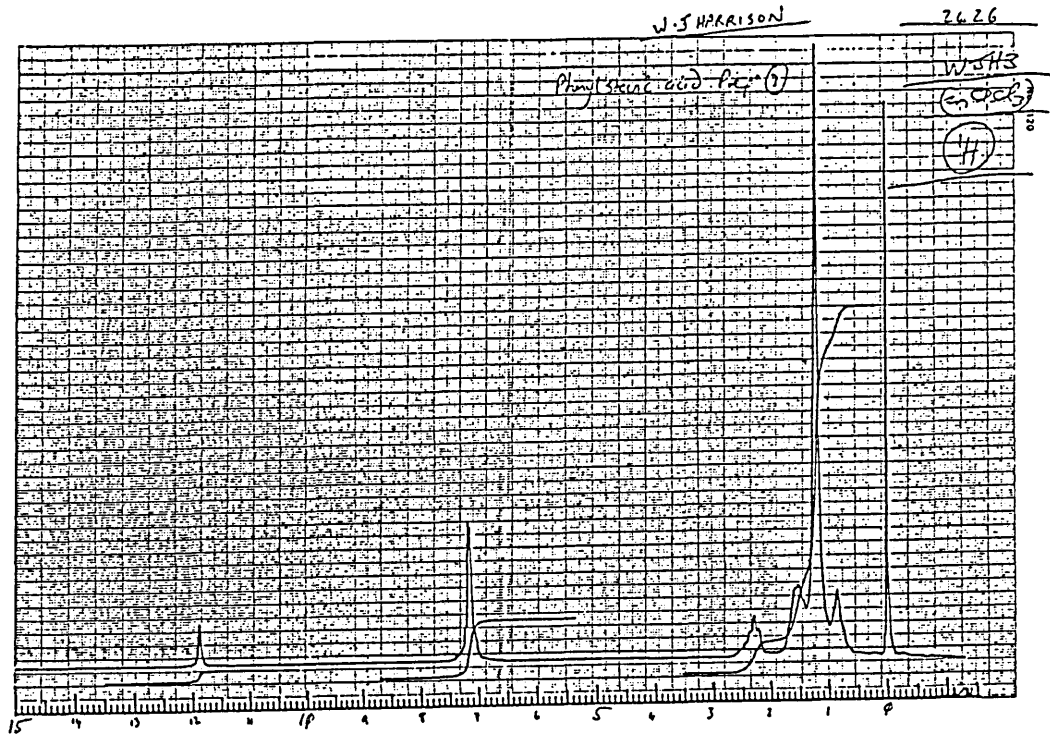


FIG. 14 :  $^1\text{H}$  NMR spectrum of phenylstearic acid

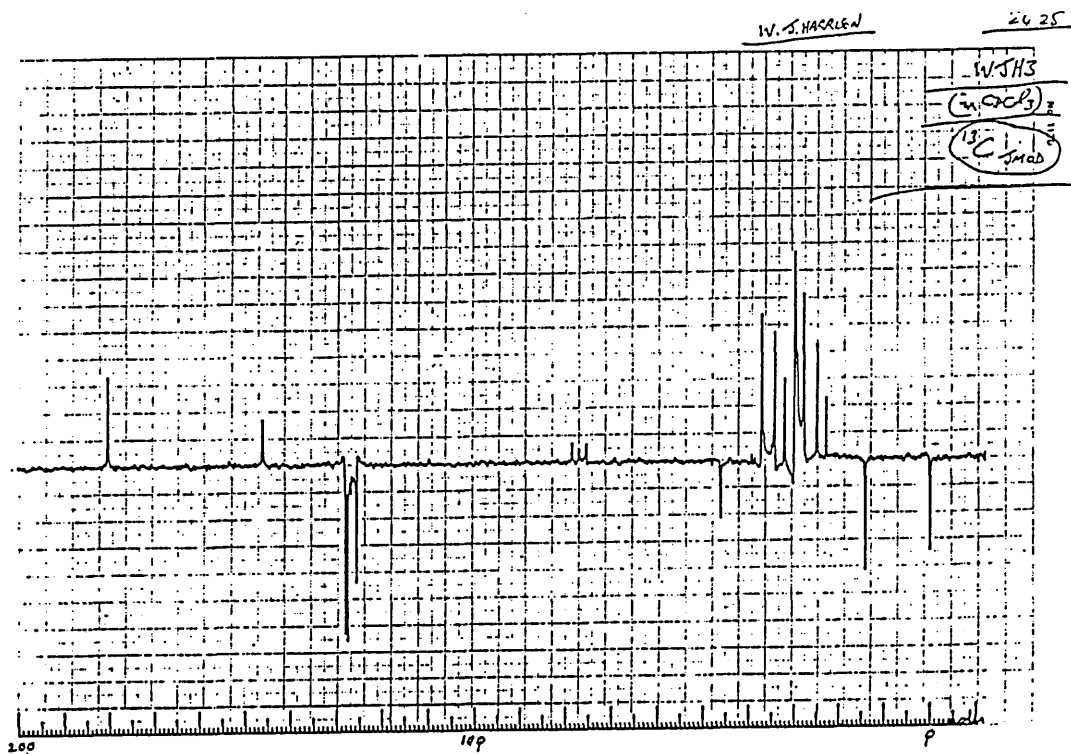


FIG. 15 :  $^{13}\text{C}$  NMR spectrum (proton-decoupled) of phenylstearic acid

<u>Chemical shift, <math>\delta</math></u>	<u><math>^1\text{H}</math> NMR</u> <u>Assignment</u>
0.8	(m, 3H, terminal $\text{CH}_3$ )
1.2 - 1.6	(m's, 28H, $\text{CH}_2$ 's)
2.3	(m, 3H, $\text{CH}_2\text{CO}_2\text{H}$ and Ph- $\text{CH}$ )
7.1	(m, 5H, phenyl protons)
11.9	(s, 1H, $\text{CO}_2\text{H}$ )

<u>Chemical shift, <math>\delta</math></u>	<u><math>^{13}\text{C}</math> NMR</u> <u>Assignment</u>
13 (-ve)	(s, terminal, $\text{CH}_3$ )
$\sim$ 20-40 (+ve)	(m's, $\text{CH}_2$ 's)
45 (-ve)	(m, Ph- $\text{CH}$ )
125-128 (-ve)	(m, phenyl $\text{CH}$ 's)
145 (+ve)	(m, phenyl $\text{C-CH}$ )
180 (+ve)	(s, $\text{COOH}$ )

#### 2.1.4 Lithium Phenylstearate

Lithium phenylstearate was prepared by neutralizing an ethanolic solution of the parent acid (see Section 2.1.3 for the method of acid synthesis) to a phenolphthalein end point by addition of a carbonate-free, 50% aqueous ethanol solution of lithium hydroxide monohydrate. After removal of the solvents and drying under vacuum over phosphorus pentoxide at 110 °C for 48 hours, the salt was isolated as a whitish, slightly hygroscopic waxy solid. The drying procedure was repeated periodically to maintain the soap in an anhydrous state.

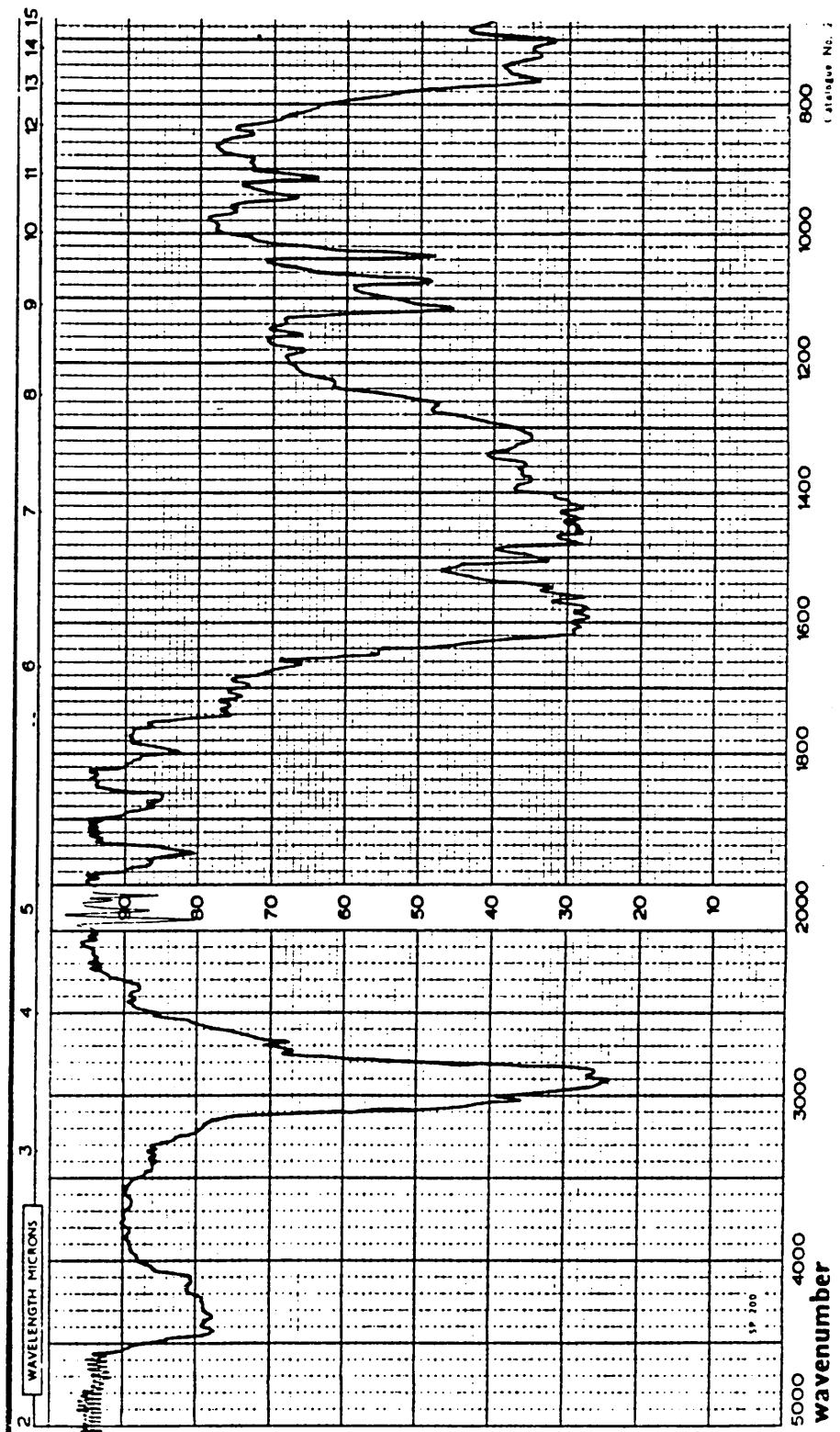


FIG. 16 : Infrared spectrum of lithium phenylstearate obtained as a thin film

When not in use the lithium phenylstearate was stored in vacuo over phosphorus pentoxide.

The infrared spectrum of the dried soap as a thin film between sodium chloride plates (film thickness unknown) showed that it contained no traces of water, ethanol or free acid impurities since the characteristic strong absorption bands at  $3300$  to  $2500\text{ cm}^{-1}$  (OH str.),  $935\text{ cm}^{-1}$  (OH b.) and  $1710\text{ cm}^{-1}$  (C=O str.) were all absent (see FIG. 16).

A sample of sodium phenylstearate was also prepared by the procedure outlined above.

It is worthy to note that Kagarise [212] concluded from I.R. studies, that no detectable amounts of absorbed water were present in a solid lithium phenylstearate film after exposure to normal atmospheres over a period of 9 days. The absorption of water was found to increase in the order  $\text{Li} < \text{Na} < \text{K}$ .

#### 2.1.5 Soap-Solvent Samples

The lithium soaps were prepared and dried as described in the previous sections.

Hydrocarbon solvents were obtained from the Aldrich Chemical Co. Ltd., Gillingham, UK. These included,

n-hexadecane (99%), squalane (99%), 1-phenylheptane (96%), benzene (99 + %, spectrophotometric grade) and toluene (99 + %, spectrophotometric grade). They were dried and stored over freshly activated type 4A crystalline sodium aluminosilicate molecular sieve beads [256]. The solvents were frequently examined for water contamination by checking for the presence of the characteristic strong absorption band in the infrared spectrum near  $3500\text{ cm}^{-1}$  (OH stretch).

The normal water used for phase studies was deionised and doubly distilled, with a typical conductivity of around  $4\ \mu\text{S cm}^{-1}$ , whilst deuterium oxide (99.8 atom %  $^2\text{H}$ ) was obtained from Fluorochem Ltd, Glossop, UK, and used as received.

To examine the phase equilibria in the two component soap-solvent systems, samples of varying composition were prepared on a weight to weight percentage basis (to within one percent) using the following method. Pyrex glass tubes (8 mm i.d. and 1 mm wall thickness) which had been flame-sealed at one end were used as sample containers. Alternatively, straight-walled Pyrex tubes containing a narrow constriction in the centre (ca. 0.5-1 mm diameter), through which the sample components could be centrifuged for mixing purposes, were used. These were supplied by the Sheffield University Glass Blowing Department. Before sample preparation, the tubes were cleaned with concentrated sulphuric acid followed by several rinses with distilled water and acetone. They were then dried in a vacuum oven

and stored in a desiccator over phosphorus pentoxide until use.

The rigorously dried anhydrous soap was introduced directly into the bottom of the sample tube via a second, slightly narrower, glass tube. This technique avoided contamination of the sample tube walls and thus prevented any sample decomposition when the tube was flame-sealed. The solvent was deposited directly onto the soap, once again avoiding contamination of the tube walls, using a Pasteur pipette. Both the soap and solvent were weighed with a precision of  $\pm 0.2$  mg using a Sartorius 1615 MP6 electronic analytical balance. Typical sample sizes of 0.3-1.0 g (depending on sample composition) were used. Between each step of the sample preparation, the tubes were tightly stoppered to minimize contamination from atmospheric moisture. Finally, the sample tubes were flushed with pure dry nitrogen and immediately flame-sealed. On cooling, the sample tubes plus contents were accurately weighed.

To obtain homogeneous soap-solvent mixtures, the methods of sample mixing varied according to the system under study.

For the binary systems of lithium stearate with both cetane (n-hexadecane) and squalane (2,6,10,15,19,23-hexamethyltetracosane), intimate mixing of the samples was achieved using methods previously employed for similar systems by Cox [51,196], Uzu [61] and Vold [195,197].

Here, the samples were rapidly heated in an oil bath to 240°C; a temperature beyond their melting points to the isotropic liquid state (see Section 2.2.2). Once melted, the samples were thoroughly mixed by agitation and immediately quench cooled by immersing them in a second oil bath maintained at the ambient temperature. This cooling process prevented a separation of the sample into layers and thus produced macroscopically homogeneous mixtures. If during the mixing cycle a loss of solvent occurred or any noticeable oxidation of the soap, as characterized by an orange-brown discolouration, fresh samples were prepared. (The onset of oxidative decomposition of the pure soap was found to occur at approximately 205°C using differential scanning calorimetry and was characterized by a broad exotherm on the heating thermogram, see FIG. 17) After mixing, the samples were stored at room temperature for a period of several days or weeks to allow equilibration before their phase behaviour was investigated.

For the binary systems of lithium phenylstearate with benzene, toluene, 1-phenylheptane and water (or D<sub>2</sub>O), homogeneous samples could be prepared simply by allowing the contacted components to stand at room temperature for sufficiently long periods of time (weeks, or months depending on sample composition). The time for these samples to reach equilibrium was significantly reduced, however, by a combination of mixing (using a spatula or by repeated centrifugation), vigorous agitation and prolonged warming. In some cases, samples were maintained at an

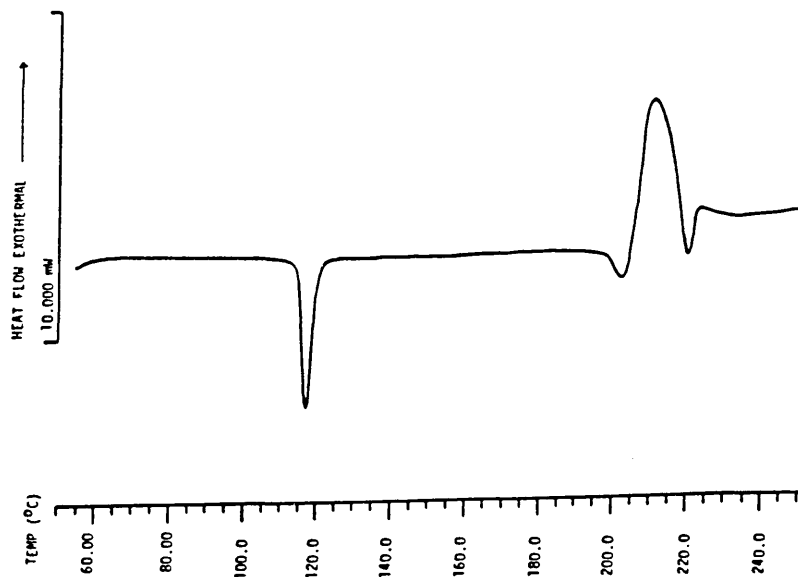


FIG. 17 : Oxidative decomposition of lithium stearate characterized by a broad exotherm at  $\sim 210$  °C (heating rate :  $10$  °C  $\text{min}^{-1}$ )

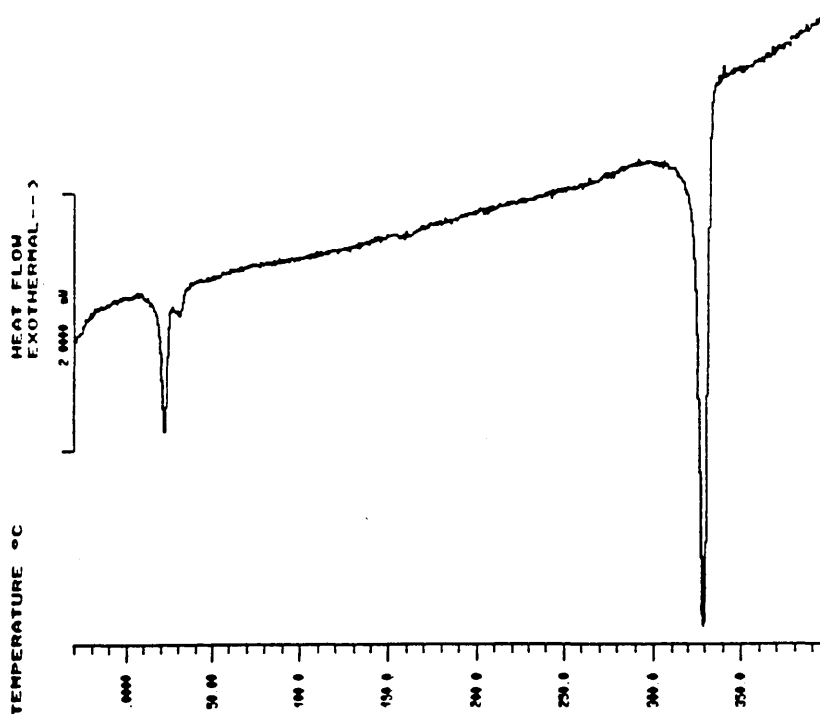


FIG. 18 : DSC thermogram obtained on heating a high pressure DSC crucible PTFE sealing gasket (heating rate :  $10$  °C  $\text{min}^{-1}$ )

elevated temperature for several days. Temperatures below 150°C were employed to prevent oxidative decomposition of the soap. On occasions, samples were also mixed by heating to the isotropic liquid state, as previously described. All samples, regardless of the method of mixing, were stored at room temperature for at least one week (sometimes for several weeks or months) before their phase behaviour was investigated. That these methods gave preparations that were in true equilibrium at room temperature was evident from the fact that mixtures having the same composition exhibited the same phase behaviour irrespective of their method of preparation.

## 2.2 Instrumental Techniques

### 2.2.1 Polarizing Microscopy

#### 2.2.1.1 Introduction

A polarizing microscope equipped with a heating stage permits visual observation of the phase transformations and the corresponding transition temperatures which occur between crystalline, mesomorphic and isotropic liquid phases as a result of changing the temperature of the specimen [36, 257] and/or the concentration of an added solvent [7, 257-260].

As a result of their ordered molecular arrangement, the great majority of mesophases are birefringent (ie the molecules constituting these mesophases possess different refractive indices for light vibrating parallel and normal to their long axes), and therefore transmit polarized light.

The broad principles of the relation between the optics of such media and their structures have been well established [257]. Simple observations of the morphology and orientation patterns (ie textures) displayed by a thin-film preparation of a liquid crystalline phase in polarized light [7, 257-260] may therefore be sufficient to establish its main structural type (eg lamellar, hexagonal, nematic etc.).

#### 2.2.1.2 Experimental Method

Microscopic observations were made on thin sample films, prepared between standard glass microscope slides and cover-slips, using a Vickers M41 Photoplan polarizing microscope. The microscope was equipped with a Kofler hot-stage (manufactured by the C.Reichert Company, Vienna) designed for a maximum operating temperature of 350°C. The heater current was controlled by a variable transformer whose temperature scale indicated the temperature of the specimen for a standard heating rate of 2°C min<sup>-1</sup>. The specimen temperature was measured by thermometers covering the ranges 20° to 230°C and 120° to 350°C.

As a preliminary method of studying lyotropic mesophase formation in soap-solvent systems, and to obtain a rough outline of the binary phase diagram, the penetration technique of Lawrence [261] was employed. Here, the microscope stage is set at the required temperature and the solvent is allowed to diffuse into the anhydrous surfactant placed between a microscope slide and cover-slip. Various liquid crystalline phases may then develop (depending on

the temperature) as separate, often well-defined, bands around the anhydrous surfactant, with the surfactant concentration decreasing monotonically towards the edge of the slide. Each band exhibits textures associated with a particular mesophase, and these, together with the relative viscosities of these phases (assessed by pressing on the cover-slip) may with experience and by comparison with literature photomicrographs, allow initial assignment of phase structure [7, 257-260]. By altering the temperature of the stage, it is then possible to record the change in phase structure with temperature. (At the higher temperatures, however, the effects of solvent loss have to be taken into account.) An alternative approach is to allow a sample of a lyotropic mesophase, formed between a slide and cover slip, to undergo peripheral evaporation. This establishes a concentration gradient with successive phases appearing towards the edge of the slide being stable at progressively higher surfactant concentrations.

To complete the phase diagrams, bulk samples of known composition were mixed (see Section 2.1.5) and their structures and phase behaviours determined by microscopy.

Appropriate reference is made in the text to illustrative photomicrographs in which the effects are those observed between crossed polars. Magnifications of 100 x were employed.

### 2.2.2 Macroscopic Visual Observations

To supplement the microscopic observations, visual observations were also made of the phase behaviour of "bulk" soap-solvent samples using methods described by Vold et al [43,189]. These methods overcame the problem of solvent loss frequently encountered in the microscope phase studies, especially at elevated temperatures.

Here, samples of known composition (typical sample size, 0.3 - 1 g) were prepared in Pyrex glass tubes (8 mm i.d. and 1 mm wall thickness), as described in Section 2.1.5, carefully flushed with pure dry nitrogen to minimize oxidative decomposition at elevated temperatures and flame-sealed to a length of approximately 10 cm. The sample tubes were then fully immersed in a thermostatically controlled transparent silicone oil bath (Aldrich Chemical Co Ltd) and subjected to repeated heating and cooling cycles at rates varying from approximately  $1^{\circ}\text{C min}^{-1}$  to  $3^{\circ}\text{C min}^{-1}$ . The maximum operating temperature of the oil bath was limited to approximately  $240^{\circ}\text{C}$ . Temperature measurements were made using thermometers accurate over the ranges  $0^{\circ}$  to  $150^{\circ}\text{C}$  and  $140^{\circ}$  to  $300^{\circ}\text{C}$ . The samples were viewed continuously through illuminated polaroid windows which could be crossed manually. Changes in sample opacity, translucency, transparency, birefringency and viscosity were used to follow their phase behaviour with changes in both temperature and composition [187]. Using this method it was often possible, depending upon the sample composition, to determine the temperature of a

liquid crystal to amorphous liquid melt with a reasonable degree of accuracy. This transition is characterized by a change from a birefringent to an isotropic appearance when viewed in polarized light. It is also accompanied by a marked decrease in sample viscosity.

### 2.2.3 Differential Scanning Calorimetry

#### 2.2.3.1 Introduction

Differential scanning calorimetry (DSC), and to a lesser extent differential thermal analysis (DTA), are powerful yet rapid thermodynamic techniques which have proven of great value in studies of the thermotropic phase behaviour of both anhydrous surfactants [47-78] and surfactant-solvent systems [51,55,59,61,195-197].

#### 2.2.3.2 Principles

In DSC, the sample and an inert reference (ie a material that does not undergo a phase transition within the temperature range of interest) are heated at identical, pre-determined rates. Thus the temperatures of the sample and reference initially increase linearly with time and the temperature difference between them is maintained at zero.

If the sample undergoes a thermally-induced event as a result of a physical transition (eg solid-solid, glass transition, fusion) or chemical reaction (eg oxidation, decomposition), the control system senses the resulting temperature differential between the sample and reference and supplies more heat to the sample or reference as

necessary to maintain the two at identical temperatures. Hence, what is recorded is not the temperature difference as in classical DTA, but the electrical input necessary for the maintenance of isothermal conditions as a function of time or temperature.

The resulting plot, or thermogram, provides information on the entire course of thermally-induced phase transitions. This includes the transition temperature, the temperature range over which the change occurs and whether the transition is first-order (endothermic or exothermic involving a discontinuous change in enthalpy,  $\Delta H$ , entropy,  $\Delta S$ , and volume,  $\Delta V$ , with temperature) or second-order (involving a discontinuous change only in the heat capacity,  $C_p$ , with temperature). Furthermore, for first-order transitions the area under the resulting peak on the DSC thermogram, when calibrated with a known standard, provides a direct and accurate measurement of the enthalpy of transition,  $\Delta H$ . The technique of DSC, unlike that of DTA, minimizes the dependence of peak area upon extraneous factors such as the heat capacity, thermal diffusivity and geometry of the sample, since the heat delivered to the entire sample is measured directly in DSC rather than the temperature differential at some point within the sample.

### 2.2.3.3 Experimental Method

DSC thermograms were recorded using a Mettler TA 3000 thermal analysis system. It consisted of a TC10 TA processor, the control unit, and a DSC 30 measuring cell

with an operating range of  $-170^{\circ}\text{C}$  to  $+600^{\circ}\text{C}$ . Controlled cooling was accomplished by means of liquid nitrogen. In addition to recording the measuring curve, the processor was equipped with a number of built-in evaluation algorithms which permitted the automatic calculation of results such as transition temperatures and enthalpies. These were used as outlined in the Mettler TA 3000 operator's manual.

The "standard" measuring sensor of the DSC 30 cell, which monitored the temperature differential between sample and reference, was a vapour-deposited, fivefold gold-nickel thermopile. This assured high accuracy and precision in the determination of enthalpy values (2% and 0.5% respectively; Mettler quoted values). It should be noted, however, that for DSC studies of the lithium phenylstearate-water system (see Section 5.2) a more robust but less sensitive nickel-nickel/chrome "metal" sensor had been fitted to the measuring cell (4% accuracy and 1% precision on enthalpy measurements; Mettler quoted values). The baseline or blank curve of the DSC cell (thermogram obtained with empty sample and reference pans) was checked regularly to ensure that it was free from peaks and discontinuities due to impurities on the sensor.

The rate at which the cell furnace must be heated in order to provide a linear temperature increase was controlled by a platinum resistance thermometer (Pt 100).

Temperature measurement with the Pt 100 sensor was calibrated every six months, the characteristic calibration parameters being obtained automatically from the fusion of pure indium, lead and zinc samples at 156.6°C, 327.4°C and 419.5°C respectively. Correct temperature measurement was checked periodically from the melting point of a sample of pure indium. To ensure high calorimetric accuracy, the heat flow was also calibrated before each set of experiments. The calorimetric sensitivity was obtained from the heat of fusion of an exactly known quantity of pure indium ( $\Delta H_f = 28.45 \text{ J g}^{-1}$ ).

Samples were contained in either standard aluminium crucibles (40  $\mu\text{l}$  net volume) supplied by Mettler Instrumente AG, Switzerland, or in mild steel, high pressure crucibles (70  $\mu\text{l}$  net volume) manufactured and supplied by R. B. Precision Engineering Co, Bracknell, UK. (The methods of sample preparation and pre-treatment are described fully in Section 2.1.) Empty crucibles of the corresponding material were used as the inert reference. Because of modifications to the standard crucible geometry (diameter and height) and mass (heat capacity), new thermometric, calorimetric and instrumental calibration parameters were determined for use with the high pressure steel pans. This was carried out in accordance with instruction sheet NR 3501 compiled by Rudolf Riesen, Application Laboratory Instruments, Mettler AG.

The standard aluminium crucibles were used for DSC investigations of the solvent-free, anhydrous soaps and for lithium stearate samples containing the high boiling point hydrocarbons cetane (b.p. 287°C) and squalane (b.p. 176°C at 0.05 mm Hg). These crucibles could be hermetically sealed to a maximum pressure of 2 bar by cold welding the pan and lid using a spring-loaded crucible press.

The high pressure steel crucibles were used to study the binary systems of lithium phenylstearate with toluene (b.p. 110.6°C), 1-phenylheptane (b.p. 233°C) and water. These crucibles could be hermetically sealed to approximately 100 bar by screwing together the pan and lid. To produce an effective seal, two circular PTFE gaskets (0.2 mm thickness, 6.5 mm diameter), cut from PTFE sheet supplied by Dalau Ltd, Clacton-on-Sea, UK, were inserted inside the lid of each crucible. These were replaced after each DSC run. FIG. 18 shows the thermogram obtained on heating a PTFE gasket as the sample between -50°C and +400°C at a rate of 10°C min<sup>-1</sup>. The sharp endotherm observed at 328.9°C was found to represent the maximum temperature to which they would sustain an effective hermetic seal (See page 67).

The hermetic sealing of all samples was carried out in a glove box under a pure nitrogen atmosphere to minimise the effects of possible sample oxidation at elevated temperatures. For samples which were not hermetically sealed, a slow stream of pure nitrogen (60 cm<sup>3</sup> min<sup>-1</sup>)

was passed through the chamber containing the sample and reference crucibles.

Typical sample weights used for each DSC run were 5 to 15 mg for pure solvent-free soaps and 30 to 70 mg for binary soap-solvent mixtures. These samples were weighed with a precision of  $\pm 5 \mu\text{g}$  using a Mettler TG 50 thermobalance. The soap-solvent samples were re-weighed after each run to ensure that no loss of solvent, and therefore no change in sample composition, had occurred. They were also re-run at a later date to check the reproducibility of the observed transitions, thus ensuring that the samples had been properly homogenized and equilibrated when originally prepared.

When performing DSC experiments, one must compromise between using a fast heating rate, thereby obtaining sharp, well defined peaks and using a slow heating rate in order to work at conditions closer to equilibrium but thereby obtaining relatively small, poorly defined peaks.

Fortunately, most liquid crystal transitions are rapid and for all systems studied heating rates of  $5^\circ\text{C min}^{-1}$  or  $10^\circ\text{C min}^{-1}$  were found to be a satisfactory compromise. Controlled cooling runs were normally performed at a rate of  $2^\circ\text{C min}^{-1}$  to minimise the effects of supercooling.

Unless otherwise stated, first-order transition temperatures were systematically taken as the apex of the curve of milliwatt of input (ordinate) versus temperature (abscissa). For a symmetrical peak, this point represents the temperature at which the transition is 50% complete [262].

For second-order transitions, the temperature recorded also corresponds to 50% completion of the transition. Transitions observed on heating and cooling will be referred to in the relevant sections by the letters H and C respectively.

#### 2.2.4 X-Ray Diffraction

##### 2.2.4.1 Introduction

A characteristic of liquid crystal structures in amphiphilic systems (both lyotropic and thermotropic) is that, while they have no short-range crystalline order ( $< 5\text{\AA}$ ), there is long-range periodic order of the secondary structure (which is composed of the structural aggregates within the system) in one, two or three dimensions [263,264].

The short-range disorder, due to the "liquid-like" conformation of the amphiphile hydrocarbon chains, is characterised by a wide diffuse reflection in the wide-angle region ( $2\theta > 10^\circ$ ) with a position corresponding to a spacing of around  $4.5\text{\AA}$ . This disordered state is dependent on the temperature and is favoured by the presence of water or an organic solvent. The identical position and appearance of a  $4.5\text{\AA}$  reflection for liquid paraffins of equivalent molecular weight [112,120,214,265,266] provides strong, but not conclusive, evidence for the liquid state of the amphiphile hydrocarbon chains. The inconclusiveness arises because hydrocarbon chains pack in a variety of ways, with the result that crystalline structures, too, can give rise to a reflection at  $4.5\text{\AA}$ ;

if the regions with long-range order are small enough ( $< 10^{-5}$  cm), this reflection can be diffuse [263]. For aqueous amphiphile systems, there is a further diffuse reflection corresponding to  $3.2\text{\AA}$  which is characteristic of liquid water. The diffraction pattern for an amphiphilic liquid crystal within the small-angle region ( $2\theta < 10^\circ$ ) is characterized by a series of sharp reflections corresponding to interplanar spacings ranging from 10 to above  $100\text{\AA}$ . The relative positions of these reflections, which have been interpreted as resulting from the long-range periodic order of the micellar units within the mesophase [263,264] vary from one type of liquid crystal to another. The pattern may be so distinctive that it is possible to recognize the phase type solely by a visual inspection of the x-ray diffraction pattern. The number of such reflections, however, depends upon the amphiphilic substance, the liquid crystal phase and the phase composition. When the number of reflections is small, it is not always possible to categorize phases according to their one-, two- or three-dimensional long-range periodicity. In such cases, guidance can be obtained from observations with the polarizing microscope and knowledge of the position of the phase on the phase diagram in relation to temperature and concentration.

Having established the lattice symmetry and mesophase structure, the structural parameters of the phase, such as the interfacial area per polar group and the dimensions of the unit aggregates, may be calculated [112,120,263,264].

#### 2.2.4.2 The Lamellar D Phase

This lamellar phase is assumed to be composed of a continuous alternation of indefinitely extended, coherent polar and non-polar layers (see FIG. 19)

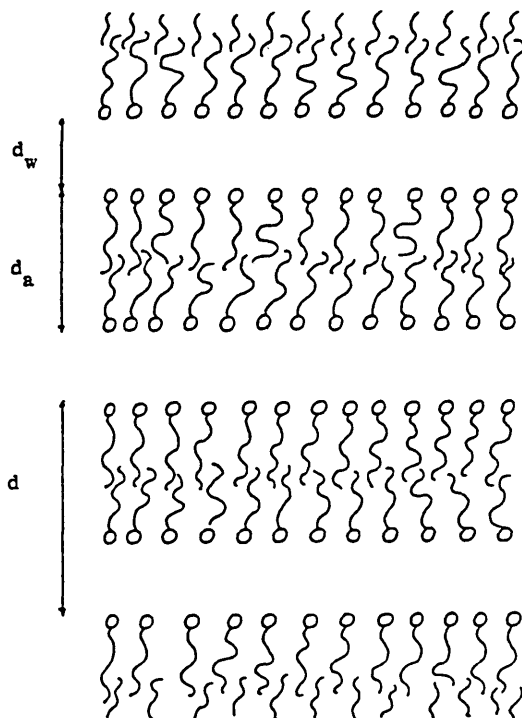


FIG. 19 : The structure of a lamellar D mesophase [263].

$d$ , the repeat distance;  $d_a$  and  $d_w$ , thickness of the amphiphile and water layers respectively.

The former are made up of the polar groups of the amphiphile (plus water molecules in aqueous mesophases). The non-polar layers contain the disordered hydrocarbon moieties of the amphiphile molecules.

Lamellar D phases [263] exhibit a diffuse reflection with spacing corresponding to  $4.5\text{\AA}$  and usually show sharp reflections in the small-angle region with  $d$ -values in the ratio,  $1 : 1/2 : 1/3 : 1/4$ .

The intensity falls off steeply for the higher orders, and often with aqueous systems only the first reflection is visible.

#### Determination of the Structure Parameters

For the lamellar phase of a two component system (amphiphile + water), the thickness of the amphiphile bilayer,  $d_a$ , is given by [263,264],

$$d_a = d\phi_a \quad (2.1)$$

where,  $d$  is the fundamental Bragg spacing corresponding to the repeat distance;

and  $\phi_a$  is the volume fraction of amphiphile defined by [264],

$$\phi_a = [1 + \bar{V}_w (1 - C_a)/\bar{V}_a C_a]^{-1} \quad (2.2)$$

where  $\bar{V}_a$  and  $\bar{V}_w$  are the partial specific volumes ( $\text{cm}^3 \text{g}^{-1}$ ) of amphiphile and water respectively (supposed independent of the composition of the system);

and  $C_a$  is the weight fraction of amphiphile (amphiphile/amphiphile + water).

Assuming that  $\bar{V}_a$  and  $\bar{V}_w$  are equal [265,267], then

$$\phi_a = C_a$$

$$\text{Therefore, } d_a = dC_a \quad (2.3)$$

The water layer thickness,  $d_w$ , is given by [265],

$$d_w = (1 - C_a)d \quad (2.4)$$

If the amphiphile is present in double-layers with the hydrophilic groups facing outwards towards the water (see FIG. 20), the interfacial area ( $\text{\AA}^2$ ) per polar group, S, will be [264],

$$S = \frac{2M\bar{V}_a}{d\phi_a N} \cdot 10^{24} \quad (2.5)$$

where, M is the molecular weight of the amphiphile and N is the Avogadro Number ( $6.022 \times 10^{23} \text{ mol}^{-1}$ ).

Assuming  $\bar{V}_a = \bar{V}_w = 1.0 \text{ cm}^3 \text{ g}^{-1}$  and  $\phi_a = C_a$ , a simplified expression for S is obtained [265],

$$S = \frac{2M}{d_a N} \cdot 10^{24} \quad (2.6)$$

where  $d_a$  is as defined in equation (2.3).

Other versions of these formulae have been reported in the literature.

The approximation that  $\bar{V}_a$  and  $\bar{V}_w$  are equal (and equal to unity) is valid since  $d_a$ ,  $d_w$  and S are only slightly dependent upon the specific volumes [215]. Having made these approximations, the relative values of the structural parameters are obtained and hence an impression of the extent to which they are dependent upon the sample composition.

#### 2.2.4.3 The Hexagonal Phase

Mesophases with two-dimensional hexagonal symmetry [263] exhibit a diffuse reflection with a spacing corresponding to  $4.5\text{\AA}$  and Bragg spacings in the small-angle region in the

ratio 1 :  $1/\sqrt{3}$  :  $1/\sqrt{4}$  :  $1/\sqrt{7}$

The above diffraction pattern is characteristic of both "normal" hexagonal mesophases (containing rod-like unit aggregates with a hydrocarbon core in an aqueous continuum) and "reversed" hexagonal mesophases (containing rod-like aggregates with a polar core in a hydrocarbon continuum; see FIG. 3, p.13), the axis of each cylinder coinciding with a six-fold axis of symmetry.

#### Determination of the Structure Parameters

The formulae used in this section are based upon those derived by Spegt and Skoulios [118,120,123,124] for the thermotropic reversed hexagonal mesophase of several anhydrous divalent metal soaps. The same formulae would be expected to apply to a lyotropic reversed hexagonal mesophase in an anhydrous amphiphile-hydrocarbon system.

The lattice parameter,  $a$ , for the two-dimensional hexagonal network (ie the distance between the centres of the polar cylinders) is obtained from the Bragg spacing,  $d_1$ , corresponding to the innermost reflection by means of the expression;

$$a = \frac{2d_1}{\sqrt{3}} \quad (2.7)$$

$n$ , the number of polar groups per unit length of rod, can be calculated from the expression,

$$n = \frac{\sqrt{3}Na^2 \delta}{2M} \quad (2.8)$$

where,  $N$ , is the Avogadro number

$a$ , is the hexagonal lattice parameter as defined in equation (2.7)

$\delta$ , is the density of the amphiphile  
and  $M$ , is the molecular weight of the amphiphile.

The radius,  $r_c$ , of the rod-shaped aggregates (assumed to be cylindrical) is obtained from the following expression,

$$r_c = \left( \frac{n \cdot V_{pol}}{N\pi} \right)^{\frac{1}{2}} \quad (2.9)$$

where  $n$  is as defined in equation (2.8)

and  $V_{pol}$  is the molar volume of the polar group (eg  $Li^+COO^-$ ).

$S$ , the interfacial area per polar group, can be obtained from the expression,

$$S = \frac{2\pi r_c}{n} \quad (2.10)$$

where  $r_c$  is as defined in equation (2.9) and  $n$  is as defined in equation (2.8).

#### 2.2.4.4 Experimental Method

X-ray diffraction experiments in the small-angle region were carried out using a Kratky camera (manufactured by Anton Paar KG, Graz, Austria) equipped with a slit collimation system. The camera length was 203 mm, the divergence slit 200  $\mu$ m and the receiving slit 300  $\mu$ m. For experiments in the wide-angle region, a Philips PW 1030 diffractometer equipped with a Philips PW 1710 control system was used. Both cameras were operated in vacuo ( $10^{-1}$  mm Hg) to reduce background scattering.

For room temperature measurements in the small-angle region, samples were sealed in 1 mm diameter Lindemann tubes or in a 1 mm diameter quartz capillary cell. For measurements at elevated temperatures, a screw-assembly glass cell of 2 mm thickness was used. For room temperature measurements in the wide-angle region, samples of approximately 2 mm thickness were sealed in a disc-shaped cell with Mylar windows. Soap-solvent mixtures were transferred to the cells using a hypodermic syringe.

Room temperature measurements were normally made at 27°C. The ambient temperature was constant to within  $\pm 1^\circ\text{C}$  throughout each experiment. Elevated temperatures were attained by electric heating of the sample holder using an Anton Paar K-HR temperature control unit with a temperature range of 25-300°C (temperature control  $\pm 1.5^\circ\text{C}$ ). Samples were held at each temperature for approximately 20 minutes to allow equilibration before data collection was started.

Copper  $K_\alpha$  radiation ( $\lambda = 1.5418\text{\AA}$ ) was used in both instruments. This was supplied by a copper target tube equipped with beryllium windows operating at 50 KV and 40 mA and powered by a Philips PW 1730 generator. Cooling of the x-ray tube was maintained by a water flow rate of 3.5 to 4.0  $\text{dm}^3 \text{min}^{-1}$ . A monochromatic x-ray beam was obtained by means of a focusing quartz crystal monochromator.

The scattered radiation was detected by a proportional counter whose output was fed into a scaling circuit via

a pulse-height discriminator. A sequential mode of data collection was employed, the scattering curve (scattered intensity as a function of the scattering angle) being scanned step-wise according to a stored programme. Typical step sizes of 50  $\mu\text{m}$  or 100  $\mu\text{m}$  were used (1  $\mu\text{m}$  corresponds to approximately  $4.5 \times 10^{-6}$  radians with the Kratky camera) with typical count times of 10 or 20 seconds per step.

The collected data was smoothed, de-smearred to compensate for slit collimation effects [268] and fitted using computer methods to yield the characteristic Bragg spacings and peak intensities.

## 2.2.5 Nuclear Magnetic Resonance Spectroscopy

### 2.2.5.1 Introduction

The majority of NMR investigations on amphiphilic liquid crystal systems involve the determination of line widths (and/or second moments) of proton magnetic resonance signals. Such studies have been used to detect phase transitions, both under anhydrous conditions and in the presence of water, and to obtain information on mesophase structure and molecular motion [91-103, 238, 248, 269].

The study of quadrupole splittings also provides a good method for the investigation of anisotropic systems [232, 270-286]. In contrast to amorphous isotropic solutions, anisotropic mesophases containing quadrupolar

nuclei give rise to NMR spectra where the electric quadrupolar interactions are not averaged to zero by the molecular motion. Therefore, important information on ionic and molecular interactions, such as amphiphile counter-ion binding and hydration phenomena, which is lost due to the rapid isotropic molecular motion in isotropic solutions is retained in the NMR spectra of these liquid crystal systems.

#### 2.2.5.2 Theory of Quadrupole Splitting

The basic theory of quadrupole interactions in the solid state is given by Cohen and Reif [287] and has been further discussed for the case of lyotropic liquid crystals (mainly aqueous amphiphile systems) in a number of articles [232, 270-286]. Only a brief outline is presented here.

All nuclei with spin quantum numbers,  $I > \frac{1}{2}$  (eg,  ${}^7\text{Li}$ ,  $I = 3/2$   ${}^2\text{H}$ ,  $I = 1$ ) have electric quadrupole moments (due to a non-spherical charge distribution) which couple to an inhomogeneous electric field. In an environment with non-cubic symmetry, as in most solids and liquid crystals, the interaction between the quadrupole moment,  $Q$ , and the electric field gradient (EFG) at the nuclear position is not averaged to zero by the molecular motion. The residual interaction, which is rather small for water deuterons or counter-ions in a liquid crystal, leads to a splitting of the NMR signal into  $2I$  equally spaced peaks centred at the Larmor frequency,  $\nu_0$ . The distance between two adjacent absorption maxima is called the quadrupole

splitting,  $\Delta$ . (Two further less pronounced maxima may also be observed at  $2\Delta$ .) For nuclei with half integral spin quantum numbers (eg  ${}^7\text{Li}$ ) the central NMR line corresponding to the transition  $m = \frac{1}{2} \leftrightarrow m = -\frac{1}{2}$  (where  $m$  is the magnetic quantum number) is not affected by the static quadrupole interaction to first order. If second order effects are considerable, due to very strong quadrupole interactions, the central line is also shifted [29].

### Macroscopically Aligned Samples

For a macroscopically aligned mesophase (a mesophase where the director has a single orientation) where there are  $i$  different binding sites, the splitting,  $\Delta$ , can be expressed as a weighted average of the  $\Delta$  values at the  $i$  sites due to rapid exchange [270] and is given by equation (2.11).

$$\Delta = \frac{3}{4I(2I-1)} \left| \sum_i \rho_i E_{Qi} S_i (3 \cos^2 \theta_{LD} - 1) \right| \quad (2.11)$$

where,  $\rho_i$  is the fraction of counter-ions (eg  ${}^7\text{Li}^+$ ) or deuterons occupying an asymmetrical site  $i$ ,

$E_{Qi}$  is the characteristic quadrupole coupling constant ( $e^2qQ/h$ ) of this site, where  $e$  is the electron charge,  $Q$  the nuclear quadrupole moment,  $q$  is the largest of the components of the EFG tensor in the principal axes system, and  $h$  is Planck's constant,

$S_i$  is an order parameter describing the degree of

orientation of the EFG's and can be expressed in terms of the time-average angle ( $\theta_{DM}$ ) between the EFG and the symmetry axis of the mesophase (ie the director).

For a uniaxial EFG, assumed to have cylindrical symmetry around the director, the asymmetry parameter term,  $\eta = (q_{xxx} - q_{yyy})/q_{zzz}$  (which describes the deviation of the EFG tensor from axial symmetry) can be neglected and  $S_i$  is given by equation (2.12),

$$S_i = \frac{1}{2} \frac{1}{(3 \cos^2 \theta_{DMi} - 1)} \quad (2.12)$$

$\theta_{LD}$  in equation (2.11) is the angle between the director and the external magnetic field.

(The director is normal to the lamellae for a lamellar mesophase and along the rod axis for a hexagonal mesophase).

For a macroscopically aligned sample where  $I = 1$  (eg  $^2\text{H}$ ) the two observed peaks are of equal intensity, while for  $I = 3/2$  (eg  $^7\text{Li}$ ) the integrated intensity ratio between the peaks is 3:4:3 (i.e. the peak intensities are proportional to  $[I(I+1) - m(m-1)]$ ).

For species which in the unperturbed state have a cubic or higher symmetry such as hydrated counter-ions, the EFG at the nucleus can arise from the electric fields due to the charged amphiphile head groups and the distortions of the hydration sheath [271, 272]. For water deuterions the electric field arises mainly from the OD bond [272].

## Powder Samples

For "powder" samples (which are made up of randomly oriented "micro-crystallites") where all values of  $\cos \theta_{LD}$  are equally probable, the NMR spectrum consists of a broad absorption curve with the distance between adjacent peaks corresponding to that for  $\theta_{LD} = 90^\circ$  in equation (2.11). The quadrupolar splitting,  $\Delta$ , for a powder sample of a lyotropic mesophase [270] is therefore given by equation (2.13),

$$\Delta = \frac{3}{4I(2I-1)} \left| \sum_i \rho_i E_{Qi} S_i \right| \quad (2.13)$$

where the parameters  $\rho_i$ ,  $E_{Qi}$  and  $S_i$  are as defined in equation (2.11).

A simplified version of equation (2.13) has been used by Bonekamp and co-workers [29-32] to calculate the  $^{23}\text{Na}$  quadrupole coupling constants ( $E_Q$ ) for the high temperature thermotropic lamellar mesophases of several anhydrous short-chain sodium carboxylates ( $^{23}\text{Na}$ ,  $I = 3/2$ ) from their first-order quadrupole splittings,  $\Delta$ . The following expression, as derived by Cohen and Rief [287] for the quadrupole splitting in solids, and valid for  $\eta = 0$  and  $I = 3/2$ , was employed,

$$\Delta = \frac{1}{4} \cdot E_Q \quad (2.14)$$

The experimental values of  $E_Q$  thus obtained were in agreement with the theoretical values necessary to reproduce the observed second-order quadrupole shifts of the central transition powder patterns.

For soap-water mesophases a simplification to equation (2.13) is also possible if we assume that the values of  $\Delta$  are dominated by the fraction of "bound" counter-ions and heavy water molecules within the surfactant head-group region close to the alkyl chain-water interface, where the anisotropy is greatest [222]. "Free" counter-ions and water molecules are considered to have zero splittings as a result of the vanishing net orientation of the EFG's [273].

Hence the quadrupolar splitting of bound counter-ions [222] such as lithium (for  ${}^7\text{Li}$ ,  $I = 3/2$ ) is given by equation (2.14),

$$\Delta^{\text{Li}} = \rho_b^{\text{Li}} \cdot \Delta_b^{\text{Li}} = \rho_b^{\text{Li}} \cdot \frac{1}{4} E_{\text{Qb}}^{\text{Li}} \cdot S_b^{\text{Li}} \quad (2.14)$$

where  $\rho_b^{\text{Li}}$  is the fraction of bound lithium ions and the subscript b denotes the properties of these ions.

Similarly for bound heavy water molecules [222], (for  ${}^2\text{H}$ ,  $I = 1$ ),

$$\Delta^{\text{w}} = \rho_b^{\text{w}} \cdot \Delta_b^{\text{w}} = \rho_b^{\text{w}} \cdot \frac{3}{4} E_{\text{Qb}}^{\text{w}} \cdot S_b^{\text{w}} \quad (2.15)$$

Assuming a constant number of bound water molecules,  $n$ , per surfactant head group over the mesophase concentration range [274], then equation (2.15) becomes,

$$\Delta^{\text{w}} = n \frac{X_A}{X_W} \cdot \frac{3}{4} E_{\text{Qb}}^{\text{w}} \cdot S_b^{\text{w}} \quad (2.16)$$

where  $X_A$  and  $X_W$  are the mole fractions of amphiphile and water respectively.

Equation (2.16) may be simplified by assuming that  $E_{Qb}^W$  and  $S_b^W$  are also invariant with concentration. This assumption is valid for the lamellar phase of a number of ionic amphiphile-water systems [232]. The deuteron quadrupole splitting for bound water can now be expressed by,

$$\Delta^W = k \frac{X_A}{X_W} \quad (2.17)$$

where  $k$  is a constant.

### Effect of Mesophase Structure

At first-order phase boundaries where the symmetry of the surfactant aggregates is altered, the value of the quadrupole splitting is expected to change abruptly since  $\rho_b$ ,  $E_{Qb}$  and  $S_b$  are all expected to be dependent on phase structure [222,272].

A change from a lamellar to a hexagonal mesophase alters the angle between the director and the surfactant-water interface by  $90^\circ$ . In general, the EFG at a nucleus in a molecule or counter-ion will be ordered at an average angle  $\theta_{DM}^{L\alpha}$  to the director in the lamellar phase ( $L_d$ ). Because the phase is uniaxial the possible directions lie on a cone. If there is no change in the microscopic ordering at the head group-water interface as the phase change occurs, then in the hexagonal phase the value of  $\theta_{DM}^H$  will take on values on a cone between  $90^\circ \pm \theta_{DM}^{L\alpha}$ . This results in a reduction of the order parameter,  $S$ , by a factor of  $\frac{1}{2}$  for all values of  $\theta_{DM}^{L\alpha}$  (see equation 2.12). The

quadrupole splitting for a lamellar mesophase should therefore be twice that of a hexagonal mesophase at the same composition if  $\rho_b$  and  $E_{Qb}$  are invariant.

It is assumed that within a single homogeneous mesophase, a rapid water molecule exchange occurs on the NMR time-scale [222,275]. In a multi-phase system, however, water exchange between different anisotropic mesophases is almost invariably slow. This results in spectra from the co-existing mesophases appearing superimposed on each other, with peak intensities proportional to the fractions of each phase present [222,276].

### 2.2.5.3 Experimental Method

Soap-solvent samples were prepared and mixed as described in Section 2.1.5, then transferred to NMR tubes (10 mm o.d., 18 cm length for  $^7\text{Li}$  studies, 9 mm o.d., 3.5 cm length for  $^2\text{H}$  studies). On occasions, samples were prepared directly in the NMR tube. The tubes were flushed with dry nitrogen and flame-sealed to avoid solvent loss and contamination from atmospheric moisture. In cases where the solvent could not be obtained in a deuterated form (eg 1-phenylheptane), and for  $^7\text{Li}$  studies of anhydrous lithium phenylstearate, a flame-sealed 5 mm NMR tube containing an appropriate solvent as the deuterium lock was positioned concentrically inside the sample tube. The choice of lock solvent was determined by the sample temperature range to be investigated. Toluene- $d_8$  (mp - 93°C) was used for low temperature studies, whilst dimethyl- $d_6$  sulfoxide (b.p. 189°C) was used for studies

at elevated temperatures. All samples were stored at room temperature for several weeks before measurements were made.

$^7\text{Li}$  NMR spectra were recorded using a Bruker WP 80 SY pulsed spectrometer operating at a resonance frequency of 31.140 MHz. The spectra were obtained from a Fourier transform of the accumulated free induction decay (FID) signals following a quadrature phase pulse sequence (QP) using a  $30^\circ$  pulse (corresponding to a pulse width of 5  $\mu\text{s}$ ) with a pulse interval of 0.1 s. (This pulse sequence was used to improve the phasing of the spectra and reduce ghost fold-back peaks.) The sensitivity (signal/noise) of the spectra was enhanced by applying an exponential multiplication to the FID using a line broadening constant of 24.0 Hz. On occasions where the observed quadrupole splitting was poorly resolved, however, a Gaussian multiplication was applied to the FID using values of -200 and + 0.025 for the line broadening and Gaussian broadening constants respectively. For studies involving anhydrous lithium phenylstearate, and its binary systems with hydrocarbon solvents such as 1-phenylheptane, a spectral width of 71.428 KHz was used with a corresponding acquisition time of 0.0573 s and 8 K data points (4 K after FT). For the lithium phenylstearate- $\text{D}_2\text{O}$  system, the spectral width was 15.151 KHz and the acquisition time 0.2703 s. Unless otherwise stated, the spectra were recorded with the sample spinning in the magnetic field at a rate of 15-25 Hz.

$^2\text{H}$  NMR spectra were recorded at a resonance frequency of 46.071 MHz using a Bruker CXP 300 pulsed spectrometer operating in the Fourier transform mode. A quadrature phase pulse sequence ("CYCLOPS") was used with a  $90^\circ$  ( $10\ \mu\text{s}$ ) pulse and a pulse interval of 0.5 s. A spectral width of 20 KHz was used with an acquisition time of 0.025 s, a line broadening constant of 20.0 Hz and 4096 data points. 80-200 transients were sufficient to record the quadrupole splittings of all samples studied. All  $^2\text{H}$  spectra were obtained with non-spinning samples.

Room temperature  $^2\text{H}$  and  $^7\text{Li}$  spectra were recorded with sample temperatures of  $22^\circ\text{C}$  and  $30^\circ\text{C}$  ( $\pm 1^\circ\text{C}$ ) respectively. For the temperature dependence studies, a Bruker BVT-1000 temperature control unit with a copper-constantan sensor was used to monitor and regulate the heater in the probe-arm (temperature control at the sample  $\pm 0.5^\circ\text{C}$ , temperature stability at the sample  $\pm 0.1^\circ\text{C}$ ). Elevated temperatures were attained using heated compressed air whilst low temperatures were achieved with a flow of cold nitrogen gas. The maximum operable temperature range of the 10 mm probe-head was  $-130^\circ\text{C}$  to  $+150^\circ\text{C}$ . All samples were thermally equilibrated at each new temperature for at least 20 minutes before data accumulation was started.

The  $^7\text{Li}$  quadrupole splittings were measured as the mean distance in Hertz from the central peak to each of the two satellite peaks. For  $^2\text{H}$ , the splitting was measured as the peak to peak distance. Reported values are the average of at least two measurements, in some cases separated by a

period of several months. The reproducibility of the measured splittings was in most cases better than  $\pm 3\%$ . Where peak width measurements were made, the values given are those measured at half maximum intensity,  $W_{\frac{1}{2}}$ .

CHAPTER THREE : THE THERMOTROPIC BEHAVIOUR OF ANHYDROUS  
LITHIUM SOAPS

3.1 Lithium Stearate

3.1.1 Differential Scanning Calorimetry

The thermograms recorded on heating samples of previously unmelted  $\text{LiC}_{18}$  between room temperature and the observed melt to the isotropic liquid, were characterized by three first-order endothermic transitions, hereafter denoted H1, H2 and H3 in order of increasing temperature. FIG. 20 shows a typical thermogram recorded at a heating rate of  $5^\circ\text{C min}^{-1}$  for a sample which had been recrystallized from absolute ethanol and dried in vacuo over  $\text{P}_2\text{O}_5$  at  $100^\circ\text{C}$  for 91 hours. All samples exhibited the same thermal behaviour in spite of their different crystal habits (refer to Section 2.1.1). No heat effects corresponding to the so-called "genotypic" temperature [289], a transition believed to occur in some soaps at a temperature close to the melting point of the parent fatty acid, were detected (m.p of stearic acid,  $68.8^\circ\text{C}$  [288]).

TABLE 2 records the mean and standard deviation values for the observed transition temperatures and the corresponding enthalpies of 25  $\text{LiC}_{18}$  samples. Heating rates of both  $5^\circ\text{C min}^{-1}$  and  $10^\circ\text{C min}^{-1}$  were used. These results are in general agreement with those previously reported in the literature [51, 54, 61].

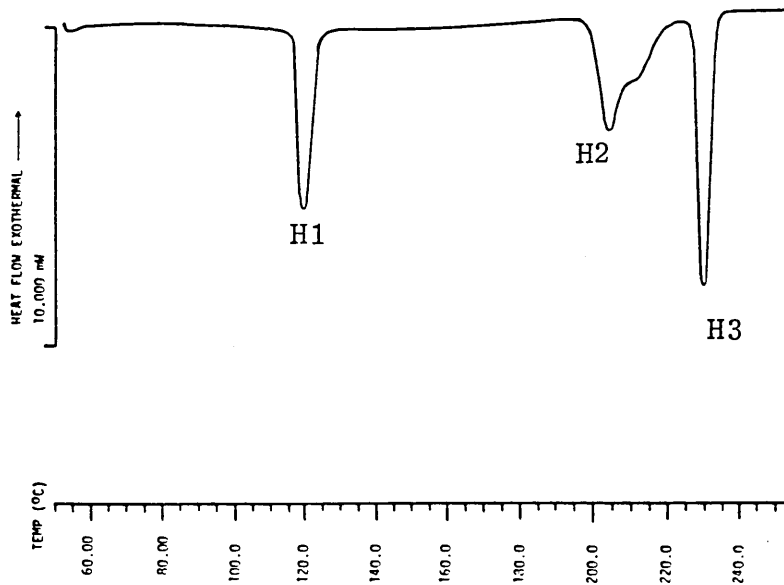


FIG. 20 : DSC heating thermogram for pure, anhydrous lithium stearate (heating rate :  $5\text{ }^{\circ}\text{C min}^{-1}$ )

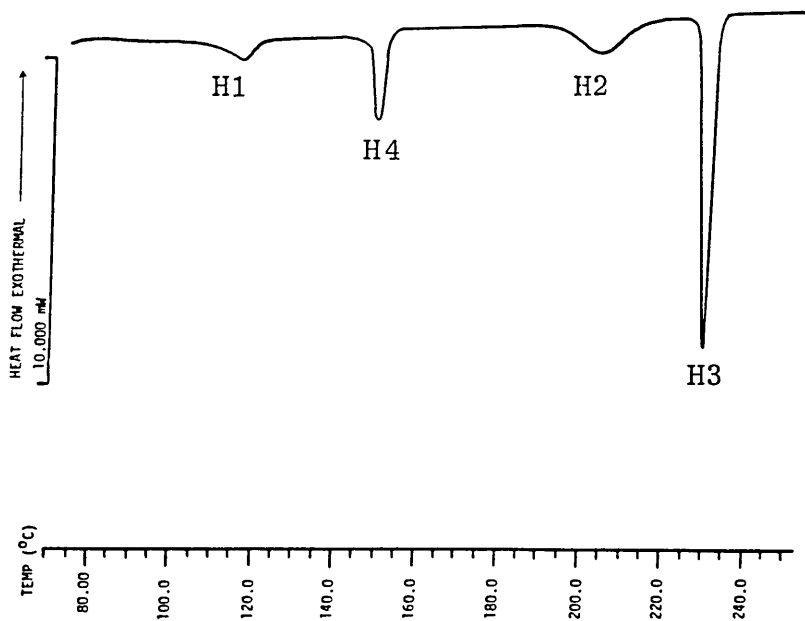


FIG. 21 : DSC thermogram for lithium stearate obtained on re-heating the sample after cooling from  $220\text{ }^{\circ}\text{C}$  to room temperature (heating rate :  $5\text{ }^{\circ}\text{C min}^{-1}$ )

TABLE 2 : Phase transition temperatures and enthalpies  
of anhydrous lithium stearate

TRANSITION	T/(°C)	$\Delta H/(\text{kJ}\cdot\text{mol}^{-1})$
H1	116.3 ± 0.8	14.7 ± 0.7
H2	202.7 ± 1.2	19.1 ± 0.9
H3	227.5 ± 0.4	19.7 ± 0.7

\* (i) The temperature tabulated for H2 corresponds to the lowest temperature transition of two unresolved transitions in the temperature range 195°C to 222°C (see FIG. 20).

\* (ii) The enthalpy,  $\Delta H$ , tabulated for H2 corresponds to the sum of the two unresolved transitions.

For valid thermodynamic data to be obtained by DSC, the system must be at equilibrium throughout the calorimetric run. Variation of the heating rate from 2°C min<sup>-1</sup> to as high as 30°C min<sup>-1</sup> showed little influence on the transition temperatures and enthalpies of the transitions. Higher heating rates, however, (those greater than 10°C min<sup>-1</sup>) were found to affect the features of the H2 peak. At the lower heating rates, the total amount of heat involved in the H2 peak was divided into two steps possibly corresponding to two separate transitions occurring at approximately 202°C and 210°C (see FIG. 20). The associated heat effects could not be measured individually owing to a superposition of the two peaks which we were unable to resolve successfully.

Provided that heating did not proceed beyond the H2 transitions, transition H1 was fully reversible in both enthalpy and temperature on cooling (supercooling within a few degrees) and on subsequent reheating. This behaviour indicated that effects due to retained solvent were absent. Similar findings were reported by Vold and Hattiangdi [65, 108] who showed that  $\text{LiC}_{18}$  was well crystallised on cooling from  $200^\circ\text{C}$  to give an X-ray diffraction pattern virtually identical with the original crystalline material despite having a thermal transition at  $113^\circ\text{C}$  (as determined by DTA) corresponding to our H1 transition at  $116.3^\circ\text{C}$ .

Cooling from  $220^\circ\text{C}$  at a rate of  $2^\circ\text{C min}^{-1}$  (a temperature beyond the H2 transitions, but before H3) gave rise to a sharp exothermic peak corresponding to H2 which was supercooled to  $140.4 \pm 0.5^\circ\text{C}$  ( $\Delta H = -22.1 \pm 1.5 \text{ kJ mol}^{-1}$ ). A broader exotherm for transition H1, which was greatly reduced in enthalpy ( $\Delta H < -6 \text{ kJ mol}^{-1}$ ), was observed at approximately  $111^\circ\text{C}$ .

Immediate reheating of the same sample to beyond the isotropic melt produced a thermogram as shown in FIG. 21. An additional first-order endothermic transition, not previously reported in the literature was observed at  $147.8 \pm 0.3^\circ\text{C}$  (hereafter denoted H4). Peaks H1 and H2, whilst occurring at their original temperatures were both considerably reduced in enthalpy. Peak H3, however, was unaffected. The features of peak H2 on reheating were also changed, now

appearing as a single broad endotherm as opposed to two partly overlapping endotherms as observed on initial heating runs (compare FIGS 20 and 21). The enthalpy of the H4 peak was not constant and varied from approximately  $2.6 \text{ kJ mol}^{-1}$  to  $7.1 \text{ kJ mol}^{-1}$  for successive samples run under identical operating conditions. As its value increased in size, a decrease was observed in the enthalpies of both H1 and H2, and vice versa. The interdependence of the H1, H2 and H4 enthalpies probably reflects the varying degrees of incomplete crystallization on cooling from beyond the H2 transitions to room temperature. The new transition, H4, may therefore be attributed to the presence of a metastable partly crystalline form of lithium stearate which contains some proportion of the supercooled higher temperature H2 phases. Information regarding the structure of this new polymorphic form could be obtained from x-ray diffraction and broad-line  $^1\text{H}$  and  $^7\text{Li}$  NMR spectroscopy studies.

In contrast, samples which had been previously melted by heating to beyond the H3 transition, exhibited only three first-order endothermic transitions when reheated (compare FIGS 21 and 22). The first two peaks H1' and H2' were observed with both lower temperatures and enthalpies than those for unmelted samples whilst H3' appeared to be unchanged (compare TABLES 2 and 3). Leaving fused samples at room temperature even for a period of several weeks before reheating was not

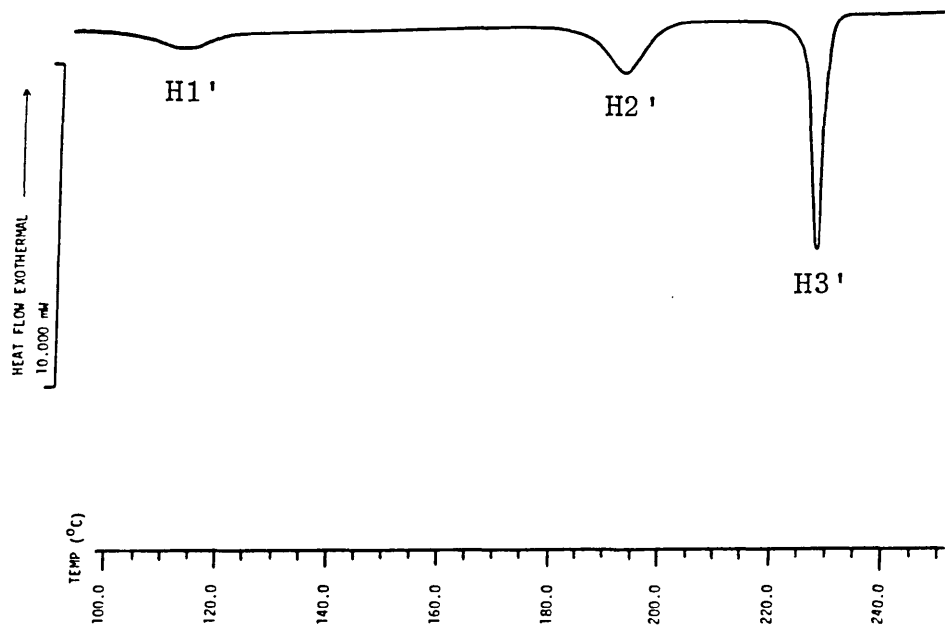


FIG. 22 : DSC thermogram for lithium stearate obtained on re-heating a sample which had been cooled from beyond the melt to room temperature (heating rate :  $10\text{ }^{\circ}\text{C min}^{-1}$ )

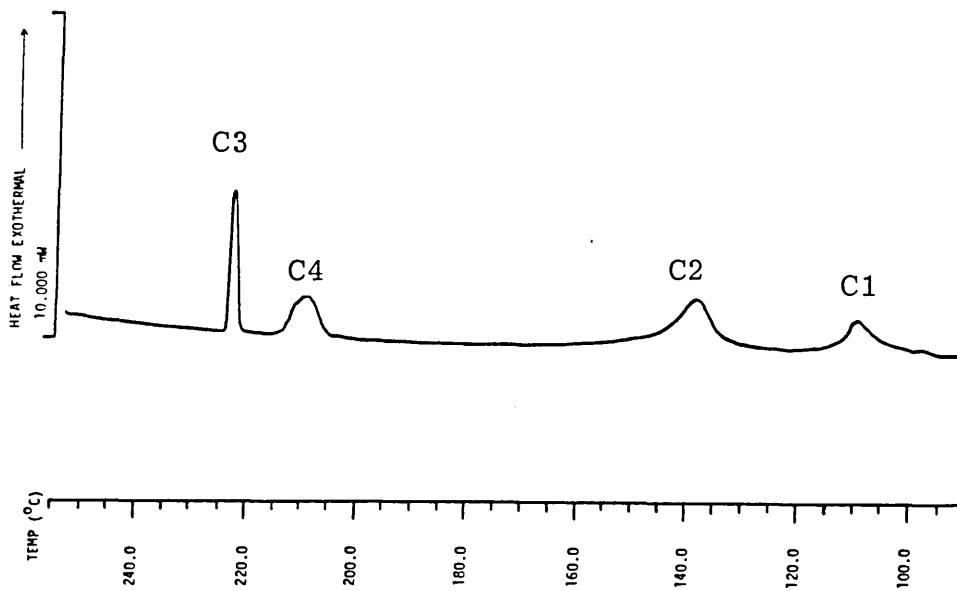


FIG. 23 : DSC cooling thermogram for pure, anhydrous lithium stearate (cooling rate :  $2\text{ }^{\circ}\text{C min}^{-1}$ )

sufficient to let peaks H1' and H2' regain their original features. The sensitivity of transition H2 to the thermal history of the sample has also been noted by

TABLE 3 : Phase transition temperatures and enthalpies of pre-melted lithium stearate\*

TRANSITION	T/°C	$\Delta H / (\text{kJ mol}^{-1})$
H1'	111.2 ± 1.8	7.9 ± 2.5
H2'	195.4 ± 3.5	11.1 ± 1.7
H3'	226.8 ± 0.3	18.9 ± 0.4

\*The above results are the mean and standard deviations of six samples which had remained at room temperature for times varying from 5 mins to 17 days after being cooled from the melt at rates ranging from 2°C min<sup>-1</sup> to approximately 90°C min<sup>-1</sup>. Subsequent reheating runs were performed at rates of 10°C min<sup>-1</sup>.

Ripmeester and co-workers [58]. In a DSC study of LiC<sub>18</sub> they found that the transition originally observed at 195°C (first deviation from the steady baseline) was shifted to 173°C after the sample had been fused under vacuum and allowed to stand at room temperature for approximately one week before reheating. (These values are in concordance with our values of 195 ± 2°C and 176 ± 3°C for transitions H2 and H2' respectively; measured at the point of first deviation of the peak from

the steady baseline). The same behaviour has also been observed in a proton NMR study of the molecular motions and phase transitions of  $\text{LiC}_{18}$  [91]. For a sample of  $\text{LiC}_{18}$  which had been fused and resolidified before the NMR spectra were recorded, a narrow component of the spectrum, present at temperatures above  $\sim 40^\circ\text{C}$ , was observed to grow in intensity until by  $170^\circ\text{C}$  (ie H2') the broad component was no longer distinguishable as a separate component. The spectrum obtained at  $171^\circ\text{C}$  for the fused sample appeared to be almost identical to that obtained for the unmelted sample at  $193^\circ\text{C}$ . These results, combined with our DSC results on fused samples, suggest that the solid soap formed on cooling from the isotropic melt is, once again, partly crystalline and possibly contains some proportion of supercooled higher temperature phases. Similar conclusions were reached by Vold et al [66] who used x-ray diffraction methods to study the structure of solid lithium palmitate ( $\text{LiC}_{16}$ ) samples cooled from the isotropic melt.

Finally, peculiar features were exhibited by peak H3 which appeared as a single transition on heating but was resolved into two separate peaks, C3 and C4, on cooling from beyond the melt due to different supercooling effects (FIG. 23). The sum of the enthalpies of C3 plus C4, occurring at approximately  $223^\circ\text{C}$  and  $209^\circ\text{C}$  respectively on cooling, were found to be equal to the enthalpy of the single peak H3 at  $227.5^\circ\text{C}$  on

reheating (TABLE 4).

TABLE 4

	PEAK C3	PEAK C4	PEAKS C3 + C4	PEAK H3
$\Delta H / (\text{kJ mol}^{-1})$	$-8.2 \pm 0.6$	$-9.6 \pm 1.3$	$-17.8 \pm 1.5$	$+18.1 \pm 0.7$

\*The above results are the mean and standard deviations of nine samples; heating and cooling rates of  $2^\circ\text{C min}^{-1}$  were used.

Moreover, peak C3 was also shown to consist of two unresolved transitions. Cooling from the melt to a temperature beyond C3, but before C4, produced a single exotherm of enthalpy  $-8.7 \pm 0.6 \text{ kJ mol}^{-1}$  (mean and standard deviation of four samples); see FIG.24. Immediate reheating, however, revealed two partly resolved endotherms, H6 and H7, at  $226.5 \pm 0.1^\circ\text{C}$  and  $227.7 \pm 0.1^\circ\text{C}$  respectively (FIG. 25). The sum of the enthalpies of these peaks was equal to  $8.9 \pm 0.8 \text{ kJ mol}^{-1}$ , with H7 accounting for  $\sim 1 \text{ kJ mol}^{-1}$  of the total enthalpy. The existence of transition H7 for  $\text{LiC}_{18}$  has not been previously reported in the literature. It was concluded from these results that lithium stearate passes through two distinct phases having only very short temperature ranges of stability before finally melting to the isotropic liquid, ie peak H3 was shown to contain a total of three transitions; H5, H6 and H7.

FIG.24

Thermogram for lithium stearate obtained on cooling from beyond the melt to 217.5 °C (cooling rate: 2 °C min<sup>-1</sup>)

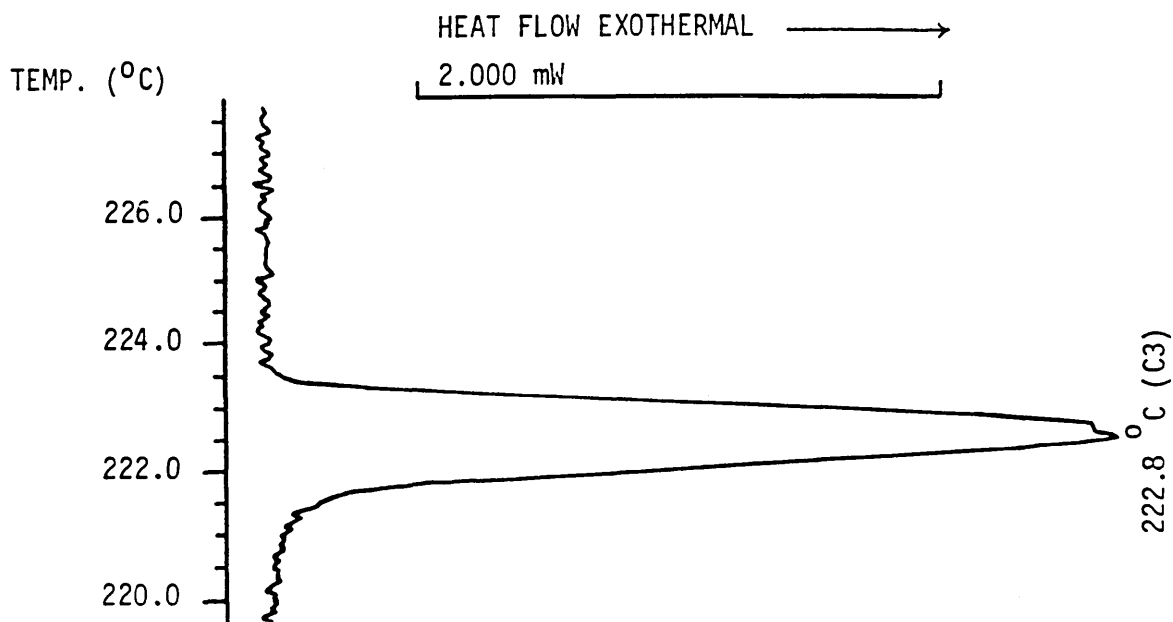


FIG.25

Thermogram for lithium stearate obtained on re-heating from 217.5 °C after cooling from beyond the melt to 217.5 °C (heating rate: 2 °C min<sup>-1</sup>)

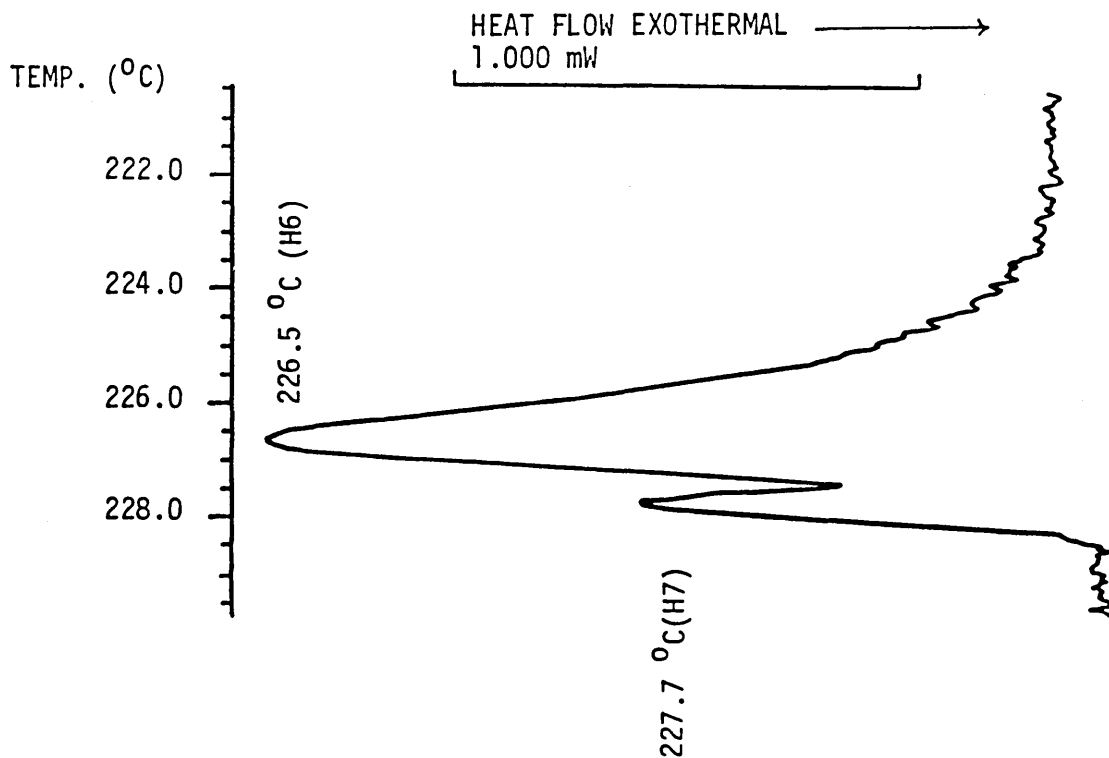


TABLE 5: A comparison of the phase transition temperatures for lithium stearate,  $\text{LiC}_{18}$ , as detected by different authors using a variety of experimental techniques.

TECHNIQUE, (REFERENCE)	TRANSITION TEMPERATURES/°C							
DTA*, [70]	49	91		177				
DTA*, [195]		114		185		221		
DILATOMETRY, [79]		115		176			229	
DTA <sup>+</sup> and, [103] microscopy		117			200	225	229	
NMR, [91]		114		>170			225	
X-ray, [19]		122		190	215		229	
Microscopy, [36]				191	215		226	
DSC <sup>+</sup> , [61]		118		203			228	
DSC, [54]		117.3		191.5			228.1	
DSC <sup>+</sup> , microscopy (this work)		116.3		202.7	210	225	226.5	227.7

\*transition temperature taken as the temperature of the first deviation from the steady base line.

+transition temperature taken as the temperature at the apex of the transition peak.

Transition H5, occurring at  $\sim 225^{\circ}\text{C}$  on heating, corresponds to the supercooled transition at  $209^{\circ}\text{C}$  (C4) on cooling from the melt. This transition was never resolved as a peak on heating, the value of  $225^{\circ}\text{C}$  being taken as the temperature of the first deviation from the baseline at the onset of H3 (see FIG. 20).

A comparison of the phase transition temperatures detected in this DSC study for previously unmelted  $\text{LiC}_{18}$ , with those detected by other workers using a variety of techniques is given in TABLE 5. This comparison is intended to be representative rather than complete.

### 3.1.2 Polarizing Microscopy and Macroscopic Visual Observations

The first transition observed microscopically was a rapidly reversible transformation from one crystal form to another occurring at approximately  $117^{\circ}\text{C} - 118^{\circ}\text{C}$ . The orientation of the optic axis within the crystals changed; consequently some crystals oriented so as to be dark between crossed polars suddenly became brightly illuminated and vice versa. This change was observed at the same temperature for  $\text{LiC}_{18}$  crystals of both lath-like and hexagonal plate-like habits, and corresponded to the calorimetrically observed H1 transition.

As the temperature was raised, a slight overall increase in sample transparency, accompanied by a softening of the crystal edges, was observed between approximately  $198^{\circ}\text{C}$  and  $203^{\circ}\text{C}$ . This was immediately followed at  $205^{\circ}\text{C}$  by a complete loss of microscopic crystallinity and a marked

increase in sample transparency. (This change corresponds to the DSC H2 transition at 202.7°C.) Individual crystals were observed to lose their sharp plane external faces and coalesce to form a highly viscous fluid. Between crossed polars, however, this patchy, birefringent phase exhibited no specific textures which would allow a well-defined structural assignment. Further increases in temperature resulted in a general decrease in sample birefringency and the appearance of isotropic or homeotropic regions (uniformly dark when viewed through crossed polars) at temperatures well below the reported melt. These changes were gradual, however, and could not be attributed to either our apparent DSC transition at  $\sim 210^\circ\text{C}$  or to a microscopically observed transition at  $215^\circ\text{C}$  (between two non-specific textures) reported by Baum et al [36]. At approximately  $230^\circ\text{C}$ , a marked decrease in viscosity and a complete loss of birefringency accompanied the final melt to a transparent, isotropic liquid. The "jelly-like, brightly birefringent, liquid-crystalline phase" observed by Cox and McGlynn [51] between  $225^\circ\text{C}$  and  $229^\circ\text{C}$  was not observed. This is probably a result of their employing a much faster heating rate since they only observed the loss of microscopic crystallinity at  $225^\circ\text{C}$ , as compared to  $205^\circ\text{C}$  in this study. Their "liquid-crystalline" phase may therefore correspond to the viscous patchy birefringent phase which was observed to form at  $\sim 205^\circ\text{C}$  in this study.

On slow cooling the sample from the isotropic melt, a uniformly homeotropic texture was observed microscopically until approximately 208°C when a non-specific dull birefringent texture (similar to that observed on initial heating) began to form. No further textural changes were observed on cooling to room temperature. The homeotropic phase corresponds to the supercooled phase detected calorimetrically between 223°C and 209°C (ie between C3 and C4). Homeotropic orientations (those in which the optic axis is normal to the plane of preparation) are frequently produced by lamellar mesophases and result from a tendency of the lamellae in the structure to arrange themselves parallel to the supporting surfaces [257]. However, it should be noted that optical effects such as bâtonnets, oily streaks, spherulites and the fanlike and mosaic textures, which are also characteristic of lamellar mesophases [257], were not observed for  $\text{LiC}_{18}$  during heating or cooling cycles.

In contrast to the homeotropic phase observed microscopically, macroscopic visual observations on bulk samples of  $\text{LiC}_{18}$  cooled from the melt (where surface orientation effects are less dominant) showed the existence of a viscous, slightly turbid, golden birefringent supercooled phase which was clearly homogeneous within the temperature range from  $\sim 220^\circ\text{C}$  to  $\sim 208^\circ\text{C}$ . This was subsequently transformed into a semi-transparent, white, waxy phase which exhibited a bright yellow-white birefringency between crossed polars. Finally, at  $\sim 144^\circ\text{C}$  (corresponding to DSC transition C2) a dull-white, opaque solid phase was formed, indicative of

"crystallization".

### 3.1.3 Discussion

#### 3.1.3.1

The x-ray powder diffraction studies of Gallot and Skoulios [19] have shown that  $\text{LiC}_{18}$  forms a three-dimensional lamellar crystalline phase (denoted LC 1) with a long spacing of  $42.0 \text{ \AA}$  at  $25^\circ\text{C}$ . In the absence of single-crystal x-ray determinations, the structure of this phase is, however, well understood. As for similar compounds [291, 292] it consists of alternating double layers of crystalline hydrocarbon chains and interdigitated polar groups. The hydrocarbon chains pack in the extended all-trans, zig-zag conformation (possibly in a monoclinic or orthorhombic manner as for lithium palmitate [48]) and are inclined at an angle,  $\alpha$ , of  $\sim 58^\circ$  with respect to the ionic basal planes.

#### 3.1.3.2

At  $122^\circ\text{C}$  (corresponding to the H1 transition observed in this study), Gallot and Skoulios [19] reported a transition for  $\text{LiC}_{18}$  to a second lamellar crystalline phase, LC 2, consisting of a change in the angle of tilt of the chain axes from  $\sim 58^\circ$  (at  $25^\circ\text{C}$ ) to  $\sim 69^\circ$  (at  $150^\circ\text{C}$ ). The packing of the polar groups remains essentially unchanged at this transition since the interfacial area per polar group,  $S$ , increases only very slightly from  $22.1 \text{ \AA}^2$  to  $22.3 \text{ \AA}^2$ . The nature of the chain packing in the higher temperature LC 2 phase is, however, less clear.

Lithium palmitate,  $\text{LiC}_{16}$ , has also been reported to undergo a LC 1 to LC 2 transition (corresponding to a change in  $\alpha$  from  $\sim 58^\circ$  to  $\sim 67.7^\circ$ ) at  $\sim 111^\circ\text{C}$  with an associated enthalpy of  $11.44 \text{ kJ mol}^{-1}$  [48]. These values are very similar to those obtained for  $\text{LiC}_{18}$  (TABLE 2, p 99). From infra-red spectroscopy studies [48] and x-ray diffraction data [48, 66] an analogy has been made between the LC 2 phase of  $\text{LiC}_{16}$  and the "a" (rotator) phase of n-alkanes. (Recent studies have also produced evidence for a rotator phase of 16-hydroxy lithium palmitate [49]). In the rotator phase, the crystalline all-trans aliphatic chains lose some of their specific chain-chain interactions, and at least some of the molecules are able to rotate a few degrees about their long axes. Because of this partial rotation, the 2-d lattice and 3-d subcell pack hexagonally, or nearly hexagonally [296].

The variation of the I.R. spectrum of  $\text{LiC}_{16}$  at the LC 1 to LC 2 transition is qualitatively similar to that observed for the n-alkanes in changing to the rotator phase [293 - 295]. Both intra- and intermolecular correlations between adjacent  $\text{CH}_2$  groups are substantially lost. Rocking ( $719 - 1050 \text{ cm}^{-1}$ ) and twisting ( $1080 - 1360 \text{ cm}^{-1}$ ) progressions almost disappear due to the broadening of the absorptions (the rotational isomers produced with each isomer having its own frequency in these regions, causes a smearing out of the spectrum) and the doublet splittings of the rocking fundamental and bending absorptions are lost (they become single

bands at  $720\text{ cm}^{-1}$  and  $1465\text{ cm}^{-1}$ , respectively).

Similarly, x-ray powder diffraction studies of LC 1 phase of  $\text{LiC}_{16}$  [48] showed that the strong reflections observed in the high-angle region, with d-spacings between  $4.24\text{ \AA}$  and  $3.95\text{ \AA}$  (associated with the regular manner of inter-chain packing) were replaced on passing into the LC 2 phase by a single strong reflection at  $4.31\text{ \AA}$  (characteristic of the rotator phase of n-alkanes [296]). Unfortunately, the corresponding high-angle x-ray data for  $\text{LiC}_{18}$  was not reported by Gallot and Skoulios [19]. However, the value of  $\sigma$ , the average cross-section available to the chains in planes perpendicular to their long axes, was shown to increase from  $18.7\text{ \AA}^2$  for the tightly packed LC 1 phase at  $25\text{ }^\circ\text{C}$  to  $20.9\text{ \AA}^2$  for the LC2 phase at  $150\text{ }^\circ\text{C}$ . The latter value compares well with the value of  $\sim 20.7\text{ \AA}^2$  for the LC 2 phase of  $\text{LiC}_{16}$  [48] and  $\sim 20\text{ \AA}^2$  for the rotator phase of n-alkanes [297].

More conclusive evidence for the existence of a rotator-type LC 2 phase was reported in a broad-line proton NMR study of  $\text{LiC}_{18}$  [91]. The results indicated that below the observed LC 1 to LC 2 transition at  $114^\circ\text{C}$  (as indicated by abrupt decreases in both line width and second moment), the molecular motion present could be explained in terms of torsional oscillations of the hydrocarbon chains. In the LC2 phase, however, the second moment was approximately one quarter of the rigid lattice value with the extent of motion being comparable

to unhindered re-orientation about the hydrocarbon chain long axes.

### 3.1.3.3

By comparing the low melting points of both n-octadecane (mp = 28.2°C [288]) and n-octadecanoic acid (mp = 68.8°C [288]) with that of LiC<sub>18</sub> (mp = 227.5°C; Section 3.1.1) it may be expected that partial melting of the soap structure involving the hydrocarbon chains would occur at a temperature significantly lower than the melt of the ionic planes. According to Busico [126], an alkyl chain in a crystalline layer environment (such as the LC 2 phase) will, with increasing temperature, exert a "lateral pressure" tending to disrupt the ionic planes, in order to increase its cross-section in the basal layer and correspondingly its conformational entropy.

At 190°C, Gallot and Skoulios [19] observed a "melting" of the lithium stearate LC 2 hydrocarbon chains; the resulting tensions breaking up the crystalline lamellae into a "semi-crystalline" ribbon phase (denoted BR 1). The symmetry and dimensions of the unit cell and the intensities of the reflections were all consistent with a structure formed by ribbon-like double sheets of polar groups, indefinitely long in one direction but of finite width ( $L = 36 \text{ \AA}$ ) and thickness, dispersed in a "liquid" matrix of disordered hydrocarbon chains. The ribbons lie parallel to one another in a 2-d rectangular centred lattice of unit cell length,  $a = 90.5 \text{ \AA}$  and width,  $b = 39.8 \text{ \AA}$ . (FIG. 1, p 7)

The value for the interfacial area per polar group on the plane of the ribbons,  $S$ , was calculated to be  $22.3 \text{ \AA}^2$  for the BR 1 phase at  $200^\circ\text{C}$ . This value is identical to the value of  $S$  for the LC 2 phase of  $\text{LiC}_{18}$  at  $150^\circ\text{C}$ , indicating that the polar groups largely retain their crystalline order. The hydrocarbon chains, however, are considered to be in a conformationally disordered liquid-like state as indicated by the diffuse reflection centred around  $4.5 \text{ \AA}$ , characteristic of molten hydrocarbons [265, 266]. This was supported by the IR spectroscopy studies of Chapman [82] who observed changes in the IR spectra of both  $\text{NaC}_{16}$  and  $\text{NaC}_{18}$  on entering the ribbon phase (a smearing out of all fine structure in the  $1800 \text{ cm}^{-1}$  to  $650 \text{ cm}^{-1}$  region) analogous to those observed in the spectra of, for example, long-chain monocarboxylic acids at their crystalline to liquid melts. Proton NMR second moment values for the ribbon phase of  $\text{LiC}_{18}$  [91] are also consistent with the structural picture suggested by x-ray studies.

In a layer organization, however, the conformational flexibility of chains with one end bound to a plane, will be reduced by the limited surface area available per chain and by intra- and intermolecular excluded volume interactions [126]. It appears that for  $S \lesssim 25 \text{ \AA}^2$ , significant conformational disorder cannot be achieved [126]. The hydrocarbon chains although being, broadly speaking, disordered are therefore necessarily to some degree ordered near to the polar ribbon planes. Here, they

retain the inclination imposed on them by the "crystalline" arrangement of the polar groups, ie on average normal to the ribbons for  $\text{LiC}_{18}$ . For a value of  $\alpha = 90^\circ$  and  $S = 22.3 \text{ \AA}$ , the average cross-section available to the chains close to the ribbon surface,  $\sigma$ , is [19]  $\sigma = \sin\alpha \cdot S = 22.3 \text{ \AA}$ , ie not much greater than the value of  $20.9 \text{ \AA}^2$ , calculated for the crystalline LC 2 phase [19]. This difference in molecular motion is reflected in the "super-Lorentzian" proton line-shapes (very sharp in the centre but having very wide wings) observed for the ribbon phases of anhydrous sodium soaps by Lawson and Flautt [96]. This appears to result from the hydrocarbon chains existing in a "liquid-like" environment on the one end and a "solid-like" environment near to the polar groups. This situation produces a distribution of correlation times, which in turn produces a resonance band which is made up of a distribution of lines having varying widths.

The width of the ribbons is determined by the equilibrium between the thermal agitation of the hydrocarbon chains and the cohesion of the polar groups. As the temperature of  $\text{LiC}_{18}$  was increased further, the width,  $L$ , of the ribbons was observed to decrease abruptly from  $36 \text{ \AA}$  to  $31 \text{ \AA}$  (with a resultant decrease in the lattice parameters  $a$  and  $b$ ) corresponding to a sharp phase transition to a second "waxy" ribbon phase, BR 2, at  $215^\circ\text{C}$  [19].

Transitions have been observed in our study by DSC at similar temperatures to those observed by Gallot and Skoulios for the BR1 and BR 2 transitions. The large heat effect associated with these transitions (TABLE 2, p 99 ) is consistent with a major structural change involving chain melting. Transition temperatures of 191°C and 215°C have also been obtained by Baum et al [36] using polarized microscopy for the formation of the BR 1 and BR 2 phases. In general, however, the majority of previous studies on the thermotropic behaviour of LiC<sub>18</sub> have reported only one "waxy" ribbon phase in this temperature region (see TABLE 5, p107).

Some doubt has been cast on the validity of the ribbon structure of these "waxy" phases. In a recent review, Fontell [298] lists the bidimensional rectangular phases proposed by Skoulios and co-workers under the "equivocal phases". Tiddy [ref 7, p 18] has also stated that "the two ribbon structures are remarkable because it is implied that the disorder of the alkyl chain zones is sufficient to disrupt the lamellar arrangements for the occurrence of these phases. One would expect that these structures would be the precursors of the liquid phase. However, they usually revert to a lamellar form before melting." Similarly, the result of a study into the polymorphism of lithium palmitate, LiC<sub>16</sub>, by Vold, Funakoshi and Vold [66] has also questioned the validity of such ribbon phases (refer to Section 1.1.2.2).

One possible way to confirm these ribbon structures would be via multinuclear NMR studies of counter-ions and alkyl chains on aligned samples. Such studies have yet to be made.

#### 3.1.3.4

At higher temperatures, Gallot and Skoulios [19] reported that a fused lamellar ("lamellar labile, LL") or anhydrous "neat" soap phase was formed by all alkali metal stearates (except lithium) as the phase immediately preceding the isotropic liquid melt.  $\text{LiC}_{18}$  was reported to melt directly from the BR 2 phase to the isotropic liquid phase at 229°C [19].

However, in this present study two distinct phases have been observed by DSC having only very short temperature ranges of stability and occurring almost simultaneously with the isotropic melt. The first of these, formed at  $\sim 225^\circ\text{C}$  (H5), is thought to be analogous to the so-called "subneat" phase formed by  $\text{NaC}_{18}$  at  $\sim 199^\circ\text{C}$  [53, 55, 112]. For  $\text{NaC}_{18}$  the structure of this phase is considered to be a rectangular-centred ribbon phase similar to the lower temperature "superwaxy" modification [112]. The formation of the subneat phase from the superwaxy phase is thought to be accompanied by some rearrangement of the polar groups. The temperature range of stability of the  $\text{LiC}_{18}$  subneat phase was observed to be less than  $2^\circ\text{C}$  on heating. However, on cooling from the isotropic melt, our results indicated that this phase was clearly homogeneous within the temperature range from  $\sim 223^\circ\text{C}$  to  $209^\circ\text{C}$ . X-ray

diffraction analysis of this supercooled phase may help to confirm the postulated structure for  $\text{LiC}_{18}$ .

### 3.1.3.5

A second high temperature phase was formed from the subneat phase of  $\text{LiC}_{18}$  at  $226.5^\circ\text{C}$  (H6), immediately preceding the final melt to the isotropic liquid state at  $227.7^\circ\text{C}$  (H7). By analogy with the thermotropic behaviour of the other alkali metal stearates, this phase is considered to be of the fused lamellar type. This mesophase was previously thought not to occur for  $\text{LiC}_{18}$ , probably because of its very narrow temperature range of stability.

The large heat effect associated with the subneat to neat transition (H6) is consistent with a major molecular rearrangement from a 2-d ribbon phase to a 1-d lamellar phase accompanied by a fusion of the polar groups. The enthalpy values reported in the literature for the subneat to neat and neat to isotropic liquid phase transitions of sodium stearate ( $\text{NaC}_{18}$ ) are comparable in size to the total enthalpy of the two high temperature transitions, H6 and H7, observed in this work for  $\text{LiC}_{18}$  ( $8.9 \pm 0.8$   $\text{kJ mol}^{-1}$ , with the H7 transition accounting for  $\sim 1$   $\text{kJ mol}^{-1}$  of the total value). Förster et al [53] reported values of  $10.13$   $\text{kJ mol}^{-1}$  for the subneat to neat transition of  $\text{NaC}_{18}$  and  $0.75$   $\text{kJ mol}^{-1}$  for the neat to isotropic liquid transition. Similarly, Stross and Abrams [59] calculated values of  $1920$   $\text{cal.mol}^{-1}$  ( $8.03$   $\text{kJ mol}^{-1}$ ) and  $140$   $\text{cal.mol}^{-1}$  ( $0.59$   $\text{kJ mol}^{-1}$ ) for

these two transitions. Finally, Pacor and Spier [56] reported values of  $\sim 2200 \text{ cal.mol}^{-1}$  ( $9.2 \text{ kJ mol}^{-1}$ ) and  $\sim 200 \text{ cal.mol}^{-1}$  ( $0.8 \text{ kJ mol}^{-1}$ ) respectively for the same two transitions of  $\text{NaC}_{18}$ .

Skoulios and co-workers [11, 112, 114, 116, 117] found that for the alkali metal stearates, the neat mesophase exists over considerable temperature ranges varying from  $\sim 34^\circ\text{C}$  for  $\text{NaC}_{18}$  to  $\sim 73^\circ\text{C}$  for  $\text{KC}_{18}$ ,  $\sim 76^\circ\text{C}$  for  $\text{RbC}_{18}$  and  $\sim 81^\circ\text{C}$  for  $\text{CsC}_{18}$ . There appears to be a possible relationship between trends in the formation,  $T_f$ , and melt,  $T_{cl}$ , of the neat phase and the nominal ionic contact radius of the cation. The values of  $T_f$  and  $T_{cl}$ , whilst increasing markedly on descending the group from lithium to potassium, are however practically independent of the nature of the cation from potassium to caesium.

The stability of this high temperature lamellar mesophase, therefore, appears to involve a special spatial equilibrium of attractive and repulsive forces between the disordered soap hydrocarbon chains. Furthermore, contact packings of oxygen atoms of the carboxyl group around an alkali cation seem to depend in a rather sensitive way not only on the cation repulsion radius, but also on the cation polarizability [14]. Consequently, whilst the carboxylates of alkali metals are predominantly ionic in nature, those of lithium show considerable covalent character [299]. This may also be a contributory factor to the reduced stability of the  $\text{LiC}_{18}$  lamellar mesophase.

### 3.1.3.6

It is interesting to note that the total value of the entropy of fusion of  $\text{LiC}_{18}$  ( $\Delta S_f = 117.0 \text{ J K}^{-1} \text{ mol}^{-1}$ ) is lower than that of the parent stearic acid ( $\Delta S_f = 165.5 \text{ J K}^{-1} \text{ mol}^{-1}$ , [288]) or that of alkane, n-octadecane ( $\Delta S_f = 203.7 \text{ J K}^{-1} \text{ mol}^{-1}$ , [288]). This might be attributed to a more organised character of the melted soaps due to Coulombic forces between the polar groups.

The small enthalpy of the neat to isotropic transition ( $\sim 1 \text{ kJ mol}^{-1}$ ) may suggest a model of an organised liquid similar to that of the neat mesophase. In fact, x-ray diffraction patterns of the isotropic liquid melt of long-chain sodium soaps [112] indicate that at temperatures near to the melt, lamellar regions of long spacing similar to that of the anhydrous neat phase, but without extended long-range order, still persist. This phenomenon may be due simply to wall orientation effects [22].

However, Busico et al [48, 49, 126, 130] have suggested that a second smectic mesophase of the lamellar neat type (denoted smectic II) may be formed at the isotropic melt by amphiphilic molecules comprising an n-alkyl chain and an ionic end-group (Section 1.1.2.2). It is claimed that the smectic II mesophase is stable up to temperatures at which thermal decomposition of the amphiphile begins [126] and that no true isotropic liquid is known for ionic n-alkyl amphiphiles. For such compounds, it is believed that temperatures of the order of  $10^4 \text{ K}$  would be necessary to stabilize the true isotropic state.

The validity of this smectic II "mesophase" could be established using quadrupole NMR techniques (Section 2.2.5.2). Such studies would indicate the existence of a true anisotropic mesophase or simply of a concentrated micellar solution (possibly made up of finite, reversed disc-shaped bilayer micelles).

## 3.2 Lithium Oleate

### 3.2.1 Differential Scanning Calorimetry

The thermograms recorded on heating samples of previously unmelted crystalline lithium oleate (LiOl) between room temperature and the observed melt to an isotropic liquid, were characterised by five first-order transitions, hereafter denoted H1, H2, H3, H4 and H5 in order of increasing temperature. TABLE 6 records the mean and standard deviation values for the observed transition temperatures and the corresponding enthalpies of 8 samples. A heating rate of 5°C min<sup>-1</sup> was used in each case.

TABLE 6 : Phase transition temperatures and enthalpies of anhydrous lithium oleate

Transition	T/(°C)	ΔH/(kJ mol <sup>-1</sup> )
H1	35.6 ± 0.3	2.2 ± 0.3
H2	132.4 ± 0.6	6.0 ± 0.6
H3	158.7 ± 0.3	17.9 ± 0.4
H4	196.4 ± 0.2	6.1 ± 0.1
H5	227.0 ± 0.3	10.1 ± 0.1

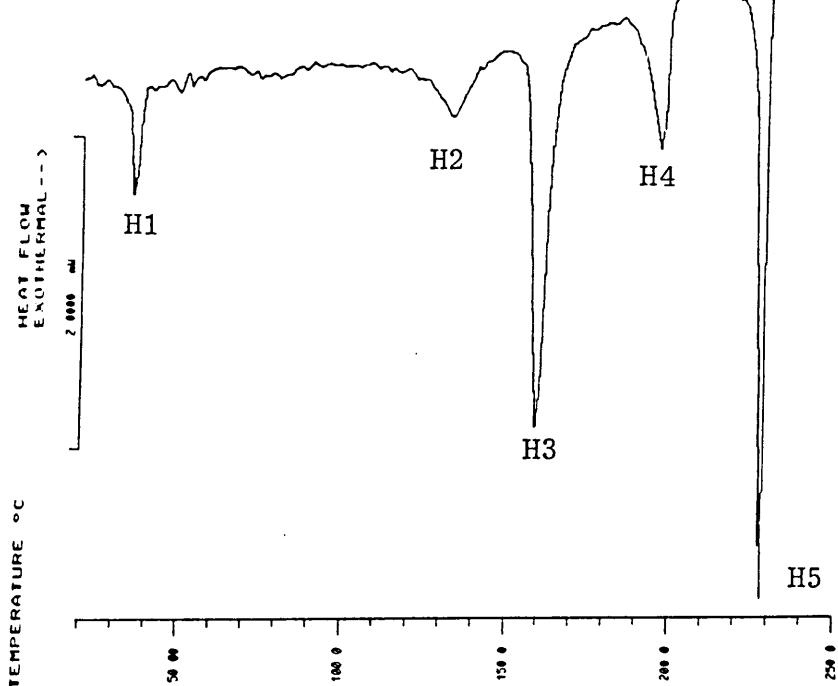


FIG. 26 : DSC heating thermogram for pure, anhydrous lithium oleate (heating rate :  $5\text{ }^{\circ}\text{C min}^{-1}$ )

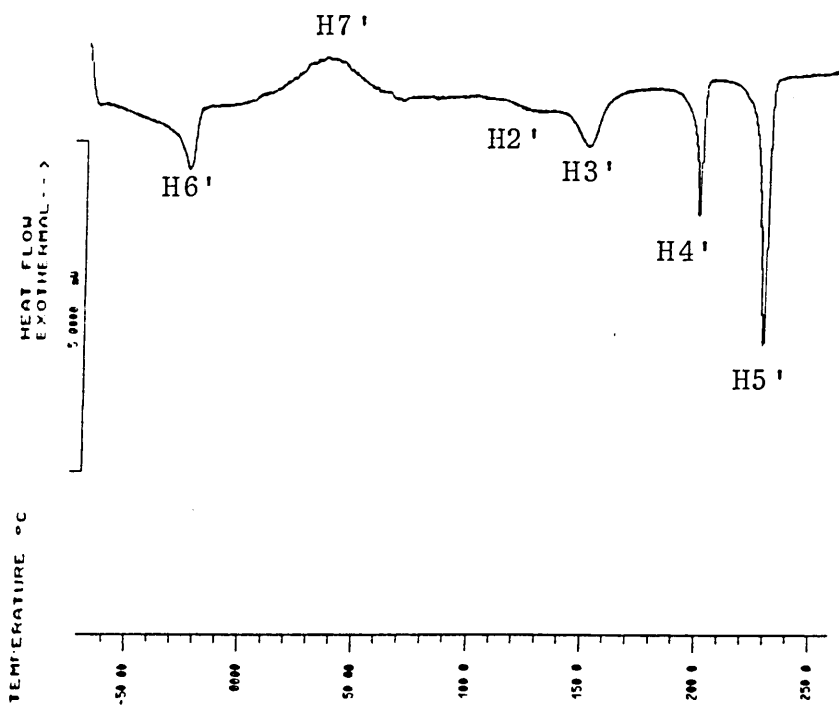


FIG. 27 : DSC thermogram for lithium oleate obtained on re-heating the sample from  $-70\text{ }^{\circ}\text{C}$  after cooling from beyond the melt (heating rate :  $5\text{ }^{\circ}\text{C min}^{-1}$ )

FIG. 26 shows a typical heating thermogram for a sample which had been dried in vacuo over  $P_2O_5$  for 48 hours. Samples obtained simply by air-drying the soap gave identical thermograms with no indication of solvent inclusion or hydrate formation. This identical polymorphic behaviour also confirmed that no metastable phases had been formed on drying the soap at an elevated temperature.

On slow cooling samples from the isotropic melt beyond H5 (cooling rate,  $2^\circ\text{C min}^{-1}$ ), only three transitions were observed. The first of these, C3, was a sharp first-order exothermic transition occurring with an almost identical temperature (supercooling within a few degrees) and enthalpy to transition H5 observed on heating. The second transition, C2, occurring at  $\sim 20^\circ\text{C}$  was difficult to detect and appeared to be second-order in nature, possibly a glass transition. Further cooling revealed a sharp exotherm, C1, at  $-31.4^\circ\text{C}$  with an associated enthalpy of only  $\sim 4.2 \text{ kJ mol}^{-1}$ .

Immediate reheating of this sample from  $-70^\circ\text{C}$  to the isotropic melt produced a thermogram as shown in FIG. 27. The observed transition temperatures and the corresponding enthalpies are recorded in TABLE 7. Transition C1, observed on cooling from the melt, appears to be fully reversible on reheating (H6'), whilst transitions H2' and H3' are considerably reduced both in temperature and enthalpy compared to the original H2 and H3 transitions (compare TABLES 6 and 7). Transition H4', whilst occurring

TABLE 7 : Phase transition temperatures and enthalpies of pre-melted lithium oleate recorded on reheating between -70°C and the isotropic liquid melt

TRANSITION	T/(°C)	$\Delta H/(\text{kJ mol}^{-1})$
H6'	- 25.4	3.8
H7'	33.3	- 14.1
H2'	$\sim 125^*$	< 2
H3'	148.3*	$\sim 4.7$
H4'	197.8	4.3
H5'	226.9	9.5

\*overlapping peaks, see FIG. 27

at essentially the same temperature as the original H4 transition, is, once again, reduced in enthalpy. Transition H5' is practically identical in both temperature and enthalpy to the original H5 transition. The exact nature of the H7' transition on reheating is not known, though the transition temperature of 33.3°C is almost identical to the temperature of the original H1 endothermic transition. The large heat effect (-14.1 kJ mol<sup>-1</sup>) and the exothermic nature of the H7' transition, however, suggests a possible recrystallization or "devitrification" process involving the amorphous hydrocarbon chain regions of the soap. This transition may well correspond to the possible glass transition observed on cooling from the melt at  $\sim 20^\circ\text{C}$  (C2).

These results indicate that lithium oleate, like lithium stearate, is incompletely or imperfectly crystallised from the isotropic melt and possibly contains some proportion of supercooled higher temperature phases.

### 3.2.2 Polarizing Microscopy

No changes in the microscopic appearance of crystalline lithium oleate were detected for either the H1 (35.6°C) or H2 (132.4°C) DSC transitions.

The major thermodynamic event occurring at transition H3 (158.7°C), however, was characterised by a loss of microscopic crystallinity to produce a "waxy" non-specific birefringent phase. A similar transition was observed microscopically for lithium stearate at  $\sim 205^\circ\text{C}$ .

A further increase in temperature to transition H4 (196.4°C) was accompanied by a pronounced decrease in sample viscosity and an increase in translucency. This transition was also accompanied by the appearance of major fluid homeotropic regions within the birefringent texture.

At transition H5 (227.0°C) a complete loss of birefringency accompanied the final melt to the isotropic liquid state. As for lithium stearate, optical effects characteristic of mesophase formation were not observed.

### 3.2.3 Discussion

Very few detailed studies concerning the polymorphism of oleate soaps, and lithium oleate in particular, have been reported [47, 52, 64, 81, 103].

#### 3.2.3.1

At room temperature, lithium oleate may be expected to possess a similar crystal structure to that of sodium oleate. Curat and Perron [52] found that by adopting the crystal structure of the low-melting form of oleic acid [290], the calculated long spacing,  $d(001)$  was in good agreement with the experimentally determined long spacing for sodium oleate ( $43.0 \text{ \AA}$  and  $43.4 \text{ \AA}$  respectively). In the low melting form of oleic acid [290], the molecules, bent at the cis-double bond, have the usual planar zig-zag conformation and adopt a side by side packing  $O' ||$  not previously found in long-chain compounds. The chain axes of the two parts have equal angles of tilt ( $56.5^\circ$ ) to the (001) planes but are tilted in opposite directions.

#### 3.2.3.2

In a broad-line  $^1\text{H}$  NMR study of lithium oleate (from approximately  $-196^\circ\text{C}$  to  $+160^\circ\text{C}$ ), Ripmeester and Dunell [103] reported decreases in both the linewidth and second moment of LiOl corresponding to a transition of 295 K ( $22^\circ\text{C}$ ). This is in agreement with the H1 transition observed in this study by DSC (but not observed microscopically) at  $35.6^\circ\text{C}$  (first deviation,  $25.3^\circ\text{C}$ ). The small  $\Delta H$  value of  $\sim 2.2 \text{ kJ mol}^{-1}$  is consistent with a transition

involving only a minor structural change. The reduction in the second moment from a value of  $\sim 16 - 20 \text{ G}^2$  above the transition suggests motional changes corresponding to an increase in the amplitude of torsional oscillation of the hydrocarbon chains. This motion is comparable to the motion in the stearate chains of  $\text{LiC}_{18}$  prior to the LC 1 to LC 2 transition where the second moment is equal to  $\sim 15 \text{ G}^2$  [91].

It is interesting to note that oleic acid is dimorphous and observations of two "melting points" have been reported. Lutton [300] obtained values of  $13.3^\circ\text{C}$  (with a change in the long spacing,  $d(001)$ , from  $40.5 \text{ \AA}$  to  $42.2 \text{ \AA}$ ) and  $16.2^\circ\text{C}$  for these two temperatures. Whether or not this transition is connected to the H1 transition of  $\text{LiOl}$  has not been established.

### 3.2.3.3

A second, broad but symmetrical, transition, H2, was observed calorimetrically at  $132.4^\circ\text{C}$  (first deviation  $101.7^\circ\text{C}$ ). The enthalpy of the H2 transition ( $\sim 6 \text{ kJ mol}^{-1}$ ) suggests a more significant structural change than that occurring at H1. This transition, however, was not reported by Ripmeester and Dunell [103], their second moment data showing only a gradual decrease from  $\sim 8 \text{ G}^2$  to  $\sim 6 \text{ G}^2$  over the temperature range of this transition.

These results, supported by the fact that this transition was accompanied by no observable change in microscopic appearance, indicate the existence of a second intercrystalline transition for LiOl. The second moment value of  $\sim 6 \text{ G}^2$  after the H2 transition is similar to the value of  $\sim 5 \text{ G}^2$  obtained for  $\text{LiC}_{18}$  after the LC 1 to LC 2 transition at  $\sim 114^\circ\text{C}$  [91]. This may correspond to a structural change for LiOl at the H2 transition involving an increase in the motion of the hydrocarbon chains comparable to re-orientations about the chain long axes.

#### 3.2.3.4

By comparing the melting points of oleic acid and stearic acid ( $16.2^\circ\text{C}$  and  $68.8^\circ\text{C}$  respectively), it may be expected that partial melting of the respective lithium soap structures involving the hydrocarbon chains would occur at a lower temperature for the unsaturated soap.

At 418 K ( $145^\circ\text{C}$ ) Ripmeester and Dunell [103] observed an abrupt decrease in the  $^1\text{H}$  second moment of LiOl from just over  $4 \text{ G}^2$  to less than  $1 \text{ G}^2$ . This transition corresponds to our H3 transition at  $158.7^\circ\text{C}$  (first deviation,  $148.3^\circ\text{C}$ ). They stated that in terms of NMR, the nature of this transition was very similar to the "chain melting" process involved in the crystalline to waxy phase transitions of the alkali metal stearates [93-95, 101] with reorientation of the hydrocarbon chains about several axes. This is also supported by the

similarity of the large heat effect associated with the H3 transition of LiOl ( $\sim 17.9 \text{ kJ mol}^{-1}$ ) with that observed for LiC<sub>18</sub> at the LC 2 - waxy H2 transitions ( $\sim 19.1 \text{ kJ mol}^{-1}$ ). Furthermore, both LiOl and LiC<sub>18</sub> experience a loss of microscopic crystallinity at this transition resulting in the formation of a "waxy" phase with a birefringent non-specific texture.

It is suggested that the oleate has a much lower crystal to waxy transition temperature than the stearate (by  $\sim 44^\circ\text{C}$ ) because of a greater degree of conformational disorder in the oleate chains on the low temperature side of the transition due to the double bond with its cis configuration.

### 3.2.3.5

At  $196.4^\circ\text{C}$  we observed a further polymorphic transition for LiOl (H4) which was accompanied by a marked decrease in sample viscosity. This transition is considered to be analogous to the waxy-subneat transition of LiC<sub>18</sub> at  $\sim 225^\circ\text{C}$ . The enthalpy change for LiOl ( $\sim 6.1 \text{ kJ mol}^{-1}$ ) is somewhat smaller than that obtained for LiC<sub>18</sub> ( $\Delta H \sim 9.6 \text{ kJ mol}^{-1}$ ; value obtained from the supercooled C4 transition) probably due to a greater degree of conformational disorder of the oleate chains in the preceding waxy phase.

Both the proposed "waxy" and "subneat" phases of LiOl are stable over a considerable range of temperature. The structures of these intermediate phases could therefore be

confirmed by x-ray diffraction studies.

### 3.2.3.6

At 227°C, a sharp first-order transition (H5) accompanied the final melt of LiOl to the isotropic liquid. The temperature of this transition is almost identical to that observed for the saturated soap, LiC<sub>18</sub>, as expected for a transition involving a fusion of the polar groups only. No "hidden" transitions, however, could be detected in the H5 peak of LiOl corresponding to the formation of a neat mesophase (as observed for LiC<sub>18</sub> ~ 1°C below the melt.) This final transition is therefore believed to involve the direct melting of the semi-crystalline "subneat" phase to the isotropic liquid state. The enthalpy involved in this transition (10.1 ± 0.1 kJ mol<sup>-1</sup>) is slightly larger than the total enthalpy involved in the subneat-neat plus neat-isotropic transitions of LiC<sub>18</sub> (8.9 ± 0.8 kJ mol<sup>-1</sup>). This may be the result of a more organized arrangement of the soap molecules in the melt of the straight-chain stearate (Section 3.1.3.6).

A similar reduction in the temperature range of stability of the neat phase exists for the corresponding sodium soaps. Whereas the neat phase of NaC<sub>18</sub> is stable over a range of 25.5°C (between 254.0°C and 279.5°C [53]), that of NaOl is stable for only 4.5°C (between 253°C and 257.5°C [52]).

The destabilizing of a bilayer mesophase, if caused by steric hindrance of neighbouring chains possessing cis double bonds, may be expected to increase as the ionic

radius of the cation decreases, ie as the average separation between neighbouring chains is reduced. This would therefore be particularly effective for lithium oleate ( $\text{Li}^+ = 0.60 \text{ \AA}$ ;  $\text{Na}^+ = 0.95 \text{ \AA}$  [301]).

The total enthalpy involved in the fusion of  $\text{LiOl}$  ( $42.2 \pm 1.4 \text{ kJ mol}^{-1}$ ) is much lower than that calculated for  $\text{LiC}_{18}$  ( $53.4 \pm 2.2 \text{ kJ mol}^{-1}$ ). Since it has been established that the enthalpy involved in the fusion of the polar groups of the two soaps is essentially the same, the difference in  $\Delta H_{\text{total}}$  may be attributed to reduced van der Waal's attractive forces and steric repulsions operating between the cis hydrocarbon chain moieties of the oleate soap molecules.

#### 3.2.3.7

By analogy to the broadly similar thermotropic behaviours of lithium and sodium stearate [19, 112], one might expect a similar polymorphism to be exhibited by the respective oleates.

In a recent study of anhydrous  $\text{NaOl}$ , however, Curat and Perron [52] reported the existence of two distinct face-centred cubic mesophases between  $119.5^\circ\text{C}$  and  $143.5^\circ\text{C}$  and  $143.5^\circ\text{C}$  and  $174.5^\circ\text{C}$  (preceding a rectangular-centred "ribbon" phase), based, significantly, on x-ray diffraction and DTA results of pre-melted samples. (Such mesophases are known not to occur for the saturated long-chain alkali metal soaps although body-centred cubic mesophases are formed by strontium and barium stearate at  $197^\circ\text{C}$  and  $220^\circ\text{C}$

respectively [121, 123]). The results of Vold and co-workers, however, based on DSC, polarizing microscopy and dilatometry, indicated the presence of a single, semi-crystalline waxy phase for NaOl over this temperature range.

Cubic mesophases can be easily recognized since they are optically clear, exceedingly viscous and non-birefringent (although they may exhibit transient strain birefringence). Such properties, however, were not exhibited by any thermotropic phase of lithium oleate. A further characteristic of "fused" cubic mesophases is that the micellar units constituting this phase possess rotational mobility and consequently they show high resolution  $^1\text{H}$  NMR spectra of the amphiphilic molecules present. The validity of the proposed cubic mesophase structures for sodium oleate requires substantiation.

Furthermore, in contrast to the results of Vold et al [47, 64, 81] Curat and Perron [52] also reported the formation of two distinct fused neat ("labile lamellar") phases for NaOl at  $242.5^\circ\text{C}$  and  $253.0^\circ\text{C}$  respectively. Although the data concerning the heats of transition of NaOl has been omitted, a qualitative interpretation of the thermograms presented suggests that the transition at  $242.5^\circ\text{C}$  is more probably a transition from the reported ribbon phase to a further ribbon structure analogous to the subneat phase. The size of the endotherm at  $253.0^\circ\text{C}$

is of the correct order for a "semi-crystalline" subneat phase to a fused neat mesophase transition but is much too large for the proposed transition between two fused neat mesophases. The transition at 257.5°C, however, appears to be of the order of magnitude expected for a neat mesophase to isotropic liquid melt, and is in concordance with the observations of Vold et al [81].

### 3.3 Lithium and Sodium Phenylstearates

#### 3.3.1 Differential Scanning Calorimetry

##### 3.3.1.1

The thermograms recorded on heating samples of anhydrous lithium phenylstearate (LiPS) between -170°C and the isotropic melt were characterised by a low temperature, second order transition, H1, and three first-order endothermic transitions, denoted H2, H3 and H4 in order of increasing temperature. FIG. 28 shows a typical heating thermogram recorded at a rate of 5°C min<sup>-1</sup> for a sample which had been dried in vacuo at ~ 115°C over P<sub>2</sub>O<sub>5</sub> for ~ 72 hours. TABLE 8 records the mean and standard deviation values for the observed transition temperatures and the corresponding heat effects of 15 samples. A heating rate of 5°C min<sup>-1</sup> was used in each case. For samples which had not been rigorously dried at an elevated temperature in vacuo, the H2 transition was practically unobservable and was not reproducible in terms of temperature or enthalpy.

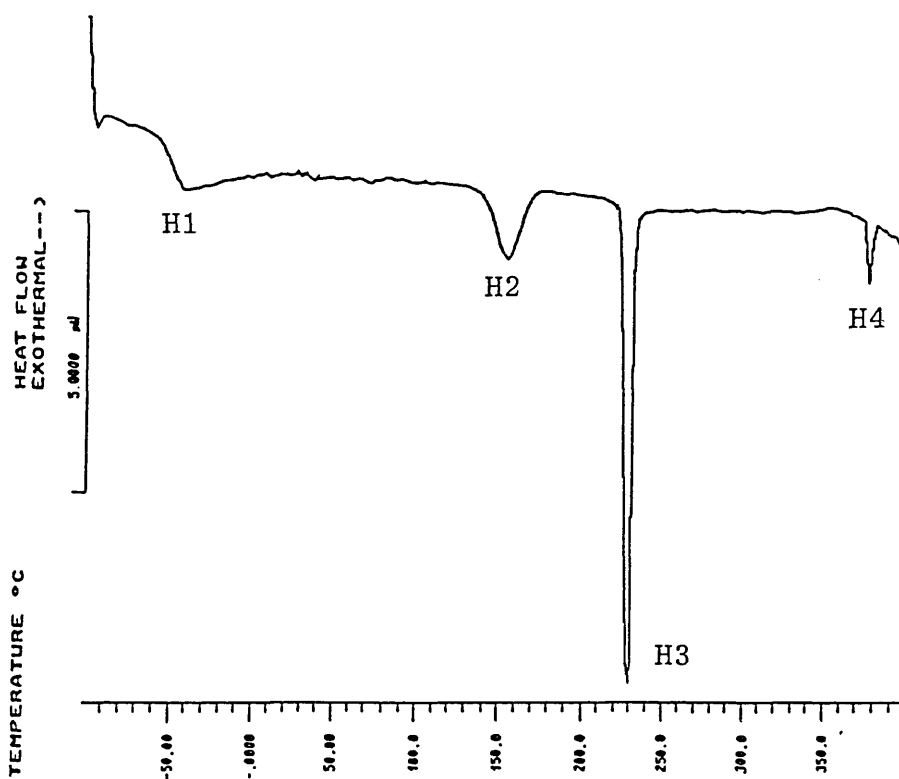


FIG. 28 : DSC heating thermogram for anhydrous lithium phenylstearate (heating rate:  $5\text{ }^{\circ}\text{C min}^{-1}$ )

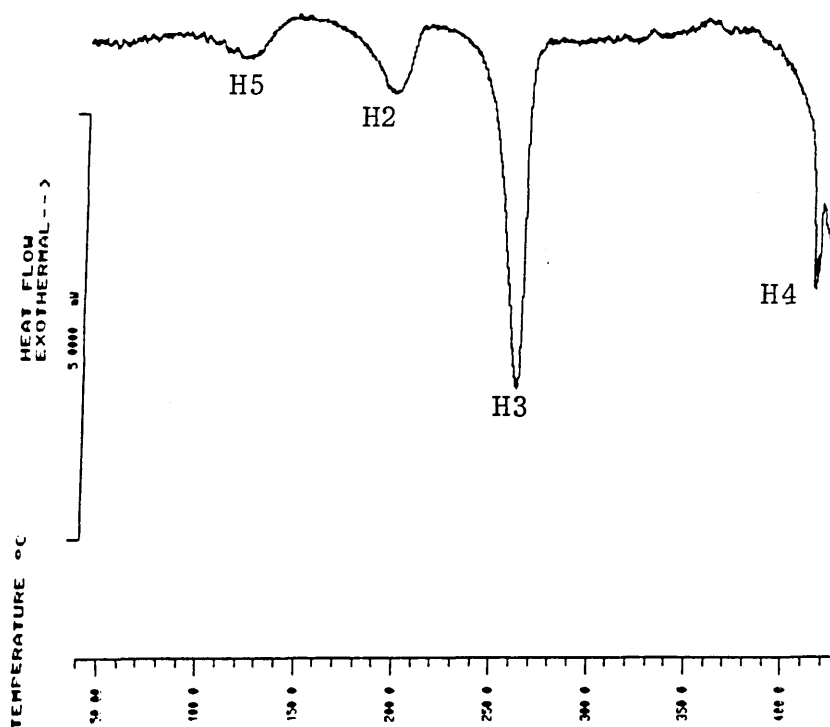


FIG 29 : DSC heating thermogram for anhydrous sodium phenylstearate (heating rate :  $5\text{ }^{\circ}\text{C min}^{-1}$ )

TABLE 8 : Phase transition temperatures and enthalpies  
of anhydrous lithium phenylstearate

TRANSITION	T/(°C)	$\Delta H / (\text{kJ} \cdot \text{mol}^{-1})$
H1*	$-49.9 \pm 1.1$	---
H2	$154.8 \pm 3.3$	$6.0 \pm 0.5$
H3	$227.0 \pm 1.0$	$11.2 \pm 0.4$
H4	$370.6 \pm 1.1$	$0.9 \pm 0.1$

\*H1 is a second-order transition with a change in heat capacity,  $\Delta C_p$ , of  $\sim 211 \text{ J} \cdot \text{mol}^{-1} \text{K}^{-1}$

The values recorded in TABLE 8 correspond to those obtained for LiPS prepared from the purest phenylstearic acid fractions (Section 2.1.3). Samples prepared from slightly less pure acid fractions (as determined by elemental analysis) exhibited almost identical H1, H2 and H3 transitions to those shown in TABLE 8 (within the limits of experimental error). The H4 transition, though accompanied by a similar enthalpy change to the purest LiPS, was, however, increased in temperature by 8-9°C.

Transitions H1, H3 and H4 appeared to be reversible on cooling (supercooling within a few degrees). However, no peak corresponding to transition H2 was observed on slow cooling from temperatures beyond either H4, H3 or H2 to -170°C. Subsequent reheating of samples which had

been cooled to room temperature from beyond H3 (260°C) and allowed to stand for varying lengths of time (in vacuo, over P<sub>2</sub>O<sub>5</sub>) gave peaks corresponding to transition H2 which varied in both temperature and enthalpy.

Immediate reheating of such samples gave peaks which were considerably reduced in enthalpy (varying between 1/3 and 1/4 of the original  $\Delta H$  value) and of a slightly lower temperature (by  $\sim 2-6^\circ\text{C}$ ). Leaving the samples at room temperature for approximately 2 days before reheating gave endotherms with very similar enthalpies but higher temperatures (by  $\sim 10^\circ\text{C}$ ) to those observed for the original H2 transition. Transitions H3 and H4 were unaffected on reheating. A similar type of behaviour has also been observed for certain transitions of anhydrous lithium stearate and lithium oleate on reheating fused samples.

Immediate reheating of samples which had been cooled from the isotropic melt beyond H4 (390°C) revealed a different thermal behaviour. Though transition H2 appeared to be absent, transition H3 gave a sharp endothermic peak at an almost identical temperature to the original sample. An additional small, broad endothermic peak, however, appeared as a shoulder to this transition at  $\sim 240^\circ\text{C}$ . In certain instances, a sharp endotherm was also observed at  $\sim 210^\circ\text{C}$ . The total enthalpy value for these overlapping peaks was not very different from the original H3 value. Transition H4, on reheating fused samples, was lowered by  $\sim 9-10^\circ\text{C}$  and appeared broader than the original

peak with a slightly smaller enthalpy change. These effects are attributed to the presence of impurities in the sample caused by partial thermal decomposition of the soap. Thermogravimetric analysis of LiPS ( $N_2$  atmosphere) showed a gradual weight loss for the sample over the approximate temperature range  $300^\circ C - 400^\circ C$  with an abrupt loss of weight from  $\sim 400^\circ C$  corresponding to extensive thermal decomposition.

### 3.3.1.2

The thermotropic polymorphism of anhydrous sodium phenylstearate, NaPS, appeared to be somewhat similar to that of LiPS but with each of the corresponding H2, H3 and H4 transitions occurring at higher temperatures for the sodium soap (compare FIGS. 28 and 29). The low temperature second-order transition exhibited by NaPS (H1) was, however, observed at an identical temperature to that of LiPS. In addition, NaPS showed a very broad, first-order endothermic transition (H5) which on occasions appeared to be second-order in nature. No analogous transition was observed for samples of LiPS. TABLE 9 records the mean and standard deviation values for the observed transition temperatures and the corresponding enthalpies of 6 samples. A heating rate of  $5^\circ C \text{ min}^{-1}$  was used in each case.

TABLE 9 : Phase transition temperatures and enthalpies  
of anhydrous sodium phenylstearate

TRANSITION	T/(°C)	$\Delta H/(\text{kJ mol}^{-1})$
H1*	$-49.8 \pm 1.0$	---
H5	$121.5 \pm 9.2$	$1.6 \pm 0.5$
H2	$187.7 \pm 4.2$	$3.3 \pm 0.3$
H3	$259.0 \pm 0.9$	$10.9 \pm 0.7$
H4	$412.9 \pm 1.3$	$1.0 \pm 0.2$

\*H1 is a second-order transition. The change in heat capacity,  $\Delta C_p$ , has not been determined.

Transitions H1, H2 and H3 were found to be fully reversible on cooling and subsequent reheating whereas transition H5 showed a similar dependence on the thermal history of the sample to that exhibited by transition H2 of LiPS. Transition H4 was accompanied by thermal decomposition of the soap and is therefore irreversible.

The values recorded in TABLE 9 correspond to those obtained for samples of NaPS prepared from a slightly less pure phenylstearic acid fraction. The large precision limits calculated for the H2 and H5 transitions may be a reflection of the degree of purity of the soap. The difficulty in obtaining sodium soaps in a completely anhydrous state may also be a major contributing factor. Samples of NaPS which had not been rigorously dried at elevated temperatures ( $\sim 115^\circ\text{C}$  in vacuo over  $\text{P}_2\text{O}_5$ ) gave peaks for transitions

H5, H2 and H3 which varied by as much as 7°C, 24°C and 6°C respectively. The enthalpy values of these transitions, however, were not seriously affected. An additional broad endotherm at ~ 70°C ( $\Delta H \sim 5 \text{ kJ mol}^{-1}$ ) was also present for these samples. It should also be noted that, as found for LiPS, the temperature value recorded for transition H4 may be higher than the true value due to the slightly impure nature of the acid fraction used.

### 3.3.1.3

Despite the isomeric nature of phenylstearic acid (Section 1.2.3.1) the anhydrous lithium and sodium soaps appear to behave as single-component systems. However, the possibility of selective separation of crystallization of one or more isomers in these soap mixtures cannot be ruled out. This may result in transitions occurring due to differences in composition within the same sample.

## 3.3.2 Polarizing Microscopy

### 3.3.2.1

At room temperature, LiPS is a whitish, wax-like solid which can be "pressed out" between a glass microscope slide and cover slip to produce regions with a patchy, non-geometric, dull birefringent texture (FIG. 30). This texture exhibits partial extinction as the microscope stage is rotated. According to Rosevear [258] and Tiddy [ref 7, p41] similar textures may be exhibited by middle (hexagonal) mesophases (category 231 in Rosevear's classification). As the temperature was increased, the

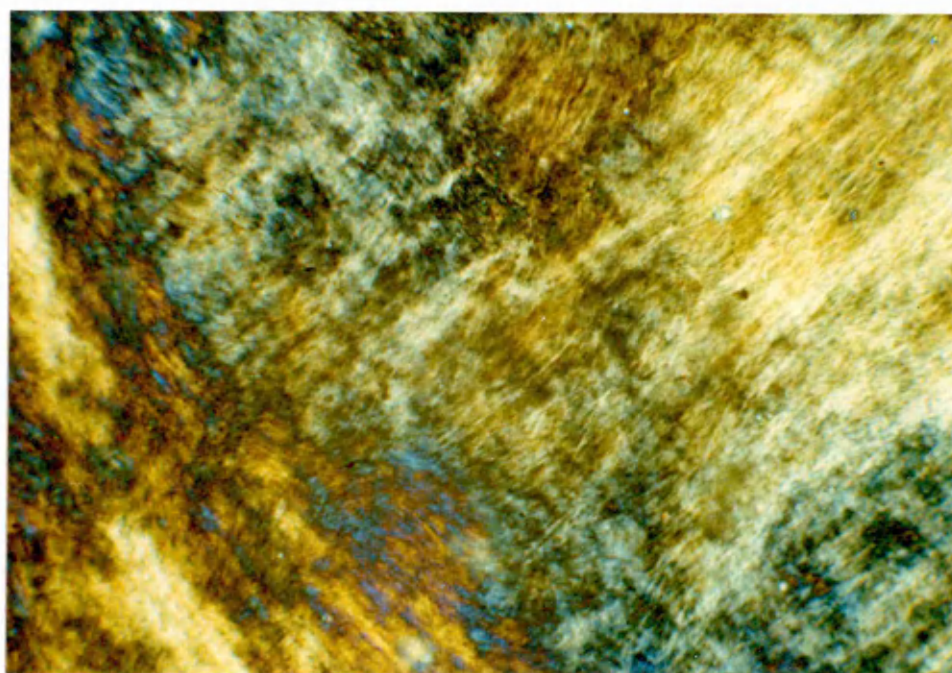


FIG. 30 : Photomicrograph of anhydrous lithium phenylstearate at room temperature (crossed polars, magnification x 100).

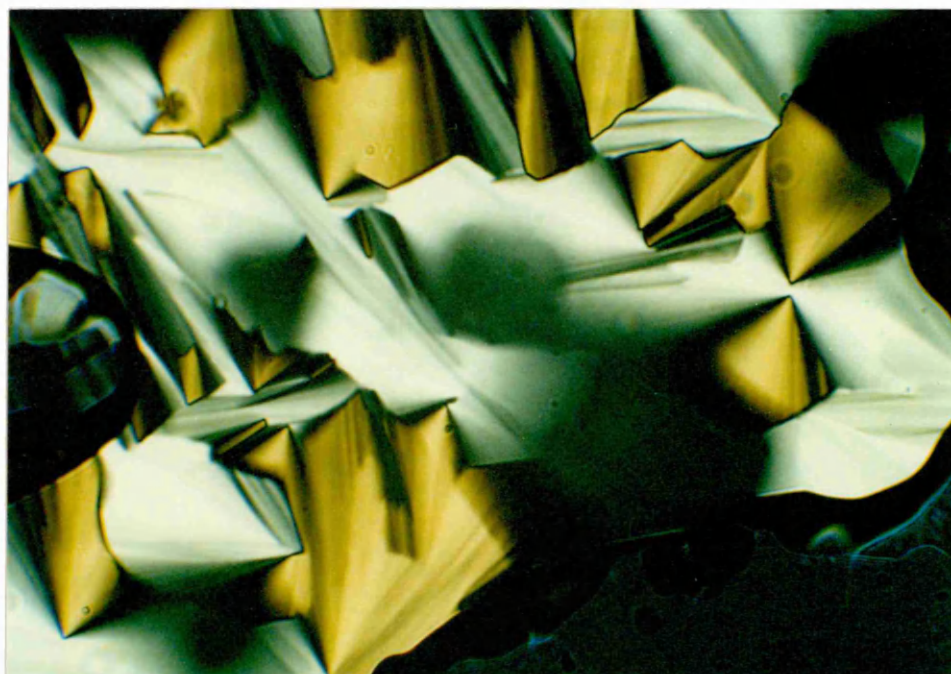


FIG. 31 : "Fanlike" focal conic texture of the reversed hexagonal mesophase exhibited by anhydrous lithium phenylstearate at 300 °C (crossed polars, magnification x 100).

sample passed through an apparent "melting" transition between  $\sim 150^{\circ}\text{C}$  and  $160^{\circ}\text{C}$ , accompanied by a marked decrease in rigidity. The sample film now exhibited a patchy, non-geometric birefringent texture throughout. (This change corresponds to the H2 transition detected by DSC at  $154.8^{\circ}\text{C}$ ). On further increase of temperature, fine striations were observed to develop in the sample and at approximately  $220^{\circ}\text{C}$ , a general decrease in the intensity of the birefringence was observed accompanied by a further decrease in viscosity to a liquid-like behaviour (corresponding to the H3 transition observed at  $227^{\circ}\text{C}$  by DSC). As the temperature was raised slowly to  $\sim 240^{\circ}\text{C}$ , a spectacular birefringent fanlike focal conic texture developed (FIG. 31). This fanlike texture (category 222.5 in Rosevear's [258] classification) is the one most commonly associated with a fused hexagonal mesophase. The boundary between two fanlike areas is a sharp discontinuity, apparently consisting only of irregular lines along which two adjacent liquid crystalline zones happen to meet and stop growing [257]. For LiPS, this fanlike texture persisted up to  $302^{\circ}\text{C}$ , the maximum attainable temperature.

### 3.3.2.2

A similar sequence of events was observed on heating a sample of anhydrous NaPS above room temperature. The first transition observed by DSC at  $\sim 121.5^{\circ}\text{C}$  (H5) was thought to be accompanied by a general softening of the

wax-like solid, although no marked change in microscopic appearance was observed. The waxy "melt" observed microscopically between approximately 185°C and 195°C corresponds to the H2 transition observed at 187.7°C by DSC. This was accompanied by the formation of a patchy, non-geometric birefringent texture, similar to that formed by LiPS after the H2 transition. An abrupt decrease in viscosity and the gradual development of a fanlike texture accompanied the H3 transition observed by DSC at 259.0°C. This fanlike texture was still apparent at 300°C, the upper limit of study.

### 3.3.3 <sup>7</sup>Li and <sup>23</sup>Na NMR Spectroscopy

#### 3.3.3.1

The <sup>7</sup>Li NMR powder spectrum of anhydrous LiPS at 22°C (obtained from a single 90° pulse at a resonance frequency of 116.641 MHz) consists of a central line flanked by two equally spaced satellites, characteristic of first-order quadrupole splitting for the case of spin I = 3/2 (FIG. 32). The values of the quadrupole splitting, Δ (as measured from satellite to central peak) and the quadrupole coupling constant, E<sub>Q</sub> (as calculated from Δ using equation (2.14), p 90) are given in TABLE 10.

TABLE 10 : Measured quadrupole splitting, Δ, and quadrupole coupling constant, E<sub>Q</sub>, for the <sup>7</sup>Li nuclei in anhydrous LiPS at 22°C

Δ/(kHz)	E <sub>Q</sub> /(kHz)
20 ± 1	80 ± 4

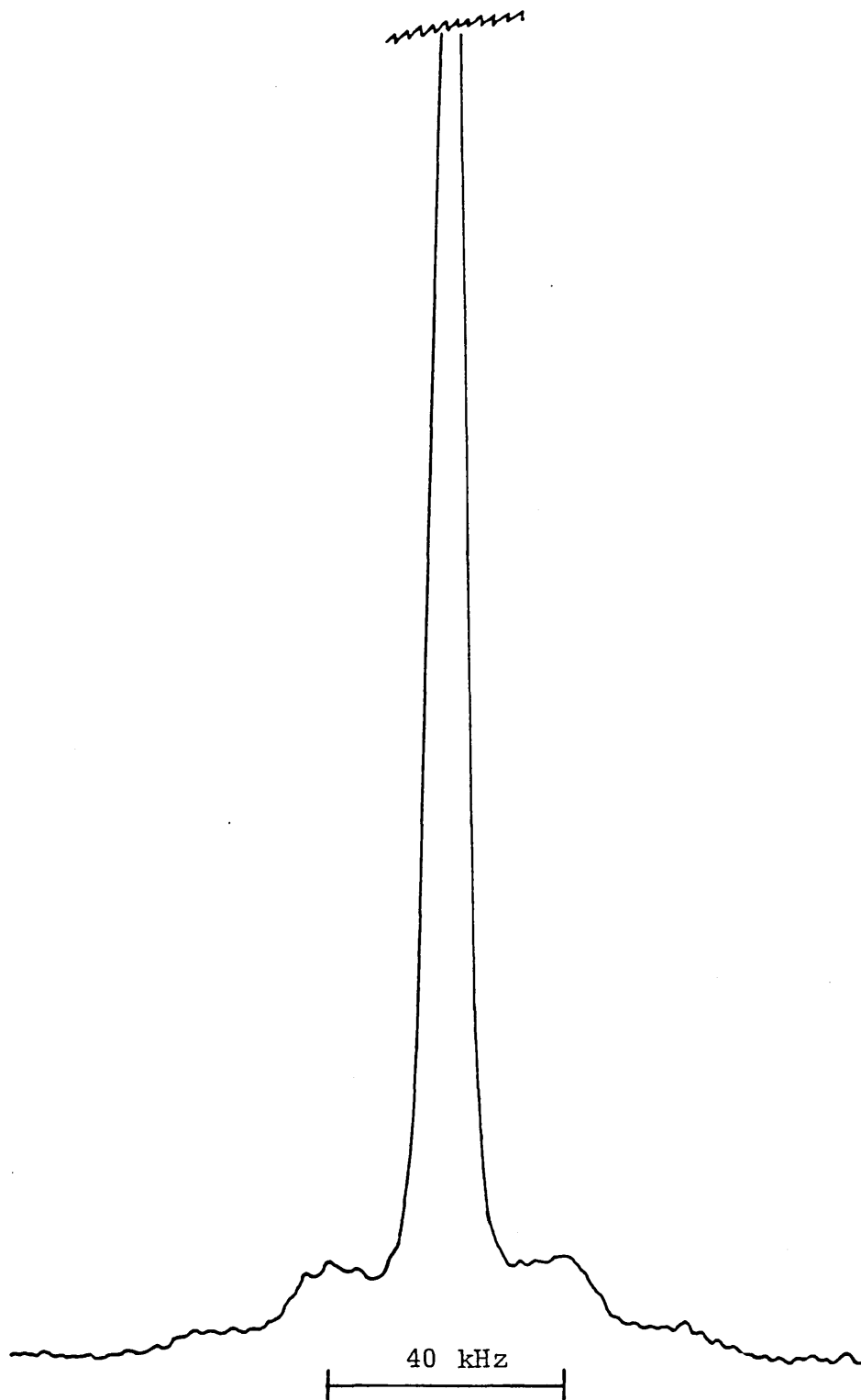


FIG. 32 :  ${}^7\text{Li}$  NMR "powder" spectrum of anhydrous lithium phenylstearate at 22 °C

In view of the fact that we are dealing with an anhydrous soap system, it is not surprising that the magnitude of  $E_Q$  is of the same order as those reported for polycrystalline samples of, for example, lithium phosphide,  $\text{Li}_3\text{P}$  [302] and lithium niobate,  $\text{LiNbO}_3$  [303], ( $68.5 \pm 3$  kHz and  $53.8 \pm$  kHz respectively).

### 3.3.3.2

The  $^{23}\text{Na}$  NMR spectrum of anhydrous NaPS at  $22^\circ\text{C}$  (SF = 79.387 MHz), however, showed no evidence of quadrupole splitting over a spectral width of 500 kHz. It is interesting to note that both sodium phosphide [304] and sodium niobate [305] have much larger  $E_Q$  values (and therefore larger  $\Delta$  values) than the corresponding lithium compounds (between 1.53 and 1.70 MHz and  $2.15 \pm 0.20$  MHz respectively). It may therefore be possible to measure the quadrupole splitting for anhydrous NaPS by employing a much larger spectral width.

### 3.3.3.3

For nuclei with half integral spin quantum numbers such as  $^7\text{Li}$  ( $I = 3/2$ ), the central NMR line is not affected by the static quadrupole interaction to first order [271]. In the solid state, however, Li-Li and Li-H dipole-dipole interactions are not averaged to zero by rapid isotropic tumbling and very broad lines result. Some non-dipolar broadening due to second-order quadrupole effects may also be present. These interactions are, however, averaged out to a greater or lesser extent by increases in molecular

motion, resulting in a narrowing of the line.

A study was therefore made of the temperature dependence of the  ${}^7\text{Li}$  central resonance absorption linewidth,  $W_{\frac{1}{2}}$ , of anhydrous LiPS (at 31.140 Mhz) over the temperature range from  $-80^\circ\text{C}$  to  $+200^\circ\text{C}$ . The results of this study are presented in TABLE 11.

TABLE 11 : Temperature dependence of the  ${}^7\text{Li}$  NMR central resonance absorption linewidth,  $W_{\frac{1}{2}}$ , of anhydrous LiPS.\*

T/( $^\circ\text{C}$ )	$W_{\frac{1}{2}}$ /(kHz)
- 80	6.73
- 30	6.77
- 17	6.70
30 <sup>‡</sup>	6.14 <sup>‡</sup>
30 <sup>†</sup>	5.51 <sup>†</sup>
50	5.82
70	5.67
90	5.60
110	5.49
130	4.60
150	2.35
170	1.78
180	1.50
190	1.15
200	0.85

\*Second-order quadrupole effects were not observed at any of the tabulated temperatures.

<sup>‡</sup> $W_{\frac{1}{2}}$  of anhydrous NaPS at  $22^\circ\text{C}$  (SF = 79.387 Mhz) was 7.2 kHz.

<sup>†</sup> $W_{\frac{1}{2}}$  measured immediately after cooling from  $200^\circ\text{C}$  over a period of  $\sim 5$  minutes. This reduction in  $W_{\frac{1}{2}}$  appears to result from an imperfect or incomplete crystallization of the polar groups and may be associated with the time-dependent reversibility of the H2 DSC transition.

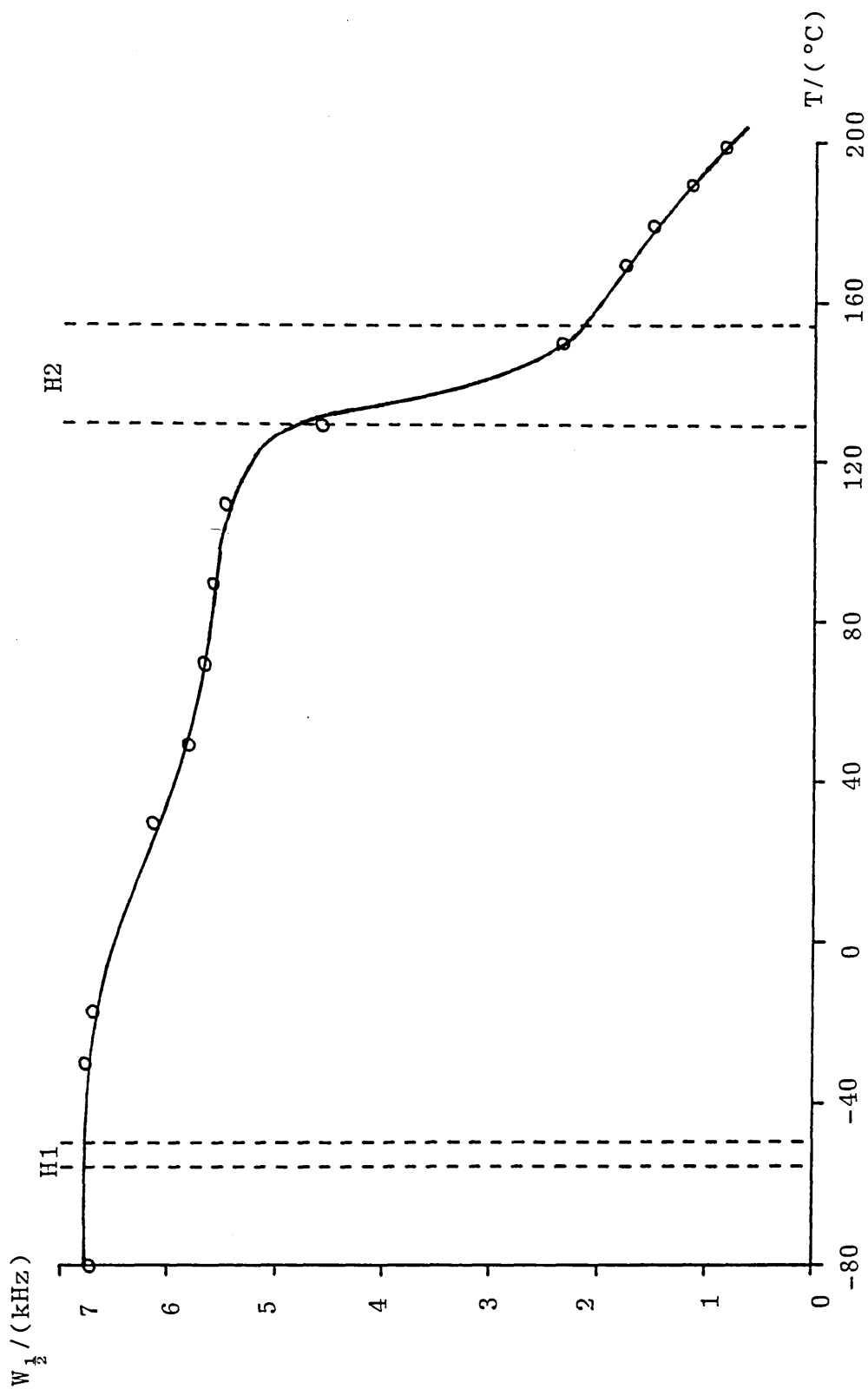


FIG. 33 : Temperature dependence of the  $^7\text{Li}$  NMR central resonance absorption linewidth,  $W_{1/2}$ , of anhydrous lithium phenylstearate

The values given in TABLE 11 have also been presented graphically (FIG. 33). The transition temperatures for the H1 and H2 DSC transitions are represented on the graph by vertical bands covering the temperature range from the onset of the transition to the point of 50% completion.

FIG. 33 shows that the  $^7\text{Li}$  linewidth is essentially constant over the temperature range from  $-80^\circ\text{C}$  to  $-17^\circ\text{C}$ , and is therefore not affected by the second-order H1 DSC transition between  $-55.7^\circ\text{C}$  and  $-49.9^\circ\text{C}$ . At room temperature, the linewidth value for LiPS is of the same order as that reported for crystalline lithium niobate ( $\sim 10$  kHz at  $24^\circ\text{C}$  [303]), suggesting a quasi-crystalline type of arrangement for the polar groups of LiPS.

With increasing temperature,  $W_{\frac{1}{2}}$  decreases very slowly up to  $130^\circ\text{C}$  (the onset of transition H2) when there is a sudden pronounced decrease in value from 4.60 kHz at  $130^\circ\text{C}$  to 2.35 kHz at  $150^\circ\text{C}$ . Between  $150^\circ\text{C}$  and  $200^\circ\text{C}$  (the maximum attainable temperature), the linewidth continues to decrease gradually to a final value of  $\sim 0.85$  kHz at  $200^\circ\text{C}$ .

Although it is difficult to state unambiguously what type of motion is the cause of the line-narrowing phenomenon for LiPS, it may be tentatively explained in terms of two motional processes. At transition H2, the line-narrowing may be attributed to a motion which only partly removes the dipolar interactions, possibly involving some

rearrangement of the RCOO<sup>-</sup> and Li<sup>+</sup> ions. As the temperature is increased towards H3 (onset  $\sim$  224°C as determined by DSC), the <sup>7</sup>Li linewidth approaches that reported by other workers (< 0.5 kHz) corresponding to rapid diffusional motion of the cations [302, 303]. Diffusional motion has been reported for the Na<sup>+</sup> ions in the smectic A (lamellar bilayer) mesophase of a number of anhydrous short-chain sodium carboxylates at elevated temperatures [28 - 32]. Here, the <sup>23</sup>Na dipolar linewidths throughout the mesophase range were as narrow as those observed for the isotropic melts.

### 3.3.4 X-Ray Diffraction

#### 3.3.4.1

At room temperature, the diffraction patterns of both LiPS and NaPS showed several sharp reflections at low angles in the ratio of  $1:1/\sqrt{3} : 1/\sqrt{4} : 1/\sqrt{7}$ , (see FIG 34 and TABLE 12). A further diffuse reflection at  $\sim 4.6 \text{ \AA}$  was also observed in the high-angle region for both LiPS and NaPS (FIG. 35).

TABLE 12 : Experimental low-angle x-ray diffraction results for anhydrous lithium and sodium phenylstearate at 27°C\*

Sample	Observed Bragg Spacings/( $\text{\AA}$ )				Lattice Symmetry
	d <sub>1</sub>	d <sub>2</sub>	d <sub>3</sub>	d <sub>4</sub>	
LiPS	31.1	17.8	15.4	11.6	2-d Hexagonal
NaPS	31.8	18.2	15.9	11.9	2-d Hexagonal

\* See overleaf

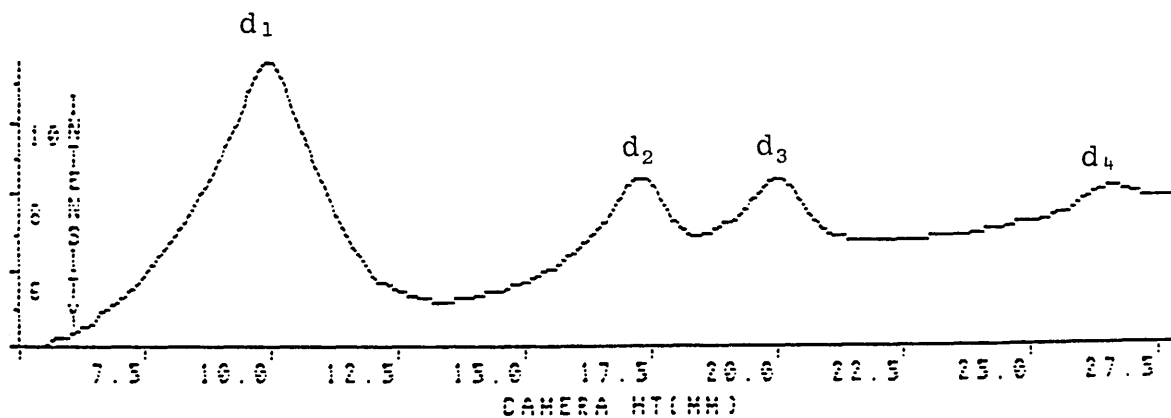


FIG. 34 : Low-angle x-ray diffraction pattern obtained from anhydrous lithium phenylstearate at 27 °C

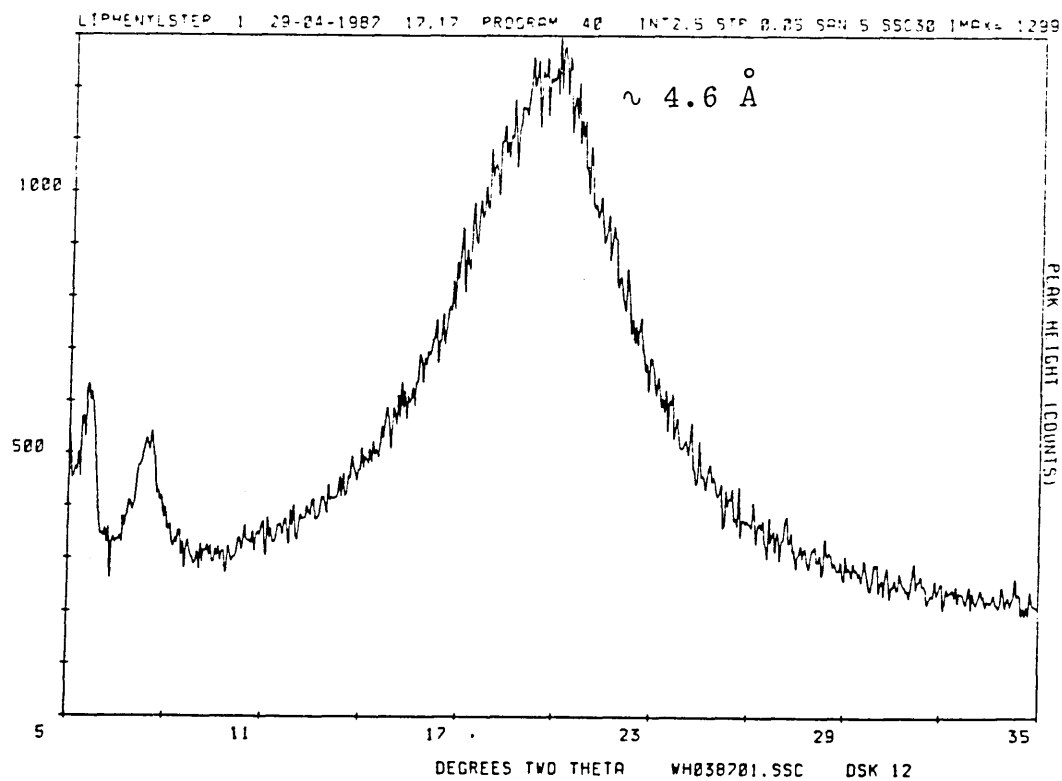


FIG. 35 : High-angle x-ray diffraction pattern obtained from anhydrous lithium phenylstearate at 27 °C

\* (i) The above data was obtained from a single experiment using samples which gave DSC results as tabulated in Sections 3.3.1.1 and 3.3.1.2. The precision limits on these values are of the order of  $\pm 0.3 \text{ \AA}$ , due to the broadness of the Bragg peaks.

(ii) The diffraction pattern for a slightly less pure sample of LiPS was also consistent with a structure having 2-d hexagonal symmetry. The  $d_1$  Bragg spacing was  $32.5 \text{ \AA}$ .

These results are consistent with structures having two-dimensional hexagonal symmetry. For a soap in the anhydrous state, a reversed hexagonal structure (containing rod-like aggregates with a polar core dispersed in a hydrocarbon continuum) is the most favourable (FIG. 3, p 13 ).

#### 3.3.4.2

From the results presented in TABLE 12, the structural parameters,  $a$  (hexagonal lattice parameter),  $n$  (the number of polar groups per unit length of rod),  $r_c$  (radius of the cylindrical-shaped aggregates) and  $S$  (the interfacial area per polar group) were calculated for LiPS and NaPS using the equations given in Section 2.2.4.3. The calculated values are given in TABLE 13.

TABLE 13 : Calculated structural parameters for the reversed hexagonal phases of anhydrous LiPS and NaPS at 27 °C\*

Sample	$a/(\text{Å})$	$n/(\text{ion } \text{Å}^{-1})$	$r_c(\text{Å})$	$S(\text{Å}^2)$
LiPS	35.9	1.82	4.8	16.5
NaPS	36.7	1.87	7.1	23.9

\* The following points should be noted:

- (i) In calculating  $n$ , the values used for the densities,  $\delta$ , of LiPS and NaPS were those determined by Honig and Singleterry [179] ( $0.991 \text{ g.cm}^{-3}$  and  $1.020 \text{ g cm}^{-3}$  respectively at  $25^\circ\text{C}$ ).
- (ii) In calculating  $r_c$ , the molar volume of the polar groups,  $V_{\text{pol}}$  ( $\text{Li}^+\text{COO}^-$  and  $\text{Na}^+\text{COO}^-$ ) were calculated by difference using the following expression [120, 123, 124],

$$V_{\text{soap}} = V_{\text{pol}} + n - 2 (V_{\text{CH}_2}) + V_{\text{CH}_3} \quad (3.1)$$

Based on DSC, polarizing microscopy and counter-ion NMR data, the polar groups of both LiPS and NaPS are considered to be in a quasi-crystalline, rather than a fused, state at room temperature. Therefore in calculating  $V_{\text{pol}}$  for the two soaps, the values of  $V_{\text{soap}}$ ,  $V_{\text{CH}_2}$  and  $V_{\text{CH}_3}$  substituted

into equation (3.1) are known values corresponding to the crystalline state.

$V_{\text{soap}}$  values were calculated from soap density values determined dilatometrically by Benton et al [79] for lithium and sodium stearate at 25°C (1.04 g cm<sup>-3</sup> and 1.00 g cm<sup>-3</sup> respectively).

The value of  $V_{\text{CH}_2}$  used (14.0 cm<sup>3</sup> mol<sup>-1</sup>) is the value obtained by Von Sydow [306] for the crystalline B-form of stearic acid with orthorhombic packed chains.

$V_{\text{CH}_3}$  (31.6 cm<sup>3</sup> mol<sup>-1</sup>) was calculated from the difference in molar volumes of two crystalline n-alkanes, eicosane (C<sub>20</sub>H<sub>42</sub>) and triacontane (C<sub>30</sub>H<sub>62</sub>) at 20°C [307].

The values of  $V_{\text{pol}}$  thus calculated were 23.6 cm<sup>3</sup> mol<sup>-1</sup> for Li<sup>+</sup>COO<sup>-</sup> and 50.8 cm<sup>3</sup> mol<sup>-1</sup> for Na<sup>+</sup>COO<sup>-</sup>.

- (iii) Due to the assumptions and approximations made in the calculation of  $V_{\text{pol}}$ , one might expect significant errors in the values of both  $r_c$  and S.

The value of  $r_c$  for LiPS is, however, comparable to those calculated by Spegt and Skoulios for the high temperature reversed hexagonal mesophases of some anhydrous divalent soaps (magnesium, 3.2 ± 0.3 Å [118], calcium 3.6 Å [120], and cadmium, 4.1 ± 0.2 Å [124]). The value of S

for LiPS is significantly lower than the value of  $22.1 \text{ \AA}^2$  calculated by Gallot and Skoulios [19] for the crystalline lamellar structure of lithium stearate at  $25^\circ\text{C}$ . This may be expected for a reversed hexagonal structure in which the polar groups are also in a "crystalline" state.

By comparison, the  $r_c$  and S values calculated for NaPS appear to be unreasonably large (the value of S for the crystalline lamellar structure of sodium stearate at room temperature is  $23 \text{ \AA}^2$  [114]). This may be due to a difference in the bonding of the polar groups of LiPS and NaPS (possibly resulting from the presence of traces of water in the "polar core" of the NaPS aggregates) or alternatively to errors introduced in the calculation of  $V_{\text{pol}}$  as a result of inaccurate soap density values.

#### 3.3.4.3

A variable temperature low-angle x-ray diffraction study of anhydrous LiPS was also carried out in order to investigate changes in structure and/or structural parameters with increasing temperature.

The results indicated that over the temperature range from  $28^\circ\text{C}$  to  $270^\circ\text{C}$ , the reversed hexagonal structure of LiPS was maintained (as evidenced by the continued presence of the  $1/\sqrt{3}$  and  $1/\sqrt{4}$  spacings at both  $190^\circ\text{C}$  and  $240^\circ\text{C}$ ) but that important structural modifications

occurred at the first-order H2 and H3 transitions detected calorimetrically. TABLE 14 shows the variation of both  $d_1$ , the Bragg spacing corresponding to the innermost reflection, and the hexagonal lattice parameter,  $a$ , with temperature.

TABLE 14 : Variation of the long spacing,  $d_1$ , and the hexagonal lattice parameter,  $a$ , of anhydrous LiPS with temperature

T/(°C)	$d_1$ /(Å)	$a$ /(Å)
28	31.1	35.9
100	31.2	36.0
120	31.3	36.1
140	31.3 + 27.2	36.1 to 31.4
155	27.4	31.6
175	27.7	32.0
190	27.9	32.2
210	28.1	32.4
220	27.1	31.3
240	26.4	30.5
270	26.6	30.7

The temperature dependence of the hexagonal lattice parameter,  $a$ , has also been presented graphically (FIG. 36). The transition temperatures for the H2 and H3 DSC transitions are represented on the graph by vertical bands covering the temperature range from the onset of each transition to the point of 50% completion.

These results show a gradual small increase in " $a$ " across the temperature range, caused by a thermal expansion of the hexagonal lattice, and abrupt decreases in " $a$ "

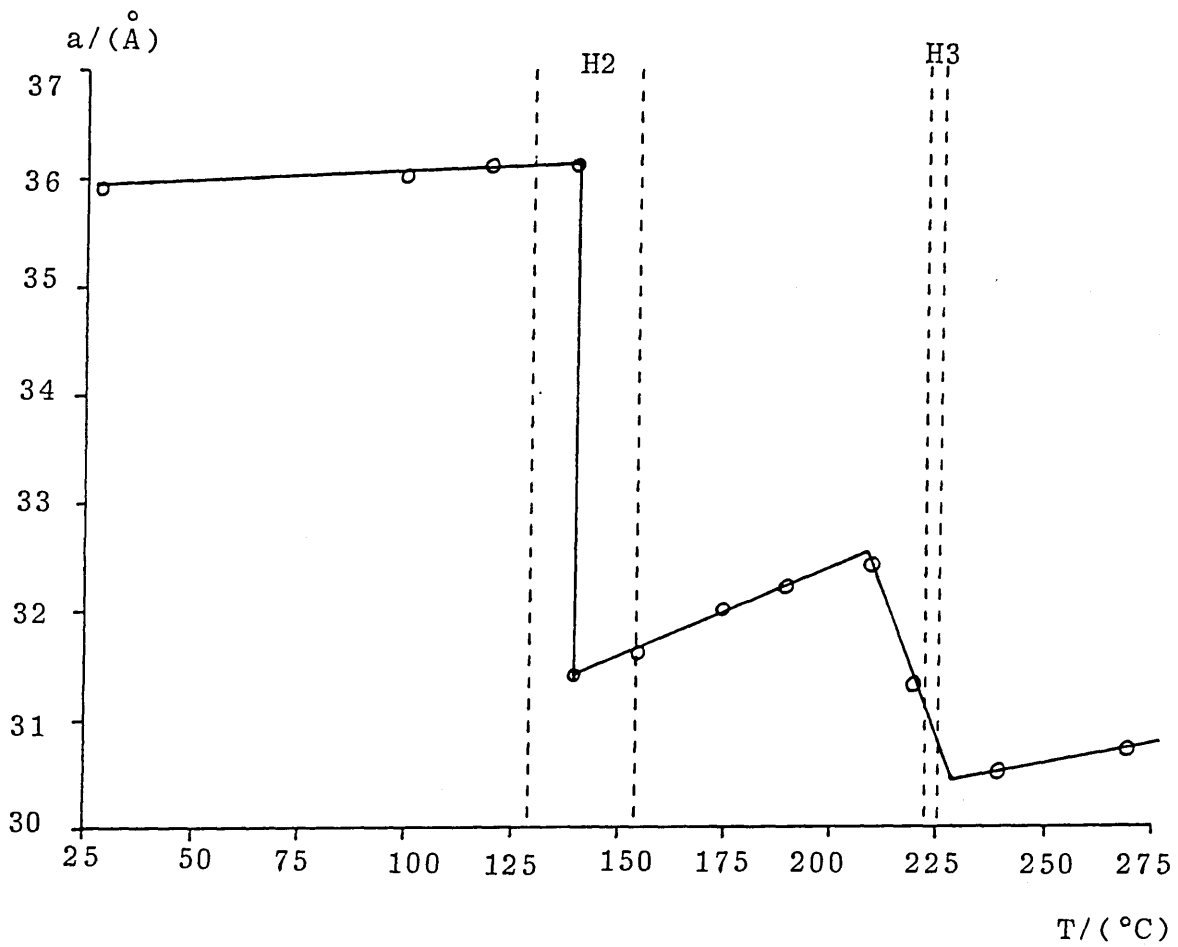


FIG. 36 : Variation of the hexagonal lattice parameter,  $a$ , of anhydrous lithium phenylstearate with temperature

corresponding to the DSC transitions between 130°C and 154.8°C (H2) and 224.0°C and 227.0°C (H3). The decreases in "a" correspond to decreases in the centre to centre distance of the "polar cylinders" i.e. the cylindrical aggregates move closer together, suggesting that the hydrocarbon chains become progressively more disordered at these transitions. In these terms the H2 transition is the more significant with a decrease in "a" of  $\sim 4.1 \text{ \AA}$ . The change in "a" at transition H3 of LiPS is comparable in size to that observed by Spegt and Skoulios [118] for anhydrous magnesium stearate at a transition between two reversed hexagonal phases ( $H_1$ ,  $a = 30.4 \text{ \AA}$  at 190°C;  $H_2$ ,  $a = 28.9 \text{ \AA}$  between 195°C and 210°C) suggesting a similar structural change. It is interesting to note that for anhydrous calcium stearate [120], which only forms a single reversed hexagonal phase, there are no abrupt decreases in "a" but only a gradual increase from 27.15  $\text{\AA}$  at 195°C to 27.8  $\text{\AA}$  at 270°C.

The value of S for the reversed hexagonal phase of calcium stearate (calculated from the values of  $r_c$  and n reported by Spegt and Skoulios [120] using equation (2.10), p 84) is 42.4  $\text{\AA}^2$  at 240°C whereas for the lower temperature  $H_1$  phases of both magnesium stearate [118] and cadmium stearate [124] the calculated values of S are only 31.1  $\text{\AA}$  and 33.8  $\text{\AA}$  respectively at 150°C. This suggests that for the stearates of magnesium and cadmium, the low temperature hexagonal phases formed at 109°C and 99°C respectively, may contain the polar groups in a more compact quasi-crystalline state, whereas in

the higher temperature hexagonal phases formed at 195°C and 211°C respectively (plus the single high temperature hexagonal phases of both calcium stearate and strontium stearate, formed at 170°C and 246°C respectively) the polar groups may be fused. Additional evidence for the different states of the polar groups in the reversed hexagonal phases of these divalent soaps is given in [reference 2, p 246-247].

Any corresponding changes in  $n$ ,  $r_c$  and  $S$  with temperature could not be determined since the temperature dependence of the density,  $\delta$ , of LiPS is not known and was not determined.

### 3.3.5 Discussion

#### 3.3.5.1

Anionic soaps and surfactants in which the lipophilic groups are of a non-compact, branched type frequently do not crystallize and the pure anhydrous salts exist as mesophases, apparently of the "fused" type, at room temperature [123, 133-136]. The best known of this type of mesogen is Aerosol OT which exists as a reversed hexagonal mesophase at room temperature [134], (FIG 4, p 16).

High and low-angle x-ray diffraction studies of anhydrous LiPS and NaPS suggest a similar type of mesomorphic behaviour at room temperature.

### 3.3.5.2

The conformationally disordered nature of the lipophilic chains at room temperature (as indicated by the diffuse 4.6 Å reflection in the high-angle x-ray diffraction pattern) is supported by DSC results. Low temperature investigations revealed the existence of a reversible second-order "glass-type" transition for both LiPS and NaPS at approximately -50°C [308, 309]. This transition occurs at a similar temperature to the major melting endotherm of the isomeric phenylstearic acid mixture (-57.3°C) and is therefore considered to involve "crystallization" of the hydrocarbon chains. True crystallization of the soap chains cannot take place because of steric hindrance considerations due to the isomeric nature of the acid. The glass so formed at this transition (H1) is therefore not crystalline but is effectively a "frozen" liquid chain configuration. This is further supported by <sup>7</sup>Li linewidth values which are invariant at this transition as expected for a transition primarily involving the hydrocarbon chain moieties of the soap molecules and not the polar groups. <sup>1</sup>H broad-line NMR investigations (line-width and/or second moment) could be used to confirm the nature of this transition.

### 3.3.5.3

Whether, however, the polar groups of LiPS and NaPS can be considered as "crystalline" or "fused" is less clear from x-ray diffraction results alone. DSC studies,

however, revealed a series of first-order transitions between room temperature and the isotropic melts of both LiPS and NaPS. Such behaviour, involving transitions of high enthalpy, would not be expected for compounds existing as fused mesophases. For example, we found, using DSC (heating rate,  $10^{\circ}\text{C min}^{-1}$ ) and polarizing microscopy, that Aerosol OT (supplied by Fluka AG, Switzerland, > 99% purity) undergoes only one endothermic transition on heating from room temperature, at  $\sim 160^{\circ}\text{C}$ , corresponding to a reversed hexagonal mesophase to isotropic liquid melt ( $\Delta H \sim 1.0 \text{ kJ mol}^{-1}$ ). Since it has been established that the hydrocarbon chains of both LiPS and NaPS are essentially in a "liquid-like" state at room temperature, these transitions have been attributed to a polymorphism of the respective polar groups which we consider to be in a quasi-crystalline state at the lower temperatures. (A similar thermotropic polymorphism of the polar groups is known to occur for the corresponding stearate and oleate soaps at elevated temperatures). The "crystalline" state of the polar groups of both LiPS and NaPS at room temperature is supported by  $^7\text{Li}$  and  $^{23}\text{Na}$  NMR linewidth values.

This behaviour may be explained by considering the nature of the amphiphiles involved. Substitution of the planar phenyl group on the fatty acid chain has been found not to occur at positions close to the polar groups (Section 1.2.3.1). One would, therefore, expect no unfavourable steric repulsions between the substituted chains close to the polar groups at the lower temperatures

which would prevent their sufficiently close lateral approach for crystallization to occur. In the anhydrous state, the polar groups of LiPS and NaPS may be held together by Coulombic forces and by co-ordination bonds between the alkali metal ion and the two equivalent carboxylate ion oxygens. This bonding was suggested by Little and Singleterry [180] for the postulated linear polymeric structure of the alkali metal phenylstearates in benzene (FIG. 8, p 35). For the solvent-free, anhydrous soaps the micellar aggregates constituting the hexagonal phases may be envisaged to result from a grouping of a number of these polymer-like chains into "cylinders" possessing polar cores. The room temperature structures of both LiPS and NaPS will therefore be referred to as semi-crystalline reversed hexagonal phases (denoted SCH 1).

#### 3.3.5.4

The H2 transition observed for LiPS by DSC may therefore be attributed to a polymorphic rearrangement of the quasi-crystalline polar groups to a second semi-crystalline reversed hexagonal phase (SCH 2). This is supported by the pronounced decrease in the  $^7\text{Li}$  NMR linewidth value. X-ray diffraction results suggest that this transition is also accompanied by a significant increase in the disorder of the hydrocarbon chains. The phenylstearate chains, which although broadly speaking are disordered at room temperature, are considered to be necessarily ordered to some degree near to the "crystalline" polar groups at the lower temperatures (as for the ribbon

structures of the straight-chain alkali metal soaps). The H2 and H5 DSC transitions of NaPS may also be attributed to polymorphic changes involving the polar groups. It is interesting to note that, as for  $\text{NaC}_{18}$  and  $\text{LiC}_{18}$ , NaPS exhibits a greater number of polymorphic transitions than the corresponding lithium soap.

#### 3.3.5.5

For LiPS and NaPS, transition H3 has been observed to occur at almost identical temperatures, and with very similar enthalpies, to a corresponding transition of the straight-chain lithium and sodium stearates. For the stearates, this transition involves a change from a semi-crystalline ribbon phase to a liquid crystalline lamellar phase and therefore involves a fusion of the polar groups. For LiPS and NaPS, the fusion of the polar groups, at  $227.0^\circ\text{C}$  and  $259.0^\circ\text{C}$  respectively, represents a transition from the semi-crystalline reversed hexagonal phase (SCH 2) to a conventional fused reversed hexagonal mesophase (commonly denoted  $\text{H}_2$  or  $\text{M}_2$ ). Polarizing microscopy studies have confirmed the formation of a fused hexagonal mesophase. X-ray diffraction and NMR linewidth results for LiPS are also consistent with this structural change.

### 3.3.5.6

The thermal stabilities of the anhydrous H<sub>2</sub> mesophases of LiPS and NaPS ( $\sim 143.6^\circ\text{C}$  and  $\sim 153.9^\circ\text{C}$  respectively) exceed by far those of the thermotropic lamellar mesophases of LiC<sub>18</sub> and NaC<sub>18</sub> ( $\sim 1.2^\circ\text{C}$  and  $\sim 25^\circ\text{C}$  [53, 55] respectively). Assuming a similar bonding of the polar groups in these two mesophases, then the increased thermal stability of the phenylstearates may be explained in terms of a greater average separation between highly disordered neighbouring chains, allowed by the curvature of the "cylindrical" aggregates in the reversed hexagonal phase, than by the planar double-layers of the lamellar phase. The reason why pure, straight-chain alkali metal soaps do not themselves form reversed hexagonal mesophases is probably that volume filling by n-alkyl chains diverging round a cylindrical core of CO<sub>2</sub><sup>-</sup> M<sup>+</sup> groups would involve geometrical difficulties.

The enthalpy of the final transition observed by DSC for both LiPS and NaPS (H4) is of the order expected for a liquid crystal to isotropic melt and is almost identical to that observed for the reversed hexagonal mesophase melt of Aerosol OT.

4.1 The Lithium Stearate-n-Hexadecane and Lithium Stearate-Squalane Systems

Equilibrium phase diagrams were constructed for lithium stearate ( $\text{LiC}_{18}$ ) in both n-hexadecane (cetane) and squalane (2,6,10,15,19,23-hexamethyltetracosane). The major first-order phase boundaries were determined by the differential scanning calorimetry analysis of soap-oil samples which had been homogenized as outlined in Section 2.1.5. Macroscopic visual observations in polarized light and polarizing microscopy observations supplemented the DSC data. When the phase boundary between different phases is first-order, one expects to find a two-phase region. The experimental techniques used in this study, however, could not always distinguish these narrow regions with certainty, making an accurate delineation difficult. For the most part, they have been omitted from the phase diagrams.

4.1.1 Differential Scanning Calorimetry

The thermograms recorded on heating both  $\text{LiC}_{18}$ -n-hexadecane and  $\text{LiC}_{18}$ -squalane mixtures of varying composition were each characterized by four reversible first-order endothermic transitions. These transitions, denoted H1, H2, H3 and H4 in order of increasing temperature (see FIGS. 37 and 38), were found to be continuous with certain transitions observed calorimetrically for the solvent-free soap itself (Section 3.1.1).

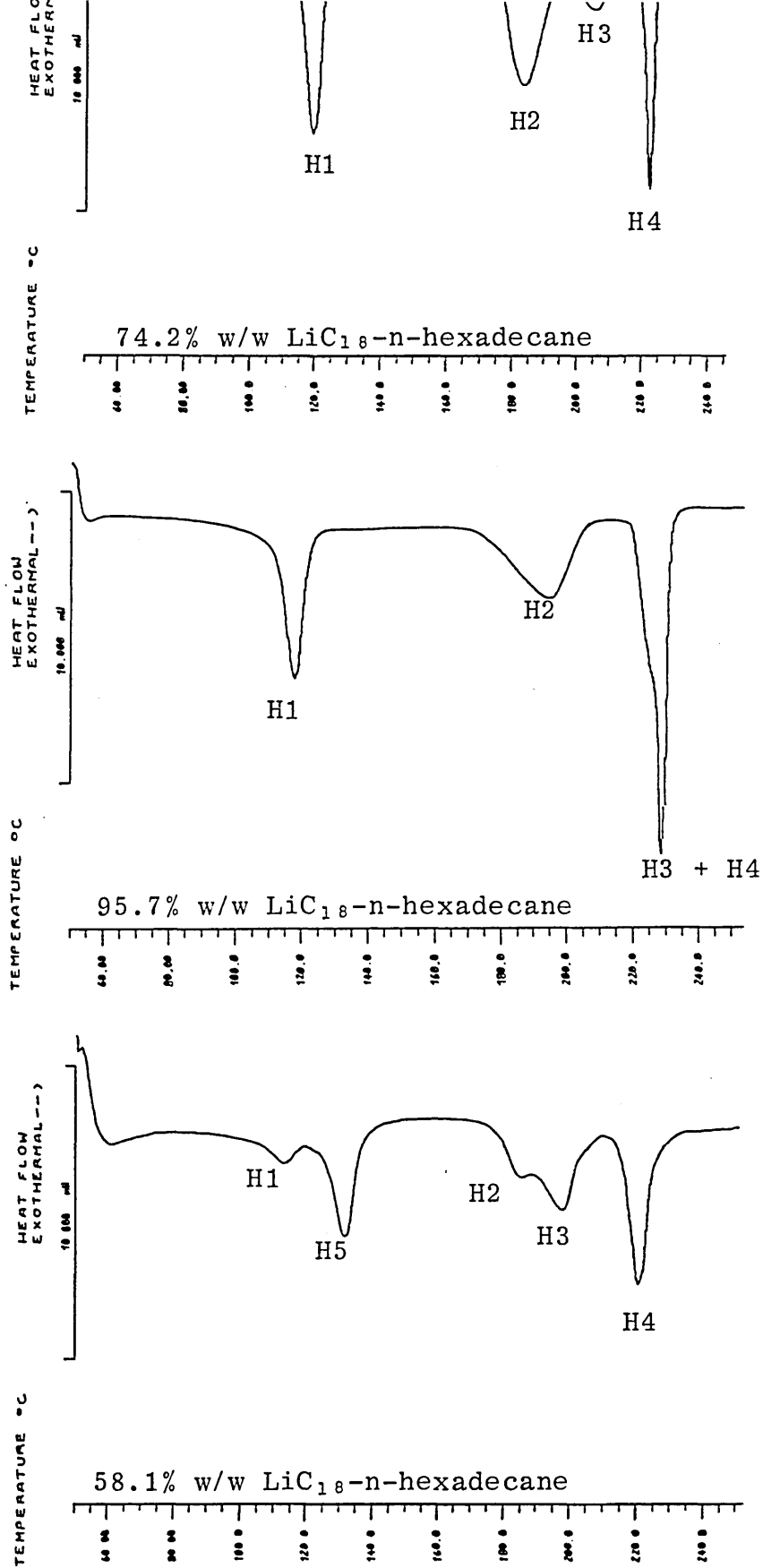


FIG. 37 : DSC heating thermograms for lithium stearate-n-hexadecane samples of varying composition (heating rates :  $5\text{ }^{\circ}\text{C min}^{-1}$ )

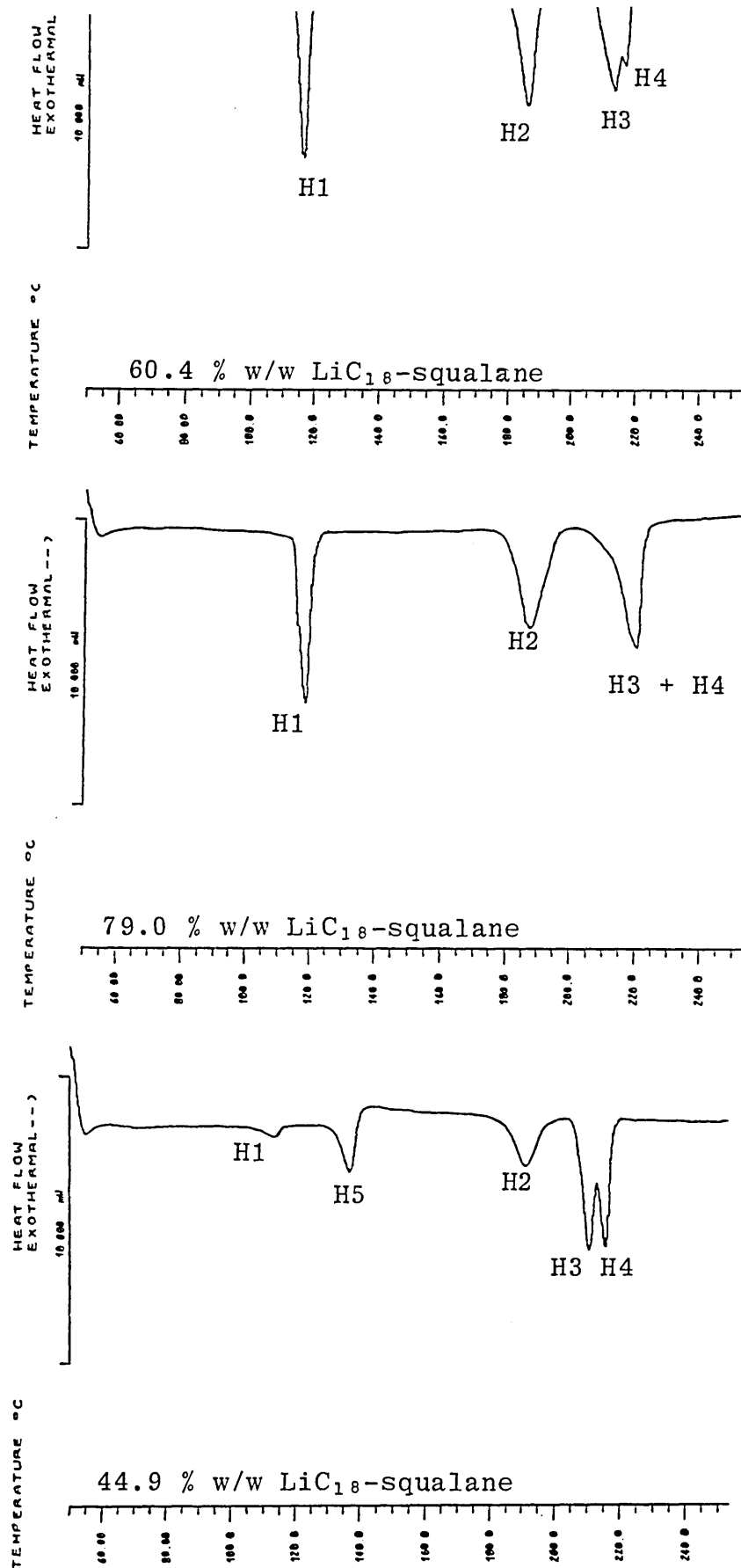


FIG. 38 : DSC heating thermograms for lithium stearate-squalane samples of varying composition (heating rates :  $5\text{ }^{\circ}\text{C min}^{-1}$ )

The temperature values obtained for these transitions at heating rates of  $5^{\circ} \text{C min}^{-1}$  are recorded in TABLES 15 and 17 as a function of sample composition. (For samples containing 2.3 mole % soap in n-hexadecane and 4.1 mole % soap in squalane, the tabulated transition temperatures were obtained using a heating rate of  $10^{\circ} \text{C min}^{-1}$ ). These values represent the mean values calculated from two or three independent heating runs at each composition. Because these temperatures were readily reproducible to within  $\pm 1^{\circ}\text{C}$  and were essentially independent of the heating rate they are considered to be equilibrium values. For the 100 mole %  $\text{LiC}_{18}$  sample, the temperature values tabulated correspond to those determined in Section 3.1.1. It should be noted that whereas the H1 and H2 transitions in both hydrocarbon systems correspond to the equivalent transitions of the solvent-free soap, the H3 and H4 transitions in these binary systems correspond to the H5 and H7 transitions of solvent-free  $\text{LiC}_{18}$ . This will be discussed in Section 4.1.4.

The corresponding phase transition enthalpies for the two hydrocarbon systems (calculated as KJ per mole of soap) are recorded in TABLES 16 and 18. The precision limits on these values are of the same order of magnitude as those indicated for the solvent-free soap (100 mole % soap). Where successive peaks overlapped and could not be resolved individually, the enthalpy values have been tabulated as the sum of these transitions

For the more concentrated soap-oil mixtures, only three distinct endotherms were observed on heating with the peak corresponding to the H3 transition concealed beneath the H4 peak (indicated by the magnitude of  $\Delta H$  for the final peak on heating and the re-appearance of this transition on cooling due to supercooling effects). The temperature values tabulated for the H3 transition of these samples therefore corresponds to the approximate point of first deviation from the steady baseline at the onset of H4.

On occasions, both  $\text{LiC}_{18}$ -n-hexadecane and  $\text{LiC}_{18}$ -squalane samples exhibited an additional endothermic transition on heating (denoted H5) at  $128.6 \pm 0.7$  °C and  $136.3 \pm 0.7$  °C respectively (see FIGS. 37 and 38). A similar transition (though considered to be possibly second-order in nature) has been observed by Vold and Vold [195] at  $\sim 140$  °C using differential thermal analysis in both the  $\text{LiC}_{18}$ -n-hexadecane and  $\text{LiC}_{18}$ -decalin systems.

The enthalpy of the H5 transition was not constant and varied from as little as  $0.6 \text{ kJ mol}^{-1}$  to  $8.7 \text{ kJ mol}^{-1}$ . As its value increased in size, a decrease was observed in the enthalpies of both H1 and H2, and vice versa. (Such samples were therefore not used for the calculation of the phase transition enthalpies recorded in TABLES 16 and 18). The temperatures of the H1 and H2 transitions were also affected with H1 occurring at a slightly lower temperature and H2 at a slightly higher temperature than

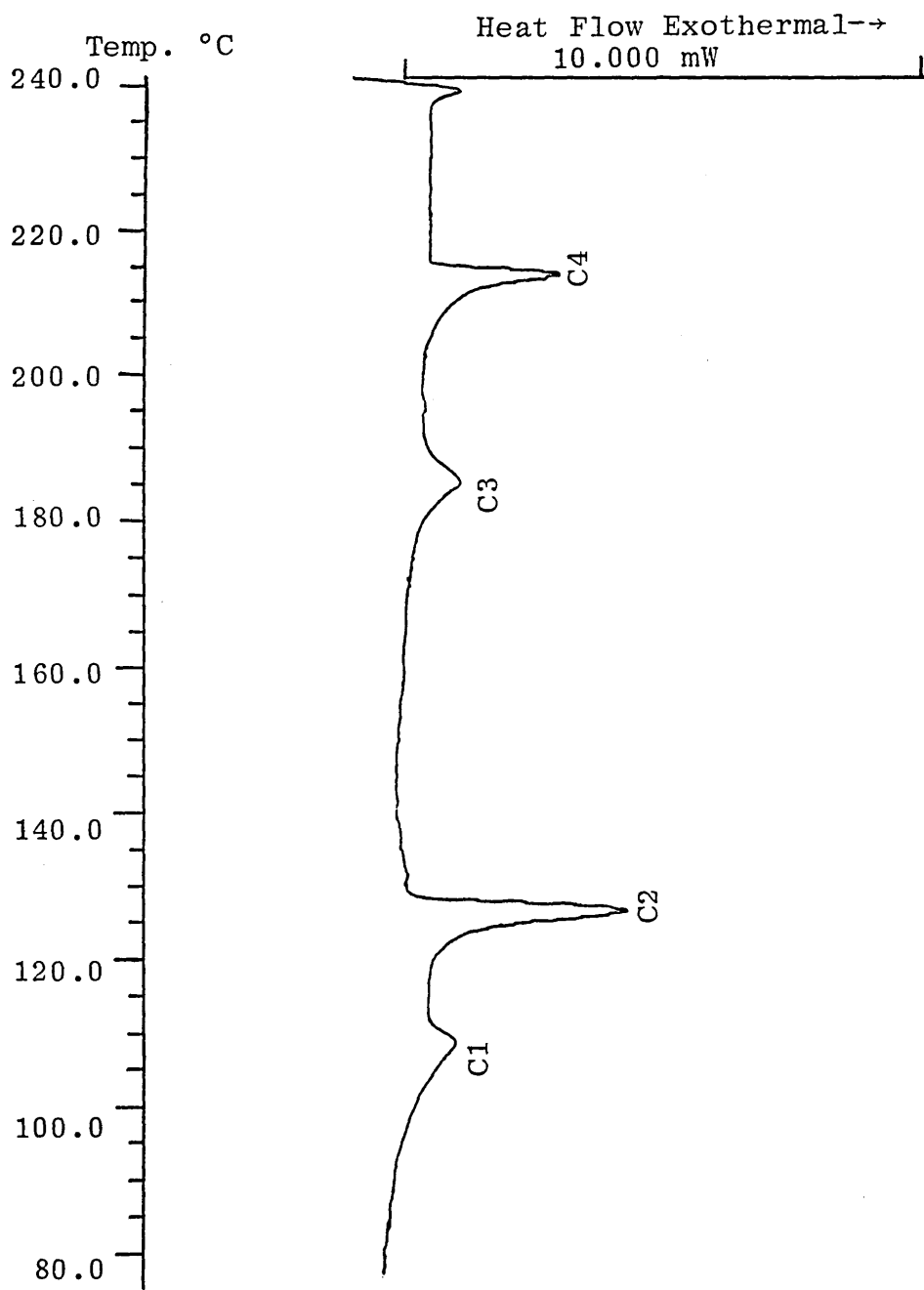


FIG. 39 : DSC cooling thermogram for a 60.4 % w/w lithium stearate-squalane sample (cooling rate : 3 °C min<sup>-1</sup>)

the mean values calculated for fully equilibrated samples. These samples have been marked in TABLES 15 and 17 with an asterisk. FIG. 39 shows the cooling thermogram obtained at a rate of  $3\text{ }^{\circ}\text{C min}^{-1}$  for a 68.9 mole %  $\text{LiC}_{18}$  in squalane sample. This trace is typical of all  $\text{LiC}_{18}$ -hydrocarbon samples studied and is similar to that exhibited by the solvent-free soap itself (FIG. 23 p 141). Whereas the H4, H3 and H1 transitions show only limited supercooling effects, the H2 transition is supercooled extensively and occurs at a temperature similar to that of the non-equilibrium H5 transition. The interdependence of the H1, H2 and H5 enthalpies probably reflects the varying degrees of incomplete crystallization of the samples after high temperature mixing and quench-cooling. The H5 transition may therefore be attributed to the presence of a metastable partly crystalline solid-soap phase containing some proportion of the supercooled higher temperature H2 phase. This transition has therefore been omitted from the equilibrium phase diagrams.

#### 4.1.1.1 The Lithium Stearate-n-Hexadecane System

See overleaf for Table 15.

TABLE 15 : Phase transition temperatures for the  
lithium stearate-n-hexadecane system

LiC <sub>18</sub> CONTENT		H1	H2	H3	H4
wt %	mole %	T/(°C)	T/(°C)	T/(°C)	T/(°C)
3.0	2.3	110.1	177.2	188.6	203.5
10.1	8.0	114.1	178.8	188.2	203.3
19.8*	16.1*	112.0	179.8	188.9	203.9
27.0	22.4	115.4	180.4	190.1	205.5
34.4	29.0	113.2	178.4	190.2	208.3
45.1	39.1	114.7	179.8	191.2	211.7
55.0	48.8	114.0	178.2	192.8	213.5
58.1*	51.9*	111.5	180.2	194.6	217.1
66.3	60.6	114.6	177.7	193.6	215.6
69.1*	63.5*	111.6	179.8	198.0	222.9
74.2	69.2	115.5	179.9	206.2	223.9
79.3*	75.0*	111.9	181.3	209.7	224.3
84.9	81.4	113.5	177.5	217.1	225.2
89.7	87.1	114.3	177.6	221.4	225.7
93.4	91.7	114.4	184.0	~ 223	225.8
95.7	94.5	115.6	194.0	~ 224	226.9
100.0	100.0	116.3	202.7	~ 225	227.7

\*These samples exhibited an additional endothermic transition (H5). Refer to text for explanation.

TABLE 16 : Phase transition enthalpies for the lithium-  
stearate-n-hexadecane system

LiC <sub>18</sub> CONTENT		H1	H2 + H3	H4
wt %	mole %	$\Delta H / (\text{kJ mol}^{-1})$	$\Delta H / (\text{kJ mol}^{-1})$	$\Delta H / (\text{kJ mol}^{-1})$
10.1	8.0	15.1	23.5	8.1
27.0	22.4	9.3	21.3	6.1
34.4	29.0	10.6	27.5	8.6
45.1	39.1	14.1	24.1	8.1
55.0	48.8	12.3	29.6	9.1
66.3	60.6	12.7	25.5	8.2
74.2	69.2	12.7	25.6	8.7
84.9	81.4	12.1	24.5	7.6
LiC <sub>18</sub> CONTENT		H1	H2	H3 + H4
wt %	mole %	$\Delta H / (\text{kJ mol}^{-1})$	$\Delta H / (\text{kJ mol}^{-1})$	$\Delta H / (\text{kJ mol}^{-1})$
89.7	87.1	11.0	14.4	18.5
93.4	91.7	12.1	14.9	18.7
95.7	94.5	10.0	12.8	19.2
100.0	100.0	14.7 ± 0.7	19.1 ± 0.9	19.7 ± 0.7

4.1.1.2 The Lithium Stearate-Squalane System

TABLE 17 : Phase transition temperatures for the  
lithium stearate-squalane system

LiC <sub>18</sub> CONTENT		H1	H2	H3	H4
wt %	mole %	T/(°C)	T/(°C)	T/(°C)	T/(°C)
2.8	4.1	112.6	189.4	207.2	209.7
9.9*	13.8*	113.1	187.2	205.8	210.8
19.7*	26.4*	113.9	189.1	207.3	212.3
28.6	36.8	115.8	186.7	208.0	212.0
29.5	37.9	114.9	185.4	208.3	212.4
36.9	46.0	115.4	187.4	208.9	212.7
38.4	47.6	116.0	185.1	209.6	213.2
44.9*	54.3*	112.4	190.6	209.1	214.5
49.2	58.5	114.2	185.9	209.3	215.5
52.8*	62.0*	113.5	188.2	208.7	215.0
53.1	62.2	116.0	185.5	210.0	214.1
60.4	68.9	114.7	185.0	211.9	216.3
70.2	77.4	116.2	186.0	214.4	218.3
79.0	84.6	116.7	185.9	~ 217	219.7
86.3	90.2	114.5	189.5	~ 223	223.7
95.6	96.9	116.4	191.6	~ 225	225.7
100.0	100.0	116.3	202.7	~ 225	227.7

\*These samples exhibited an additional endothermic transition (H5). Refer to text for explanation.

TABLE 18 : Phase transition enthalpies for the lithium  
stearate-squalane system

LiC <sub>18</sub> CONTENT		H1	H2	H3 + H4
wt %	mole %	$\Delta H / (\text{kJ mol}^{-1})$	$\Delta H / (\text{kJ mol}^{-1})$	$\Delta H / (\text{kJ mol}^{-1})$
28.6	36.8	12.6	16.8	19.8
29.5	37.9	12.5	16.9	19.1
36.9	46.0	13.3	16.1	20.1
38.4	47.6	13.1	18.0	19.7
49.2	58.5	11.3	14.6	19.8
53.1	62.2	12.9	17.3	19.4
60.4	68.9	12.8	16.6	20.1
70.2	77.4	12.5	15.7	17.5
79.0	84.6	13.0	17.1	18.4
86.3	90.2	11.1	14.1	19.0
95.6	96.9	11.7	15.0	16.7
100.0	100.0	$14.7 \pm 0.7$	$19.1 \pm 0.9$	$19.7 \pm 0.7$

#### 4.1.2 Macroscopic Visual Observations and Polarizing Microscopy

At room temperature the homogenized soap-hydrocarbon samples formed opaque white gels or solids depending on the LiC<sub>18</sub> concentration. For the more dilute soap samples, it was possible to distinguish regions of clear solvent which had separated by syneresis.

As the temperature of these samples was raised, no visible changes in either macroscopic or microscopic appearance were observed corresponding to the H1 DSC transition.

At the H2 transition, however, a marked decrease in sample opacity occurred to produce semi-translucent white wax-like samples. Between crossed polars, these bulk samples transmitted light with a dull orange colour. Microscopically they possessed very dull, non-specific patchy birefringent textures. On occasions, it was possible to observe increases in translucency within some bulk samples at temperatures well below the H2 transition. This translucency was, however, non-uniform and is thought to correspond to the non-equilibrium H5 transition observed for a number of soap-oil samples by DSC.

At higher temperatures, the H3 transition was accompanied by changes to a liquid-crystalline type behaviour. The bulk samples were now almost entirely transparent (slightly turbid) viscous liquids which transmitted light between crossed polars with a uniform intense golden colour. At the lowest soap concentrations, however, this birefringency became vanishingly dim. Microscopically these samples exhibited bright non-specific birefringent textures similar to those of the preceding "waxy" phase. No well-defined focal conic structures or other optical effects which could be associated with specific liquid crystal phases were observed.

The final H4 transition was accompanied in each case by a marked reduction in sample viscosity and a complete loss of birefringency to produce isotropic solutions.

Because a number of the higher temperature transitions frequently occurred within a narrow temperature range for the two systems studied (and because of temperature gradients within the oil bath and the possibility of some phase separation on initial mixing) it was often possible to observe a number of co-existing phases within the same bulk sample. Furthermore small quantities of free isotropic solution in the "waxy" and "liquid crystalline" matrices were not easy to identify positively macroscopically or microscopically. The determination of high temperature equilibrium two-phase regions was therefore not possible using these experimental techniques.

The phase changes observed at each of the reported transitions, though supercooled to varying extents, were reversible.

#### 4.1.3 The Equilibrium Phase Diagrams

The equilibrium phase diagrams constructed for the lithium stearate-n-hexadecane and lithium stearate-squalane systems are shown in FIGS. 40 and 41. The nomenclature used to describe the structure of phases occurring in these systems is that used previously for the phases of solvent-free lithium stearate (Section 3.1.3).

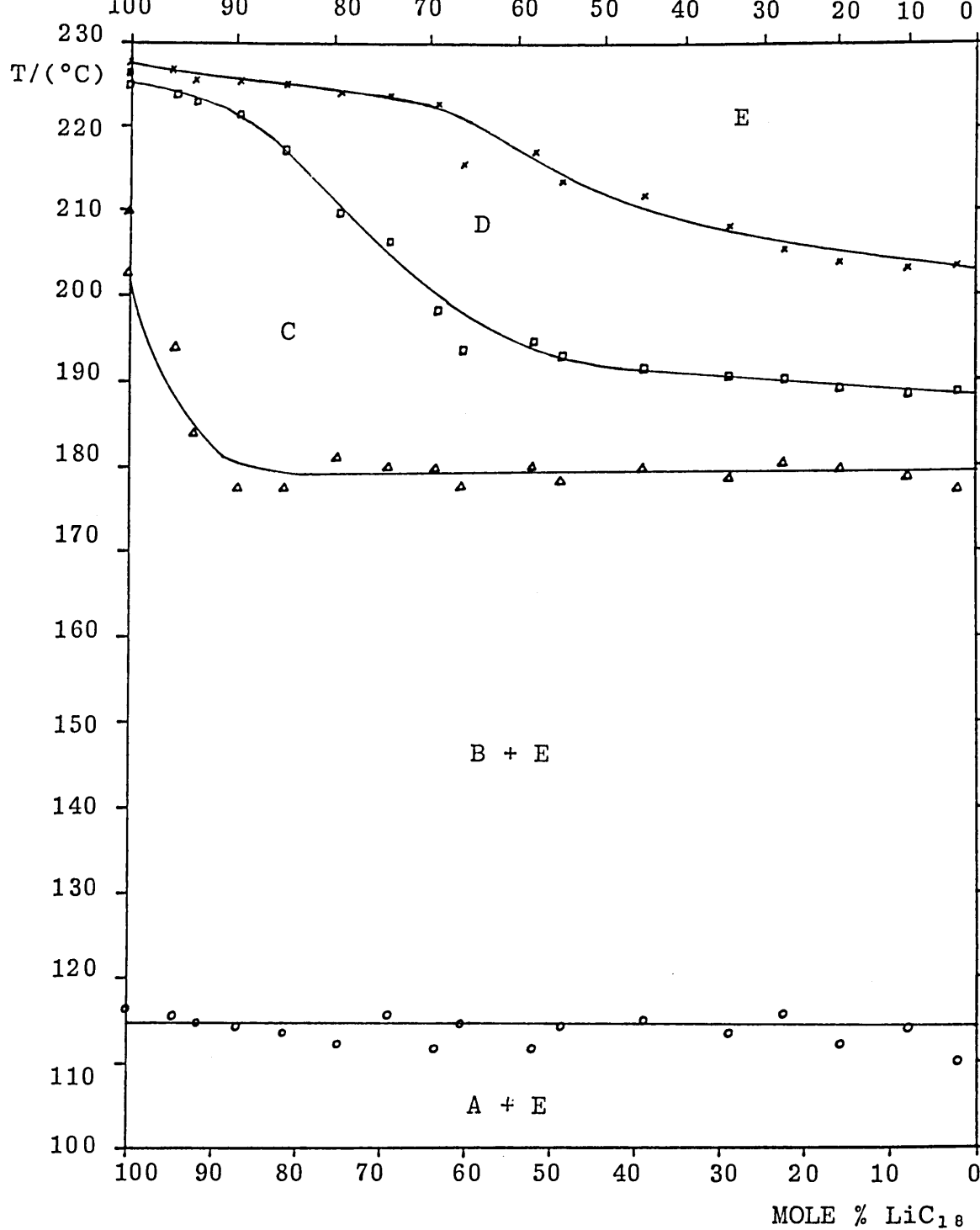


FIG. 40 ; An equilibrium phase diagram for the system  
LITHIUM STEARATE - n-HEXADECANE

A, crystalline  $\text{LiC}_{18}$  1; B, crystalline  $\text{LiC}_{18}$  2;  
C, waxy  $\text{LiC}_{18}$ ; D, subneat  $\text{LiC}_{18}$ ;  
E, isotropic solution

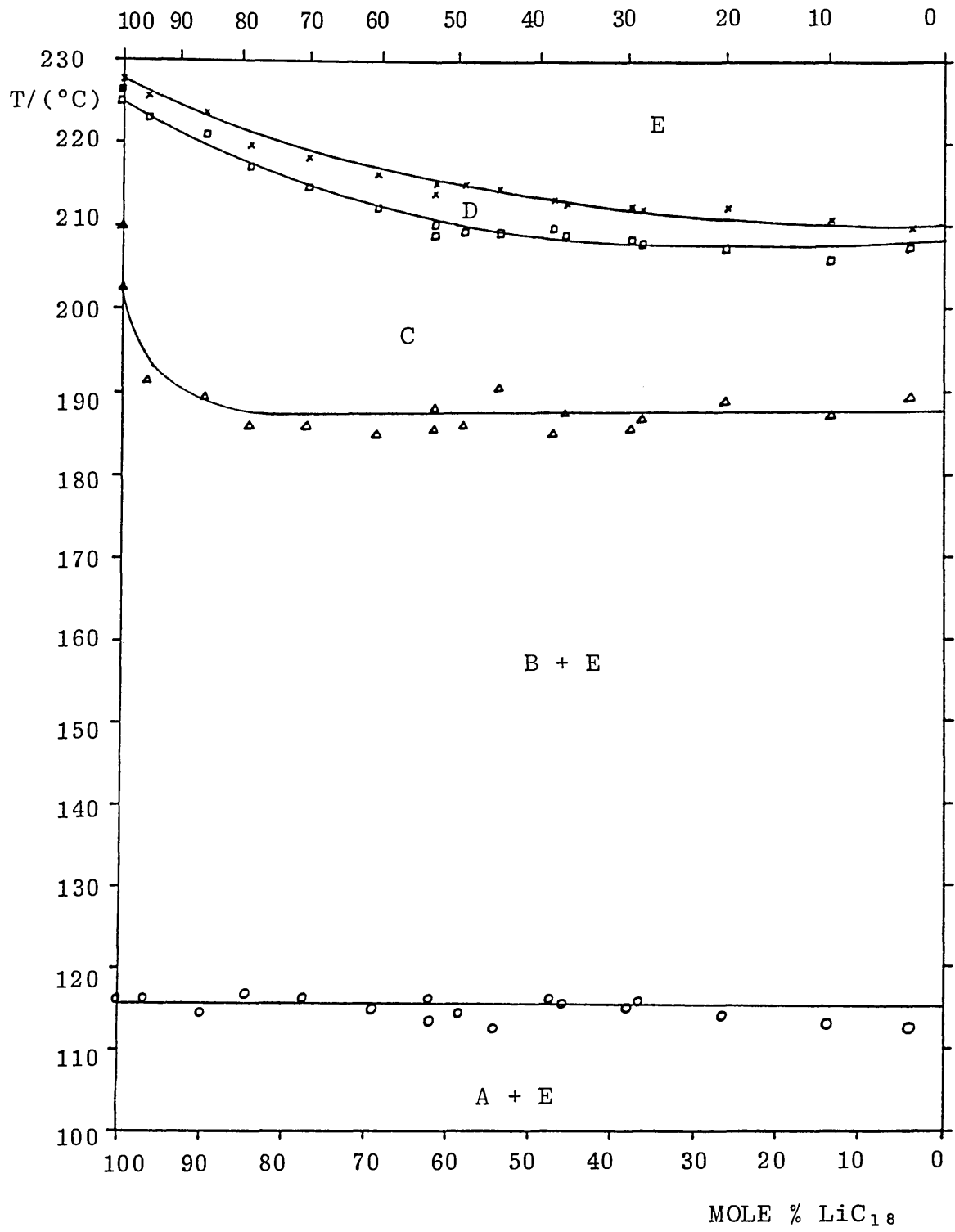


FIG. 41 : An equilibrium phase diagram for the system  
 LITHIUM STEARATE-SQUALANE  
 A, crystalline  $\text{LiC}_{18}$  1; B, crystalline  $\text{LiC}_{18}$  2;  
 C, waxy  $\text{LiC}_{18}$ ; D, subneat  $\text{LiC}_{18}$ ;  
 E, isotropic solution

#### 4.1.4 Discussion

The equilibrium phase diagrams for the lithium stearate-hydrocarbon systems (FIGS. 40 and 41) show that in each case the number and nature of the phases found is remarkably similar, with each soap-containing phase being continuous with a phase of the solvent-free soap itself. Apparently these solvents cannot overcome the ionic and coordination forces operating between the lithium carboxylate groups so the process of stepwise melting still exists even in the dilute hydrocarbon systems. Similar observations have been reported by Cox [196] and Uzu [61] for a number of different  $\text{LiC}_{18}$ -mineral oil and n-paraffin systems. It is interesting to note that the temperatures at which large amounts of hydrocarbons can be incorporated into the soap lattice correspond to the temperature range over which the inter-chain Van der Waals forces are overcome in sharply defined steps in the pure solvent-free soap.

At room temperature the cohesive forces operating between the soap molecules in the crystalline state are relatively unaffected by the hydrocarbon solvents (ie the lattice energy of the soap greatly exceeds the solvation free energy of the hydrocarbons) and lithium stearate may be considered to be practically insoluble in both n-hexadecane and squalane. (A typical value for the solubility of  $\text{LiC}_{18}$  in both n-heptane and isooctane at  $27^\circ\text{C}$  is of the order of  $4 \times 10^{-5} \text{ mol dm}^{-3}$  [143]). The negligible interaction between the crystalline LC 1 phase of lithium stearate and the two hydrocarbons was

shown by the failure of the solvents to significantly lower the temperature of the intercrystalline transition of the pure soap (H1) at any soap-oil concentration observed (mean values of  $114.1 \pm 1.5$  °C and  $115.3 \pm 1.2$  °C were calculated for the H1 transition in the n-hexadecane and squalane systems respectively, as compared to  $116.3 \pm 0.8$  °C for the solvent-free soap). It is interesting to note that for samples not exhibiting the non-equilibrium H5 transition, the mean enthalpy values of the intercrystalline H1 transition ( $12.0 \pm 1.7$  kJ mol<sup>-1</sup> in the n-hexadecane system and  $12.4 \pm 0.8$  kJ mol<sup>-1</sup> in the squalane system) were still significantly lower than that obtained for the solvent-free soap itself ( $14.7 \pm 0.7$  kJ mol<sup>-1</sup>). Similar findings were reported by Uzu [61] for the H1 transition of LiC<sub>18</sub> in systems containing n-docosane ( $7.74$  kJ mol<sup>-1</sup>) and n-octadecane ( $8.12$  kJ mol<sup>-1</sup>). He considered this to result from differences in the degree of crystallinity of the soap samples due to imperfect crystallization after high temperature mixing.

At higher temperatures, however, the transition from the crystalline LC 2 phase of lithium stearate to the waxy BR 1 phase (H2) was lowered from 202.7 °C at 100 mole % LiC<sub>18</sub> to 177.6 °C by as little as 12.9 mole % of n-hexadecane. Similarly in the squalane system this transition was lowered to 185.9 °C on addition of only 15.4 mole % hydrocarbon. The differences in the H2

transition temperatures of these two systems may be related to the entropy of mixing between the soap and solvent. This entropy contribution would lower the free energy of the system and in this instance appears to be greater for the smaller, straight-chain hydrocarbon, n-hexadecane.

It should be noted that no evidence of a transition to a second waxy phase, BR 2, (thought to occur at  $\sim 210$  °C in the pure soap) was observed at any soap-oil composition studied. The peaks corresponding to the H2 transition were symmetrical in each case and of lower enthalpy than that calculated for the solvent-free soap. These effects, however, were also observed on reheating samples of the solvent-free soap which had been previously fused (Section 3.1.1) and do not preclude the existence of a second higher temperature waxy phase.

The constancy of the H2 transition temperature in both hydrocarbon systems over most of the composition range ( $178.6 \pm 1.1$  °C between 12.9 mole % and 97.7 mole % n-hexadecane and  $186.2 \pm 1.3$  °C between 15.4 mole % and 95.9 mole % squalane) may indicate that the waxy phase (or phases) is capable of incorporating only limited quantities of these hydrocarbon solvents into its ribbon structures).

For the  $\text{LiC}_{18}$ -n-hexadecane system, Vold and Vold [195] reported that a waxy phase of  $\text{LiC}_{18}$ , stable between 185 °C and 224 °C, could dissolve nearly one mole of

n-hexadecane (cetane) per mole of soap (see FIG. 5 p 26 ).

It is also interesting to note that in an x-ray diffraction study of the  $\text{NaC}_{18}$ -n-tetradecane system, Skoulios [144] found that the subwaxy phase of  $\text{NaC}_{18}$  ( which may be isomorphous with the waxy BR 1 phase of  $\text{LiC}_{18}$ , as suggested by the similarity in unit cell dimensions of the respective ribbon structures of the solvent-free soaps [19,112,114]) could incorporate less than 5 wt. % tetradecane into its structure whereas the higher temperature waxy phase of  $\text{NaC}_{18}$  (which may be isomorphous with the waxy BR 2 phase of  $\text{LiC}_{18}$  [19,112,114]) could incorporate nearly 50 wt % tetradecane with the solvent penetrating into the most disordered regions of the ribbon structure. This resulted in the length 'a' of the rectangular centred lattice unit cell increasing with added hydrocarbon whilst the width 'b' remained constant, ie the swelling proceeded in a direction parallel to the ionic basal planes (see FIG. 1 p 7 ). (Additional evidence for the possible isomorphism of these phases is offered by the similarity in the magnitudes of  $\Delta H$  for the anhydrous soaps at the corresponding transitions. The sum of the individual enthalpies for the crystal to subwaxy (117 °C, 7.62 kJ mol<sup>-1</sup>) and the subwaxy to waxy (135 °C, 11.89 kJ mol<sup>-1</sup>) transitions of  $\text{NaC}_{18}$  ( $\Delta H_{\text{tot}} = 19.51 \text{ kJ mol}^{-1}$  [53]) is almost identical to the values obtained in this study (TABLE 2, p 99 ) for the sum of the crystal LC 2 to waxy BR 1 (at 202.7 °C) and the waxy BR 1 to waxy BR2 (at ~ 210 °C) transitions of  $\text{LiC}_{18}$  ( $\Delta H_{\text{tot}} = 19.1 \pm 0.9 \text{ kJ mol}^{-1}$ ).

In this present study, however, the position of the boundaries between the two waxy phases of  $\text{LiC}_{18}$  and the two-phase waxy-solution region could not be positively established using the experimental techniques employed. It is worthy to note that for a sample containing as little as 13.8 mole %  $\text{LiC}_{18}$  in squalane, no distinct phase separation between the waxy and solution phases was observed macroscopically during heating or cooling cycles.

The constancy of the H2 transition temperature in a number of  $\text{LiC}_{18}$ -hydrocarbon systems has led other workers [51, 196, 196] to suggest the presence of a possible eutectic system between the crystalline LC 2, waxy and solution phases (see FIG. 6, p 26). This was not proven experimentally, however, and is therefore not indicated on the present phase diagrams.

The next transition in both solvent systems was to a golden birefringent "liquid crystal"-type phase. This phase was also found to be continuous with a high temperature phase of the solvent-free soap. No evidence for the existence of a liquid crystal "phase island" as postulated by Vold and Vold [195] for the  $\text{LiC}_{18}$ -n-hexadecane (cetane) system between 41.5 mole % and 78 mole % soap and 190 °C and 222 °C (Section 1.2.2.2) was found. These results are therefore in agreement with those of Cox and co-workers [51,196]. The marked differences in phase behaviour may be attributed to the presence of traces of water in the Vold system [51, 189].

Only one peak, however, could be detected in each solvent system (H3) corresponding to the formation of a single "mesophase" despite the fact that two high temperature transitions, H5 and H6, are known to exist in the pure soap, corresponding to the formation of the subneat and neat phases respectively (Sections 3.1.3.4 and 3.1.3.5). The magnitude of  $\Delta H$  for the final transition to the isotropic liquid state in both solvent systems (H4) suggests, however, that the golden birefringent "liquid crystal" phase previously observed by Cox and co-workers [51, 196] and Vold and Vold [195] is probably a subneat, semi-crystalline ribbon-type phase. (An enthalpy of the order of  $1 \text{ kJ mol}^{-1}$  would be expected for the H4 transition involving a fused lamellar (neat) mesophase melt.) This is supported by the polarizing microscopy observations of this phase which detected no well-defined focal conic structures commonly associated with lamellar mesophases. (A structure for this "liquid crystal" phase, made up of "long chain-like aggregates of soap molecules" was postulated by Cox [196] based on DTA and polarizing microscopy studies of  $\text{LiC}_{18}$ -mineral oil systems). The bilayer structure of the lamellar mesophase, which is stable for only  $\sim 1 \text{ }^\circ\text{C}$  below the melt of the solvent-free soap (Section 3.1.3.5), may be de-stabilized on addition of hydrocarbon solvents which are capable of penetrating between the disordered soap hydrocarbon chains forcing the "fused" polar lattice apart.

In both systems studied, the solvent-swollen subneat phase was observed to extend to below 5 mole % soap. The DSC thermograms of the 2.3 mole %  $\text{LiC}_{18}$ -n-hexadecane sample and the 4.1 mole %  $\text{LiC}_{18}$ -squalane sample still clearly showed four peaks marking all the major first-order boundaries. The experimental techniques used in this study could not, however, distinguish two-phase regions here with certainty (the isotropic solution and subneat phases had so nearly the same density that stratification into layers did not occur readily).

The phase boundary marking the transition from the waxy phase to the subneat phase was lowered gradually in both systems (though more markedly in the n-hexadecane system) by increasing percentages of hydrocarbon down to  $\sim 39.1$  mole % soap in the n-hexadecane system and  $\sim 37.9$  mole % soap in the squalane system. At lower soap concentrations, these boundaries were practically constant at  $189.5 \pm 1.1$  °C and  $207.3 \pm 1.0$  °C respectively. This behaviour may indicate that the subneat phase is capable of incorporating greater quantities of hydrocarbon solvent into its structure than the lower temperature waxy phases before entering a two-phase subneat-solution region. Alternatively, the constancy of the H3 transition temperature may be interpreted as arising from a eutectic system involving the waxy, subneat and solution phases. The validity of this eutectic system has not been substantiated experimentally and it has therefore been omitted from the phase diagrams. Similar observations

have been reported by Cox and co-workers [51, 196] for the  $\text{LiC}_{18}$ -n-hexadecane system (see FIG. 6, p 26) and for a number of  $\text{LiC}_{18}$ -mineral oil systems.

The temperature of the final transition to the isotropic liquid state (H4) was lowered in a gradual manner by increasing concentrations of the hydrocarbons throughout the composition range studied.

Despite the general similarity between the two  $\text{LiC}_{18}$ -hydrocarbon phase diagrams (FIGS. 40 and 41) definite differences exist; the major difference being the temperature range of existence of the subneat phase. The most obvious characteristics of the hydrocarbon which might be expected to influence soap-oil inter-solubility are its molecular shape, type and weight.

A study into the variables affecting the phase changes in several  $\text{LiC}_{18}$ -mineral oil systems carried out by Cox [196] (and later extended by Uzu [61] to include a number of n-paraffins from tetradecane to docosane) attempted to correlate the transition temperatures of formation of the waxy (H2), "liquid crystal" (H3) and solution phases (H4) with the molecular weight of the oils and with each of the three carbon-type compositions present in the mineral oil mixtures (paraffinic, naphthenic and aromatic). The phase change temperatures for each system, taken at 10 and 30 mole % soap, were found to be closely similar at either concentration. The results indicated that the temperatures of the waxy (H2) and solution transitions (H4) appear to

depend slightly on the paraffin content of the oils with the temperatures falling within the range of  $184 \pm 5$  °C (H2) and  $207 \pm 5$  °C (H4). The mean transition temperatures for the H2 and H4 transitions in both n-hexadecane (calculated at 8.0 mole % and 29.0 mole % soap) and squalane (calculated at 13.8 mole % and 26.4 mole % soap) were found to be  $178.6 \pm 0.2$  °C and  $188.2 \pm 1.3$  °C (H2) and  $205.8 \pm 3.5$  °C and  $211.6 \pm 1.1$  °C (H4) respectively.

Cox [196] also discovered a linear relationship between the equilibrium phase change temperatures of the waxy to "liquid crystal" transition (H3), at 10 mole % soap, and the molecular weight of the hydrocarbons. The additional data obtained by Uzu [61] was reported to follow this linear trend. The values obtained in this study for the H3 transition in n-hexadecane (at 8.0 mole % soap) and squalane (at 13.8 mole % soap) were  $188.2 \pm 1.0$  °C and  $205.8 \pm 1.0$  °C respectively. These values appear to fit the linear plot published by Cox [196] with the lower temperature H3 transition being obtained in n-hexadecane, the linear hydrocarbon of lower molecular weight.

## 4.2 The Lithium Phenylstearate-Hydrocarbon Systems

### 4.2.1 The Lithium Phenylstearate-1-Phenylheptane System

An equilibrium phase diagram was constructed for the system, lithium phenylstearate (LiPS) in 1-phenylheptane and is presented in FIG. 55, p 233 . Since the soap used in this study consisted of a complex mixture of positional

isomers (Section 2.1.3.1) the two-component phase diagram may not fully obey the Gibbs phase rule. It was found experimentally, however, that the phase transitions observed in the hydrocarbon system were as rapid and well-defined as those observed for the solvent-free soap (Section 3.3).

The positions of the major first-order phase boundaries were established by the differential scanning calorimetry analysis of LiPS-hydrocarbon samples which had been homogenized as outlined in Section 2.1.5. (The extent of the two-phase regions which exist at these boundaries over a number of degrees was not determined accurately and they have been omitted from the phase diagram).

Macroscopic and microscopic observations in polarized light supplemented the DSC data. The positions of the boundaries indicated by broken lines are tentative.

Variable-temperature, small-angle x-ray diffraction and  $^7\text{Li}$  NMR techniques were used to provide structural information on the phases encountered.

#### 4.2.1.1 Differential Scanning Calorimetry

The thermograms recorded on heating LiPS-1-phenylheptane samples between room temperature and the isotropic melt were characterized by two or three first-order endothermic transitions depending upon the sample composition (see FIG. 42). These transitions, denoted H2, H3 and H4 in order of increasing temperature, were found to be continuous

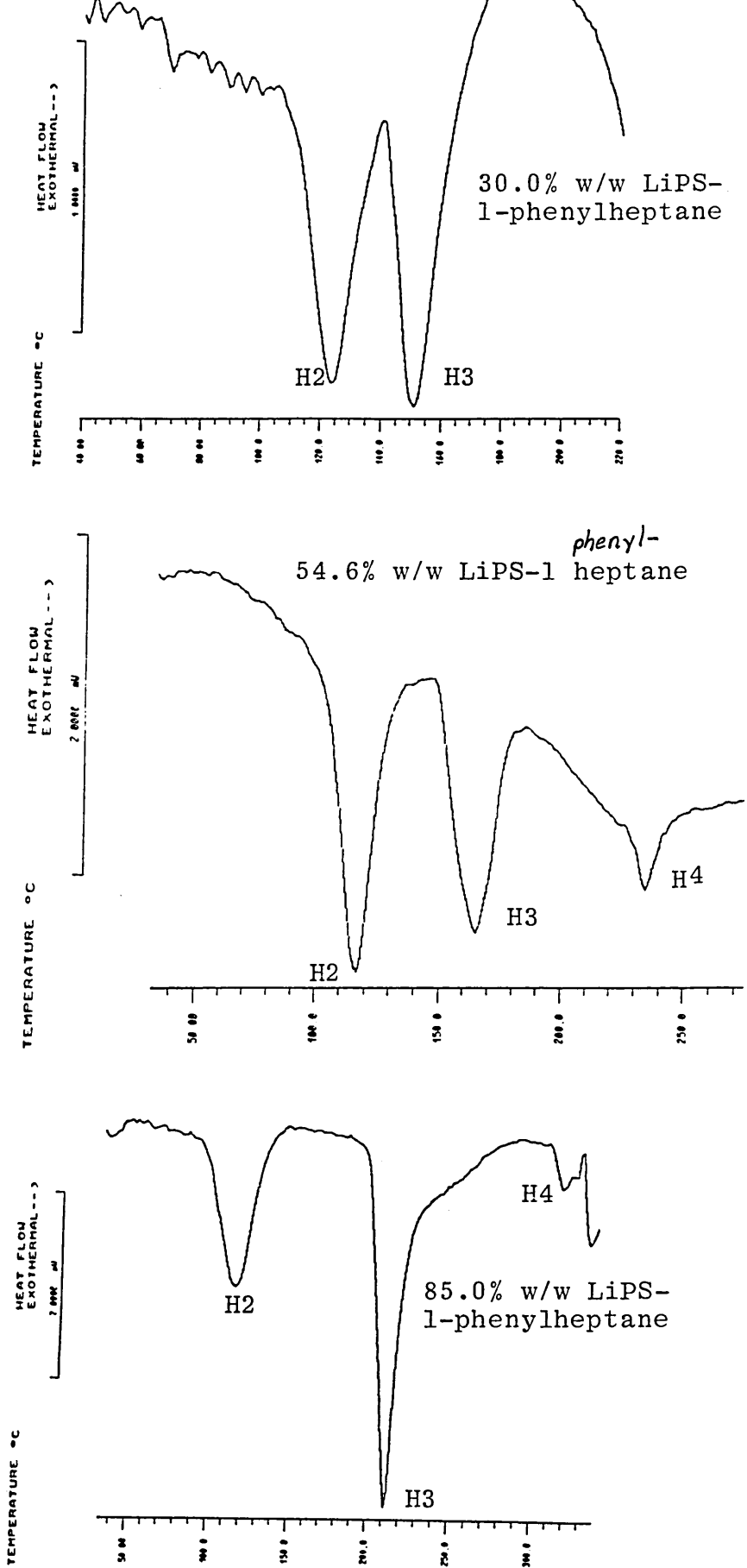


FIG. 42 : DSC heating thermograms for lithium phenylstearate-l-phenylheptane samples of varying composition (heating rates :  $5\text{ }^{\circ}\text{C min}^{-1}$ )

with the calorimetrically observed transitions of solvent-free LiPS itself (Section 3.3.1.1.). (The effect of added hydrocarbon on the low-temperature second-order transition (H1) of LiPS was not studied.)

The temperature values obtained for each transition at heating rates of 5 °C min<sup>-1</sup> are recorded in TABLE 19 as a function of sample composition. These values

TABLE 19 : Phase transition temperatures for the lithium phenylstearate-1-phenylheptane system

LiPS CONTENT		H2	H3	H4
wt %	mole %	T/(°C)	T/(°C)	T/(°C)
5.1	2.5	126.9	144.1	-
10.6	5.4	121.9	143.0	-
20.4	11.0	122.2	149.9	~ 158*
30.0	17.1	122.3	150.9	~ 185*
40.4	24.6	122.2	155.8	~ 208*
45.1	28.3	119.5	158.0	217.4
50.0	32.5	121.3	161.4	225.3
54.6	36.7	116.9	169.4	233.3
59.5	41.4	109.8	179.9	242.1
65.2	47.4	108.5	182.8	253.7
70.7	53.7	109.0	189.7	262.7
75.6	59.9	108.2	198.3	277.8
79.4	65.0	109.9	203.8	294.5
85.0	73.2	114.9	210.4	315.8
89.8	80.9	127.3	218.9	> 328.9 <sup>†</sup>
100.0	100.0	154.5	227.1	378.5

\* Transition temperature determined by polarizing microscopy.

† Transition temperature beyond the maximum hermetic sealing temperature of the DSC crucibles.

represent the mean values calculated from two independent heating runs at each composition. The temperatures were readily reproducible to within  $\pm 1$  °C and are considered to be equilibrium values. Each of the transitions was reversible, though the reversibility of the H2 transition was time-dependent as observed for the solvent-free soap (Section 3.3.1.1).

The corresponding phase transition enthalpies (calculated as kJ per mole of soap) are recorded in TABLE 20. The estimated precision limits on these values are of the

TABLE 20 : Phase transition enthalpies for the lithium phenylstearate-1-phenylheptane system

LiPS CONTENT		H2	H3	H4
wt %	mole %	$\Delta H / (\text{kJ mol}^{-1})$	$\Delta H / (\text{kJ mol}^{-1})$	$\Delta H / (\text{kJ mol}^{-1})$
20.4	11.0	4.2	5.2	*
30.0	17.1	4.1	5.6	*
40.4	24.6	4.4	5.5	< 0.1
45.1	28.3	3.9	4.1	$\sim 0.2$
50.0	32.5	3.4	4.9	0.5
54.6	36.7	4.7	3.2	0.6
59.5	41.4	5.0	5.7	1.0
65.2	47.4	5.6	4.8	1.0
70.7	53.7	5.2	5.6	1.0
75.6	59.9	5.4	5.9	0.5
79.4	65.0	4.8	6.2	0.6
85.0	73.2	5.4	7.2	0.5 - 1.0
89.8	80.9	4.3	7.9	†
100.0	100.0	5.8 $\pm$ 0.6	11.2 $\pm$ 0.4	1.0 $\pm$ 0.1

\* No transition detected by DSC.

†  $\Delta H$  not calculated. Refer to text for explanation.

order of 5% to 12% and were dependent upon the sharpness and resolution of the individual peaks and the stability of the baseline.

For samples containing less than 24.6 mole % LiPS, only two distinct endotherms could be detected calorimetrically corresponding to the H2 and H3 transitions. For the 17.1 mole % and 11.0 mole % LiPS samples, the temperatures of the final H4 transitions were determined by polarizing microscopy (Section 4.2.1.2). Samples containing less than 11.0 mole % LiPS were observed to melt directly to the isotropic liquid state at the H3 transition. The enthalpy values for the H2 and H3 transitions of the two most dilute LiPS samples (containing 2.5 mole % and 5.4 mole % LiPS) have been omitted from TABLE 20 as a result of badly sloping baselines and poor resolution of the overlapping peaks. The total enthalpy values (H2 + H3) for both samples was of the order of 6 - 9 kJ mol<sup>-1</sup>. For the samples containing greater than 73.2 mole % LiPS, the temperature and enthalpy of the final H4 transition could not be determined. At these compositions this transition occurred at temperatures beyond the maximum hermetic sealing temperature of the DSC crucibles (> 328.9 °C). For the 73.2 mole % sample itself, the enthalpy value of H4 could not be measured accurately as this transition overlapped with a transition of the DSC crucible hermetic sealing gasket (see FIG. 42 and FIG.18). Its enthalpy was estimated to be around 0.5 to 1.0 kJ mol<sup>-1</sup>.

It is interesting to note that whereas transitions H3 and H4 show monotonic decreases in temperature with increasing solvent concentration, the H2 transition exhibits a more complicated behaviour.

Between 5.4 mole % and 32.5 mole % LiPS, the H2 transition is essentially constant at  $121.6 \pm 1.1$  °C. Similarly between 41.4 mole % and 79.4 mole % LiPS, it is constant at  $109.1 \pm 0.8$  °C, before starting to increase at higher LiPS concentrations towards that of the solvent-free soap (100 mole % LiPS). The marked difference in these two temperatures may be due simply to the methods employed for sample homogenization. Samples containing a maximum of 32.5 mole % LiPS had been mixed by heating to the isotropic liquid state (i.e. beyond H4) whilst samples containing higher LiPS concentrations were mixed mechanically and by prolonged heating to temperatures below the H2 transition. (It has already been demonstrated (Section 3.3.1.1.) that reheating samples of solvent-free LiPS which had been previously heated to beyond the H3 transition, increased the temperature of the H2 transition on subsequent reheating by  $\sim 10$  °C, whilst the H3 and H4 transitions were unaffected). The behaviour of a sample of intermediate composition suggests, however, that this conspicuous change in temperature of H3 with composition may be attributed to a phase change. For example, the sample containing 36.7 mole % LiPS exhibited a H2 transition at a temperature halfway between those of the more dilute

and those of the more concentrated LiPS samples.

The transition enthalpies also displayed a marked variation with sample composition.

For the H2 transition, the mean enthalpy value over the composition range 11.0 mole % to 80.9 mole % LiPS was  $4.8 \pm 0.8 \text{ kJ mol}^{-1}$ . This is similar in magnitude to that of the solvent-free soap ( $5.8 \pm 0.6 \text{ kJ mol}^{-1}$ ).

The enthalpy value of the H3 transition, however, was greatly reduced upon addition of the solvent. For samples containing a maximum of 53.7 mole % LiPS,  $\Delta H$  appears to be essentially invariant ( $5.0 \pm 0.8 \text{ kJ mol}^{-1}$ ) and equal to almost half that of 100 mole % LiPS. As the soap concentration increased beyond 53.7 mole % LiPS,  $\Delta H$  gradually increased in size though the values are still significantly lower than that of solvent-free LiPS.

Finally, the enthalpy of the H4 transition was found to be similar to that of the solvent-free soap over the range 73.2 mole % to 32.5 mole % LiPS, but was significantly reduced as the solvent concentration increased beyond 67.5 mole % 1-phenylheptane. For the 17.1 mole % and 11.0 mole % LiPS samples, no H4 transitions could be detected by DSC (either first or second-order) corresponding to the microscopically observed melts at  $\sim 185 \text{ }^\circ\text{C}$  and  $\sim 158 \text{ }^\circ\text{C}$  respectively.

It should be noted that the lithium phenylstearate used in this study was prepared from a slightly impure acid fraction as indicated by the temperature of the H4 transition for the 100 mole % LiPS sample in TABLE 19 (refer to Section 3.3.1.1.). The tabulated H4 transition temperatures for the LiPS-1-phenylheptane system are therefore considered to be higher than those expected for samples containing absolutely pure LiPS. For example, a sample containing 32.5 mole % pure LiPS in 1-phenylheptane subsequently gave temperatures and enthalpies for the H2 and H3 transitions which were in concordance (within experimental error) with those given in TABLES 19 and 20 whilst the temperature corresponding to the H4 transition was  $\sim 9$  °C lower for the pure sample.

The qualitative phase behaviour of the LiPS-1-phenylheptane system, as reported in the following sections, appeared to be unaffected, however, by slight differences in the purity of the LiPS used.

#### 4.2.1.2 Polarizing Microscopy and Macroscopic Visual Observations

As a preliminary means of studying possible lyotropic mesophase formation in the LiPS-1-phenylheptane system, the polarizing microscopy penetration technique (Section 2.2.1.2) was employed.

At room temperature, the solvent-contacted LiPS film exhibited a patchy, non-geometric birefringent texture similar to that displayed by the solvent-free soap (see FIG. 30, p 141). As the temperature of the sample was

raised, no well-defined textural changes were observed until approximately 160 °C. Around this temperature a pronounced decrease in viscosity was observed at the LiPS-solvent interface resulting in the formation of a fluid birefringent phase with a readily identifiable "schlieren" or "nucleated domains" texture [257]. (The fluidity of this phase was demonstrated by the fact that any particles of dust present in the preparation could be seen moving freely through the material under the influence of convection currents.) Between crossed polars, this texture showed an irregular network of dark brushes branching out from a number of scattered points or nuclei. (It should be noted, however, that these optical features were not as well-defined as those commonly observed with thermotropic molecular nematic mesophases [257]). The application of slight pressure to this phase produced a texture made up of almost parallel thread-like lines which, on release of pressure, reverted to the schlieren texture.

The schlieren texture and pronounced fluidity displayed by this phase are characteristic properties of lyotropic nematic (also known as micellar nematic) mesophases. Such mesophases possess no long-range positional order of the micellar units (oblate spheroids of disc-like shape or prolate spheroids of rod-like shape) making up the phase whilst long-range orientational order is retained [254, 310, 311].

As the temperature was increased slowly towards  $\sim 180$  °C, a second distinct mesophase was formed at the soap-rich boundary of the nematic phase. (FIG.45) This was identified as a fused hexagonal mesophase by its characteristic "angular" texture (category 222.6 in Rosevear's classification [258]) and relatively high viscosity. Since the lyotropic nematic phase was intermediate to a micellar hexagonal phase (most probably of the reversed  $H_2$  type) at higher temperatures/higher concentrations of LiPS and an isotropic micellar solution phase at lower temperatures/lower concentrations of LiPS, the nematogenic unit in the nematic phase was considered, by inference, to be a reversed cylindrical or rod-like micelle.  $^7\text{Li}$  NMR spectroscopy may be used to confirm this.

FIG. 43 shows a photomicrograph, taken with crossed polars, of the mesophases formed by penetration of 1-phenylheptane into a thin film of anhydrous LiPS at 201 °C. The phases pictured from top left to bottom right, as the solvent concentration decreased monotonically, are isotropic solution, micellar nematic and hexagonal mesophases. (The patchy, non-geometric birefringent phase formed at even higher LiPS concentrations, and still present at 201 °C, is not shown). It is interesting to note that close to the hexagonal phase boundary the texture adopted by the nematic phase appears to be continuous with the angular units of the hexagonal phase. At higher solvent concentrations, the more characteristic schlieren texture is clearly visible (FIG. 44). At the

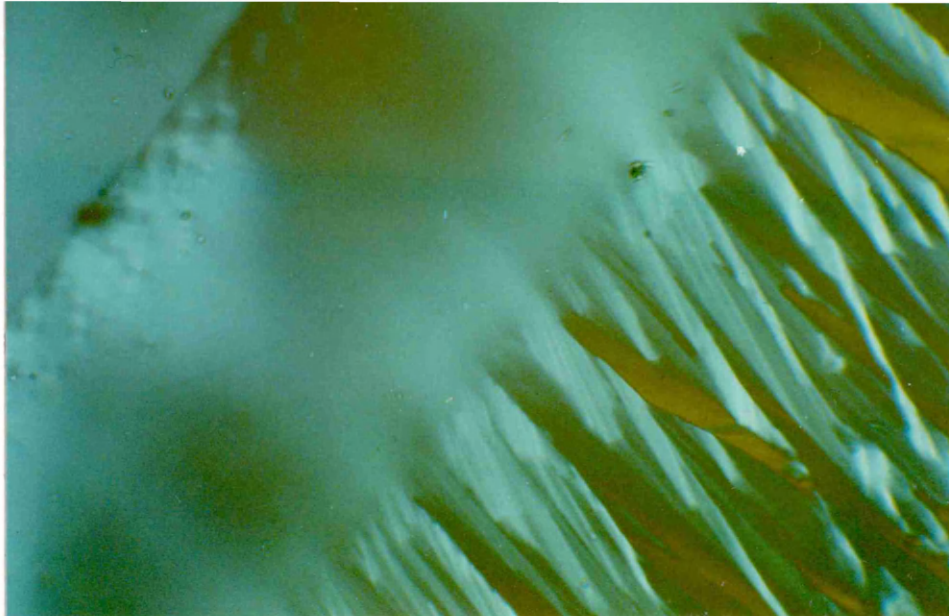


FIG. 43 : Penetration of 1-phenylheptane into anhydrous lithium phenylstearate at 201 °C. Phases pictured from top left to bottom right are; isotropic solution, micellar nematic and hexagonal mesophases (crossed polars, magnification x 100).



FIG. 44 : As above, showing more clearly the Schlieren texture of the micellar nematic mesophase (far left) formed at 183 °C at the higher 1-phenylheptane concentrations.

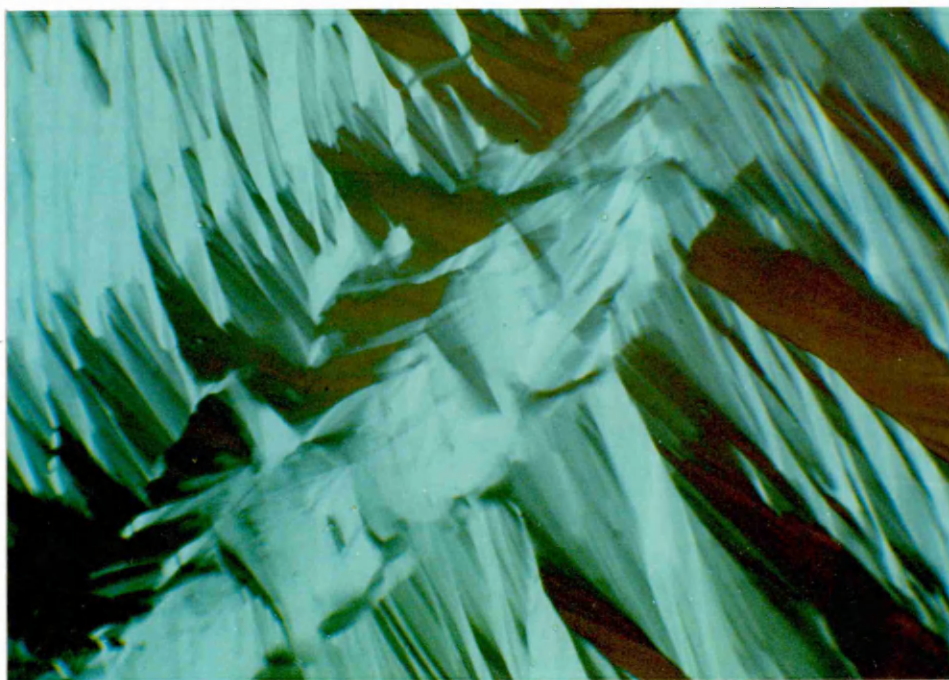


FIG. 45 : Reversed hexagonal mesophase "angular" texture formed in the lithium phenylstearate-1-phenylheptane penetration experiment at  $\sim 180^\circ\text{C}$  (crossed polars, magnification x 100).



FIG. 46 : Formation of the micellar nematic mesophase Schlieren texture from the spherical droplets deposited on cooling the isotropic solution phase in the lithium phenylstearate-1-phenylheptane system (crossed polars, magnification x 100).

isotropic solution-nematic phase boundary, a network of small isotropic holes can be clearly seen as the nematic phase formed at lower concentrations melts (see FIG. 43). On cooling, the nematic phase was deposited from isotropic solution in the form of typical free-form spherical droplets which then coalesced to form the schlieren texture (FIG. 46). Nematic droplets are said to characterize a type-texture of the nematic phase since they occur nowhere else (ref. 5, p 19).

As the temperature was increased to  $\sim 225$  °C, no additional liquid crystal phases were formed. At this temperature the sample consisted mainly of the angular hexagonal mesophase which was continuous with a very narrow region of melting nematic phase. No signs of a hexagonal mesophase melt were observed however. Microscopic observations were limited to these temperatures because of the boiling point of the solvent (233 °C).

The transitions reported above were reproduced on several independent heating cycles.

In order to ascertain approximate values for the temperature and composition ranges of existence of the phases described, the phase behaviour of bulk samples of known composition was studied using macroscopic and then microscopic observations in polarized light.

The addition of anhydrous LiPS in low concentrations to 1-phenylheptane at room temperature produced completely transparent highly viscoelastic solutions which exhibited slightly non-Newtonian flow. (As little as 1.0 wt %, 0.5 mole %, LiPS was sufficient to produce solutions with such properties). At greater LiPS concentrations, transparent viscous gels were formed.

Between crossed polars, these bulk samples were birefringent, though their appearance depended upon the sample composition. Samples containing a minimum of 32.5 mole % LiPS displayed a uniform intense golden birefringency, whilst those containing greater concentrations of hydrocarbon exhibited a more heterogenous birefringency composed of multihued (predominantly golden; plus blue, green and crimson) birefringent patches, streaks and swirls. (This heterogenous birefringency was often more pronounced after vigorous agitation or moderate heating of the sample.) For samples containing less than  $\sim 17.1$  mole % LiPS, isotropic regions could also be distinguished. At soap concentrations less than  $\sim 2.5$  mole % LiPS, the birefringency became vanishingly dim, though such samples exhibited marked flow and shear birefringence.

As the temperature of these bulk samples was increased, marked changes in appearance were observed at each of the calorimetrically detected first-order transitions.

At both the H2 and H3 transitions, a temporary loss of transparency, to produce translucent white samples, was accompanied by a significant decrease in intensity of the birefringence. (The observed degree of opacity was more pronounced at the H3 transition.) These changes occurred at the respective transitions over temperature intervals of approximately 25 °C and 15 °C, and are thought to result from the formation of two-phase regions at each of the first-order phase boundaries. For samples containing less than 5.4 mole % LiPS, however, these changes could not be detected.

As the temperature was increased beyond the H3 transition, a very pronounced decrease in viscosity was observed for the samples containing less than 32.5 mole % LiPS. For the samples containing 28.3 mole % to 11.0 mole % LiPS, this resulted in the formation of a fluid multihued birefringent phase whilst for the more dilute samples the viscosity beyond H3 approached that of the pure solvent, with H3 corresponding to the final isotropic melt.

Samples containing a minimum of 41.4 mole % LiPS also experienced a reduction in viscosity at H3 (though not as pronounced as that experienced by the more dilute LiPS samples) to produce viscous solutions displaying a uniform golden birefringency between crossed polars.

For samples of intermediate composition (32.5 mole % and 36.7 mole % LiPS) viscous uniformly golden birefringent

solutions were initially formed at H3 whilst at significantly higher temperatures ( $\sim 193$  °C and  $\sim 215$  °C respectively) a further reduction in viscosity was observed producing the fluid multihued birefringent phase. No signs of isotropic solution could be detected in the fluid phases at these temperatures however.

As the temperature was increased towards  $\sim 240$  °C (the maximum operating temperature of the oil bath) samples containing a maximum of 41.4 mole % LiPS were observed to melt to the isotropic solution state at their respective H4 transition temperatures. Samples containing greater LiPS concentrations continued to display a uniform golden birefringency at this temperature.

Each of the phase changes reported above were reproducible on subsequent heating systems.

At room temperature, all thin film preparations of LiPS-1-phenylheptane mixtures when viewed microscopically in polarized light exhibited patchy, non-geometric textures with incipient striations, independent of sample composition.

Increasing the temperature of the samples beyond their respective H2 transitions resulted in more highly striated textures. Their appearance beyond H3 however varied markedly with sample composition.

For the samples containing less than 32.5 mole % LiPS a very abrupt decrease in viscosity and formation of the nematic schlieren texture accompanied the H3 transition. It was also noticed that such samples displayed a characteristic textural change  $\sim 10$  °C below this transition producing a more stippled or grainy appearance. Samples containing a minimum of 41.4 mole % LiPS also experienced a reduction in viscosity at H3 which was accompanied by the gradual development of the angular hexagonal texture.

At intermediate compositions, however, (32.5 mole % and 36.7 mole % LiPS) the samples were first observed to undergo a change to a viscous patchy non-geometric hexagonal texture (no angular features were observed) followed by the formation of the nematic schlieren texture at higher temperatures (between  $\sim 179$  °C - 183 °C and  $\sim 200$  - 205 °C respectively). These observations established the approximate position, with respect to temperature and composition, of the hexagonal-nematic mesophase boundary. The transition between these two distinct liquid crystal phases was not detected by DSC, however, suggesting the existence of a very weak first- (or possibly a second-) order transition at this phase boundary.

Samples containing less than 11.0 mole % LiPS melted directly to the isotropic solution state at H3 without the formation of the nematic phase. As the temperature was

increased further, samples containing 11.0 mole % to 36.7 mole % LiPS were observed to melt from the liquid crystal phase to the isotropic state at the H4 transition. The more concentrated samples continued to exhibit the angular texture up to  $\sim 230$  °C (the upper limit of study).

The microscopically observed transitions reported above were reproducible and in general agreement with those observed macroscopically and by DSC.

#### 4.2.1.3 X-Ray Diffraction

The diffraction patterns obtained from LiPS-1-phenylheptane mixtures in the low-angle region at room temperature were dependent upon the sample composition (see TABLE 21)

Samples containing a minimum of 36.7 mole % LiPS exhibited three reflections at low-angles in the ratio,  $1:1/\sqrt{3}:1/\sqrt{4}$ . These results are characteristic of structures possessing two-dimensional hexagonal periodicity. The increase in  $d_1$  and the corresponding increase in the hexagonal lattice parameter,  $a$ , (i.e. the centre to centre distance between the cylindrical micellar aggregates) with increasing hydrocarbon concentration is consistent with the dilation of a reversed hexagonal structure. The disordered nature of the soap hydrocarbon chains in the semi-crystalline reversed hexagonal (SCH 1) phase of solvent-free LiPS at room temperature (Section 3.3.5.2) allows the hydrocarbon to penetrate into the structure between the reversed rod

TABLE 21 : Low-angle x-ray diffraction results for the lithium phenylstearate-1-phenylheptane system at 27 °C\*

LIPS CONTENT		OBSERVED BRAGG SPACINGS/(Å)			LATTICE SYMMETRY	HEXAGONAL LATTICE PARAMETER, a/(Å)
wt %	mole %	d <sub>1</sub>	d <sub>2</sub>	d <sub>3</sub>		
30.0	17.1	56.0 ± 2 <sup>†</sup>	-	-	Micellar <sup>†</sup>	-
45.1	28.3	51.0 ± 1 <sup>†</sup>	-	-	Micellar <sup>†</sup>	-
54.6	36.7	47.0 ± 0.4	26.2 ± 0.2	22.6 ± 0.2	2-d Hexagonal	54.3 ± 0.4
59.0	40.9	42.5 ± 0.3	24.0 ± 0.1	20.7 ± 0.1	2-d Hexagonal	49.1 ± 0.3
69.6	52.4	39.0 ± 0.3	22.2 ± 0.1	19.4 ± 0.1	2-d Hexagonal	45.0 ± 0.4
100.0	100.0	31.1 ± 0.3	17.8 ± 0.1	15.4 ± 0.1	2-d Hexagonal	35.9 ± 0.4

\*These samples also exhibited a diffuse reflection in the high-angle region at  $\sim 4.6^\circ$  Å.

<sup>†</sup>d<sub>1</sub> corresponds to the maximum scattering intensity of the liquid-type scattering function. The diffraction pattern in this case is considered to result from a semi-crystalline micellar nematic phase, SCN<sub>c</sub> 1 (refer to text for explanation).

micelles to produce a solvent-swollen SCH 1 phase at these compositions.

As the solvent concentration was increased to 71.7 mole % 1-phenylheptane, however, the long-range positional order between the indefinitely long rod micelles was lost and the hexagonal reflections were replaced by a single broad scattering maximum (see FIG. 47) characteristic of liquid-type interparticle interference [312]. Further studies on samples of intermediate composition (between 28.3 mole % and 36.7 mole % LiPS) are required to establish the position of this phase boundary with a greater degree of accuracy.

Similar diffraction maxima have been reported by Philippoff [313] and Siegel [198] for concentrated isotropic solutions of Aerosol OT in benzene, cyclohexane, n-decane and n-dodecane. The maximum scattering intensity observed in the present study, however, is considered to result from mutual interactions between orientationally ordered reversed rod micelles.

Doi and Edwards [314] have shown in a theoretical study that the rotation of stiff rod micelles becomes restricted when the rotational volumes of the rods begin to overlap. The free spatial angle in which a rod can rotate before it bumps into a neighbouring rod becomes smaller and smaller with increasing concentration of the rods. At the extreme, the rod would be completely locked in position by neighbouring overlapping rods. This situation becomes especially severe for rods which are much longer

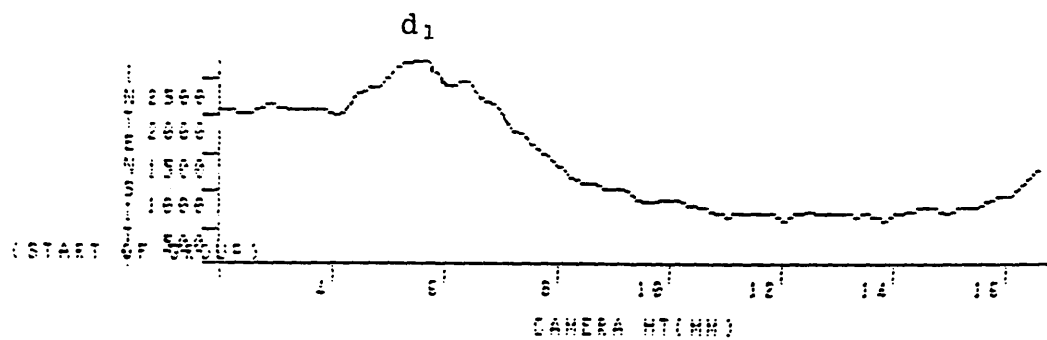


FIG. 47 : Low-angle x-ray diffraction pattern  
 obtained from a 30.0 % w/w LiPS-  
 1-phenylheptane sample at 27 °C

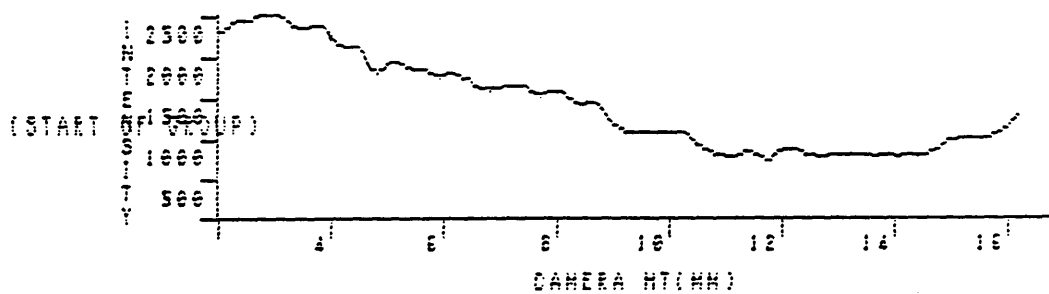


FIG. 48 : Low-angle x-ray diffraction pattern  
 obtained from a 30.0 % w/w LiPS-  
 1-phenylheptane sample at 180 °C

than the mean distance of their centre of masses.

This would appear to be the case in the LiPS-1-phenylheptane system since samples containing 17.1 mole % and 28.3 mole % LiPS are birefringent at room temperature (indicating some degree of micellar order) and form micellar nematic mesophases at elevated temperatures. These high temperature mesophases possess no long-range positional (translational) order of the rod micelles making up the phase whilst long-range orientational order is retained [254, 310, 311]. Their room temperature phase structure have accordingly been denoted  $SCN_C 1$  (to signify a semi-crystalline nematic phase composed of orientationally ordered reversed cylindrical micelles which possess quasi-crystalline polar groups (Section 4.2.1.4) and disordered hydrocarbon chains.) The outward shift of the scattering maximum with increasing hydrocarbon concentration may therefore be interpreted as the effect of increasing thicknesses of solvent layers between the rod micelles. The phase boundary between the  $SCN_C 1$  phase and isotropic micellar solution could not be positively established using low-angle x-ray diffraction. Macroscopic visual observations in polarized light, however, have indicated that it may occur at very low soap concentrations (< 2.5 mole % LiPS) with the phases being possibly separated by a two-phase region.

A variable temperature low-angle x-ray diffraction study was carried out on several LiPS-1-phenylheptane mixtures in order to investigate changes in structure and/or structural parameters with increasing temperature. The results are presented in TABLE 22.

For both the 30.0 wt % and 69.6 wt % LiPS samples, no overall qualitative change in appearance of the diffraction patterns (micellar nematic and 2-d hexagonal respectively) was observed on heating the samples from 27 °C to beyond their respective calorimetrically observed H2 and H3 transitions (TABLE 19). At the H4 transition, however, the diffraction pattern of the 30.0 wt % LiPS sample (and also the 54.6 wt % LiPS sample) showed a pronounced change. The scattering maximum observed at lower temperatures was replaced by a monotonic decrease in scattering intensity (see FIG. 48) characteristic of isolated single-particle scattering without interference [312]. The absence of interparticle interference (together with a complete loss of birefringency) probably results from the break up of the long ordered, reversed rod micelles through increasing thermal fluctuations to produce much smaller rods possessing a low anisotropy or isometric  $S_2$  micelles at the mesophase to isotropic solution transition.

More interesting was the observation of a well-defined change in the diffraction pattern of the 54.6 wt % LiPS sample at  $\sim 180$  °C (a temperature intermediate between

TABLE 22 : Variable temperature low-angle x-ray diffraction results for the lithium phenylstearate-1-phenylheptane

wt % LiPS	T/(°C)	OBSERVED BRAGG SPACINGS /(Å)			PHASE TYPE*
		d <sub>1</sub>	d <sub>2</sub>	d <sub>3</sub>	
30.0	27	~ 56.0	-	-	SCN <sub>C</sub> 1
	90	~ 52.2	-	-	SCN <sub>C</sub> 1
	140	~ 45.7	-	-	SCN <sub>C</sub> 2
	160	~ 43.7	-	-	N <sub>C2</sub>
	180	-	-	-	S <sub>2</sub>
54.6	27	47.0	26.2	22.6	SCH 1
	50	48.5	26.8	23.8	SCH 1
	100	50.5	29.5	24.6	SCH 1
	130	41.6	23.1	-	SCH 2
	155	41.9 + 39.8	-	-	SCH 2 to N <sub>C2</sub>
	180	~ 39.5	-	-	N <sub>C2</sub>
	200	~ 41.6	-	-	N <sub>C2</sub>
	230	-	-	-	S <sub>2</sub>
69.6	27	39.0	22.2	19.4	SCH 1
	100	36.2	20.9	18.1	SCH 1/SCH 2
	150	32.1	18.6	16.1	SCH 2
	200	33.7 + 32.0	-	-	SCH 2 to H <sub>2</sub>
	220	27.8	16.0	13.9	H <sub>2</sub>

\*Refer to Section 4.2.1.5 for explanation of the phase notations.

the calorimetrically observed H3 and H4 transitions) from a 2-d hexagonal pattern to a "micellar" pattern (similar to that obtained from the 30.0 wt % LiPS sample at 160 °C in the micellar nematic phase). This distinct transition was not observed by DSC but was observed for this sample using polarizing microscopy and corresponded to a hexagonal to micellar nematic phase change. This indicates the presence of a very weak first- (or possibly second-) order, transition at the hexagonal H<sub>2</sub>-micellar nematic phase boundary. It should be noted, however, that for a first-order transition between these two mesophases, the technique of low-angle x-ray diffraction would not be very sensitive to the presence of the intervening two-phase region in this case.

The data presented in TABLE 22 also indicates, however, that each sample, irrespective of composition and room temperature phase structure (TABLE 21) appears to undergo similar quantitative structural modifications on heating. As observed for solvent-free LiPS (Section 3.3.4.3) these changes were manifested in abrupt decreases in the value of  $d_1$  (and consequently the lattice parameter,  $a$ , for the 2-dhexagonal phases) at temperatures corresponding to the first-order H2 and H3 transitions (TABLE 19). The decreases in  $d_1$  were of the same order of magnitude for each LiPS-1-phenylheptane sample studied and were similar to those observed for the solvent-free soap. (It should be noted that on occasion the decrease in  $d_1$  was observed at a lower temperature than the transition

temperatures given in TABLE 19. The values given in TABLE 19, however, correspond to the point of 50% completion of the transition. The approximate onset of these DSC transitions, as measured from the points of first deviation of the peaks from the steady baseline, was found to be 17-33 °C, 15-24 °C and 10-12 °C lower for the H2, H3 and H4 transitions of these samples respectively).

As reported in Section 4.2.1.1, each of the phase transitions observed for the LiPS-1-phenylheptane samples studied here (H2, H3 and H4) were found to be continuous with thermotropic phase transitions of the solvent-free soap itself. Since the phase structures of these samples are considered to be composed of the same basic micellar aggregates which make up solvent-free LiPS, it is suggested that the structural modifications occurring in the solvent system are very similar to those occurring in the solvent-free soap (Sections 3.3.5.4 and 3.3.5.5).

It would appear, therefore, that even in the more dilute LiPS samples the non-polar hydrocarbon solvent cannot overcome the strong ionic and co-ordination forces operating between the quasi-crystalline lithium carboxylate groups (as evidenced by the magnitude of the respective  $\Delta H$  values at the H2 and H3 transitions; TABLE 20), so that the process of stepwise melting persists in the hydrocarbon system. Similar effects were observed in the  $\text{LiC}_{18}$ -hydrocarbon systems.

#### 4.2.1.4 <sup>7</sup>Li NMR Spectroscopy

In order to extract information concerning the molecular dynamics of the phases encountered in the LiPS-1-phenylheptane system (specifically the strength of counter-ion binding), a study of the temperature dependence of the <sup>7</sup>Li central resonance ( $m = -\frac{1}{2} \leftrightarrow m = +\frac{1}{2}$ ) absorption linewidth,  $W_{\frac{1}{2}}$ , was made for samples of varying composition over the temperature range from 30 °C to 200 °C. The results are presented in TABLE 23. For several of these samples (where the lyotropic and thermotropic phase behaviour is considered to be well established) the phases present have been indicated in parentheses after the linewidth values. The phase notations are those outlined in Section 4.2.1.5. It should be noted, however, that the temperatures indicated do not necessarily correspond to the actual transition temperature between successive phases (refer to TABLE 19, p 190).

For linewidths in the approximate region of  $\leq 100$  Hz, the estimated errors may be as large as 10-20%, while for larger linewidths the errors are considerably less. For the purpose of this study, however, knowledge of the absolute values was not critical.

At room temperature each sample, irrespective of composition, gave rise to very broad lines with values ranging from  $\sim 2.4$  kHz (at 2.0 wt %, 1.0 mole % LiPS) to  $\sim 3.2$  kHz (at 59.9 wt %, 41.8 mole % LiPS). Though considerably narrower than the linewidth observed for

TABLE 23 : Temperature dependence of the  $^7\text{Li}$  NMR central resonance absorption linewidth,  $W_{\frac{1}{2}}$ , in the lithium phenylstearate-1-phenylheptane system. <sup>†</sup>

T/(°C)	$^7\text{Li}$ NMR LINEWIDTH, $W_{\frac{1}{2}}$ (kHz)				
	w/w % LiPS				
	10.0	20.2	30.0	50.0	59.9
30	2.42*	2.46	3.07 (SCN <sub>C</sub> 1)	3.28 (SCH 1)	3.16 (SCH 1)
50		2.41	2.67		
70			2.44		
75		1.81		2.35	
90			1.97		
100	0.94	0.94	1.45	1.60	
115	0.87				
125	0.66	0.77			
130	0.14		1.12 (SCN <sub>C</sub> 2)	1.19 (SCH 2)	
135	0.10	0.16	0.77		
140	0.10	0.16	0.31	0.91	0.89 (SCH 2)
145	0.09	0.12		0.31	0.24
150	0.09	0.09	0.19 (N <sub>C2</sub> )	0.31	0.27
155		0.09			
160		0.07	0.17	0.25 (H <sub>2</sub> )	0.21
170			0.17	0.23 (H <sub>2</sub> )	0.20
180		0.05	0.05	0.21 (N <sub>C2</sub> )	0.17 (H <sub>2</sub> )
190					0.17 (H <sub>2</sub> )
200			0.03 (S <sub>2</sub> )		0.17

\*Similar  $W_{\frac{1}{2}}$  values were also obtained for 2.0 wt % and 5.0 wt % LiPS-1-phenylheptane samples at 30 °C.

<sup>†</sup>The experimental linewidths were not corrected for magnetic field inhomogeneity.

solvent-free LiPS at room temperature (6.14 kHz at 30 °C; Section 3.3.3.3), the values obtained in the hydrocarbon solvent system were orders of magnitude greater than those observed for counter-ions in conventional aqueous mesophases and micellar solutions [239, ref 269, p 212]. The value obtained for the 2.0 wt % LiPS-1-phenylheptane sample was almost identical to that reported graphically by Wang et al [324] for  $^{23}\text{Na}$  in the reversed micellar phase of Aerosol OT in n-heptane at 3% w/v surfactant containing  $\sim 0.2$  % v/v  $\text{H}_2\text{O}$ . (For the Aerosol OT system, this corresponds to a molar ratio  $\text{H}_2\text{O}/\text{Na}^+$  of 1.64. It is interesting to note that when in excess of 1% v/v  $\text{H}_2\text{O}$  had been added to this solution, i.e. on completion of the counter-ion solvation shell where  $\text{H}_2\text{O}/\text{Na}^+ > \sim 6$ , the  $^{23}\text{Na}$  NMR central linewidth was reduced to  $< 350$  Hz). These results are consistent therefore with the possible presence of only a very low concentration of water in the LiPS-1-phenylheptane system.

With increasing temperature, gradual motional narrowing of the  $^7\text{Li}$  lines was observed with discontinuous changes at their respective first-order DSC transitions.

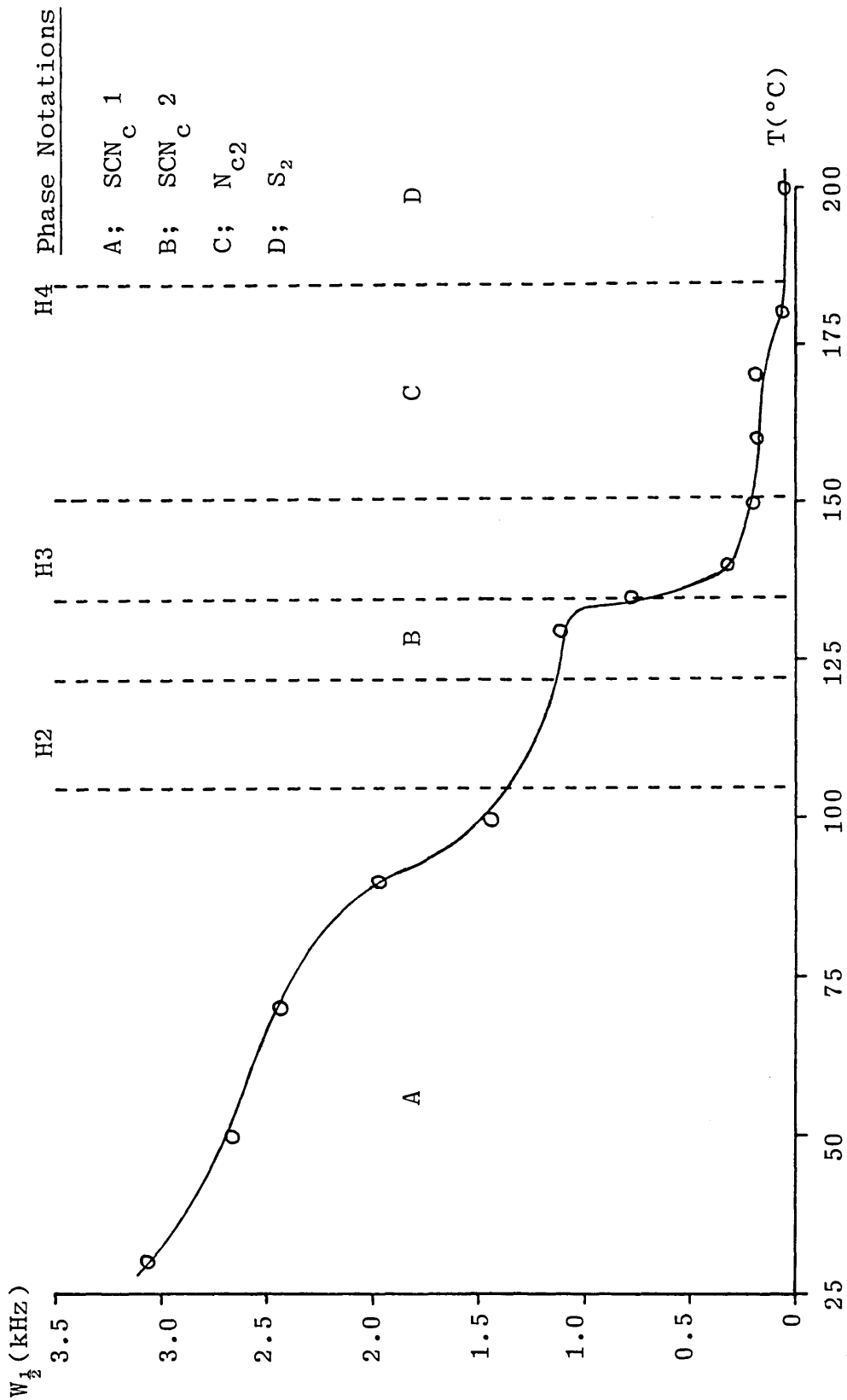


FIG. 49 : Temperature dependence of the <sup>7</sup>Li NMR central resonance absorption linewidth, W<sub>1/2</sub>, for a 30 % w/w lithium phenylstearate-1-phenylheptane sample

This is clearly evident in FIG. 49 where the temperature-linewidth data for the 30.0 wt % (17.1 mole %) LiPS sample has been presented graphically. The transition temperatures for the H2 and H3 DSC transitions of this sample have been represented on the graph by vertical bands covering the temperature range from the onset of each transition (the first deviation from the steady baseline) to the point of 50% completion (the apex of the symmetrical peak). The temperature of the H4 transition, as determined by polarizing microscopy is also shown. The H4 transition of this sample, corresponding to a micellar nematic mesophase melt, was not detected by DSC but on the basis of the present linewidth data is considered to be weakly first-order.

This behaviour is qualitatively very similar to that observed for the solvent-free soap. (The possible motional processes responsible for this line-narrowing have been discussed for the case of solvent-free LiPS in Section 3.3.3.3. The interpretation given is considered to be equally valid for the hydrocarbon system). The magnitude of the linewidth decrease at H2 was, however, much smaller in the 1-phenylheptane system as a direct consequence of the significantly narrower linewidths immediately preceding this transition. It would appear that the addition of the hydrocarbon solvent causes a loosening of the quasi-crystalline polar groups of LiPS at moderately low temperatures. It is suggested that this occurs not through direct interaction with the polar groups, but

indirectly by increasing the disorder of the soap hydrocarbon chains.

Beyond the respective H2 transitions, and immediately prior to the H3 transitions, the linewidth values of the solvent-containing and solvent-free systems were very similar. For the samples containing a minimum of 30.0 wt % (17.1 mole %) LiPS, the dipolar linewidths observed between the H3 and H4 transitions (i.e. the region of liquid crystal H<sub>2</sub> and N<sub>C2</sub> formation) were practically invariant and correspond to a diffusional motion of the Li<sup>+</sup> cations (Section 3.3.3.3). The observed reduction in W<sub>1/2</sub> upon entering the isotropic melt may indicate that "free" translational diffusion along the surface of the reversed rod-like micellar aggregates, in both the micellar nematic, N<sub>C2</sub> and hexagonal, H<sub>2</sub> mesophases, is partially restricted.

The data presented in TABLE 23 were reproducible on subsequent heating cycles. However, it is worthy to note that the room temperature <sup>7</sup>Li NMR spectra recorded after cooling samples from temperatures beyond their respective H3 transitions, were significantly different from their original room temperature spectra. This is shown in FIG. 50 for the 59.9 wt % (41.8 mole %) LiPS sample. The former spectrum of this sample was characterized by a very narrow resonance signal superimposed on a broad line, both centred at the Larmor frequency. The intensity of the broad line accounted for ~ 35-40% of the total

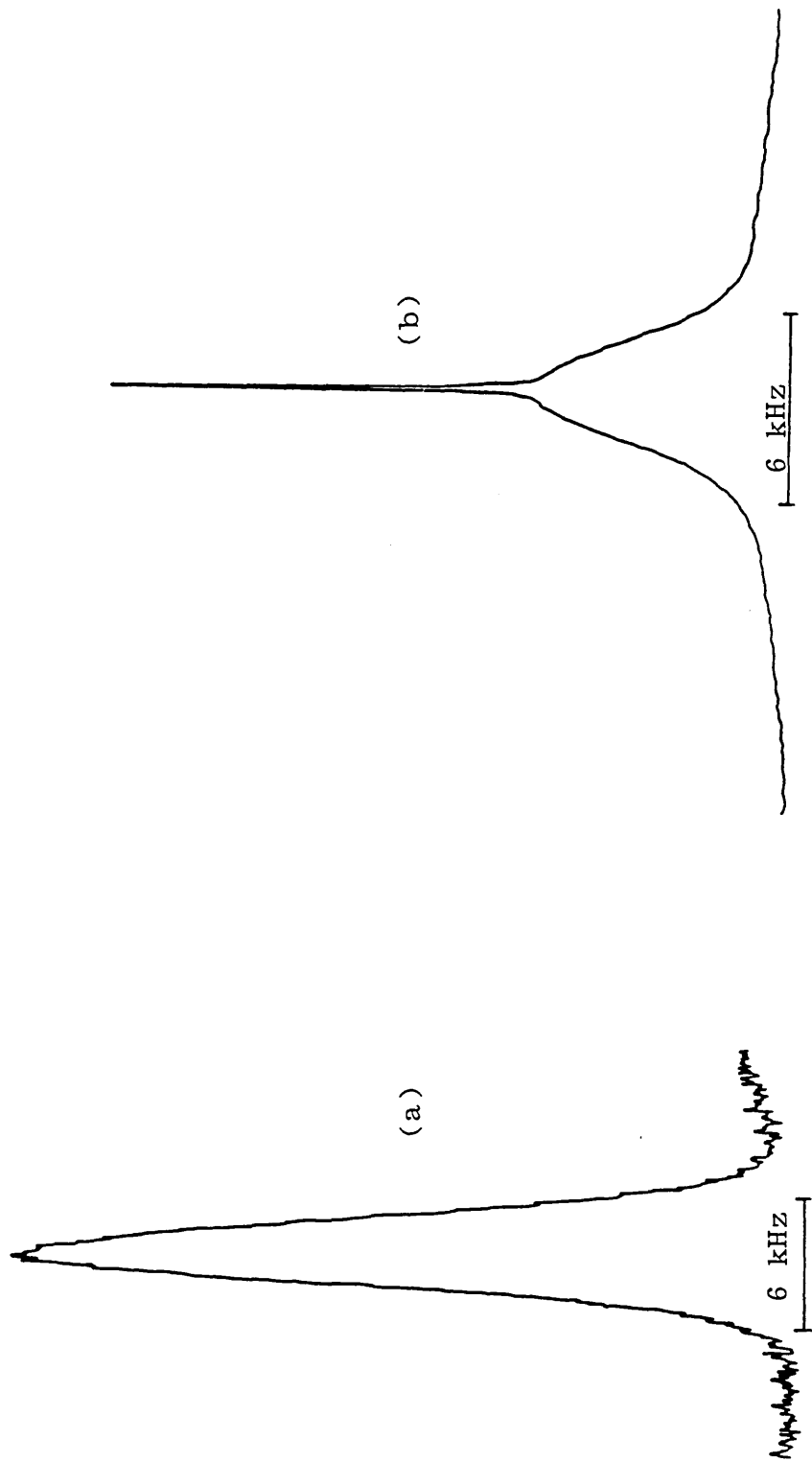


FIG. 50 :  ${}^7\text{Li}$  NMR central resonance absorption spectra for a 59.9% w/w lithium phenylstearate - 1-phenylheptane sample. (a) at 30 °C (b) at 30 °C after cooling from 200 °C

signal intensity whilst the ratio between the two signals appeared to be somewhat dependent upon the sample cooling rate, with faster cooling rates increasing the overall intensity of the narrow signal. The linewidth value obtained for the broad line was very similar to the original value whilst the  $W_{\frac{1}{2}}$  value for the narrow line (measured at the midpoint of the distance from the baseline to the apex of the narrow line) was 0.18 kHz; a value almost identical to that observed for this sample in the hexagonal,  $H_2$  mesophase. This spectrum, recorded after allowing the sample to stand at the ambient temperature for six months after cooling from 200 °C, indicates that the sample probably contains some proportion of the supercooled mesophase, and suggests that complete recrystallisation of the LiPS polar groups may be hindered in the hydrocarbon solvent system.

Samples containing a minimum of 30 wt % (17.1 mole %) LiPS when heated to the temperature interval between their respective H3 and H4 transitions were also observed to exhibit a first-order quadrupole "powder" splitting,  $\Delta$ , of the  $^7\text{Li}$  NMR resonance signal (see FIG. 51). The observation of quadrupole splittings provides conclusive evidence for the anisotropic nature of the fused micellar nematic  $N_{C2}$  (at 30.0 wt %, 17.1 mole % LiPS) and fused hexagonal,  $H_2$  (at 50.0 and 59.9 wt % LiPS; 32.5 and 41.8 mole % LiPS respectively) mesophases formed at these

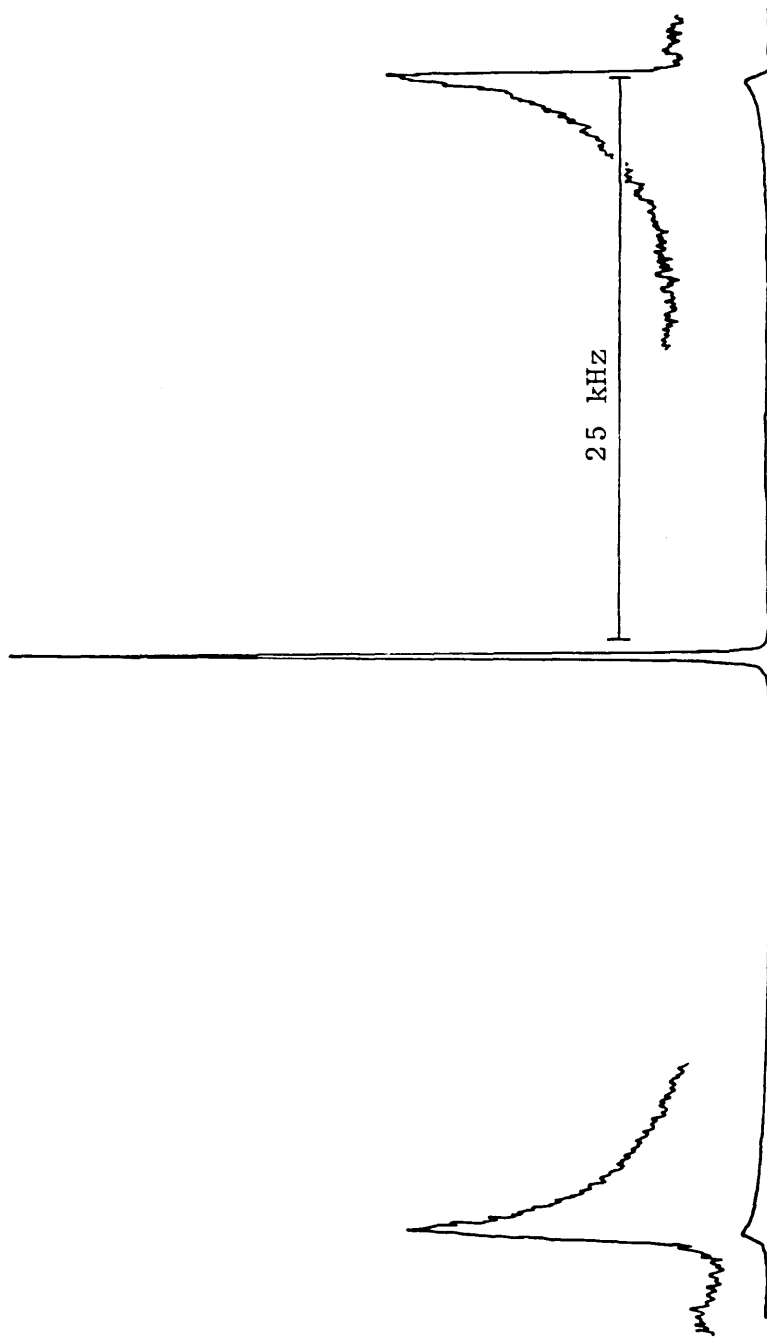


FIG. 51 :  ${}^7\text{Li}$  NMR "powder" spectrum for a 59.9% w/w lithium phenylstearate -  
1-phenylheptane sample at 190 °C ( $\text{H}_2$  mesophase)

temperatures (Section 2.2.5.2).

The similarity in magnitude of  $\Delta$  for both mesophases (TABLE 24) is consistent with the micellar nematic  $N_{C2}$  phase being composed of cylindrical (as opposed to disc-like,  $N_D$ ) aggregates. (In this present study, the  $^7\text{Li}$  spectra were recorded at a resonance frequency of 31.140 MHz and consequently the very weak "powder" satellites observed for solvent-free LiPS (at 116.641 MHz) at 22 °C were not discernible until temperatures were attained corresponding to a "fusion" of the polar groups. The increase in molecular motion of the  $\text{Li}^+$  cations at these temperatures resulted in a significant improvement in resolution of the quadrupole splitting.)

The magnitudes of  $\Delta$  (and of the quadrupole coupling constants,  $E_Q$ , as calculated from  $\Delta$  using equation (2.14), p 90 ) observed for these mesophases (TABLE 24) are, however, closer to that of solvent-free "solid" LiPS ( $\Delta = 20 \pm 1$  KHz; Section 3.3.3.1) than those reported in the literature for conventional aqueous soap mesophases where the soap molecules are extensively hydrated. For example, the  $^7\text{Li}$  quadrupole splittings in the lamellar phase of the lithium octanoate-decanol- $\text{D}_2\text{O}$  system vary monotonously between 0.45 and 0.67 kHz over the entire phase domain [284].

TABLE 24 : Temperature dependence of the  ${}^7\text{Li}$  quadrupole splitting,  $\Delta$ , and quadrupole coupling constant,  $E_Q$ , in the lithium phenylstearate-1-phenylheptane system

w/w % LiPS	T/(°C)	$\Delta$ /(kHz)	$E_Q$ (kHz)	PHASE TYPE*
30.0	140	$23.7 \pm 0.7$	$94.8 \pm 2.8$	$\uparrow$ $N_{C_2}$ $\downarrow$
	150	$24.1 \pm 0.8$	$96.4 \pm 3.2$	
	160	$23.6 \pm 0.8$	$94.4 \pm 3.2$	
	170	$22.6 \pm 1.4$	$90.4 \pm 5.6$	
50.0	145	$24.2 \pm 1.4$	$96.8 \pm 5.6$	$\uparrow$ $H_2$ $\downarrow$ $N_{C_2}$
	150	$26.2 \pm 0.9$	$104.8 \pm 3.6$	
	160	$26.2 \pm 0.4$	$104.8 \pm 1.6$	
	170	$26.0 \pm 0.4$	$104.0 \pm 1.6$	
	180	$25.5 \pm 0.7$	$102.0 \pm 2.8$	
59.9	150	$26.2 \pm 0.7$	$104.8 \pm 2.8$	$\uparrow$ $H_2$ $\downarrow$
	160	$26.5 \pm 0.5$	$106.0 \pm 2.0$	
	170	$26.1 \pm 0.4$	$104.4 \pm 1.6$	
	180	$26.0 \pm 0.2$	$104.0 \pm 0.8$	
	190	$25.5 \pm 0.4$	$102.0 \pm 1.6$	
	200	$25.0 \pm 0.5$	$100.0 \pm 2.0$	

\*Refer to Section 4.2.1.5 for explanation of the phase notations.

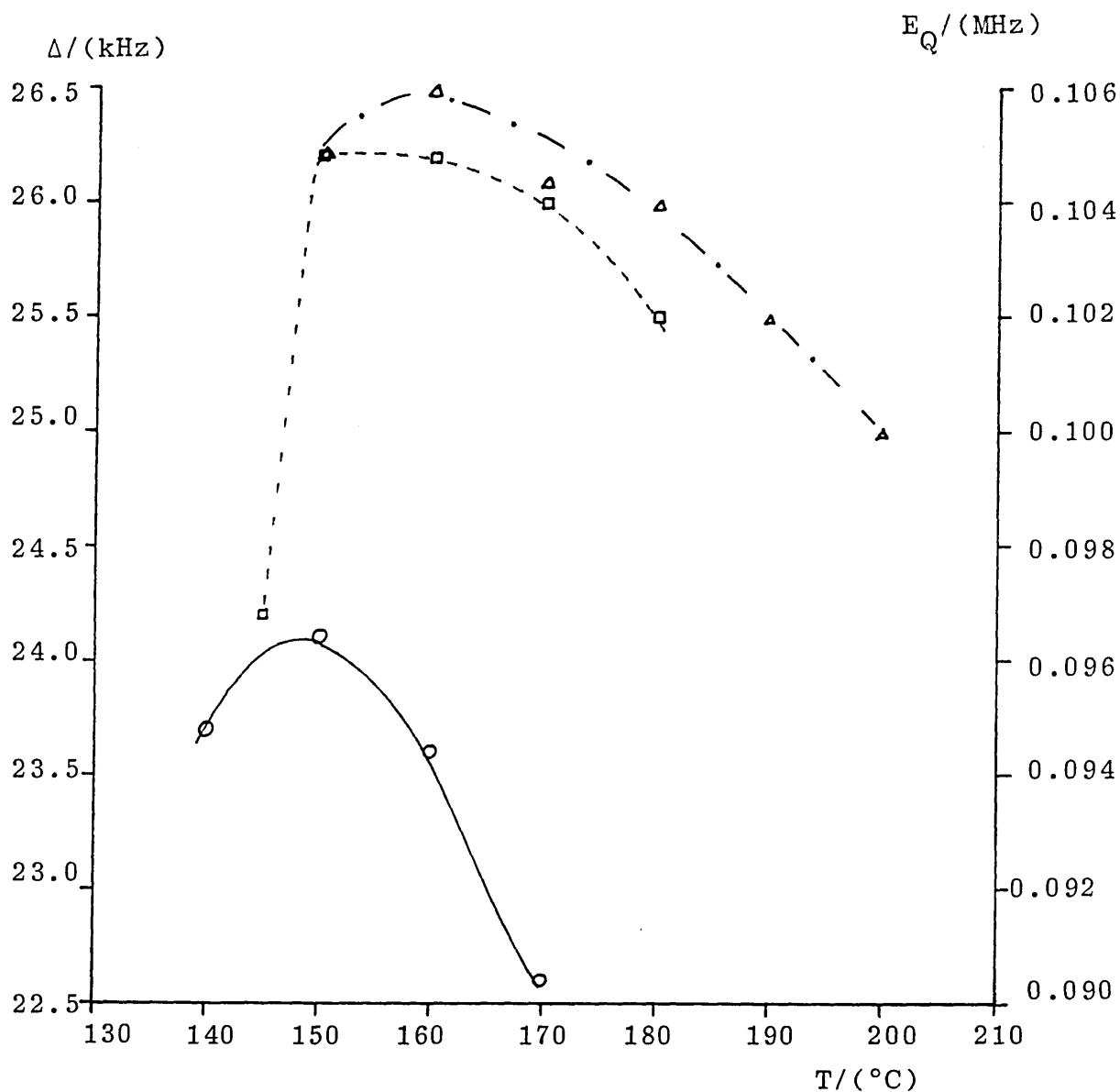


FIG. 52 : Temperature dependence of the  ${}^7\text{Li}$  quadrupole splitting,  $\Delta$ , and quadrupole coupling constant,  $E_Q$ , for lithium phenylstearate - 1-phenylheptane samples containing:

- 30.0% w/w LiPS
- 50.0% w/w LiPS
- △ 59.9% w/w LiPS

In the 1-phenylheptane system, the samples studied appeared to exhibit very weak temperature dependent  $\Delta$  and  $E_Q$  values (see FIG. 52). In spite of the relatively large precision limits on these values (see TABLE 24) it would appear that each sample experiences an initial increase in  $\Delta$  and  $E_Q$  at the H3 transition followed by a very gradual decrease with increasing temperature. (A comparable behaviour has been reported for  $^{23}\text{Na}$  in the thermotropic smectic A (lamellar) mesophase formed by a number of anhydrous short-chain sodium carboxylates at elevated temperatures (see FIG. 53).) It is worthy to note that the 50.0 wt % (32.5 mole %) LiPS sample,

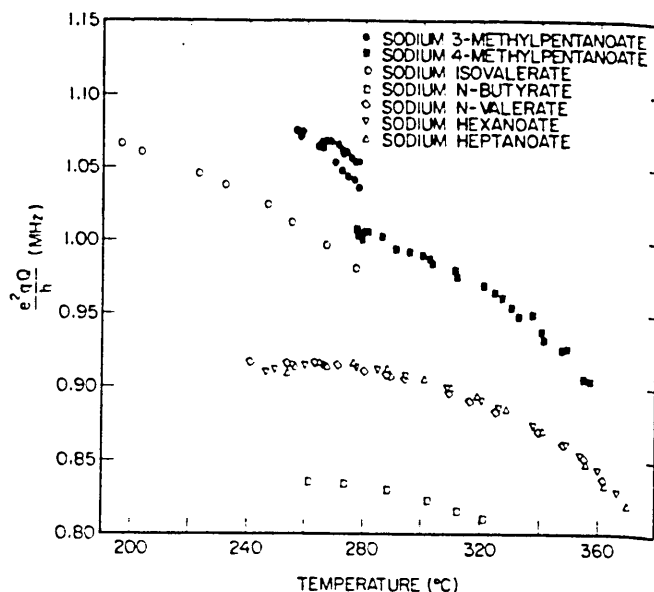


FIG. 53 : Temperature dependence of the absolute value of the  $^{23}\text{Na}$  quadrupole coupling constant  $|e^2qQ/h|$  in the mesophase of short-chain sodium carboxylates [32].

which has been observed to undergo a transition from a reversed hexagonal  $H_2$  mesophase to a micellar nematic  $N_{C2}$  mesophase at  $\sim 180$  °C by polarizing microscopy shows

no discontinuity in the quadrupole splitting - temperature curve. This behaviour indicates a very weak first- (or possibly a second-) order transition between the two mesophases which is in concordance with the DSC study where no transition was detected.

The vast majority of studies on the variation of counter-ion quadrupole splittings with temperature have been concerned with aqueous soap mesophases (for example, [280] and [285]) where changes in  $\Delta$  have been attributed to changes in the value of the order parameter,  $S$  (Section 2.2.5.2). Such changes were often complex and depended upon a large number of factors such as the nature of the amphiphile polar head ( $\text{CO}_2^-$ ,  $\text{OSO}_3^-$ ,  $\text{SO}_3^-$ ), the type and degree of counter-ion binding, the extent of amphiphile hydration and the presence of added components such as long-chain alcohols.

The precise origins of the temperature variation of  $\Delta$  in the 1-phenylheptane system are not clear. However, it seems reasonable to explain the decrease in  $\Delta$  tentatively in terms of reductions in the value of  $S$  due to changes in the time average of the EFG's sampled by the lithium nucleus. This may result from increasing diffusional and re-orientational motions of the  $\text{Li}^+$  and  $\text{RCOO}^-$  ions with increasing temperature. Similarly, the slight difference in the absolute values of  $\Delta$  for the micellar nematic  $N_{c2}$  and reversed hexagonal  $H_2$  mesophases may result from changes in the average EFG tensor (and therefore  $S$ ) caused

by greater order fluctuations in the former, less well-ordered mesophase. The cause of the initial increase in  $\Delta$  at the onset of the H3 transition is also uncertain and cannot be deduced from the available evidence. It is suggested, however, that this may arise from re-orientations of the  $\text{Li}^+ \text{RCOO}^-$  ion pairs before the onset of rapid diffusional motion, where a change in the time average value of  $\Theta_{\text{DM}}$  produces an increase in the value of S (refer to Section 2.2.5.2). A change in the EFG due to a modification of the electron density distribution (chemical bonding) resulting from the "fusion" of the polar groups at the H3 transition may also be a possible reason for the initial increase in the quadrupole splitting [303].

Lyotropic nematic mesophases may be oriented in a strong static magnetic field to produce a uniform macroscopic alignment of the constituent micellar aggregates with the principal or optic axis of the mesophase (the director) parallel or perpendicular to the applied field [254, 310, 311].

For uniaxial micellar nematic phases, the direction of alignment is determined by the diamagnetic susceptibility anisotropy of the mesophase measured parallel and perpendicular to the director,  $\Delta\chi = (\chi_{11} - \chi_{\perp})$ . It is clear that  $\Delta\chi$  may be zero, in which case the phase is

isotropic, at least, as far as diamagnetism is concerned. A positive value of  $\Delta x$  leads to a tendency for the director to align parallel to the magnetic field (Forrest and Reeves' [254] type I behaviour) whilst a negative value of  $\Delta x$  results in a tendency to align the director in all directions in the perpendicular plane to the applied magnetic field (Forrest and Reeves' [254] type II behaviour).

NMR spectroscopy may be used to determine the sign of  $\Delta x$  by observing the evolution of the mesophase quadrupole splittings from a completely random distribution of directors in space (the "powder" spectrum) to one which is more favourable to the field direction. For the micellar nematic  $N_{C2}$  phase formed in the LiPS-1-phenylheptane system, the sign of  $\Delta x$  was determined in the following manner.

A 30.0 wt % (17.1 mole %) LiPS sample was heated to the isotropic liquid state (200 °C) in the NMR magnet (working field strength 1.88 Tesla, 18.8 KGauss) and then cooled to the nematic mesophase region (160 °C) with the sample tube stationary (non-spinning). The  $^7\text{Li}$  NMR spectrum recorded for this sample after remaining stationary for 5 hours at 160 °C in the magnetic field is shown in FIG. 54(a). The corresponding powder spectrum is shown in FIG.54(b).

It is evident from these spectra that the resonance signals from the directors at  $\theta_{LD} = 0^\circ$  have become

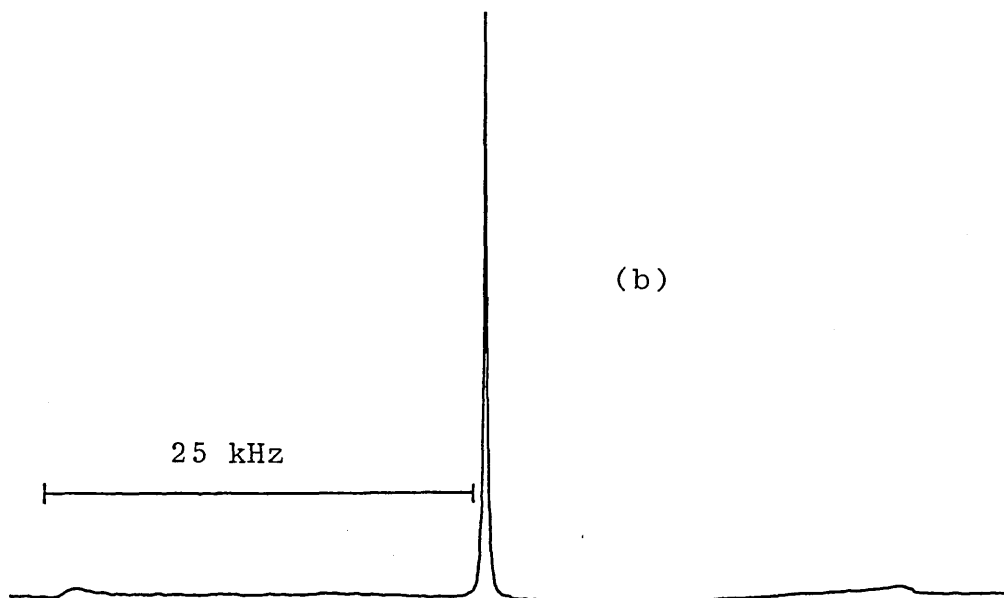
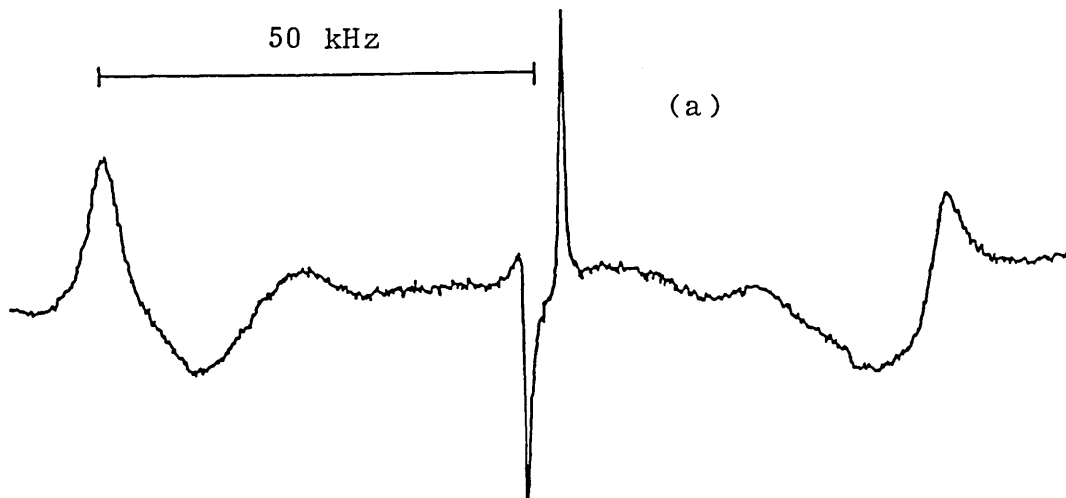


FIG. 54:  ${}^7\text{Li}$  NMR spectra for a 30.0% w/w lithium phenylstearate - 1-phenylheptane sample at 160 °C (micellar nematic mesophase)

- (a) aligned sample
- (b) "powder" sample

accentuated at the expense of all other angles as the process of parallel alignment has proceeded. The sign of  $\Delta x$  for this micellar nematic  $N_{C_2}$  phase is therefore positive ( $\Delta x > 0$ ). As a consequence of the  $(3\cos^2\theta_{LD} - 1)$  term in equation (2.11), p 88, this alignment has resulted in an increase of  $\Delta$  by a factor of two ( $\Delta = 48.4 \pm 0.9$  kHz) over the corresponding powder spectrum ( $\Delta = 23.6 \pm 0.8$  kHz). FIG. 54(a) shows, however, that the spectrum of the aligned sample was far too broad ( $\sim 100$  kHz) to be detected without serious distortion of the lineshape using the narrow band, high resolution spectrometer employed in this study. It should also be noted that a homogeneous "single-crystal" alignment of this sample could not always be attained (as evidenced by significant differences in the intensities of the quadrupole splitting satellites at  $\theta_{LD} = 0$ ). The reasons for this behaviour are not clear and this problem warrants further investigation.

The sign of  $\Delta x$  was confirmed by spinning the aligned sample about an axis perpendicular to the applied magnetic field (at an angular velocity of  $\sim 17$  Hz) for several hours. This motion destroyed the uniform alignment of the mesophase and produced a typical "powder" spectrum as shown in FIG. 54(b).

Whilst the existence of micellar nematic mesophases composed of finite sized "normal" disc micelles ( $N_{D_1}^+$ ,  $N_{D_1}^-$ ) and "normal" cylindrical micelles ( $N_{C_1}^+$ ,  $N_{C_1}^-$ ) have been reported for binary ionic amphiphile-water

systems, and also for ternary and quaternary aqueous systems containing added electrolytes and/or cosurfactants [254, 310, 311], this is believed to be the first reported case of a non-aqueous lyotropic nematic mesophase formed by an ionic amphiphile which is composed of "reversed" cylindrical micelles. Using the terminology of Boden, Radley and Holmes [315] this mesophase has been denoted  $N_{c_2}^+$  (with the + sign denoting a positive diamagnetic susceptibility anisotropy and the subscript  $c_2$  denoting the presence of reversed cylindrical micelles).

#### 4.2.1.5 The Equilibrium Phase Diagram

The equilibrium phase diagram constructed for the lithium phenylstearate-1-phenylheptane system is shown in FIG. 55. The positions of the boundaries indicated by broken lines are tentative.

The phase notations employed in FIG. 55 and throughout Section 4.2 are summarized below. It should be noted that the micellar aggregates constituting each phase (with the possible exception of the  $S_2$  phase) are of the reversed "cylindrical" type. Phases referred to as semi-crystalline possess a quasi-crystalline arrangement of the amphiphile polar groups and liquid-like hydrocarbon chains.

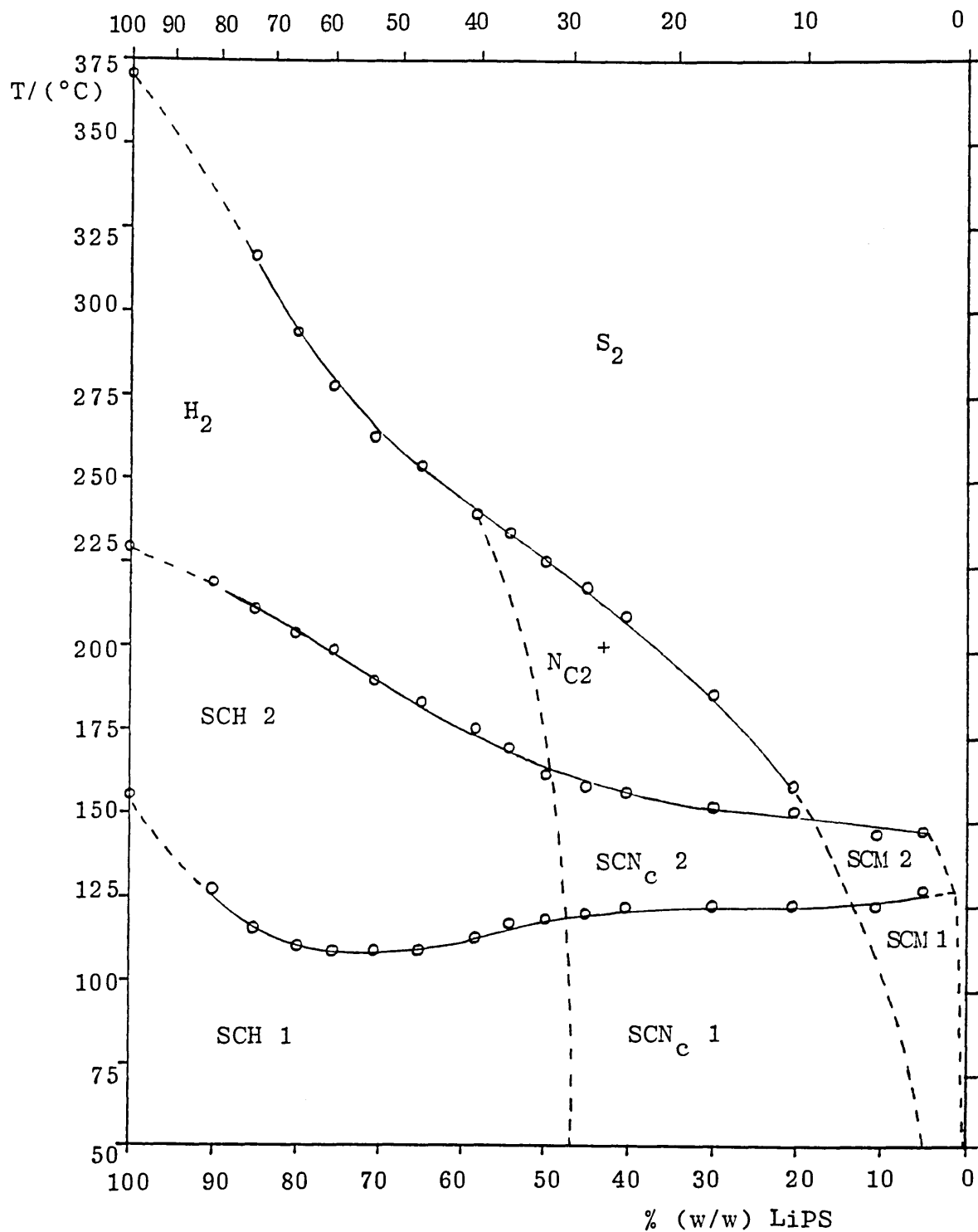


FIG. 55 : An equilibrium phase diagram for the system  
LITHIUM PHENYLSTEARATE - 1-PHENYLHEPTANE

SCH, semi-crystalline hexagonal phase  
SCN<sub>c</sub>, semi-crystalline nematic phase  
SCM, semi-crystalline "isotropic" micellar phase  
H<sub>2</sub>, fused hexagonal mesophase  
N<sub>c2</sub><sup>+</sup>, fused nematic mesophase possessing a positive  
diamagnetic susceptibility  
S<sub>2</sub>, fused isotropic micellar solution.

#### 4.2.2 The Lithium Phenylstearate-Benzene and Toluene Systems

The phase behaviour of lithium phenylstearate with aromatic hydrocarbon solvents such as benzene and toluene, appeared to be qualitatively similar to that observed with 1-phenylheptane.

Addition of these solvents to anhydrous LiPS at room temperature also produced transparent viscoelastic birefringent solutions and gels. Low-angle x-ray diffraction studies of these samples revealed the formation of a solvent-swollen 2-d hexagonal phase (SCH 1) or a concentrated "micellar" phase (SCN<sub>c</sub> 1) depending upon sample composition (TABLE 25).

TABLE 25 : Low-angle x-ray diffraction results for the lithium phenylstearate-benzene and toluene systems at 27 °C\*

LIPS CONTENT wt % mole %	OBSERVED BRAGG SPACINGS/(Å)			LATTICE SYMMETRY	HEXAGONAL LATTICE PARAMETER, a/(Å)
	d <sub>1</sub>	d <sub>2</sub>	d <sub>3</sub>		
IN BENZENE					
30.9	8.7	54.0 ± 2 <sup>†</sup>	-	Micellar <sup>†</sup>	-
39.6	12.3	41.3 ± 0.3	23.8 ± 0.1	2-d Hexagonal	47.7 ± 0.3
49.3	17.2	38.7 ± 0.3	22.3 ± 0.1	2-d Hexagonal	44.7 ± 0.3
57.3	22.2	38.1 ± 0.3	22.0 ± 0.1	2-d Hexagonal	44.0 ± 0.3
IN TOLUENE					
39.9	14.3	NOT MEASURED <sup>†</sup>	-	Micellar	-
49.5	19.8	40.4 ± 0.3	23.1 ± 0.1	2-d Hexagonal	46.6 ± 0.4
59.9	27.3	39.9 ± 0.3	22.9 ± 0.1	2-d Hexagonal	46.1 ± 0.3

\*These samples also exhibited a diffuse reflection in the high-angle region at  $\sim 4.6 \text{ \AA}$ .  
<sup>†</sup>d<sub>1</sub> corresponds to the maximum scattering intensity of a liquid-type scattering function. The diffraction pattern in this case is considered to result from a semi-crystalline reversed micellar nematic phase, SCN<sub>C</sub> 1 (refer to Section 4.2.1.3 for explanation).

It would appear that, as a result of their much smaller molecular volumes, greater quantities of these solvents can be incorporated into the disordered hydrocarbon regions of the LiPS reversed hexagonal SCH 1 structure without producing major dilations of the lattice (as revealed by the small changes in "a" with solvent concentration). The hexagonal (SCH 1) to nematic (SCN<sub>c</sub> 1) phase boundary is consequently observed at correspondingly lower solvent concentrations (1-phenylheptane < toluene < benzene) as the molecular volume of the solvent increases in size.

Irrespective of sample composition, however, <sup>7</sup>Li NMR central linewidth values obtained for the LiPS-toluene system, indicated that, once again, the polar groups of LiPS cannot be considered as "fused" at room temperature even in the more dilute samples. For samples containing between 0.1 and 8.5 wt % (0.025 and 2.3 mole %) LiPS, the <sup>7</sup>Li  $W_{\frac{1}{2}}$  values were essentially invariant at  $2.4 \pm 0.1$  kHz. This was further supported by the observation of a stepwise melting process for the soap-solvent samples in both systems involving transitions accompanied by considerable changes in enthalpy. The results obtained by DSC for several LiPS-toluene samples are given in TABLE 26. (It should be noted that the LiPS used in this study was prepared from a batch of pure phenylstearic acid. The H4 transition temperatures given in TABLE 26 are therefore considered to be the true values whereas those obtained for the 1-phenylheptane system

TABLE 26 : Phase transition temperatures and enthalpies  
for the lithium phenylstearate-toluene system

LiPS CONTENT		H2		H3		H4	
wt %	mole %	T/(°C)	$\Delta H/$ (kJmol <sup>-1</sup> )	T/(°C)	$\Delta H/$ (kJmol <sup>-1</sup> )	T/(°C)	$\Delta H/$ (kJmol <sup>-1</sup> )
20.0	5.9	75.1	*	100.1	*	~155 <sup>†</sup>	-
28.5	9.1	75.6	*	107.3	*	~190 <sup>†</sup>	-
39.2	13.9	91.3	*	117.8	*	213.8	1.2
50.2	20.2	88.1	4.1	122.1	2.8	222.2	1.5
61.6	28.7	74.5	4.4	138.0	5.1	251.8	1.6
68.5	35.3	91.8	3.9	157.6	4.7	273.3	1.6

\*Total enthalpy for the overlapping H2 and H3 transitions was ~ 8-10 kJ mol<sup>-1</sup>.

<sup>†</sup> Transition temperature determined by macroscopic visual observations in polarized light (birefringent to isotropic).

(TABLE 19, p 190) are considered to exceed the true values by ~ 9 °C).

Comparing the results obtained by DSC for the LiPS-toluene and LiPS-1-phenylheptane systems on a weight to weight percentage basis, it would appear that the respective H2 and H3 transitions are significantly lower in the toluene system. The temperatures of the H4 transition (corresponding to the formation of the isotropic melt and determined ultimately by the strength

of cohesion between the "fused"  $\text{Li}^+$  and  $\text{RCOO}^-$  ions) appear to be greater, however, in the toluene system, suggesting that the phase structures present preceding the final melt are destabilized to a lesser degree by toluene. (DSC results obtained for a 49.3 wt % (17.2 mole %) LiPS-benzene sample were very similar to those obtained for the corresponding toluene sample, allowing for the slight differences in sample composition, suggesting a similar phase behaviour for the two systems).

Due to the high volatilities of both benzene and toluene, structural investigations of their LiPS containing systems were not carried out at elevated temperatures. It is anticipated, however, that the equilibrium phase diagrams of LiPS with both benzene and toluene may be qualitatively similar to that constructed for the 1-phenylheptane system.

#### 4.2.3 The Lithium Phenylstearate-Non-Aromatic Hydrocarbon Systems

In contrast to the phase behaviour of the LiPS with the aromatic hydrocarbons, preliminary investigations involving saturated alkane solvents of different molecular shape and weight revealed some marked differences in behaviour.

Addition of 51.4 wt % n-heptane to anhydrous LiPS at room temperature produced a heterogenous opaque gel whereas n-hexadecane in approximately the same concentration produced a swollen "solid" sample. The addition of squalane, however, appeared to have very little visible effect on the "solid" soap. Similar effects were also observed on addition of approximately 80 wt % of these solvents.

Macroscopic visual observations suggested that complete miscibility of these soap-solvent samples was only achieved on heating past the respective H2 transition temperatures for the n-heptane and n-hexadecane systems and past the H3 transition temperature for the squalane system.

DSC studies of the n-hexadecane and squalane samples (which had been homogenized by heating to the isotropic liquid state; Section 2.1.5) indicated that these solvents were far less effective than 1-phenylheptane (and also toluene and benzene) in reducing the H2 and H3 transition temperatures of the solvent-free soap, though lower temperatures were observed for the H4 isotropic melt transition. (The LiPS used in these studies was of a similar purity to that used for the 1-phenylheptane system, so a direct comparison of the transition temperatures can be made).

For a 51.1 wt % (39.2 mole %) LiPS in n-hexadecane sample, values of 141.5 °C ( $\Delta H = \sim 5.6 \text{ kJ mol}^{-1}$ ), 184.3 °C ( $\Delta H = \sim 6.3 \text{ kJ mol}^{-1}$ ) and 210.7 °C ( $\Delta H = \sim 1.7 \text{ kJ mol}^{-1}$ ) were obtained for the H2, H3 and H4 transitions respectively.

For a 48.2 wt % (51.8 mole %) LiPS-squalane sample, the corresponding H2 and H3 transition temperatures were 143.7 °C and  $\sim 209.3 \text{ °C}$  (no  $\Delta H$  data was obtained). The endothermic peak corresponding to the H4 transition was concealed beneath the H3 peak as revealed by

macroscopic visual observations.

DSC studies were not performed on the LiPS-n-heptane sample, however macroscopic visual observations in polarized light indicated that the H2 and H3 transition temperatures were approximately 15-20 °C higher than those observed for a 1-phenylheptane sample of similar composition. Unfortunately, observations of the n-heptane sample had been limited to 190 °C and so a direct comparison of the respective H4 transition temperatures cannot be made.

Though comprehensive structural investigations of these hydrocarbon systems were not performed, polarizing microscopy penetration experiments provided a general insight into their phase behaviour at elevated temperatures.

For the LiPS-n-hexadecane system, the onset of sample dissolution to the isotropic liquid state was apparent between  $\sim$  170 °C and 180 °C. Further increases in temperature resulted in the formation of a micellar nematic mesophase at the LiPS-solvent interface (recognised by its pronounced fluidity and characteristic schlieren texture). The temperature range of stability of this mesophase, between approximately 195 °C and 209 °C, was far less than that observed in the 1-phenylheptane system. At a slightly higher temperature the angular texture characteristic of fused hexagonal mesophases became apparent. This phase was stable to at least 250 °C, the upper limit of study.

For the LiPS-squalane system, general dissolution of the sample only became apparent at  $\sim 198$  °C. Careful observations indicated that the micellar nematic mesophase was absent from this system, though the fused hexagonal mesophase is believed to occur.

#### 4.2.4 Discussion

The study of dilute solutions of ionic amphiphiles of low crystallizing tendency, the so-called "oil-soluble soaps", has been reported in a variety of organic solvents by a number of investigators [137, 140, 171, 178-180]. The solubility phenomena exhibited by these surfactants are too complex and depend upon too many factors to justify any hope of systematizing all the data by means of one simple theory.

The results of this present study suggest, however, that the theory proposed by Little and Singleterry [171] to explain the solubility behaviour of the alkali metal dinonylnaphthalenesulphonates (DNNS) in low polarity organic solvents may be extended in part to the phenylstearates.

It may be noted that when Kissa [209] mixed the lithium salts of nine pure branched-chain acids, the room temperature solubility was increased 400-fold over the sum of their separate solubilities (Section 1.2.3.2). Little and Singleterry [171] have suggested that the major change in the thermodynamic situation when these pure salts are mixed (as in the case of lithium phenylstearate;

Section 1.2.3.1) is that the condensed soap phase becomes effectively a solid solution of geometrically unlike molecules which approaches the character of the viscous liquid phase postulated for the sulphonates [171]. The solubility then becomes that appropriate to liquid-liquid mixtures. This is thought not to be the case, however, for the isomeric lithium phenylstearate soap mixture.

It has been established (Section 3.3.5) that solvent-free "solid" LiPS forms an ordered semi-crystalline 2-d reversed hexagonal structure (SCH 1) at room temperature and not a heterogenous "solid solution". The solubility characteristics of LiPS in hydrocarbon solvents will therefore be partly determined by the composition and properties of the exterior parts of the constituent cylindrical micelles which are located so that they can interact with the molecules of the solvent. To a very rough approximation, this portion of the micelle consists of the disordered phenylstearate radicals: the lithium carboxylate portion of the soap molecules are considered to be located in the central region of the micelle forming a quasi-crystalline polar core. As a result of this structure, the solubility of LiPS in hydrocarbon solvents may be expected to parallel that of the branched hydrocarbon phenyloctadecane, again to a rough first approximation. (It may be expected, however, that this approximation will be affected at low temperatures due to the attachment of the phenylstearate chains at one end

to the ordered quasi-crystalline polar groups).

Little and Singleterry [171] found that the solubility parameter,  $\delta$ , of Hildebrand and co-workers [317], rather than the dielectric constant or the dipole moment, was the property of a solvent which most accurately forecast the micellar solubility of the alkali suphonates in that solvent. The parameter  $\delta$  is equal to  $\sqrt{-E}/V_e$  where  $-E$  is the energy of vaporization to zero pressure and  $V_e$  is the liquid molar volume. It effectively measures the square root of the "internal pressure" or "cohesive energy density" of the liquid. The cohesive energy density is a measure of intermolecular attraction, and in this theory it is assumed that molecules of equal cohesive energy density have equal intermolecular interaction and therefore form ideal solutions. However, if solutes have a different cohesive density than the solvent, the solutions are not ideal and solubility of the solute is decreased from ideality by an amount predictable from the difference in cohesive energy densities of solute and solvent. Miscibility in all proportions is characteristic of liquid pairs whose solubility parameters do not differ by more than approximately 3.5 units [317]. The degree of mismatch tolerated is less if the effective molecular volumes differ by an order of magnitude.

The fact that "solid" LiPS appears to be miscible with several aromatic hydrocarbons (1-phenylheptane, toluene and benzene) in all proportions at room temperature (forming homogenous viscous solutions or gels), partially

miscible with n-heptane, swells in n-hexadecane but is essentially insoluble in squalane may be directly related to critical differences in the respective solvent solubility parameters. In the absence of a known value for the solubility parameter of phenyloctadecane, those of the solvents benzene, n-hexadecane, n-heptane and squalane are reported to be 9.15, 8.0, 7.45 and 7.1 respectively [171]. It is tentatively suggested that when the solubility parameter mismatch is significant, resulting in negligible or limited LiPS solubility at room temperature, complete solubility may only be achieved at a certain critical temperature which corresponds to a 'melting' transition of the solvent-free soap structure itself (c.f. the solubility behaviour of crystalline lithium stearate in hydrocarbons; Section 4.1).

Low angle x-ray diffraction studies of the LiPS-aromatic hydrocarbon solvents have shown that significant quantities of these solvents can be incorporated into the disordered lipophilic regions between the reversed micellar aggregates of the 2-d hexagonal soap structure at room temperature. This results in a gradual dilation of the lattice, though long-range 2-d hexagonal periodicity is retained. (This behaviour appears to be in direct contrast to that of the oil-soluble surfactant, Aerosol OT, which forms a "fused" reversed hexagonal,  $H_2$ , mesophase in the solvent-free state at room temperature; Section 1.2.2.4). These solvents will be distributed so that

their concentrations are highest in that locality where their activity coefficients are lowest, i.e. in that locality which it most resembles in solvent type or solubility parameter. Therefore, 1-phenylheptane might be expected to be distributed uniformly among the soap hydrocarbon chains close to the substituted phenyl groups. Benzene and toluene on the other hand, as a result of their much smaller molecular volumes and their polarizable nature, may also show considerable electrostatic "solvation" interactions with the polar groups (ref 4, p 28). These solvents will therefore show a lower activity coefficient when close to the polar groups than would molecules of a less polarizable hydrocarbon such as n-heptane. This difference in distribution of the dissolved hydrocarbons may explain the significantly lower H<sub>2</sub> and H<sub>3</sub> transition temperatures observed in the benzene and toluene systems compared with the other LiPS-hydrocarbon systems studied. (It should be noted, however, that for each system studied, the interaction of the hydrocarbon solvent was not sufficient to overcome the strong quasi-crystalline bonds existing between the lithium carboxylate groups at room temperature. This was evidenced by the magnitudes of the <sup>7</sup>Li NMR lines down to soap concentrations as low as 0.1 wt % (0.025 mole %) LiPS in the toluene system.)

At higher solvent concentrations the long-range positional ordering between these indefinitely long reversed

cylindrical micelles is lost and a concentrated micellar solution of orientationally ordered rigid rod micelles (the  $SCN_C$  1 phase) is believed to result. (In the 1-phenylheptane system, such solutions may give rise, depending upon same composition, to a micellar nematic mesophase ( $N_{C2}$ ) at temperatures corresponding to a "fusion" of the quasi-crystalline polar groups.)

Due to the strong bonding which exists between the polar groups of these micelles at room temperature, and the low dielectric constants of the hydrocarbon solvents, it may be envisaged that in the absence of significant quantities of water or other polar contaminants, the size of the LiPS micelles may well prove to be essentially concentration independent and very long (if not indefinitely long as in the parent hexagonal phase) micelles may persist down to very low soap concentrations.

The results of the present investigations indicate, therefore, that the high viscosity, shear-birefringence and non-Newtonian flow reported for the dry phenyl-stearate-benzene solutions [178, 179] probably arise, for the lithium phenylstearate system at least, from the presence of long rigid reversed cylindrical micelles and not as originally suggested by Honig and Singleterry [180] from the aggregation of these soap molecules into single, coordinately bonded linear polymer-like chains (FIG. 8, Section 1.2.3.3) analogous to those proposed for the aluminium and cobalt hydroxy monooleate soaps in hydrocarbon solvents (Section 1.2.1.3).

This may not be the case, however, for all alkali metal phenylstearates. Honig and Singleterry [180] have reported that LiPS in 0.9 wt % concentration in benzene ( $\sim 2.2 \times 10^{-2} \text{ mol dm}^{-3}$ ) formed a viscous solution whereas the caesium soap even at 2.65 wt % concentration ( $\sim 4.7 \times 10^{-2} \text{ mol dm}^{-3}$ ) gave a solution only slightly more viscous than pure benzene (Section 1.2.3.3). These observations suggest that for caesium phenylstearate the size and shape of the aggregates formed may be either concentration dependent or strongly influenced by the strength of the caesium carboxylate interactions.

A similar dependence of aggregation size on the nature of the surfactant counter-ion, but of the reversed order (an increase in the size of the cation resulted in an increase in the aggregation number but also an increase in the tendency to form concentration dependent aggregates), has been observed for the alkali metal derivatives of Aerosol OT in solvents such as benzene, cyclohexane, n-heptane and isooctane at 25 °C [164, ref 140, p 103]. For example, in isooctane, the aggregation numbers for the Li and Na derivatives were practically constant at 17-18 surfactant molecules (between  $\sim 2$  and  $5 \text{ mol dm}^{-3}$  surfactant) whereas that of the caesium derivative increased from  $\sim 40$  to  $\sim 55$  over the same concentration range (ref 140, p 103).

It has been reported that for typical oil-soluble soaps such as Aerosol OT, sodium DNNS and many petroleum

sulphonates [137], specific atom to atom coordination bonds are not formed between the polar groups and the condition of the ions in the central core of these micelles approximates to that in a fused salt [318]. For such surfactants, the formation of small approximately spherical micelles is sterically favoured since this geometry allows the loosest packing of the bulky hydrocarbon radicals around a core of given volume (with the prolate ellipsoid next with regard to packing density). The number of molecules per micelle is therefore sterically limited by the relative cross-sections and volumes of the hydrocarbon chains and polar heads respectively [137].

In this present study, attempts to obtain precise information concerning the size and shape of the micelles present in dilute toluene and 1-phenylheptane solutions (containing  $\sim 1$  wt % LiPS) using light scattering techniques [319, 320] were unsuccessful. This was due to the insignificant differences in the refractive indices between the solvents and their respective micellar solutions. It is hoped to obtain this information, however, by small-angle neutron scattering experiments [321, 322] on dilute solutions of LiPS (1 and 2 wt %) in both toluene- $d_8$  and n-heptane- $d_{16}$ .

The preceding discussion has to be judged with the view that minute amounts of water in all organic systems, even under particular precautions, cannot be

completely excluded. It is also obvious that the tendency of reversed micellar aggregates in nonpolar hydrocarbon solvents to solubilize minute amounts of polar impurities, particularly water, is pronounced [140]. It has been shown [323] that the amount of water necessary to form a minimum number of hydrogen-bonds significant to support the growth of the aggregates and to stabilize the final particles is far below the detectable amount present in organic solvents. (It is also worthy to note that the strength of the hydration interaction of the alkali metals increases from caesium to lithium.) These statements lead to some interesting consequences; the question arises whether or not it is reasonable at all to discuss a surfactant in oil as a true binary system except by way of an extrapolation.

An equilibrium phase diagram was constructed for the lithium phenylstearate (LiPS)-water system and is presented in FIG. 56, p 323. The ordinate gives the temperature ( $^{\circ}\text{C}$ ) and the abscissa the sample composition. The latter is given as the weight per cent of amphiphile (LiPS) on the lower axis and as the mole ratio of water ( $^2\text{H}_2\text{O}$ ) to amphiphile,  $X_{\text{W}}/X_{\text{A}}$ , on the upper axis.

The positions of the major first-order phase boundaries were established by differential scanning calorimetry, with macroscopic and microscopic observations in polarized light supplementing this data. The positions of the boundaries indicated by broken lines are tentative. Variable-temperature low-angle x-ray diffraction and quadrupole NMR ( $^7\text{Li}$  and  $^2\text{H}$ ) techniques were used to provide structural information on the phases encountered.

It should be noted that, due to the complex isomeric composition of lithium phenylstearate (Section 2.1.3.1), the two-component phase diagram may not fully obey the Gibbs phase rule. For the purpose of this study, however, the soap was regarded as a single component.

The phase notations used in FIG. 56 and systematically employed throughout Chapter 5 are those devised by Ekwall et al [260] where  $L_1$  and  $L_2$  are isotropic solution phases; D and B represent the lamellar mesophase and G corresponds to solid material.

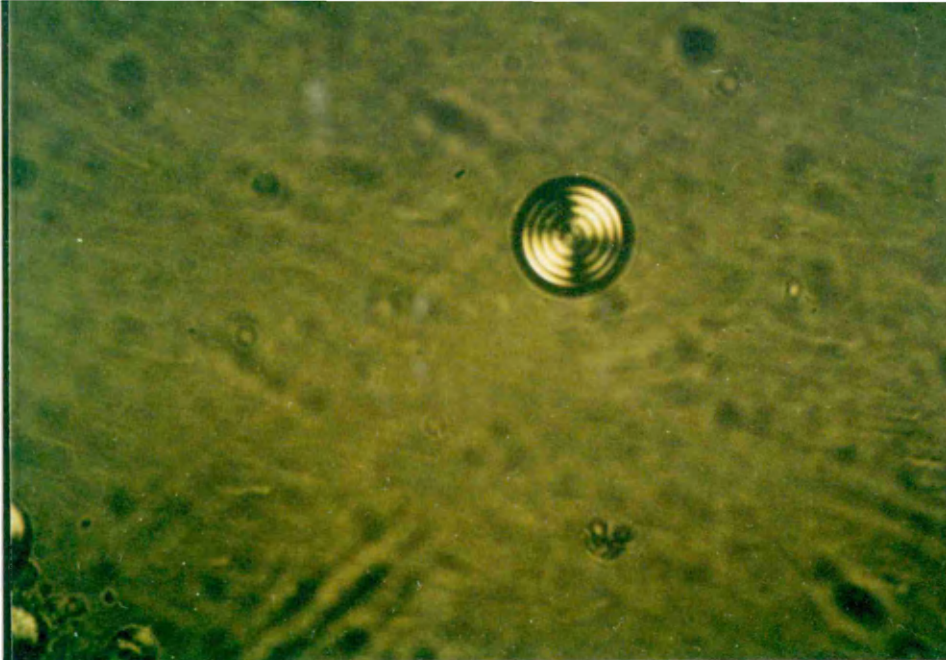
## 5.1 Polarizing Microscopy and Macroscopic Visual Observations

### 5.1.1 Microscopy Penetration Experiment

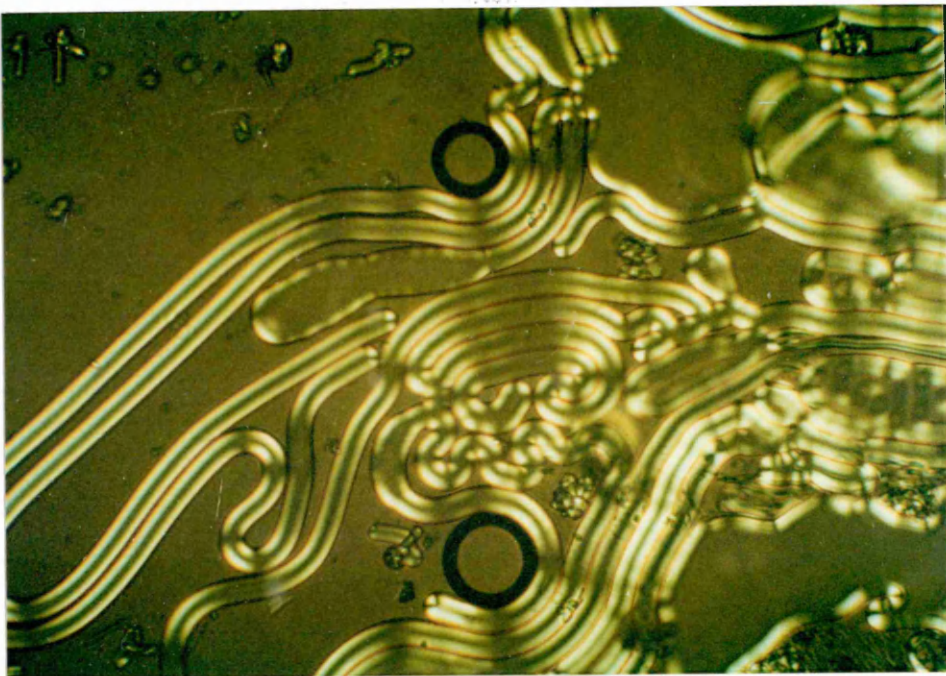
As a preliminary means of studying possible lyotropic mesophase formation in the LiPS-water system, the polarizing microscopy penetration technique (Section 2.2.1.2) was employed.

In contrast to the long straight-chain crystalline lithium soaps ( $n_c > 12$ ) which are quite insoluble in water, their Krafft points being above 100 °C [316], water was observed to penetrate instantaneously into a thin film of LiPS at room temperature producing a lyotropic lamellar mesophase. This phase was easily recognized by the spherulitic (where the lamellar bilayers are believed to be arranged concentrically like the layers in an onion [257]) and myelenic optical structures observed in the most dilute soap regions (FIG. 57 (a) and (b) respectively).

On allowing the water-contacted soap film to stand at room temperature for several hours, to assist the diffusion of the solvent, a re-examination of the sample revealed the presence of a mobile brightly birefringent more soap-rich region (which was continuous with the features described above) possessing a so-called "mosaic" texture (category 122.1 in Rosevear's [258] classification). Application of slight pressure to these regions produced a largely homeotropic texture containing numerous small spherulites and transversely striated "oily-streaks" (categories 112 and 122.2 in Rosevear's [258] classification).



(a)



(b)

FIG. 57 : Lamellar mesophase optical structures formed on contacting a thin film of lithium phenylstearate with water at room temperature;

(a) spherulite (crossed polars, magnification x 200)

(b) myelinic tubes (crossed polars, magnification x 100)

On release of pressure, however, this texture reverted to a fine-grained mosaic texture. These observations were also consistent with the formation of a lamellar bilayer mesophase (commonly referred to in the literature as McBain's "neat" phase, Luzzati's " $L_{\alpha}$ " phase, Winsor's "G" phase and Ekwall's "D" phase).

At higher LiPS concentrations, the lamellar phase was succeeded by a more viscous phase possessing a dull birefringent patchy non-geometric texture (resembling Rosevear's [258] "middle" or hexagonal phase texture, category 231) which appeared to be continuous with the "solid" soap.

As the temperature of the sample was increased beyond  $\sim 74$  °C, a marked change in microscopic appearance was observed corresponding to a gradual transformation of this dull viscous non-geometric phase into the mobile bright golden birefringent lamellar phase mosaic texture. By  $\sim 95$  °C, the upper limit of study, an apparently homogeneous lamellar neat phase was present at all LiPS-water concentrations up to the boundary with the "solid" soap phase. The reversibility of this thermotropic transition was difficult to detect microscopically, though the phase behaviour reported above was reproducible for all successive preparations.

In order to ascertain approximate values for the temperature and composition ranges of existence of the phases described, the phase behaviour of bulk soap-water samples of known composition was studied using macroscopic and then microscopic observations in polarized light.

### 5.1.2 Macroscopic Observations

The LiPS-water ( $^2\text{H}_2\text{O}$ ) samples could be divided broadly into four main groups according to gross appearance and consistency. In the intervening regions there was a continuous transition of these physical properties.

At compositions between approximately 1 wt % and 20 wt % LiPS, fluid milky solutions were formed. On standing at room temperature for  $\sim 24$  hours, samples containing 1 wt % and 3 wt % LiPS separated spontaneously into two distinct layers composed of a milky fluid (upper layer) and a slightly turbid isotropic solution (lower layer). The samples in this composition range were therefore believed to result from heterogeneous equilibria involving a two-phase dispersion of a lamellar liquid crystal in dilute soap solution.

Between approximately 30 wt % and 45 wt % LiPS, greyish translucent slightly anisotropic mucous-like samples with relatively low viscosities were formed, with the degree of transparency increasing slightly with decreasing water concentration. On heating these samples, a reversible transition to a completely transparent, highly anisotropic (uniform bright golden birefringent) state was complete by  $\sim 140$  °C in each case. At significantly higher temperatures a complete loss of birefringency accompanied by a marked decrease in sample viscosity marked the transition to the isotropic liquid melt.

At slightly higher soap concentrations ( $\sim 50$  wt % to 65 wt % LiPS) the samples prepared at room temperature were of a more viscous mucous-like consistency. They were also translucent, but cloudy, and optically anisotropic. The cloudy appearance of these samples was, however, heterogeneous and was attributed to incomplete mixing of the soap and solvent. After heating the samples to the isotropic liquid melt and cooling to room temperature, completely transparent highly anisotropic homogenous materials were obtained. These underwent no further changes in appearance after storing at room temperature for over 12 months.

At even higher LiPS concentrations (between  $\sim 70$  wt % and 75 wt % LiPS) the homogenized samples formed stiff, semi-translucent, slightly anisotropic but cloudy heterogeneous gels. As the water content was reduced further to  $\sim 6$  wt %, completely opaque wax-like "solids" were formed. These observations indicated the existence of a second two-phase region possibly involving a liquid crystal phase + "solid" soap, with the mesophase concentration decreasing with decreasing water concentration.

On heating each of these samples to  $\sim 100$  °C, the opacity cleared (at increasingly higher temperatures as the water concentration was reduced), producing transparent homogeneous bright golden birefringent viscous liquids which melted at correspondingly higher temperatures to the isotropic liquid state. At the highest soap concentration studied, a sample containing  $\sim 96$  wt % LiPS

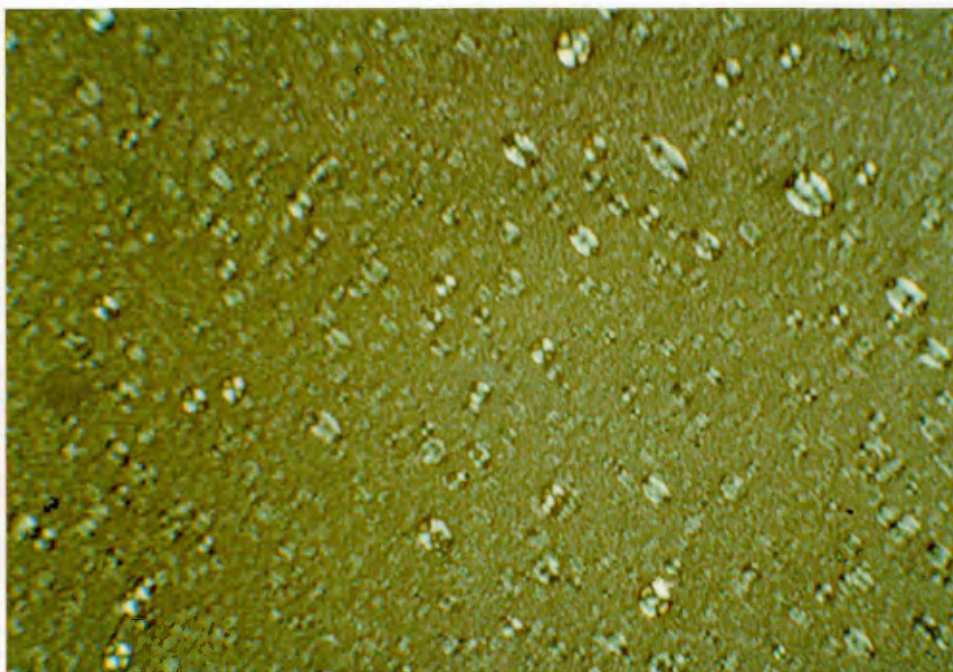
(in contrast to all other samples containing a minimum of 70 wt % soap, where the opacity reappeared on cooling to room temperature) remained transparent and highly anisotropic after cooling from beyond the isotropic melt and standing at room temperature for  $\sim 12$  months.

### 5.1.3 Microscopic Observations

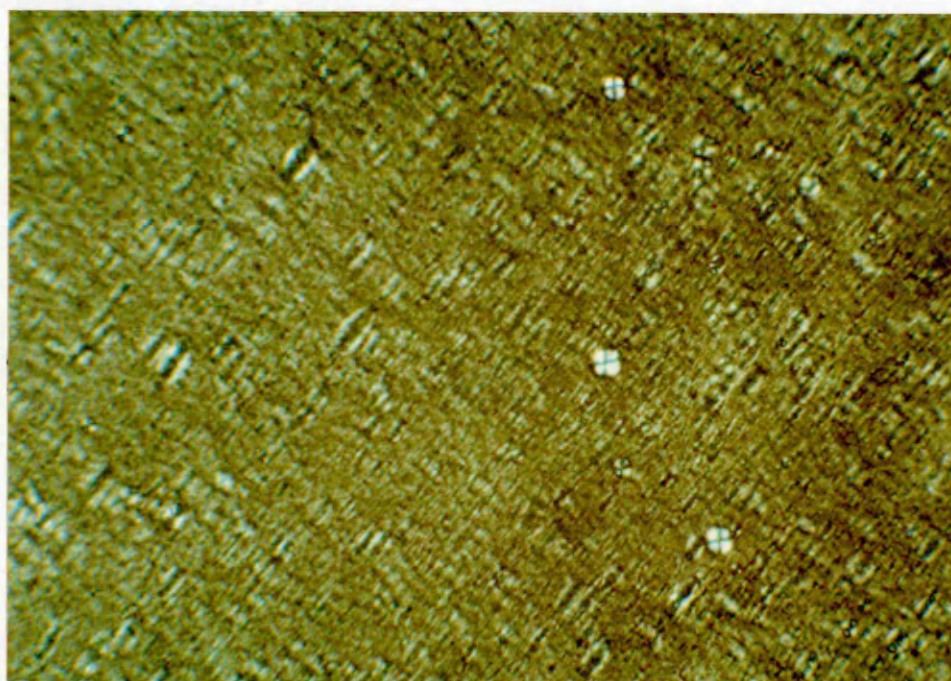
Polarizing microscopy observations of the samples studied macroscopically allowed a preliminary assignment of the phases formed at known soap-water compositions.

Samples containing in excess of  $\sim 77$  wt % water (ie in the two-phase lamellar + isotropic solution region) exhibited a weakly birefringent "diffuse woven" background texture containing a large number of spherulites with extinction crosses plus deformed spherulitic structures (FIG. 58). As the soap concentration increased, however, from  $\sim 23$  wt % to  $\sim 45$  wt % LiPS, an almost uniform "woven" texture, with few or no spherulites, was observed (FIG. 59). These microscopic features were reminiscent of the textures reported by Mandell and Ekwall [260] for a lamellar B phase (coherent "rippled" bilayers [325]) formed at room temperature in the most water-rich regions of the ternary system sodium octanoate-decanol-water. No distinct textural changes were observed on heating these aqueous LiPS samples to  $\sim 95$  °C, the upper limit of study.

As the soap concentration was further increased to a maximum of  $\sim 65$  wt % LiPS, textures more characteristic



(a)



(b)

FIG. 58 : Optical textures formed at room temperature by dilute lithium phenylstearate-water two-phase samples (lamellar mesophase + isotropic solution) showing a weakly birefringent "diffuse woven" background + spherulites (crossed polars, magnification x 100).

(a) 9.8% (w/w) LiPS- $^2$ H $_2$ O

(b) 19.8% (w/w) LiPS- $^2$ H $_2$ O

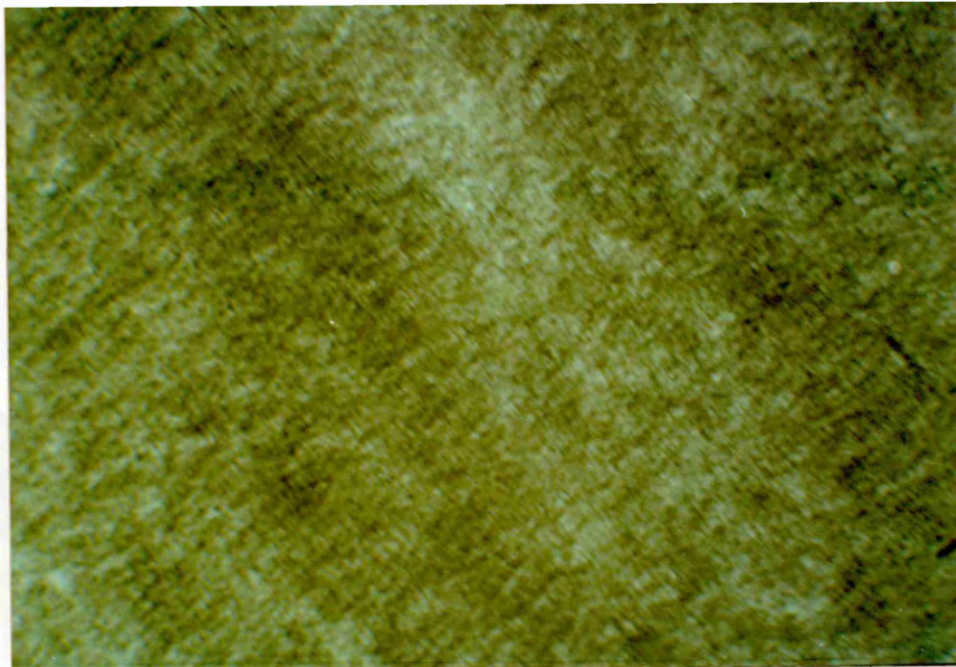


FIG. 59 : Lamellar mesophase texture formed by a 28.1% (w/w) lithium phenylstearate- $H_2O$  sample at room temperature showing an almost uniform weakly birefringent "woven" texture (crossed polars, magnification x 100).

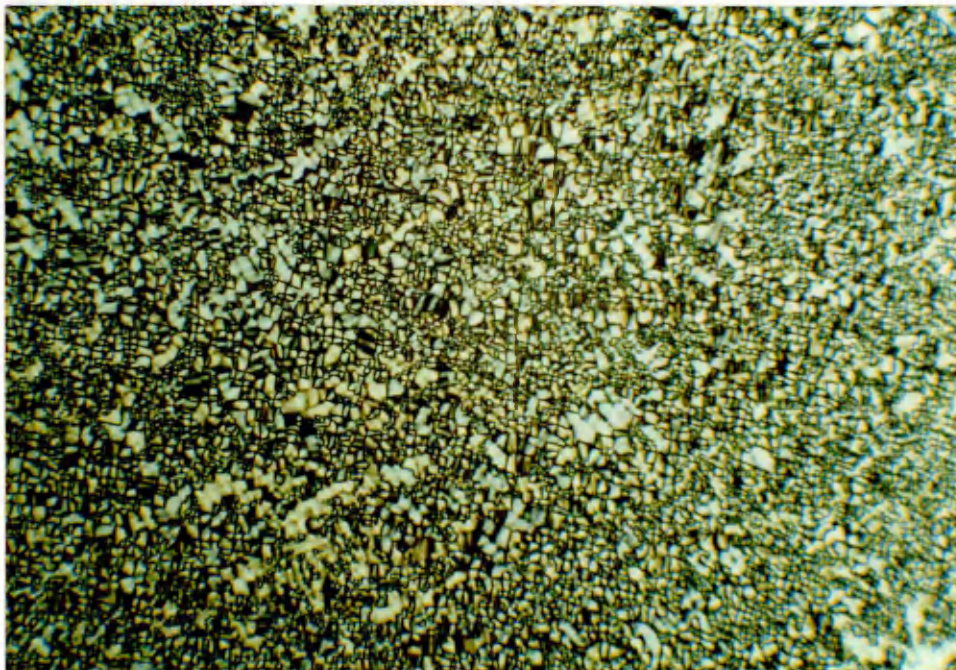
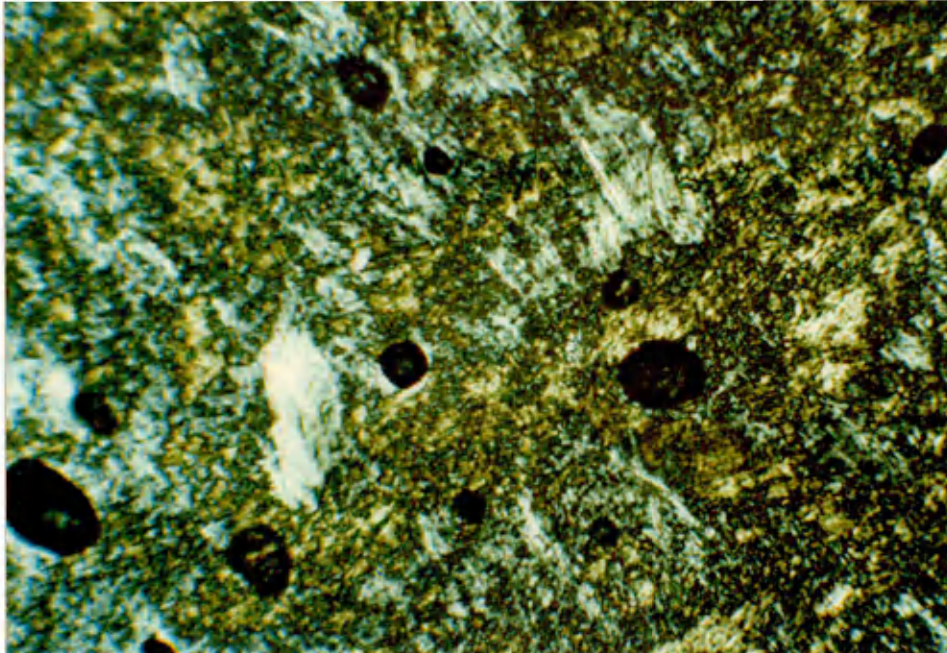
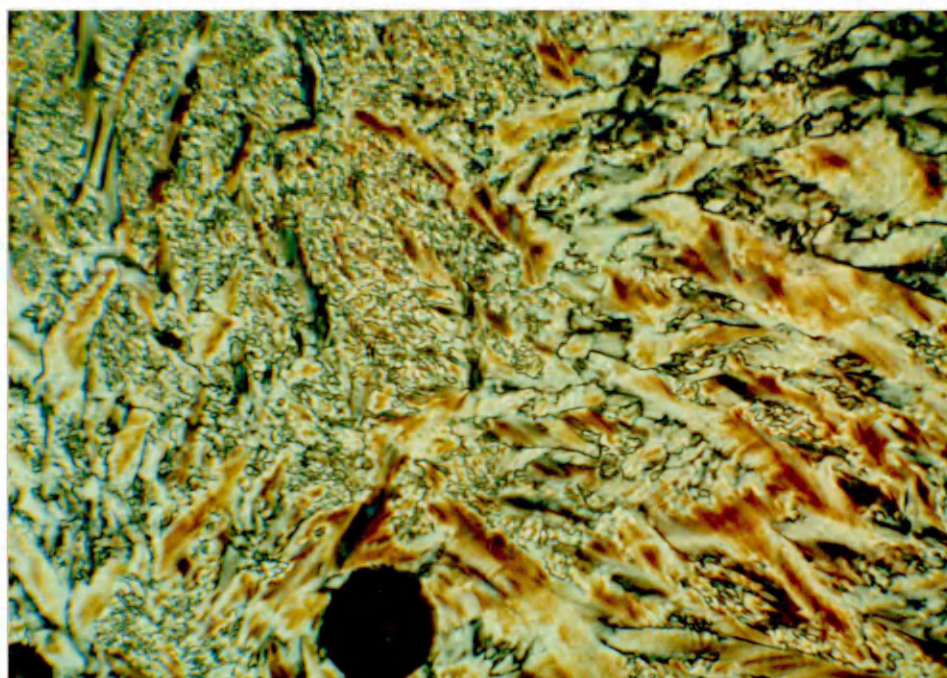


FIG. 60 : Lamellar mesophase "mosaic" texture formed by a 64.9% (w/w) lithium phenylstearate-water sample at 83 °C (crossed polars, magnification x 100).



(a)



(b)

FIG. 61 : Optical textures formed by a 75.0% (w/w) lithium phenylstearate- $H_2O$  sample (crossed polars, magnification x 100).

- (a) At room temperature (two-phase lamellar mesophase + "solid" LiPS).
- (b) At 91 °C (homogeneous lamellar mesophase) showing a "broken-fan" type texture.

of Ekwall's lamellar D phase (the conventional "neat" bilayer structure) were observed; namely transversely striated "oily-streaks", spherulites and the "mosaic" texture (FIG. 60). (It is important to note, however, that for samples in the composition range  $\sim$  50-65 wt % LiPS, if not thoroughly mixed by heating to beyond  $\sim$  100 °C, the textures displayed at room temperature were of a non-geometric patchy birefringent type. On heating these samples to  $\sim$  90-95 °C very mobile lamellar D phase textures developed which were retained indefinitely on cooling to room temperature, provided that water loss was prevented. This phenomenon has been attributed to incomplete soap "dissolution" on initial sample preparation).

The results of these observations suggested initially that two different lamellar phase types (B and D) may have existed in the LiPS-water system over different composition ranges and that between them there was a transition zone where one type replaced the other. Whether there was a continuous transition between the two types within the same phase or whether there existed a heterogeneous equilibrium between two different mesophases could not be decided solely on the basis of microscopic and macroscopic observations.

In the two-phase region (lamellar + "solid" soap) formed at higher LiPS concentrations ( $>$   $\sim$  70 wt % LiPS) textures characteristic of the lamellar D phase (FIG. 61(a)) were gradually replaced with decreasing water concentration by a more viscous patchy non-geometric dull birefringent texture which was indistinguishable from that exhibited

by the anhydrous "solid" soap at room temperature (FIG. 30, p 141). However, on heating these samples to their macroscopic "clearing" transitions, a lamellar D phase mosaic texture was formed (identical to FIG. 60). Maintaining the sample under isothermal conditions for a short period of time ( $\sim 30$  minutes) subsequently transformed this texture into a lamellar "broken-fan" type texture (FIG. 61(b)) which reverted to the mosaic texture after applying slight pressure to the microscope cover-slip. For a sample containing  $\sim 94$  wt % LiPS, no change in texture was observed on heating to  $\sim 97$  °C, the upper limit of study. This was in accordance with the "clearing" transition at this composition occurring at a temperature beyond the boiling point of water.

## 5.2 Differential Scanning Calorimetry

### 5.2.1 Above Room Temperature

The thermograms recorded on heating LiPS-water samples between room temperature and the isotropic melt were characterized by one or two reversible first-order endothermic transitions depending upon sample composition (FIG. 62). These have been denoted H1 and H2 in order of increasing temperature.

The transition temperatures and the corresponding enthalpy values (calculated as kJ per mole of LiPS), obtained at heating rates of  $5$  °C  $\text{min}^{-1}$ , are recorded as a function of sample composition (where  $X_W/X_A$  corresponds to the mole ratio of water to amphiphile) in TABLE 27. They represent

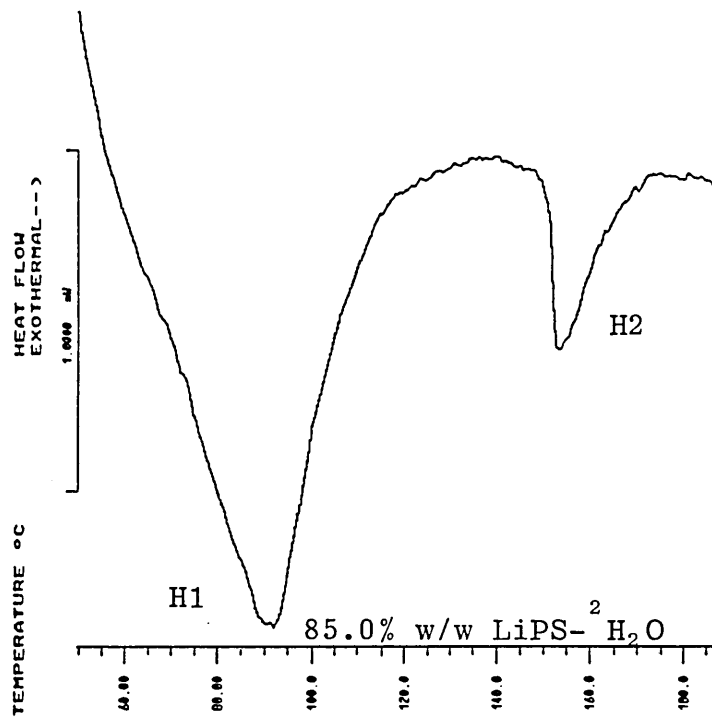
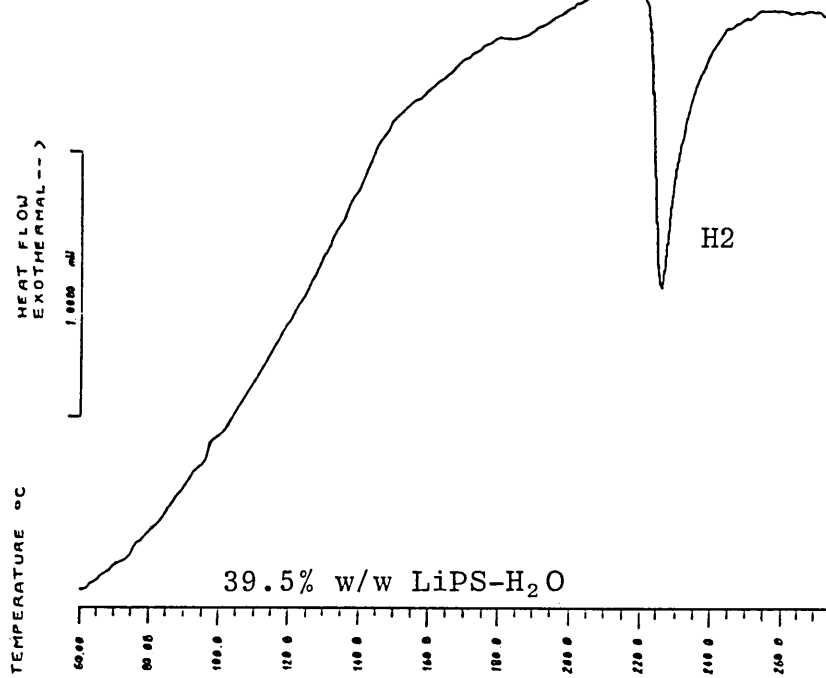


FIG. 62 : DSC heating thermograms for lithium phenylstearate-water samples of varying composition (heating rates : 5 °C min<sup>-1</sup>)

TABLE 27 : Phase transition temperatures and enthalpies  
for the lithium phenylstearate-water system

wt % LiPS	$X_W/X_A$	Transition H1		Transition H2	
		T/(° C)	$\Delta H/(\text{kJ mol}^{-1})$	T/(° C)	$\Delta H/(\text{kJ mol}^{-1})$
22.4	70.5	-	-	197.9	0.3
28.1	52.0	-	-	216.9	0.7
39.5	31.2	-	-	224.3	2.0
48.6*	19.4	-	-	223.8	2.0
50.0	20.3	-	-	224.5	2.3
59.2	14.0	-	-	219.6	1.9
64.8	11.0	-	-	216.3	1.8
69.6	8.9	-	-	208.6	1.5
75.0*	6.1	-	-	190.6	1.0
80.0*	4.6	76.7	1.9	170.9	0.6
85.0*	3.2	89.4	4.0	151.7	0.6
89.8	2.1	99.1	3.8	140.3	0.2
94.1*	1.1	†	4.5 <sup>†</sup>	127.1 <sup>†</sup>	†
95.9*	0.8	†	-	~156 <sup>‡</sup>	-

\* These samples contain heavy water ( $^2\text{H}_2\text{O}$ ) as opposed to normal water.

† Transitions H1 and H2 occur almost simultaneously. The tabulated  $\Delta H$  is the sum of the two unresolved transitions.

‡ Transition temperature determined by macroscopic visual observations.

the mean values calculated from at least 3 independent heating runs at each composition. The temperatures were readily reproducible to within  $\pm 1$  °C in each case and are considered to be equilibrium values. As a result of the small enthalpy changes associated with these transitions and the baseline instability often experienced when operating at very high instrument sensitivities, the enthalpy values are only approximate with estimated precision limits of the order of 6% to 20%.

Little or no effect on the transition temperatures and enthalpies was observed on substituting heavy water ( $^2\text{H}_2\text{O}$ ) for normal water (compare the results for the 48.6 wt % LiPS- $\text{D}_2\text{O}$  and 50.0 wt % LiPS- $\text{H}_2\text{O}$  samples). It may be anticipated, however, that the appearance of the H1 transition may be shifted to a slightly higher LiPS concentration for samples containing the latter (as a result of larger  $X_{\text{W}}/X_{\text{A}}$  values for samples of equal composition by weight but containing normal as opposed to deuterated water).

In the soap concentration range from 22.4 wt % to 75.0 wt % LiPS, only one transition (H2) was observed which has been attributed (on the basis of the  $\Delta\text{H}$  values and polarizing microscopy observations) to a lamellar meosphase melt. The H2 transition temperatures therefore correspond to the position of the  $T_1$  curve (Section 1.3.1.1) over this composition range. Even when operating at the

highest instrument sensitivities, no heat effect could be detected corresponding to a phase boundary between a homogeneous lamellar mesophase and the two-phase lamellar + dilute soap solution region believed to exist between  $\sim 20$  wt % and 25 wt % soap at room temperature. Similarly, no transitions were observed corresponding to a possible heterogeneous equilibrium between two different lamellar mesophases (types B and D) as suggested in Section 5.1. Furthermore, no transitions were detected corresponding to the macroscopic "clearing" of samples containing between  $\sim 30$  and 45 wt % LiPS at  $\sim 140$  °C (Section 5.1.2) or to the microscopically observed textural change for heterogeneous soap-water samples containing  $\sim 50$ -65 wt % LiPS at 90-95 °C (Section 5.1.3).

At low water contents ( $< 25$  wt %  $^2\text{H}_2\text{O}$ ), a further reversible broad endothermic transition (H1) was observed which was considered (on the basis of both macroscopic and microscopic observations in polarized light and the magnitude of  $\Delta H$ ) to be continuous with the H3 transition of the anhydrous soap (corresponding to a "fusion" of the quasi-crystalline polar groups;

Section 3.3.5.5). This behaviour is reminiscent of the  $T_c$  curve observed in the aqueous systems of the long-chain crystalline soaps (Section 1.3.1.1). These results are consistent with visual observations suggesting that beyond  $\sim 70$  wt % LiPS a two-phase region composed of a lamellar liquid crystal + "solid" soap (D + G) was present at room temperature. It is interesting to note that,

whereas these experimental observations indicated this two-phase region to extend to soap concentrations as low as 70 wt % LiPS in  $^2\text{H}_2\text{O}$ , no H1 transition could be detected calorimetrically for the 69.6 wt % or 75.0 wt % LiPS samples in normal and heavy water respectively. It is suggested that the amount of "solid" soap present at these compositions was possibly too small to be detected upon their "dissolution" into the lamellar mesophase.

It would appear, therefore, that a critical minimum concentration of water is required for the formation of the homogeneous lamellar mesophase at room temperature. This amount corresponds to a minimum mole ratio, water to amphiphile of between 8 and 10 (based on macroscopic visual observations). As the temperature of the system was raised beyond H1, however, this requisite minimum appeared to decrease slightly and the boundary between the homogeneous lamellar phase (D) and the two-phase lamellar + "solid" soap (D + G) region was displaced towards lower water contents (see FIG. 56, p 323). On decreasing the water content to  $\sim 5.9$  wt %  $^2\text{H}_2\text{O}$ , the H1 and H2 transitions were observed to occur practically simultaneously. It would appear, therefore, that the upper temperature limit of stability of this lamellar mesophase was also influenced by the fact that the water concentration fell below a critical value (corresponding to a minimum  $X_W/X_A$  value of  $\sim 1$  in this case).

The phase equilibrium operating at the lowest water contents was, however, uncertain. It was not clear whether the two-phase (D + G) region extended to the boundary with the anhydrous "solid" soap (where  $X_W/X_A = 0$ ) or whether it was succeeded at some minimum water content by a single hydrated "solid" soap phase.

### 5.2.2 Below Room Temperature

A number of LiPS-water samples, containing between  $\sim 30.4$  wt % and 94.1 wt % surfactant, were also studied over the temperature range from  $-165$  °C to 25 °C using DSC. On heating, each sample, irrespective of composition, exhibited three reversible first-order endothermic transitions denoted H3, H4 and H5 in order of increasing temperature (see FIG. 63).

The transition temperatures and the corresponding enthalpy values, obtained at heating rates of  $5$  °C  $\text{min}^{-1}$ , are recorded in TABLE 28 for two samples which formed homogeneous lamellar D phases at room temperature . These results were obtained from single heating runs at each sample composition. A qualitative study of the thermograms suggested that significant errors may be expected in both the temperature and enthalpy values of H3 and H4 due to the small size and poor resolution of the peaks. It was noticed, however, that the respective H5 transitions appeared to shift to slightly higher temperatures on substituting the normal water by heavy water. This may result from the difference in the melting points of bulk  $\text{H}_2\text{O}$  and  $^2\text{H}_2\text{O}$  (4 °C). All three transitions

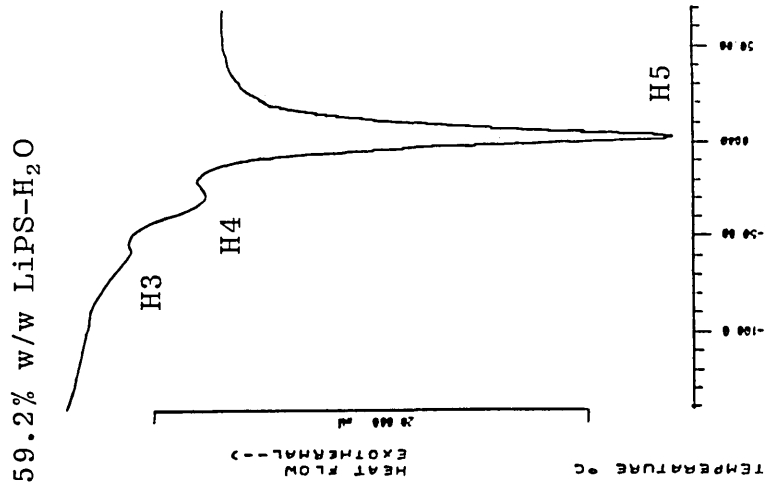
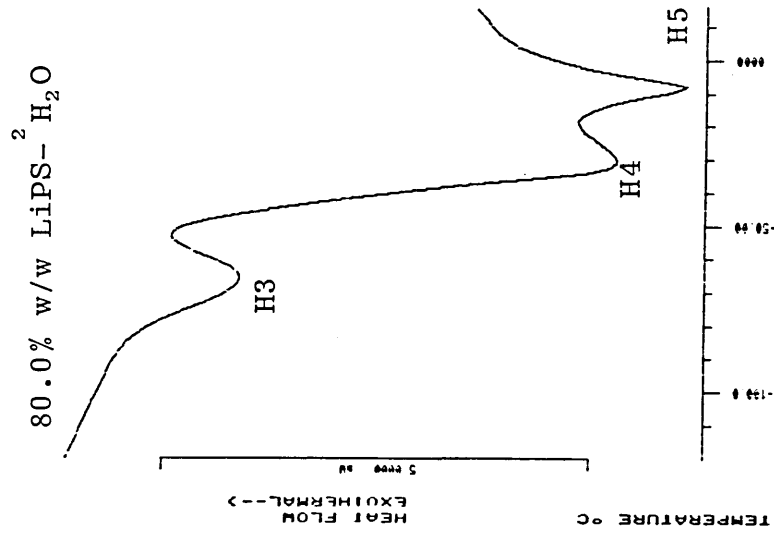


FIG. 63 : Low temperature DSC heating thermograms for lithium phenylstearate-water samples of varying composition

TABLE 28 : Phase transition temperatures and enthalpies for the lamellar D phase in the lithium phenylstearate-water system below 0 °C

wt % LiPS	$X_W/X_A$	Transition H3		Transition H4		Transition H5		
		T/(°C)	$\Delta H/kJ mol^{-1}$ of LiPS	T/(°C)	$\Delta H/J g^{-1}$ of sample	T/(°C)	$\Delta H/J g^{-1}$ of sample	$\Delta H/kJ mol^{-1}$ of $H_2O$
50.0	20.3	- 60	<< 1	- 33	~ 3.3	- 2.4	3.1	86
59.2	14.0	- 60	< 1	- 33	~ 4.2	- 3.1	2.7	62

were still present at LiPS concentrations up to 94.1 wt % with H3 and H4 increasing in enthalpy and H5 decreasing in both size ( $\Delta H$ ) and temperature with increasing soap concentration. A quantitative evaluation of the thermodynamic data for these heterogenous two-phase (D + G) samples would, however, be meaningless without more detailed knowledge of the actual phase equilibria.)

Similar DSC results have recently been reported by Blum et al [235] as part of a study into the temperature dependence of the molecular motion in smectic (lamellar) liquid crystals of hydrated sodium 4-(1'-heptylnonyl)-benzenesulphonate (SHBS); Section 1.3.2.2.

For a 75 wt % SHBS-H<sub>2</sub>O sample ( $X_W/X_A = 7.5$ ) which forms a homogeneous lamellar mesophase at 25 °C, endotherms at approximately - 70 °C, - 39 °C, - 23 °C and - 13 °C were observed. The approximate enthalpy value of the - 70 °C transition was reported to be  $1.62 \pm 0.22$  kcal. mol<sup>-1</sup> ( $6.78 \pm 0.92$  kJ mol<sup>-1</sup>) of surfactant. From variable temperature carbon-13 NMR spectroscopy, this transition was identified as the freezing-in of motion of the aliphatic soap hydrocarbon chains. The total heat involved in the latter 3 transitions was estimated to be  $15 \pm 3$  cal g<sup>-1</sup> ( $63 \pm 13$  J g<sup>-1</sup>) of lamellar phase (SHBS + H<sub>2</sub>O). These transitions were shown, using a combination of <sup>13</sup>C, <sup>23</sup>Na and <sup>2</sup>H NMR spectroscopy to result primarily from the immobilization of bilayer water with the water most bulk-like freezing in at the highest temperature. (Similar results have recently been reported for the Aerosol OT-D<sub>2</sub>O

system [336] based on DSC, <sup>1</sup>H NMR and quasi-elastic neutron scattering measurements. Other studies of this nature have also been carried out on the aqueous lamellar mesophases formed by a number of phospholipids [326 - 328] and straight-chain sodium soaps [55].) The transition occurring at - 23 °C was attributed specifically to a freezing in of motion of the benzenesulphonate head groups and the "bound" sodium ions and water molecules associated with these ionic groups.

Whilst a quantitative comparison of the results obtained in this present study with those of Blum et al [235] would be difficult (due to differences in the molecular structure of the surfactants and the associated differences in water binding capacity of their head groups and counter-ions and also the difference in water content of the respective mesophases) a qualitative comparison of the thermograms suggests a very similar behaviour for the two systems.

On the basis of this comparison, it is suggested that the H3 transition observed at approximately - 60 °C in the LiPS-water system corresponds to a freezing-in of motion of the hydrocarbon chains. This temperature is similar to the calorimetrically observed "crystallization" temperature of the parent phenylstearic acid (- 57.3 °C; Section 2.1.3.1) and to the glass transition of the anhydrous soap (ca. - 50 °C; Section 3.3.5.2). The small enthalpy change recorded at H3 may be attributed to the complex isomeric composition of the soap (Section 1.2.3.1). The nature of this transition could be confirmed by <sup>1</sup>H or

$^{13}\text{C}$  NMR linewidth measurements.

The H4 transition at ca. - 33 °C is therefore attributed to the combined immobilization of the carboxylate head groups, the "bound" lithium counter-ions and the water molecules specifically bound to these groups by hydrogen bonding and ion-dipole attractions. (This was supported by variable temperature  $^7\text{Li}$  NMR data; Section 5.4.2.3). No heat effect corresponding to the - 23 °C transition (SHBS-H<sub>2</sub>O) system was detected in the LiPS-H<sub>2</sub>O system, however.

Similarly, the H5 transition is believed to correspond to a freezing-in of "free" (unbound) bilayer water. On the basis of an approximate calculation (assuming the "free" bilayer water to have a similar heat of fusion to normal bulk water; 6.01 kJ mol<sup>-1</sup>), the enthalpy values obtained for the H5 transitions of the 50.0 wt % and 59.2 wt % LiPS-H<sub>2</sub>O samples were found to account for the melting of only ~ 51% and ~ 45% of the total amount of water present. This gave apparent values of approximately 10 and 8 respectively for the number of moles of "bound" water per mole of soap. These values are in good agreement with those reported in the literature [10, 272] corresponding to that amount required for more or less complete hydration of the lithium ions (7-8 moles) and carboxylate groups (2-3 moles) of typical soap molecules. They are also in concordance with the value estimated in the previous section for the minimum concentration of water required for the formation of a homogenous lamellar phase

in the LiPS-water system at room temperature.

## 5.3 X-Ray Diffraction

### 5.3.1 At Room Temperature

The diffraction patterns obtained from LiPS-water samples in the low-angle region at room temperature were dependent upon the sample composition (see TABLE 29).

A number of samples in the composition range 30.2 wt % to 56.6 wt % LiPS exhibited two sharp reflections with spacings in the ratio of 1:1/2 (FIG. 64) characteristic of structures possessing a 1-d lamellar periodicity (Section 2.2.4.2). For two of these samples a very weak reflection corresponding to a further higher order 1:1/3 lamellar spacing was also observed. (Due to the sharpness of these reflections, even at the lower soap concentrations, the lamellar mesophase structures have been designated as the conventional "neat" or D type (see FIG. 19, Section 2.2.4.2) as opposed to Ekwall's B phase where the two lamellar reflections were reported as being both weak and diffuse [263, 325]). For a sample containing 18.3 wt % LiPS, however, the two observed reflections, (especially  $d_1$ ), were very weak and diffuse. Macroscopic and polarizing microscopy observations, however, have suggested the onset of a two-phase region at similar soap compositions, composed of a lamellar mesophase + dilute isotropic soap solution.

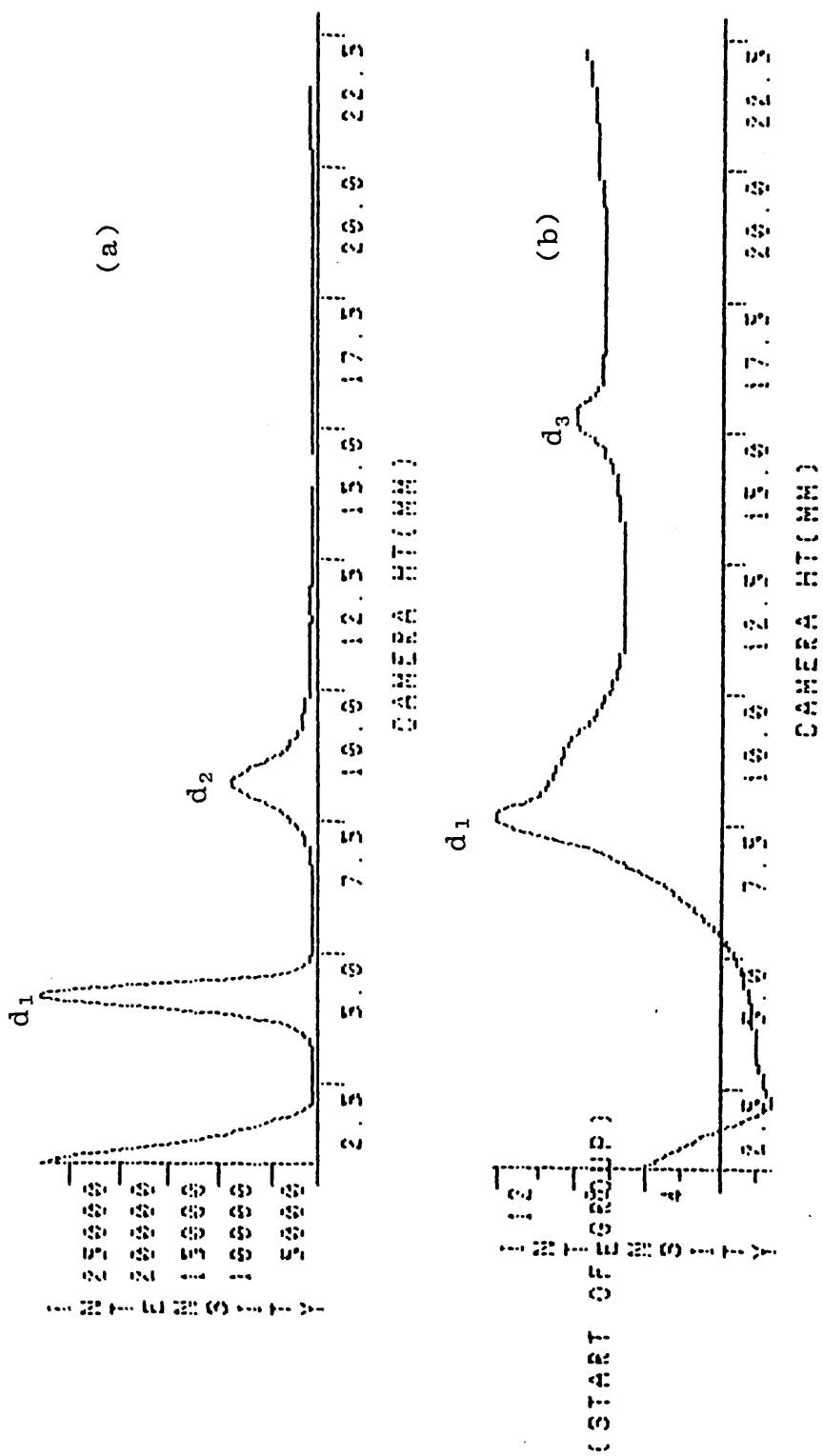


FIG. 64 : Low-angle x-ray diffraction patterns obtained at 27 °C from lithium phenylstearate - <sup>2</sup>H<sub>2</sub>O samples containing:  
 (a) 35.0% w/w LiPS (lamellar mesophase)  
 (b) 80.0% w/w LiPS (lamellar mesophase + "solid" LiPS)

TABLE 29 : Low angle x-ray diffraction results for the lithium phenylstearate-<sup>2</sup>H<sub>2</sub>O system at 27 °C

wt % LiPS	X <sub>w</sub> /X <sub>A</sub>	OBSERVED BRAGG SPACINGS/(Å)				PHASE STRUCTURE
		d <sub>1</sub>	d <sub>2</sub>	d <sub>3</sub>	d <sub>4</sub>	
18.3 <sup>†</sup>	81.7	68 ± 4	42 ± 1			L <sub>1</sub> + D
30.2	42.3	90.7 ± 1.0	45.7 ± 0.2			D
35.0	34.0	74.2 ± 0.9	37.6 ± 0.2	26.2 ± 0.1		D
40.1	27.3	72.0 ± 0.9*				D
41.8 <sup>†</sup>	25.5	66.3 ± 0.7	33.5 ± 0.2			D
44.9	22.5	62.6 ± 0.7*				D
49.7	18.5	57.0 ± 0.5*				D
56.6 <sup>†</sup>	14.0	50.2 ± 0.4	25.5 ± 0.2	16.7 ± 0.1		D

Table 29 continued overleaf .....

Table 29 continued . . . .

wt % LiPS	$X_W/X_A$	OBSERVED BRAGG SPACINGS / ( $\text{\AA}$ )				PHASE STRUCTURE
		$d_1$	$d_2$	$d_3$	$d_4$	
59.6	12.4	$48.6 \pm 0.4^*$				D
65.0	9.9	$43.9 \pm 0.4^*$				D
70.0	7.8	$43.3 \pm 0.3^*$				D + G
74.5	6.3	$41.1 \pm 0.3$	$24.9 \pm 0.2$	$20.7 \pm 0.1$		D + G
80.0	4.6	$40.3 \pm 0.3$	$25.6 \pm 0.1$	$20.2 \pm 0.1$		D + G
89.9	2.1	$39.3 \pm 0.3$ + $35.8 \pm 0.2$	$23.2 \pm 0.2$	$19.2 \pm 0.1$	$17.8 \pm 0.1$	D + G
95.9	0.8	$34.6 \pm 0.3$	$24.5 \pm 0.2$	$18.4 \pm 0.1$	$17.2 \pm 0.1$	G + D

# The high angle region was not studied for this system.

† These samples were prepared with normal water. The tabulated compositions have therefore been corrected for the difference in molecular weight between normal and heavy water ( $^2\text{H}_2\text{O}$ )

\* The position of the fundamental Bragg peak only was recorded.

It should be noted that for samples marked with an asterisk in TABLE 29, the position of the fundamental Bragg peak only was recorded. Macroscopic and polarizing microscopy observations have indicated that each of these samples (with the possible exception of that containing 70 wt % LiPS) possess lamellar phase structures and they have been designated accordingly. For the 70 wt % LiPS-<sup>2</sup>H<sub>2</sub>O sample, however, the recorded Bragg peak was slightly asymmetric indicating a possible two-phase sample.

For the more concentrated aqueous soap samples containing 74.5 wt % and 80.0 wt % LiPS, the fundamental Bragg peak was distinctly asymmetrical (see FIG. 64b), with a less intense broad shoulder occurring at higher angles (lower spacings). The apex of this latter reflection was, however, not resolved and its position cannot therefore be estimated accurately. In addition to the two sharp lamellar spacings observed for these samples, an extremely weak reflection was also present which may be indexed tentatively as a  $1:1/\sqrt{3}$  spacing characteristic of a phase structure with 2-d hexagonal periodicity (Section 2.2.4.3). These results are considered to be indicative of a two-phase region composed of lamellar mesophase + "solid" (possibly hydrated) soap. (It has been established in Section 3.3.4.1 that anhydrous LiPS has a 2-d hexagonal phase structure at room temperature).

As the water content of the system was reduced to only 10 wt %  $^2\text{H}_2\text{O}$ , the diffraction pattern was apparently composed of two distinct sets of reflections which may be indexed independently as 1-d lamellar + 2-d hexagonal. The intensities of the fundamental Bragg peaks were approximately equal whilst the higher order reflections were equally weak.

At the highest soap concentration studied (95.9 wt % LiPS) the  $d_1$  Bragg peak at  $\sim 34.6 \text{ \AA}$  was very broad but symmetrical and corresponded, possibly, to two reflections with the weaker of the two positioned at a spacing of  $\sim 36\text{-}37 \text{ \AA}$  (since a very weak higher order reflection with a spacing of  $18.4 \text{ \AA}$  was resolved, corresponding to a possible lamellar phase). It is suggested that the  $24.5 \text{ \AA}$  (very weak) and  $17.2 \text{ \AA}$  (weak) reflections may correspond to the 2-d hexagonal  $1/\sqrt{3}$  and  $1/\sqrt{4}$  spacings of the predominating "solid" LiPS phase.

### 5.3.2 Mechanism of Water Uptake

It has been reported that the fundamental Bragg spacing of the lamellar D ("neat") phase (corresponding to the repeat interlayer distance; refer to FIG. 19, Section 2.2.4.2) changes with the water content in quite distinct ways for different amphiphiles, and even in different composition ranges of the neat phase of a particular system [10]. These differences point to variations in the mechanism of water uptake of the neat phases.

If added water is intercalated between the double layers of amphiphile molecules, the uptake being accompanied by typical one-dimensional swelling, the slope of the curve of  $\log d$  against  $\log (1/\phi_a)$ , the reciprocal of the volume fraction of amphiphile, should be unity for an amphiphile which is insoluble in water (as implied by the logarithmic version of equation (2.1), Section 2.2.4.2). In these "expanding" lamellar phases, the thickness of the amphiphile layers,  $d_a$ , and the interfacial area per polar group,  $S$ , are almost independent of the water content [10]; that is to say no additional water appears to be incorporated between the molecules of the amphiphile layers, all of it being intercalated in the region between the layers,  $d_w$  (see FIG. 19, Section 2.2.4.2).

For the "non-expanding" type of neat phase, however, the slope of  $\log d$  against  $\log (1/\phi_a)$  is close to zero and in many of these lamellar phases the slope is actually zero [10]. The incorporation of water also results in a marked rise in the interfacial area per polar group and some reduction in the thickness of the amphiphile double layers (for instance in the neat phase of potassium oleate at 20 °C, the area,  $S$ , increases from 33 to 40 Å<sup>2</sup> and the thickness,  $d_a$ , decreases from about 31 to 27 Å [10]). As the water content is increased, the packing of the amphiphile molecules thus becomes less dense; it would seem that the water molecules penetrate the layers between the amphiphile molecules forcing them apart and reducing the thickness of the layer. This reduction

compensates for the increase in the thickness of the water layer,  $d_w$ , so that the phase as a whole becomes "non-expanding".

In order to establish the mechanism of water uptake for the lamellar mesophase(s) formed in the LiPS- $^2\text{H}_2\text{O}$  system at room temperature, graphs of  $\log d$  versus  $\log (1/c_a)$ , FIG. 65, and weight per cent  $^2\text{H}_2\text{O}$  versus both  $S$  and  $d_a$  (FIG. 66) were plotted for the soap concentration range from 30.2 wt % to 65.0 wt % LiPS.

The parameters, presented in TABLES 30 and 31, were calculated assuming the presence of a single homogeneous lamellar D mesophase at each sample composition. In the absence of a measured value for the partial specific volume of the amphiphile (and consequently  $\phi_a$ ; refer to Section 2.2.4.2) a valid approximation using the quantity  $c_a$  (the weight fraction of amphiphile) was employed [215]. The values of  $d_a$ ,  $d_w$  and  $S$  were calculated using equations (2.3), (2.4) and (2.6) respectively as outlined in Section 2.2.4.2.

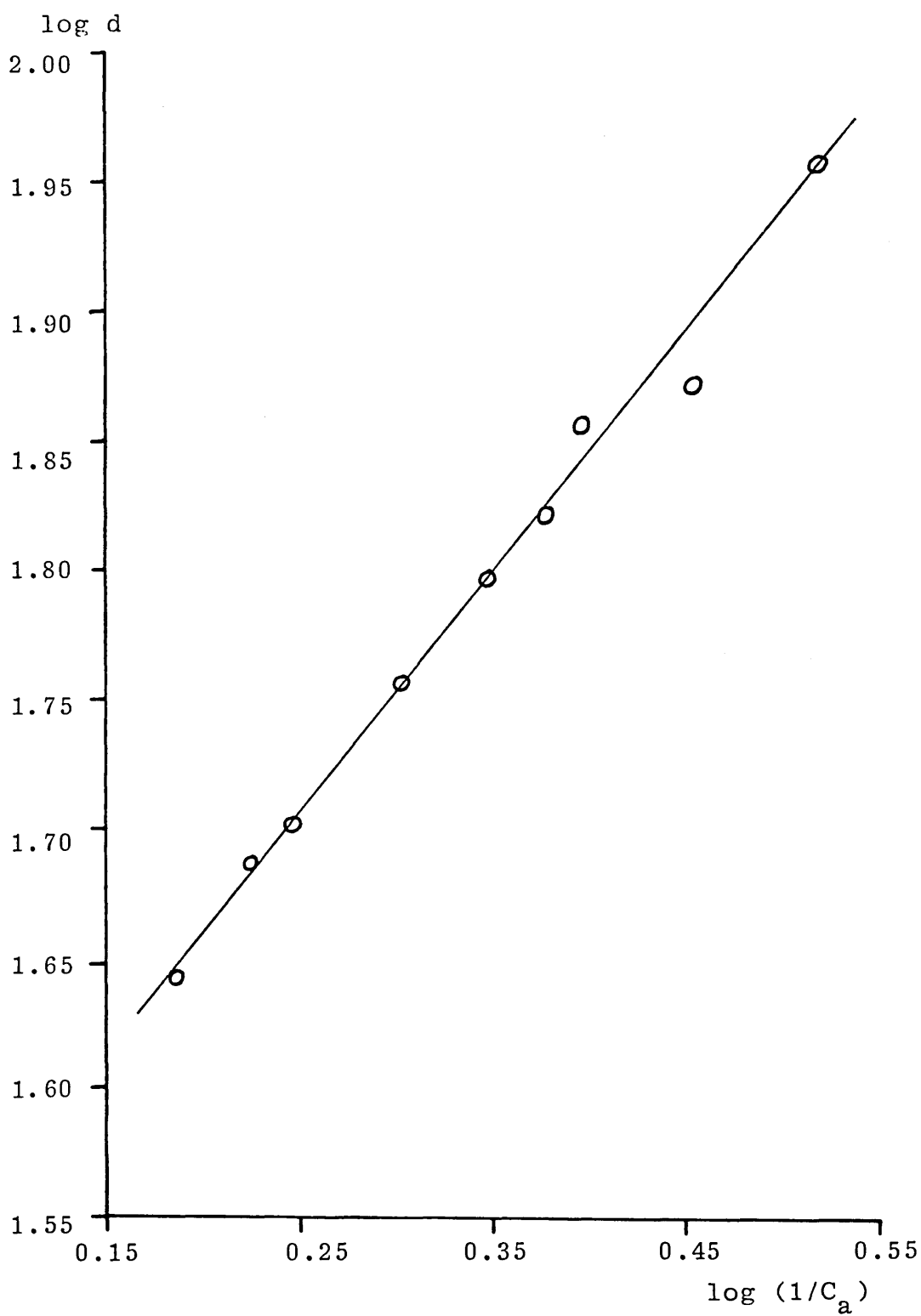


FIG. 65 : Variation of the fundamental interplanar repeat distance,  $d$ , with the weight fraction of amphiphile,  $C_a$ , for the lamellar mesophase formed in the LiPS-<sup>2</sup>H<sub>2</sub>O system at 27 °C

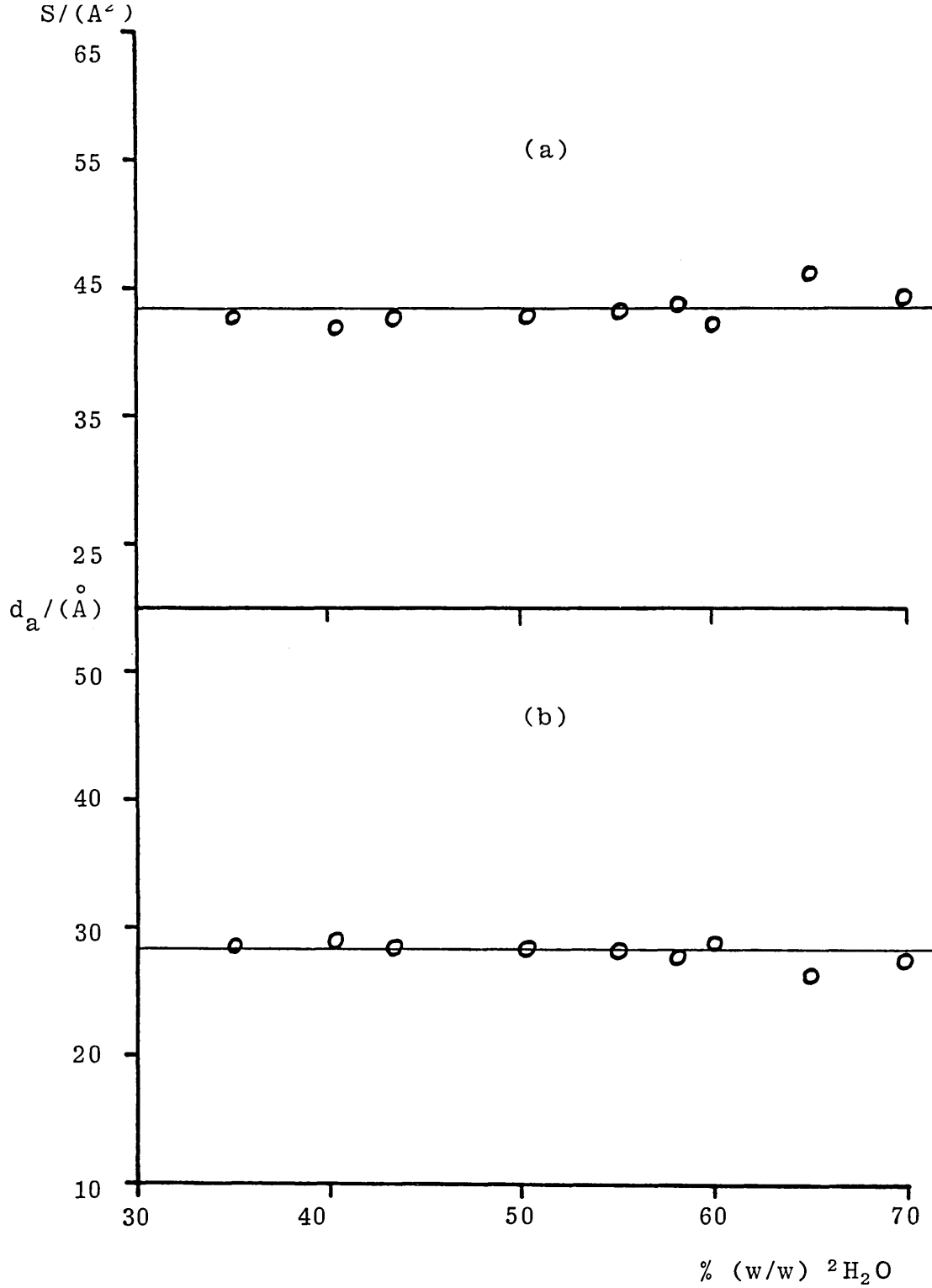


FIG. 66 : Variation of (a) the interfacial area per polar group,  $S$ , and (b) the thickness of the amphiphile bilayers,  $d_a$ , with  $^2\text{H}_2\text{O}$  content for the lamellar mesophase formed in the lithium phenylstearate -  $^2\text{H}_2\text{O}$  system at  $27^\circ\text{C}$ .

TABLE 30 : Variation of the fundamental interplanar repeat distance,  $d$ , with the weight fraction of amphiphile,  $c_a$ , for the lamellar mesophase formed in the lithium phenylstearate- $^2\text{H}_2\text{O}$  system at 27 °C

$c_a$	$\log (1/c_a)$	$d/(\text{Å})$	$\log d$
0.302	0.520	90.7	1.958
0.350	0.456	74.2	1.871
0.401	0.397	72.0	1.857
0.418	0.379	66.3	1.822
0.449	0.348	62.6	1.797
0.497	0.304	57.0	1.756
0.566	0.247	50.2	1.701
0.596	0.225	48.6	1.687
0.650	0.187	43.9	1.643

The results of this x-ray diffraction study have indicated that the lamellar mesophase formed in the LiPS- $^2\text{H}_2\text{O}$  system over the soap concentration range from 30.2 wt % to 65.0 wt % LiPS, exhibits typical one-dimensional swelling and is therefore of the "expanding" type.

The graph of  $\log d$  versus  $\log (1/c_a)$ , FIG. 65, has a gradient of  $\sim 0.93$  over this composition range whilst the gradients of the graphs of wt %  $^2\text{H}_2\text{O}$  versus  $S$  and  $d_a$  (FIG. 66) are both essentially zero, indicating that these parameters are independent of the  $^2\text{H}_2\text{O}$  content, with values

TABLE 31 : Variation of the interfacial area per polar group,  $S$ , and the thickness of the amphiphile layers,  $d_a$ , and water layers,  $d_w$ , with  $^2\text{H}_2\text{O}$  content for the lamellar mesophase formed in the lithium phenylstearate- $^2\text{H}_2\text{O}$  system at 27 °C.

wt % $^2\text{H}_2\text{O}$	$S/(\text{Å}^2)$	$d_a/(\text{Å})$	$d_w/(\text{Å})$
69.8	44.4	27.4	63.3
65.0	46.3	26.3	48.2
59.9	42.2	28.9	43.1
58.2	43.9	27.7	38.6
55.1	43.3	28.1	34.5
50.3	43.0	28.3	28.7
43.4	42.8	28.4	21.8
40.4	42.0	29.0	19.6
35.0	42.7	28.5	15.4

of  $43.4 \pm 1.3 \text{ Å}^2$  and  $28.1 \pm 0.8 \text{ Å}$  respectively.

The absence of discontinuities in these plots indicates the existence of a single lamellar D mesophase over this composition range with the lamellar B phase (whose possible existence was suggested on the basis of polarizing microscopy observations) being merely a continuation of the lamellar D "neat" phase at high water concentrations.

### 5.3.3 Above Room Temperature

A variable temperature low-angle study was also carried out on a concentrated aqueous soap sample in the two-phase lamellar + "solid" soap (D + G) region (containing 80 wt % LiPS) to investigate changes in structure with increasing temperature. The results are presented in TABLE 32.

With increasing temperature, the  $d_1$  and  $d_3$  reflections characteristic of the lamellar mesophase were observed to decrease monotonically, corresponding to slight decreases in the interlayer repeat distance. At each of the tabulated temperatures the weak  $d_2$  reflection, corresponding approximately to the  $1/\sqrt{3}$  spacing of the 2-d hexagonal "solid" LiPS structure, was resolved although at 90 °C this reflection was extremely weak and diffuse and only just visible above the background intensity. At 90 °C, a corresponding improvement in the resolution of the fundamental Bragg peak ( $d_1$ ) was also observed, resulting from a marked decrease in intensity of the weaker broad "solid" LiPS component at higher angles.

TABLE 32 : Variable temperature low-angle x-ray diffraction results for an 80.0 wt % LiPS-<sup>2</sup>H<sub>2</sub>O two-phase (D + G) sample

T/(°C)	OBSERVED BRAGG SPACINGS/(Å)		
	d <sub>1</sub>	d <sub>2</sub>	d <sub>3</sub>
27	40.3 ± 0.3	25.6 ± 0.1	20.2 ± 0.1
27*	40.4 ± 0.3	25.7 ± 0.1	20.3 ± 0.1
50	39.8 ± 0.3	23.5 ± 0.1	19.9 ± 0.1
70	39.2 ± 0.2	23.1 ± 0.1	19.6 ± 0.1
80	38.7 ± 0.2	22.5 ± 0.2	19.3 ± 0.1
90	38.2 ± 0.2	23.5 ± 0.1	19.2 ± 0.1

\*Sample held isothermally at 27 °C for 24 hours after cooling from 90 °C

DSC investigations have revealed the presence of a broad endothermic transition (H1) for this sample between ~ 55 °C (transition onset; first deviation from the steady baseline) and ~ 100 °C (completion of transition; return to steady baseline). The result of this x-ray study indicate that this transition corresponds to a dissolution of the "solid" LiPS component of the two-phase sample into the lamellar D mesophase at elevated temperatures. This behaviour is also consistent with polarizing microscopy observations.

It should be noted that the room temperature diffraction pattern obtained from this sample 24 hours after cooling from 90 °C was identical with the original pattern (within the limits of experimental error) and is in concordance with the calorimetrically observed reversibility of the H1 transition.

## 5.4 NMR Spectroscopy

### 5.4.1 <sup>2</sup>H NMR

#### 5.4.1.1 At Room Temperature

NMR measurements of the quadrupole splitting of deuterium in labelled water,  $\Delta^W(^2\text{H})$ , (FIG. 67) were made as a function of sample composition at 22 °C in order to obtain information on the mechanism of amphiphile hydration (the fraction of "bound" water and its ordering) and to verify the proposed phase equilibria (Section 2.2.5.2) in the LiPS-<sup>2</sup>H<sub>2</sub>O system.

The results are presented in TABLE 33 (where  $X_A$  and  $X_W$  represent the mole fractions of amphiphile, LiPS, and water, <sup>2</sup>H<sub>2</sub>O respectively). The reproducibility of these measured splittings was better than ± 3%. For cases where the quadrupole splitting could not be resolved (denoted by an asterisk), the tabulated value corresponds to the linewidth,  $w_{\frac{1}{2}}$ , of the "isotropic" signal positioned at the Larmor frequency.

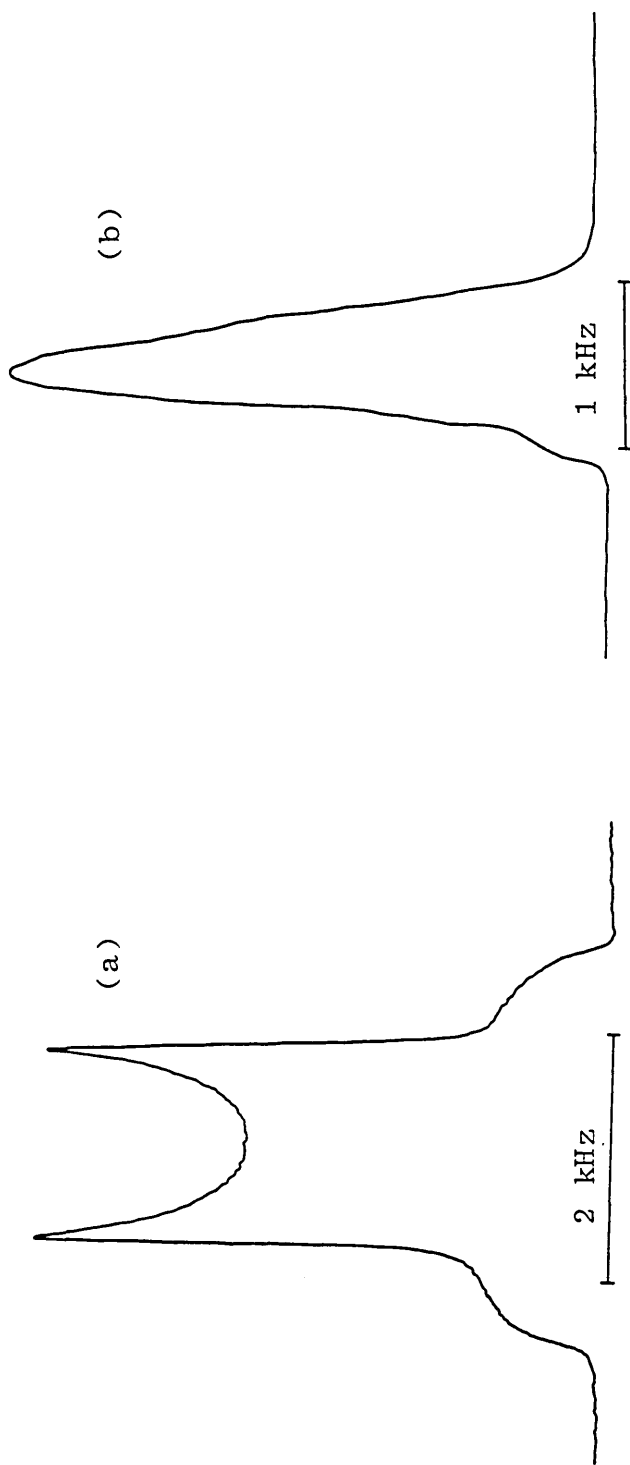


FIG. 67 : Water  $^2\text{H}$  NMR "powder" spectra for lamellar mesophase samples in the lithium phenylstearate- $^2\text{H}_2\text{O}$  system containing:

(a) 54.3% w/w LiPS- $^2\text{H}_2\text{O}$

(b) 30.4% w/w LiPS- $^2\text{H}_2\text{O}$

TABLE 33 : Water deuterium NMR quadrupole splittings,  $\Delta^W(^2\text{H})$ , as a function of sample composition for the LiPS- $^2\text{H}_2\text{O}$  system at 22 °C

wt % LiPS	$X_W/X_A$	$X_A/X_W$	$\Delta^W(^2\text{H}) / (\text{kHz})$	PHASE DESIGNATION
9.8	168.4	0.006	0.12*	L <sub>1</sub> + D
19.8	74.1	0.013	0.12*	L <sub>1</sub> + D
30.4	41.9	0.024	0.58*	D
39.9	27.6	0.036	0.73	D
50.0	18.3	0.055	1.24	D
54.3	15.4	0.065	1.52	D
59.9	12.2	0.082	1.96	D
64.9	9.9	0.101	2.35	D
69.5	8.0	0.125	2.74	D + G
75.1	6.1	0.165	3.62	D + G
79.8	4.6	0.216	4.12	D + G
85.0	3.2	0.310	4.56	D + G
89.9	2.1	0.486	3.99	D + G

\*  $\Delta(^2\text{H})$  not resolved. This value corresponds to the linewidth ( $W_{\frac{1}{2}}$ ) of the "isotropic" signal positioned at the Larmor frequency. Refer to text for explanation.

The observation of a single "doublet" spectrum for samples in the composition range from 39.9 wt % to 89.9 wt % LiPS (FIG. 67a) indicated the presence of a single homogeneous mesophase at each sample composition. (For a heterogeneous system consisting of two or more phases, one expects to observe a superposition of the  $^2\text{H}$  spectra characterizing the phases provided that deuteron exchange between the phases is slow on the NMR time-scale; Section 2.2.5.2). It should be noted that samples containing a minimum of  $\sim 70$  wt % LiPS have been shown to constitute heterogeneous two-phase mixtures of lamellar liquid crystal (D) plus "solid" LiPS (G). The "solid", probably hydrated, soap did not, however, show any signal in the  $^2\text{H}$  NMR spectrum. This may be explained by the existence of a strong quadrupole interaction resulting in large quadrupole splittings with very broad lines.

For samples containing in excess of  $\sim 60$  wt %  $^2\text{H}_2\text{O}$  (ie at compositions corresponding to the originally proposed lamellar B phase and the two-phase lamellar plus isotropic soap solution region) it was not possible to measure  $\Delta^{\text{W}}$  values due to the "isotropic"  $^2\text{H}$  signal (see FIG. 67b, p288). The most likely explanation of these effects is that very rapid deuteron exchange between lamellar "crystallites" having different orientations in the powder sample resulted in an averaging of  $\Delta$  [329]. Kleman et al [330] have reported that the number of defects increases with added water in the lecithin lamellar mesophase. It would appear from the results of the present

study that the same phenomenon occurs in the LiPS- $^2\text{H}_2\text{O}$  system with the lamellar crystallite size decreasing with increasing water content. This is in accordance with our observations that the more dilute lamellar samples (originally designated as a lamellar "B" phase) are cloudy, ie scatter light. Thus the transition from a "doublet" spectrum to an "isotropic" spectrum with increasing water concentration cannot be taken as an indication of the position of the lamellar to lamellar + isotropic soap solution phase boundary in this instance. No attempt was made to store these samples for prolonged equilibration to allow the annealing of the structural defects.

The interaction between  $^2\text{H}_2\text{O}$  and the amphiphile soap molecules is reflected in the measured order parameters which contain information about the average molecular orientation [269, 272, 278, 284]. If the simple two-site model (outlined in Section 2.2.5.2) involving the rapid exchange of "free" and "bound" water molecules applies to this system, then equation (2.16) may be used to calculate an absolute value (but not the sign) for the order parameter  $S_b^W$  of the O- $^2\text{H}$  bond of the bound  $^2\text{H}_2\text{O}$  molecules.

If  $n|E_{Qb}^W S_b^W|$  does not vary with composition, then a plot of the observed deuterium quadrupole splittings,  $\Delta^W(^2\text{H})$ , versus the mole ratio of amphiphile to water ( $X_A/X_W$ ) will give a straight line with zero intercept and a gradient equal to the quantity  $0.75 n|E_{Qb}^W S_b^W|$ . (It is commonly assumed that the electric field gradient of the water

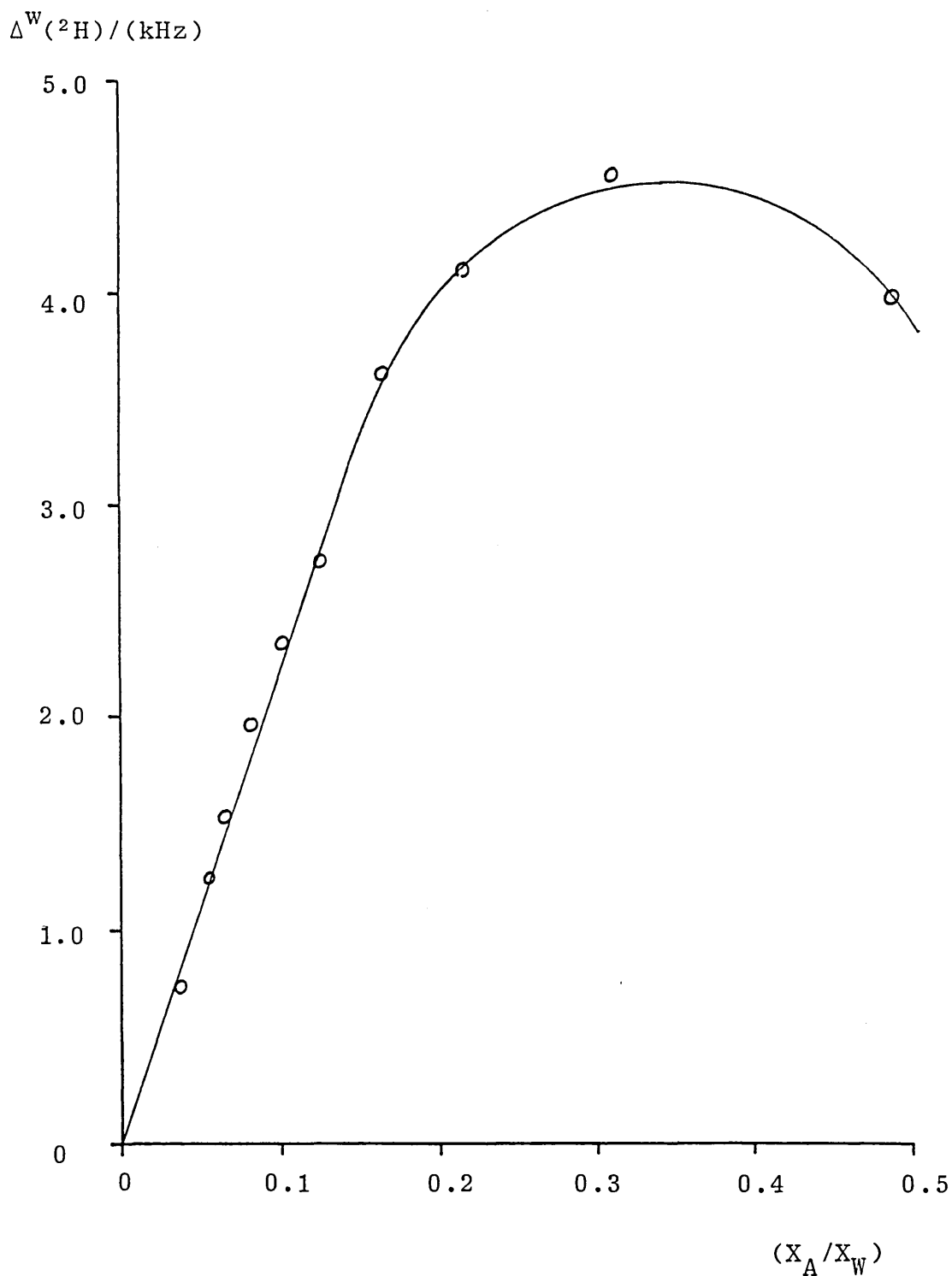


FIG. 68 : Water  $^2\text{H}$  NMR quadrupole splittings,  $\Delta^W(^2\text{H})$ , as a function of the mole ratio amphiphile/water,  $X_A/X_W$ , for the lithium phenylstearate- $^2\text{H}_2\text{O}$  system at 22 °C

O-<sup>2</sup>H groups arises from intramolecular effects [271, 331] and as indicated by relaxation studies on heavy water solutions [332] the value of  $E_Q$  is approximately constant under different hydrogen bonding conditions. The order of magnitude of  $S_b^W$  can therefore be estimated by using the assumption that  $E_{Qb}^W$  is approximately equal to the value in solid <sup>2</sup>H<sub>2</sub>O, 215 kHz [333]. It is also interesting to note that low-angle x-ray diffraction measurements on the LiPS-<sup>2</sup>H<sub>2</sub>O system have indicated a typical 1-d swelling behaviour for the lamellar mesophase formed at these sample compositions with added water being intercalated between the amphiphile bilayers apparently as "free" water. The constant value obtained for the interfacial area per polar group suggests a constant value of "n", the number of moles of bound water per mole of LiPS).

The evaluation of the <sup>2</sup>H quadrupole splittings as a function of  $X_A/X_W$  (FIG. 68) proves that this is in fact the case for the single homogeneous lamellar phase formed at sample compositions between 39.9 wt % and 64.9 wt % LiPS.

It is interesting to observe that the data for samples containing 69.5 wt % and 75.1 wt % LiPS, which are considered to be two-phase (D + G), comply with this linear relationship. This suggests that only a minor proportion of the total sample is composed of "solid" soap at these compositions with the lamellar phase component apparently retaining the constant "n" value found at the

lower LiPS concentrations. However, as the proportion of the "solid" soap phase increases, at compositions beyond 75.1 wt % LiPS (where  $X_W/X_A < 6.1$ ), marked deviations from the linear plot can be observed.

However, by taking the data point at 64.9 wt % LiPS as the upper composition limit of stability of the homogeneous D phase at room temperature (corresponding to a value of 9.9 for the static "time-average" value of 'n', the "constant" number of bound water molecules per amphiphile molecule [329]) the order of magnitude of  $S_b^W$  can be estimated having calculated the gradient of the linear region of the plot to be  $\sim 22.2$  kHz and assuming  $E_{Qb}^W$  to be  $\sim 215$  kHz [333].

By this procedure, the value of  $S_b^W$  was found to be  $\sim 0.01$  for the "expanding" lamellar D phase. (Alternatively if the data point at 75.1 wt % LiPS is taken, corresponding to the actual observed upper limit of linearity where  $n = 6.1$ , the calculated value of  $S_b^W$  increases slightly to 0.02). These values are very similar to those found in many other surfactant systems [269, 272, 278, 284] and indicate a substantial motional freedom of the water molecules of amphiphile hydration [284].

In order to fully define the orientation of the water molecule, however, two independent orientation matrix elements  $S_{11}$  and  $S_{22}$  are required [272, 334, 335], and without knowledge of both it is not worthwhile discussing a detailed model of orientation.

#### 5.4.1.2 Above Room Temperature

The influence of temperature on the deuterium quadrupole splitting,  $\Delta^W(^2\text{H})$ , of  $^2\text{H}_2\text{O}$  in samples containing 50.0 wt % LiPS (lamellar D phase) and 85.0 wt % LiPS (two-phase, D + G) was also studied. The results presented in TABLE 34 have also been presented graphically (FIG. 69).

TABLE 34 : Water  $^2\text{H}$  NMR quadrupole splittings  $\Delta^W(^2\text{H})$  as a function of temperature at different sample compositions in the LiPS- $^2\text{H}_2\text{O}$  system.

wt % LiPS	$X_W/X_A$	T/(°C)	$\Delta^W(^2\text{H})$ /(kHz)	PHASE DESIGNATION
50.0	18.3	22	1.24	D
		40	1.21	D
		65	1.12	D
		90	1.00	D
85.0	3.2	22	4.56	D + G
		30	4.38	D + G
		40	3.97	D + G
		60	3.66	(D + G) → D
		80	3.52	(D + G) → D
		90	3.25	(D + G) → D
		100	2.98	(D + G) → D

It can clearly be seen from FIG. 69 that  $\Delta^W(^2\text{H})$  decreases with increasing temperature for both samples between 22 °C and 90 °C (by ~ 20% and ~ 29% respectively) with an apparent discontinuity in this decrease being observed for the (D + G) sample between ~ 60 °C and ~ 80 °C. It should also be noted that for the two-phase (D + G) sample a sharp reversible isotropic central component, which

$\Delta^W(^2\text{H}) / (\text{kHz})$

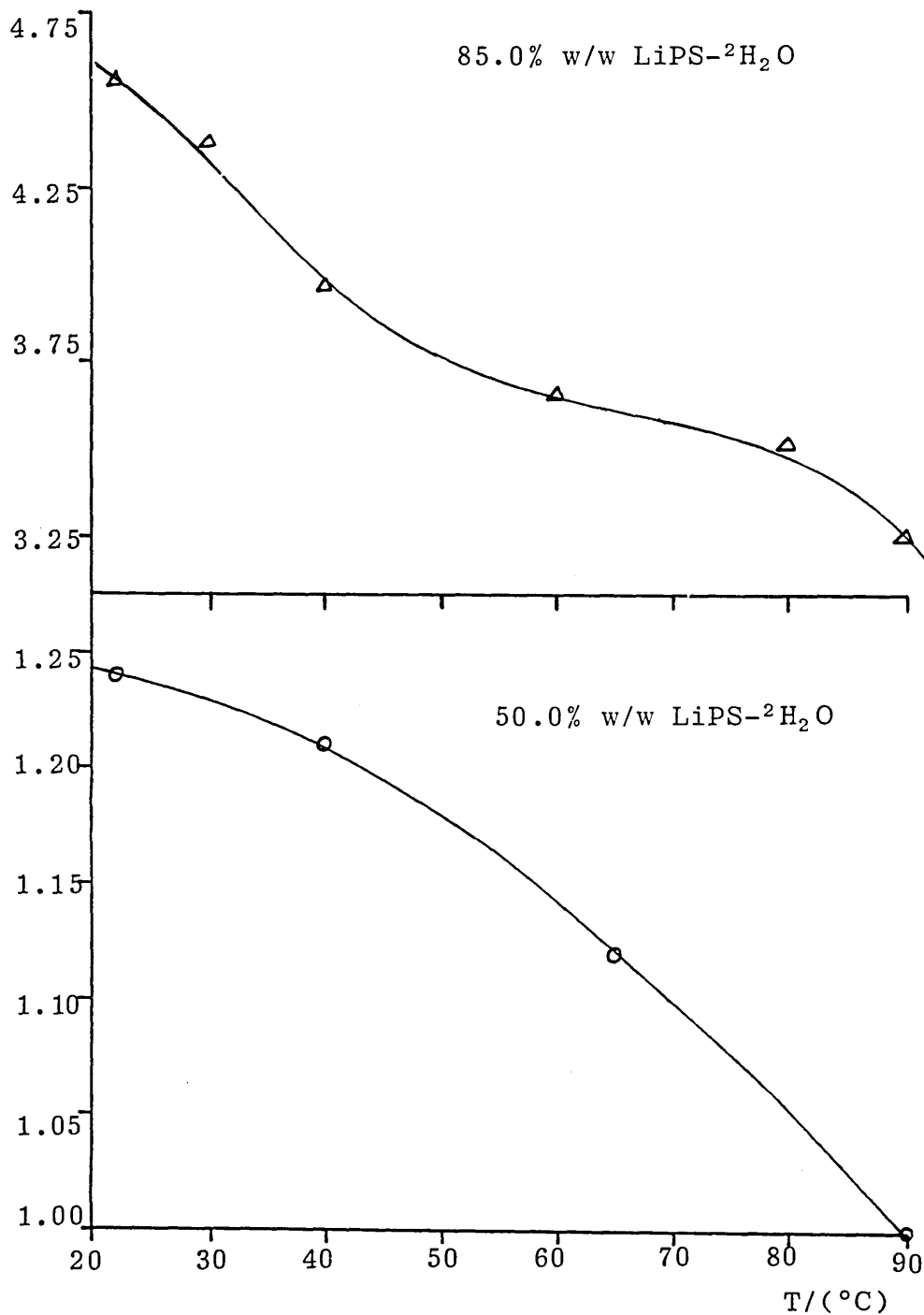


FIG. 69 : Water <sup>2</sup>H NMR quadrupole splittings,  $\Delta^W(^2\text{H})$ , as a function of temperature at two different sample compositions in the lithium phenylstearate-<sup>2</sup>H<sub>2</sub>O system

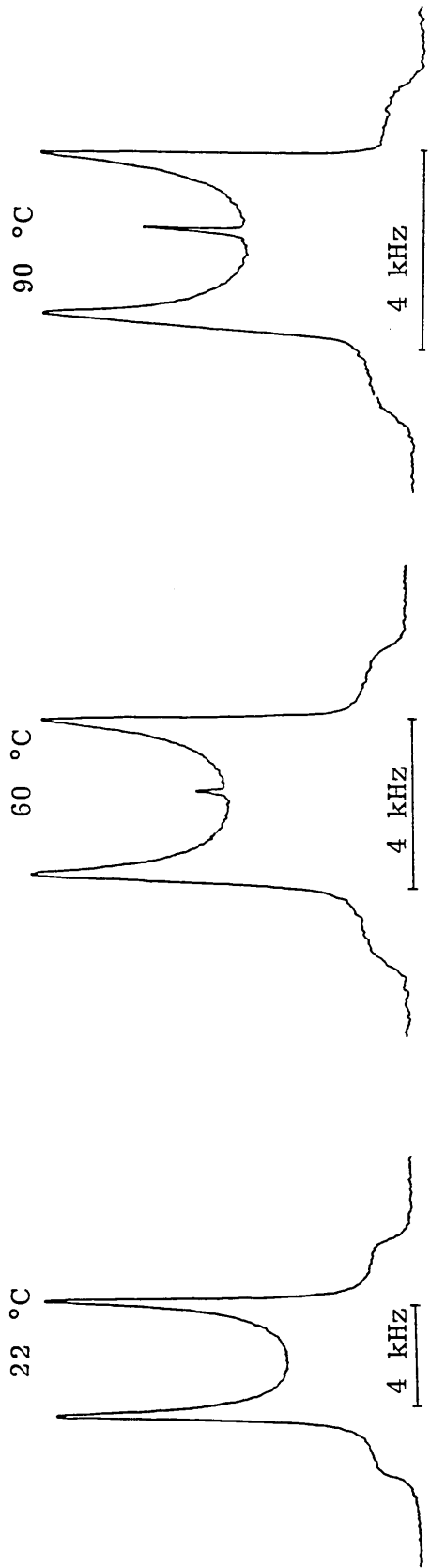


FIG. 70 : Changes in the water  $^2\text{H}$  NMR "powder" spectrum of an 85.0% w/w lithium phenylstearate- $^2\text{H}_2\text{O}$  sample as a function of temperature

became superimposed upon the lamellar mesophase "doublet" at 60 °C was observed to grow in intensity with increasing temperature (see FIG. 70). This reversible change in appearance of the  $^2\text{H}$  NMR spectrum was in accordance with the observation of a broad reversible endothermic transition (H1) for this sample between  $\sim 60$  °C (onset) and  $\sim 115$  °C (completion) by DSC. This transition corresponds to the first order boundary between the (D + G) two-phase region and the homogeneous lamellar D mesophase (see FIG. 56, p 323).

The  $^2\text{H}$  spectra recorded for the 85.0 wt % LiPS- $^2\text{H}_2\text{O}$  sample at the higher temperatures ( $> 60$  °C) are believed to result, therefore, from co-existing non-equilibrium lamellar D + isotropic soap solution ( $L_2$ ) phases; the latter arising from the hydrated "solid" soap (G) phase melt at the H1 transition. This non-equilibrium mixture apparently permits the slow exchange of water between the two phases simply as a result of the diffusion of  $^2\text{H}_2\text{O}$  molecules across "phase boundaries" within the sample matrix.

No comparable changes in the  $^2\text{H}$  NMR lineshape of the 50.0 wt % LiPS- $^2\text{H}_2\text{O}$  sample were detected between 22 °C and 90 °C. This was in agreement with DSC and polarizing microscopy studies which indicated the presence of a single homogeneous lamellar D phase over this temperature range.

The temperature dependence of the quadrupole splitting  $\Delta^{\text{W}}(^2\text{H})$  may be interpreted in terms of changes in the

values of the parameters  $E_{Qb}^W$ ,  $P_b^W$  and  $S_b^W$  with temperature (refer to equation (2.15), Section 2.2.5.2). The quadrupole coupling constant,  $E_Q$ , of deuterium in  $^2\text{H}_2\text{O}$  is considered to be relatively insensitive to changes in temperature [278, 332] and therefore the changes in  $\Delta^W(^2\text{H})$  may, to a good approximation, be attributed primarily to changes in the fraction of "bound" water molecules,  $P_b^W$ , and/or the order parameter  $S_b^W$  of this bound water.

For the case of water in lyotropic liquid crystals, it is now generally accepted that the non-zero, net electric field gradients giving rise to quadrupole coupling occur within the surfactant head-group region close to the alkyl chain/water interface [222, 329]. ("Free" water molecules are considered to have zero quadrupole splittings as a result of the vanishing net orientation of the EFG's).

The water molecules bound to the carboxylate headgroups through ion-dipole attraction and hydrogen bonds would be expected to give the biggest contribution to  $\Delta^W$  since these groups are situated in the most ordered part of the mesophase. (Hydrogen bonding interactions involving the carboxylate groups, a moderately strong Lewis base, may be particularly important in the case of the lithium soap due to the ability of the  $\text{Li}^+$  ions to polarize the surrounding water molecules).

The lithium counter-ions with their high surface charge density will be strongly hydrated and therefore water of counter-ion hydration will be partially oriented with respect to the lamellae for "bound"  $\text{Li}^+$  ions. However, this water can occupy a number of sites at the counter-ion with exchange between them due to rotation [272] and the contribution to  $\Delta^W$  from this source is therefore expected to be smaller.

It has been shown directly that the hydration of the counter-ions of ionic amphiphiles diminishes as the temperature of the system is increased [10]. There is less reliable information, however, on the extent to which the binding of water to the ionized amphiphile head groups decreases, but that it does is indisputable [10]. This decrease in water binding (ie in  $P_b^W$ ) will clearly be an important factor governing the temperature dependence of  $\Delta^W$ .

Similarly, higher temperatures will mean an increased amplitude of the thermal motion of both the bound water molecules and the amphiphile head groups and consequently  $S_b^W$  will be reduced [272, 331].

Tiddy et al [272] have reported similar monotonic decreases in  $\Delta^W(^2\text{H})$  with temperature (from  $\sim 0.95$  kHz at  $\sim 25$  °C to  $\sim 0.75$  kHz at  $\sim 55$  °C) for a lamellar D mesophase sample (formed at a composition  $X_A/X_W = 0.077$ ;  $X_W/X_A = 13.0$ ) in the lithium perfluorooctanoate-water system.

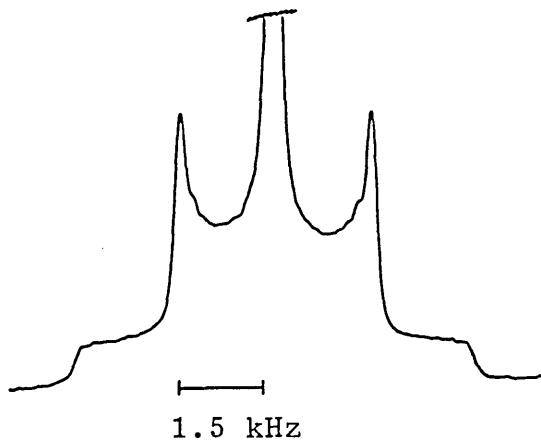
## 5.4.2 <sup>7</sup>Li NMR

### 5.4.2.1 At Room Temperature

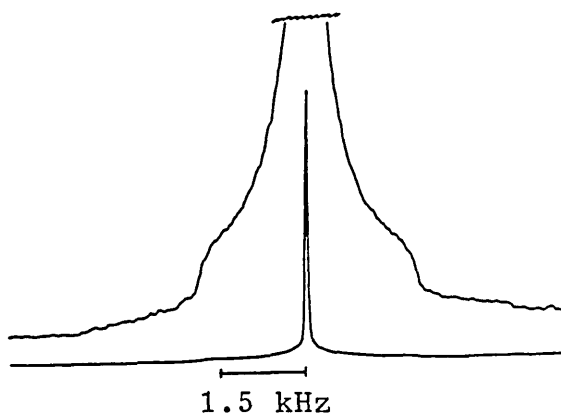
NMR measurements of the quadrupole "powder" splitting of lithium-7 ions,  $\Delta(^7\text{Li})$ , in the lithium phenylstearate- $^2\text{H}_2\text{O}$  system were made as a function of sample composition at 30 °C (see FIG. 71) in order to study the nature of the binding between the surfactant counterions ( $\text{Li}^+$ ) and head groups ( $\text{RCOO}^-$ ).

The results are presented in TABLE 35 (where  $\Delta(^7\text{Li})$  represents the distance from each "satellite" peak to the central peak positioned at the Larmor frequency as defined by equation (2.13), Section 2.2.5.2). The reproducibility of these  $\Delta$  values was in most cases better than  $\pm 3\%$ .

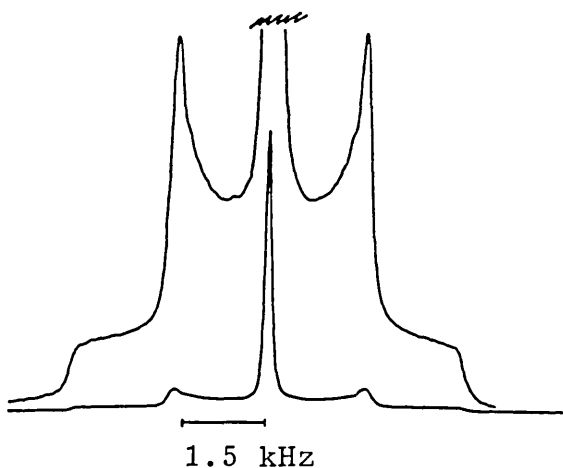
For a number of samples containing relatively high water contents (marked with an asterisk in TABLE 35, and originally designated as a lamellar "B" type phase on the basis of polarizing microscopy observations) the quadrupole splittings were, however, poorly resolved and too broad for  $\Delta(^7\text{Li})$  to be measured accurately; see for example FIG. 71b. (It was possible to improve the resolution of such spectra, however, by using an appropriate combination of values for the line broadening and Gaussian broadening NMR constants; refer to Section 2.2.5.3. In these instances, the estimated errors may be as large as 10%)



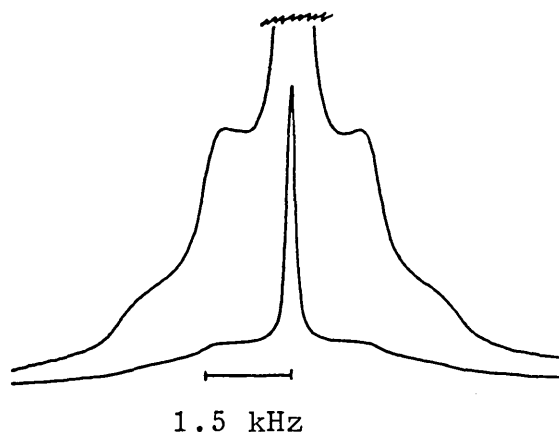
(a) 20.0% w/w LiPS-<sup>2</sup>H<sub>2</sub>O



(b) 29.4% w/w LiPS-<sup>2</sup>H<sub>2</sub>O



(c) 64.9% w/w LiPS-<sup>2</sup>H<sub>2</sub>O



(d) 94.1% w/w LiPS-<sup>2</sup>H<sub>2</sub>O

FIG. 71 : <sup>7</sup>Li NMR "powder" spectra obtained from lithium phenylstearate-<sup>2</sup>H<sub>2</sub>O samples of varying composition at 30 °C

TABLE 35 : Lithium-7 NMR counterion quadrupole "powder" splittings,  $\Delta(^7\text{Li})$  as a function of sample composition for the LiPS- $^2\text{H}_2\text{O}$  system at 30 °C

wt % LiPS	$X_W/X_A$	$\Delta(^7\text{Li})/(\text{kHz})$	PHASE DESIGNATION
3.0	591.6	1.65	$L_1 + D$
5.9	291.8	1.61	$L_1 + D$
9.9	166.5	1.60	$L_1 + D$
20.0	73.2	1.71	$L_1 + D$
29.4	43.9	$\sim 1.8^*$	D
35.2	33.7	$\sim 1.8^*$	D
39.9	27.6	$\sim 1.8^*$	D
50.0	18.3	1.75	D
63.5	10.5	1.68	D
64.9	9.9	1.72	D
79.4	4.7	1.47	$D + G$
94.1	1.1	$\sim 1.4$	$G + D$

Similar difficulties have been reported by Lindblom et al [270] in recording the  $^{23}\text{Na}$  NMR spectra of lamellar "B" phase samples formed at high water contents in the sodium octanoate-decanol-water system at room temperature. This phenomenon was attributed to an intermediate rate of exchange of the  $\text{Na}^+$  ions on the NMR timescale between very small lamellar "crystallites" having different macroscopic orientations in the "powder" sample. At an intermediate rate of transfer of the ions, ie when the lifetime in a region with a particular orientation is

longer than the inverse Larmor frequency but shorter than the inverse splitting, the lines of the  $m = 3/2 \leftrightarrow 1/2$  and  $m = -1/2 \leftrightarrow -3/2$  transitions would become too broad for  $\Delta$  to be measured but would not contribute significantly to the central observed resonance [270].

An alternative explanation for this phenomenon offered by Boden et al [285], was based upon large scale undulations of the lamellae at high water contents where the lamellar phase undergoes one-dimensional swelling. (The existence of a 1-d swelling mechanism has established for the lamellar mesophase formed in the LiPS-<sup>2</sup>H<sub>2</sub>O system by low-angle x-ray diffraction.) They proposed that the fluctuations in the quadrupolar splitting associated with the fluctuations in the orientation of the local lamellar director would similarly give rise to an exchange broadening of the quadrupole "satellites" when the rate of these fluctuations was comparable with the magnitude of  $\Delta$ .

Where it was possible to measure  $\Delta(^7\text{Li})$  values for the proposed "B" phase in the LiPS-<sup>2</sup>H<sub>2</sub>O system (denoted by an asterisk in TABLE 35), the values were very similar to those obtained for lamellar D phase samples at higher soap concentrations. It seems likely that the "B" phase is simply a continuation of the D phase at high water content (as indicated by both <sup>2</sup>H NMR and x-ray diffraction results) and that no first-order B/D phase change exists. These samples have therefore been designated as D and not B in TABLE 35.

A similar conclusion was reached by Lindblom et al [270] to account for the "B" phase originally proposed by Ekwall et al [260] in the sodium octanoate-decanol-water system. In the original paper Ekwall et al [260] concluded that the x-ray evidence for the co-existence of B + D phases was not unequivocal. The phase boundaries were obtained by analysis of separated samples after prolonged high-speed centrifugation. It is possible that the gravity gradient along the centrifuge tubes caused the separation observed. Certainly it is hard to find a physical reason why lamellar phase samples with  $\sim 64 \text{ \AA}$  water layers should separate from samples with  $\sim 72 \text{ \AA}$  water layers as was observed [260].

On increasing the water content of the present system from  $\sim 70.6 \text{ wt } \%$  to  $80.0 \text{ wt } \% \text{ } ^2\text{H}_2\text{O}$ , a marked improvement in the resolution of the quadrupole split  $^7\text{Li}$  spectrum was observed (see FIG. 71 a). This is believed to result from a slow exchange of  $\text{Li}^+$  ions between the lamellar phase crystallites and dilute isotropic soap solution in the heterogenous two-phase ( $L_1 + D$ ) region. These results established the approximate position of the boundary between the homogenous lamellar phase (D) and the two-phase ( $D + L_1$ ) region at a composition between  $20.0 \text{ wt } \%$  and  $29.4 \text{ wt } \% \text{ LiPS}$ .

It should be noted that for such two-phase equilibria (eg  $D + L_1$ ) the  $^7\text{Li}$  NMR signal corresponding to the isotropic component ( $L_1$ ) is not resolved as a separate distinct signal (as observed for the quadrupole split  $^2\text{H}$

spectra of similar systems) but is directly superimposed upon the central  ${}^7\text{Li}$  mesophase signal corresponding to the  $m = 1/2 \leftrightarrow m = -1/2$  transition. The  ${}^7\text{Li}$  NMR spectrum obtained from the isotropic soap solution phase of the 3.0 wt % LiPS phase separated sample (refer to Section 5.1.2) was, however, characterized by a single sharp line centred at the Larmor frequency. The linewidth ( $W_{1/2}$ ) of this absorption signal was of the same order of magnitude as that observed for both the two-phase ( $L_1 + D$ ) samples and an isotropic  $\text{LiCl}-2\text{H}_2\text{O}$  sample ( $\sim 4.5 \text{ mol.dm}^{-3}$ ) recorded using identical experimental operating conditions ( $\sim 37 \text{ Hz}$ ). Linewidth values measured for the single phase lamellar samples were estimated to be approximately twice as large as those measured for the  $L_1 + D$  samples, indicating that the firmness of binding of the lithium counterion is greater in the lamellar D phase than in the isotropic soap solution phase  $L_1$  [273, 335].

For the 79.4 wt % LiPS sample in the two-phase D + G region, no overall change in appearance of the  ${}^7\text{Li}$  NMR spectrum was observed, although a slight decrease in the value of  $\Delta({}^7\text{Li})$  was recorded for the liquid crystal (D) component. The  ${}^7\text{Li}$  absorption signal from the "solid" LiPS phase (where the counter-ions are expected to undergo much slower re-orientations) would be strongly broadened due to rapid quadrupole relaxation [269, 335]). The intensity of this signal was therefore spread over a large frequency range thus reducing the peak amplitudes

to values too small to be detected under the experimental conditions employed. The  $^7\text{Li}$  lineshape recorded for the 94.1 wt % LiPS sample, however, (FIG. 71d), where the "solid" material (G) is considered to be the major component, indicated a more conspicuous contribution from the "solid" soap resulting in a marked decrease in resolution of the mesophase satellite signals. It was also noted that the linewidth ( $W_{\frac{1}{2}}$ ) of the  $^7\text{Li}$  central line was considerably increased at this composition to  $\sim 200$  Hz. As discussed in several NMR investigations of counterion bonding in amphiphile-water systems [273, 335], an increase in the linewidth can often be interpreted as resulting from a stronger binding of the counterions to the amphiphile molecules. Such an effect might be expected on reducing the water content of the lamellar mesophase component below a certain concentration corresponding to that required for complete hydration of the counterions and head groups.

It can clearly be seen from TABLE 35 that the  $\Delta(^7\text{Li})$  values are essentially constant with changes in sample composition across the whole of the lamellar D phase region (within the limits of experimental error).

On the basis of a crude two-site model (Section 2.2.5.2) involving counter-ions "bound" to the amphiphile head groups (in general having  $\Delta > 0$ ) and those free in solution ( $\Delta = 0$ ), these results imply that the parameters  $P_b^{\text{Li}}$ ,  $E_{\text{Cb}}^{\text{Li}}$  and  $S_b^{\text{Li}}$  (equation (2.14)) are also invariant for the lamellar D phase.

A change in the lithium electric field gradient (and hence  $E_{Qb}^{Li}$ ) would be associated with an alteration of the average position of water and head groups at the interface and would be expected to give rise to a change in the measured  $\Delta(^2H)$  values [272]. This was not observed.

Similarly, x-ray diffraction studies have shown that at the relatively high water contents involved, the hydration of the interface is complete with additional water causing a 1-d swelling behaviour. The interfacial area per polar group (which in a lamellar micelle is equal to the effective cross-sectional area per amphiphile molecule) was consequently found to be constant in this region ( $S \sim 43 \text{ \AA}^2$ ) and therefore no change in  $\Theta_{DM}$  and consequently ( $S_b^{Li}$ ) would be expected.

The constancy of  $P_b^{Li}$  can be explained in terms of the ion-condensation model developed by Wennerström and co-workers [282] for the case of aqueous lamellar mesophases formed by ionic amphiphiles. This model predicts that when the thickness ( $2a$ ) of the water lamellae exceeds a critical value which depends upon the surface charge density  $\sigma$ , a fraction ( $\sim 0.5$ ) of the counterions, which depends upon  $\sigma$ , coalesce onto the surface. For values of  $(|\sigma|a)$  larger than the critical value, the number of bound ions is predicted to be independent of both the water content and temperature (since the ion-binding process is entropy driven). In lamellar liquid crystalline phases stable to high water

contents a typical charge density is one unit charge per  $80\text{\AA}^2$ , while considerably higher charge densities can appear at lower water contents [282]. With  $\sigma = 1e/80\text{\AA}^2$ , the critical distance between the lamellae is  $7.5\text{\AA}$  and above this distance ion condensation behaviour is expected. The distances are usually larger in systems with small charge density [282]. For the lamellar D phase formed in the LiPS- $^2\text{H}_2\text{O}$  system, however, the value of  $\sigma$  is much higher ( $\sim 1$  charge per  $43\text{\AA}^2$ ) and the minimum water layer thickness was calculated to be  $\sim 15\text{\AA}$  and therefore an ion-condensation type behaviour would be expected.

Since changes in the populations of counter-ions bound to different anisotropic sites would be reflected in variations in  $\Delta(^7\text{Li})$ , these results are consistent with the assumption that the splitting is proportional to the fraction population,  $P_b^{\text{Li}}$ , of a single "bound" site over the entire composition range of the lamellar D phase [282]. Similar results have been reported for aqueous ionic amphiphile systems containing, for example, sodium octylsulphate [337], sodium octylsulphonate [270] and sodium di-2-ethylhexylsulphosuccinate [337]. In sodium octanoate systems of lower water content, however, several (two or more) binding sites are thought to be involved in the direct counterion binding [270, 338].

Lindman et al [284] have reported that the  $\text{Li}^+$  ion with its greater charge density is more strongly hydrated than

the  $\text{Na}^+$  ion and thus the quadrupole splittings of the  $\text{Li}^+$  ions are less sensitive to alterations in their environment (such as changes in polar head group and charge density on the amphiphile aggregates, or temperature variations; refer to Section 5.4.2.2). As an example it was mentioned that the  $^7\text{Li}$  quadrupole splitting in the lamellar phase of the lithium octanoate-decanol- $^2\text{H}_2\text{O}$  system [284] varied monotonously between 0.45 and 0.67 kHz over the entire phase domain in contrast to the complicated variations found with the corresponding sodium system [270]. Similarly Everiss et al [272] have reported  $\Delta(^7\text{Li})$  values of between  $\sim 0.40$  and 0.55 kHz for the lamellar D mesophase formed in the lithium perfluorooctanoate-water system between  $\sim 0.077$  and  $\sim 0.085$  mole fraction of soap at 25 °C.

It is worthy of note that there appears to be a tendency for the splittings to decrease slightly in the  $\text{LiPS-}^2\text{H}_2\text{O}$  system at the highest water concentrations (corresponding to the  $L_1 + D$  region) though this apparent decrease is clearly within the limits of experimental error. A genuine decrease in the value of  $\Delta(^7\text{Li})$ , however, may be explained in terms of an increased counter-ion dissociation from the lamellae [273] (ie a decrease in the fraction of  $\text{Li}^+$  ions experiencing a residual anisotropy in the field gradients) or alternatively to an increasing curvature in the lamellae (resulting in an increase in the angular amplitude of the field gradient fluctuations thereby reducing the order parameter) since the repulsion between the lamellae is weak

at high water contents [282].

The origins of the observed decrease in  $\Delta(^7\text{Li})$  at the highest soap concentrations (corresponding to the two-phase D + G region) is however less clear. It may be explained tentatively in terms of a change in the molecular organization at the amphiphile-water interface of the lamellae (thereby changing  $\Theta_{\text{DM}}$  and consequently the order parameter, S; equation (2.12)) caused by either a decrease in hydration of the amphiphile molecules and/or by the preferential "crystallization" of certain isomeric soap molecules from the lamellar D mesophase to form the "solid" G phase.

#### 5.4.2.2 Above Room Temperature

In order to gain some insight into the factors determining the magnitude of the  $^7\text{Li}$  counterion quadrupole splitting,  $\Delta(^7\text{Li})$  the temperature dependence was investigated for samples of varying composition and phase type. The results presented in TABLE 36 have also been presented graphically (FIG. 72).

Each sample, irrespective of composition and phase type, displayed similar increases in  $\Delta(^7\text{Li})$  with increasing temperature. (Additional lamellar D phase samples at soap concentrations of 35.2 wt % LiPS ( $X_{\text{W}}/X_{\text{A}} = 33.7$ ) and 63.5 wt % LiPS ( $X_{\text{W}}/X_{\text{A}} = 10.5$ ) also exhibited small increases in  $\Delta(^7\text{Li})$  over similar temperature ranges). It is interesting to note that for the homogeneous lamellar D phase sample (where  $X_{\text{W}}/X_{\text{A}} = 18.3$ ) and for the two-phase

TABLE 36 : Lithium-7 NMR counterion quadrupole "powder" splittings,  $\Delta(^7\text{Li})$ , as a function of temperature at different sample compositions in the LiPS- $^2\text{H}_2\text{O}$  system

T/(°C)	$\Delta(^7\text{Li})/(\text{kHz})$		
	LiPS CONTENT/(wt %)		
	20.0 (L <sub>1</sub> + D)	50.0 (D)	79.4 (D + G)
30	1.71	1.75	1.47
40	1.77	1.81	1.52
50	1.81	1.88	1.59
55	1.84	1.90	-
60	1.86	1.94	1.68
65	1.89	1.96	-
70	1.91	1.99	1.83
75	1.93	2.00	-
80	1.95	2.05	1.89
85	-	2.07	-
90	-	2.08	1.93
95	-	2.09	-

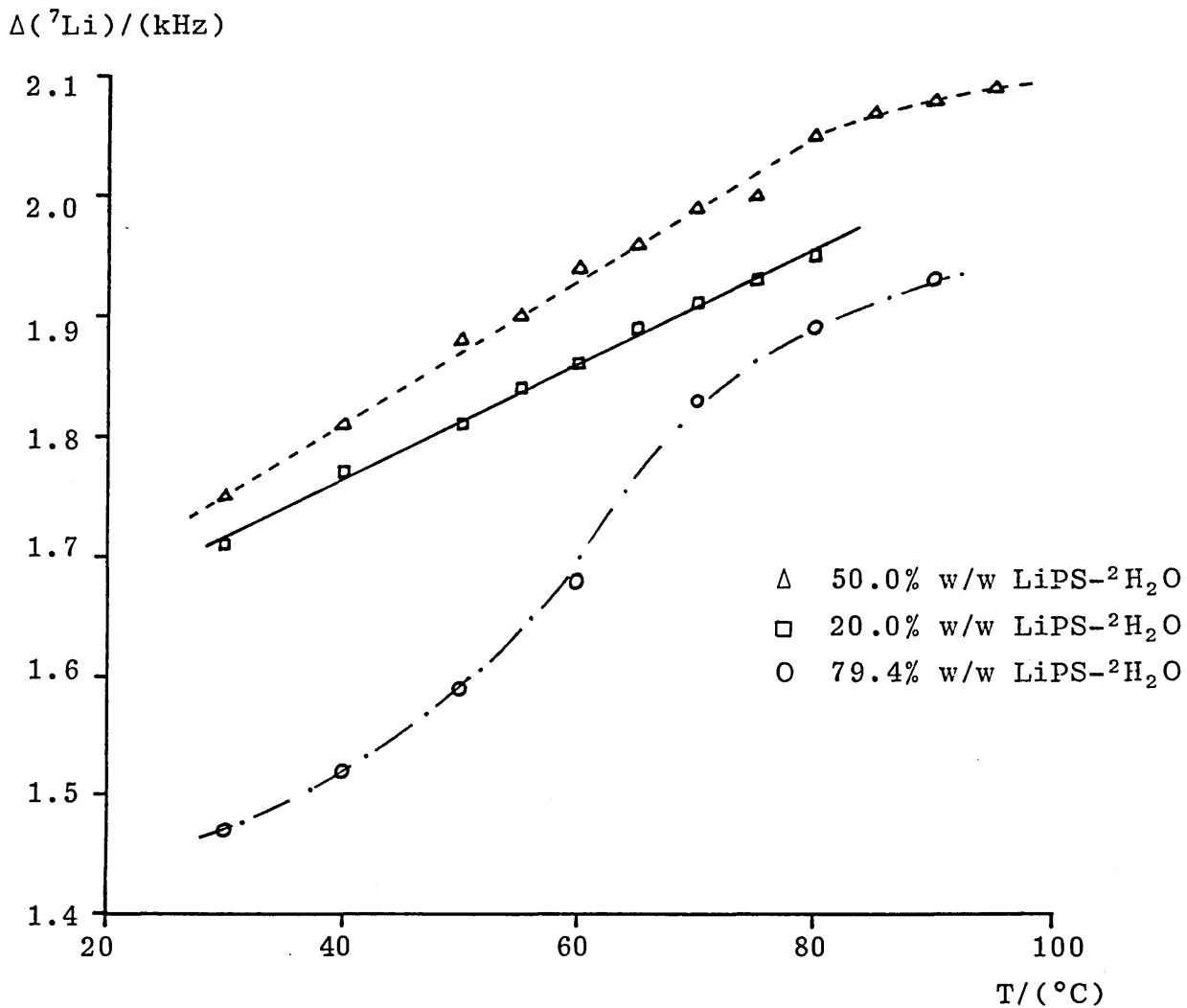


FIG. 72 :  $^7\text{Li}$  NMR counterion quadrupole "powder" splittings,  $\Delta(^7\text{Li})$ , as a function of temperature at different sample compositions in the lithium phenylstearate- $^2\text{H}_2\text{O}$  system

lamellar + "solid" soap (D + G) sample (where  $X_W/X_A = 4.7$ ), the rate of increase in  $\Delta(^7\text{Li})$  appears to fall off slightly beyond  $\sim 80$  °C. A similar, though unexplained, behaviour was reported by Boden et al [285] for the  $^{39}\text{K}$  counterion quadrupole splitting in the lamellar D phase of the potassium oleate-water system (at  $X_W/X_A = 7.6$ ) beyond  $\sim 60$  °C. For the D + G sample, an apparent discontinuity in the plot of  $\Delta(^7\text{Li})$  versus temperature was also observed between  $\sim 60$  °C and  $70$  °C. This may well correspond to the calorimetrically observed H1 transition for a sample of similar composition between  $\sim 55$  °C (onset) and  $\sim 100$  °C (completion) at the first-order (D + G) to G phase boundary.

A model based upon the variation of  $\theta_{DM}$  (the time average angle between the EFG and the normal to the lamellae), and consequently the order parameter, S, (refer to equations (2.12) and (2.14); Section 2.2.5.2) has previously been used to explain the temperature dependence of counter-ion quadrupole splittings in the lamellar D phase of the sodium octanoate-water system [270] and in the ternary systems containing decanol [270, 338] pentanol [273] and octanoic acid [270].

The complex quadrupole splitting variations observed for these systems indicated that over wide concentration and temperature ranges  $\theta_{DM}$  takes on large values in the vicinity of the magic angle ( $54^\circ 44'$ ) where the order parameter term  $3 \cos^2 \theta_{DM} - 1$  vanishes. A location of specifically bound sodium ions between adjacent carboxylate

groups involving hydrogen bonding between water of counterion hydration and these surfactant head-groups was considered to be a plausible model to explain the results.

If an increase in the thermal energy of the system may be supposed to increase the distance between the counterions and the charged lamellae, a temperature increase will result in a decrease in the average value of  $\Theta_{DM}$ . The accompanying increase in the order parameter of these bound counterions (ie more positive or less negative depending upon the original value of  $\Theta_{DM}$ ) may, depending upon its sign, give either an increase or a decrease in the splitting. Thus if the splitting increases with increasing temperature, the order parameter should be positive.

If the above single binding site model is applied to the lamellar D phase in the LiPS-<sup>2</sup>H<sub>2</sub>O system, the  $\Delta(^7\text{Li})$  NMR data is consistent with a positive quadrupole splitting (ie order parameter). This would be indicative of partial penetration of the specifically bound hydrated lithium ions between the surfactant carboxylate head groups with a  $\Theta_{DM}$  value of  $< 54^\circ 44'$  and with a limited range of variation (as implied by the weak change in  $\Delta(^7\text{Li})$  with temperature). The falling off in the rate of increase of  $\Delta(^7\text{Li})$  at higher temperatures in this case, may therefore be indicative of  $\Theta_{DM}$  approaching a limiting value.

Temperature dependent counterion quadrupole splittings may also be interpreted in terms of a two-site model for counterion bonding at a charged surface [270, 285] illustrated in FIG. 73.

In this model, two distinct binding sites are envisaged (which can be regarded as two different sites in equation (2.13)). In site I the ions are specifically bound between neighbouring carboxylate head groups (corresponding to a Stern layer) whilst in site II, though essentially still bound, they are distributed in a Gouy-Chapman type diffuse layer and are not associated with any one specific surfactant group.

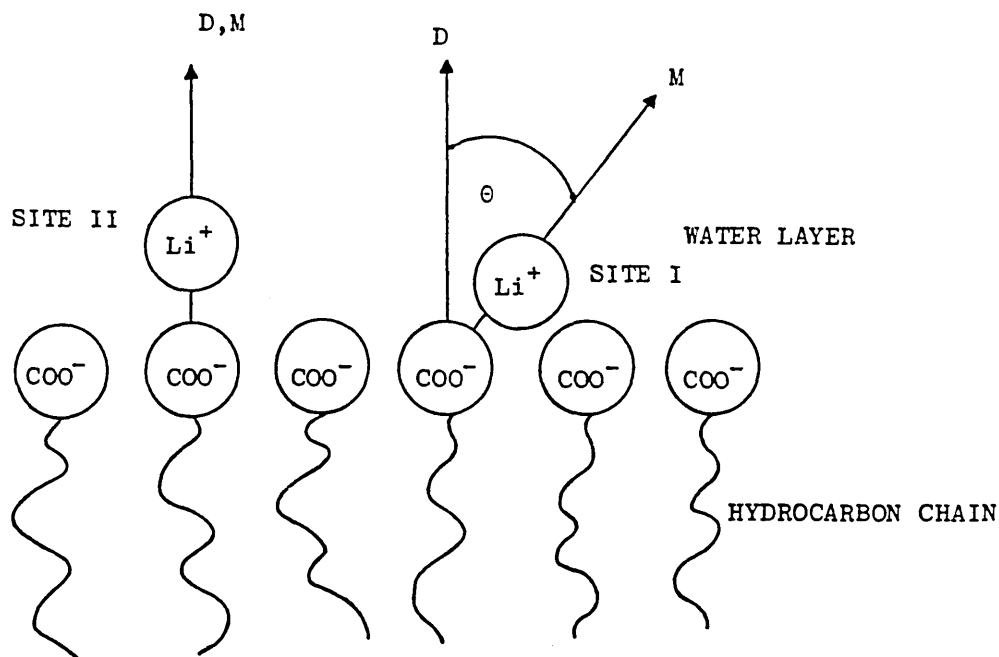


FIG. 73 Two site model for counterion binding at a lamellar surface. Refer to text for explanation.

For ions in site II, the electric field gradient,  $M$ , is expected to be parallel to the mesophase director ( $D$ ); thus  $S_{II} > 0$  and  $\Delta_{II} > 0$  provided  $E_{QII} > 0$ . Conversely, for an ion in site I the EFG will be included at an angle  $\Theta_{DM}$  which is considered to be greater than  $54^\circ 44'$  (the magic angle), thereby making  $S_I < 0$  and  $\Delta_I < 0$ . Both order parameters,  $S_I$  and  $S_{II}$ , are assumed to be approximately temperature invariant [270]. A free-energy difference  $\Delta G$  between the two sites is also assumed and it is anticipated that site I (specific) will be energetically more favourable than site II (diffuse) at lower temperatures and water contents. (Indeed an arrangement in which the counterions are interposed between carboxylate head groups will minimize the coulombic energy).

An increase in temperature is considered to be accompanied by an increase in the population of ions in site II at the expense of site I. This will cause an increase in the magnitude of  $\Delta$  (the observed splitting is a weighted average over the two sites) if initially it is positive and a decrease if initially it is negative.

On the basis of this two-site model, the  $\Delta(^7\text{Li})$  NMR data for the  $\text{LiPS}-^2\text{H}_2\text{O}$  system is once again consistent with a positive quadrupole splitting. The falling off in the rate of increase of  $\Delta(^7\text{Li})$  at higher temperatures, in this case, may be explained in terms of the attainment of a limiting equilibrium value for the relative populations of the two binding sites.

Irrespective of which particular model is invoked, the temperature dependence of the counterion quadrupole splittings in the LiPS-<sup>2</sup>H<sub>2</sub>O system is far less complex than that reported for aqueous sodium surfactant systems (where  $\Delta$  has been observed to change sign with increasing temperature [270, 338]) and is indicative of positive quadrupole splitting variations. This may be a consequence of differences in the strength and degree of hydration of the respective counterions and also of the strength of the counterion-head group interactions. Similar small, monotonic increases in  $\Delta(^7\text{Li})$  with temperature have also been reported for the lamellar mesophases formed in the lithium perfluorooctanoate-water [272] and lithium octanoate-decanol-<sup>2</sup>H<sub>2</sub>O [284] systems.

#### 5.4.2.3 Below Room Temperature

Changes in the <sup>7</sup>Li NMR lineshape of a 50.0 wt % LiPS -<sup>2</sup>H<sub>2</sub>O lamellar phase sample were studied as the temperature of the system was decreased monotonically below 30 °C (see FIG. 74). The counterion quadrupole splitting,  $\Delta(^7\text{Li})$ , and central resonance absorption linewidth,  $W_{\frac{1}{2}}$ , values have been recorded in TABLE 37 as a function of temperature.

In most cases, the estimated errors on the tabulated  $\Delta$  values are of the order of 3-4%. For the spectrum recorded at -20 °C, however, the satellite peaks were considerably broadened and poorly resolved (see FIG. 74b) resulting in a possible error of ~ 12%. For the linewidth values of approximate magnitude < 0.1 kHz, the estimated errors

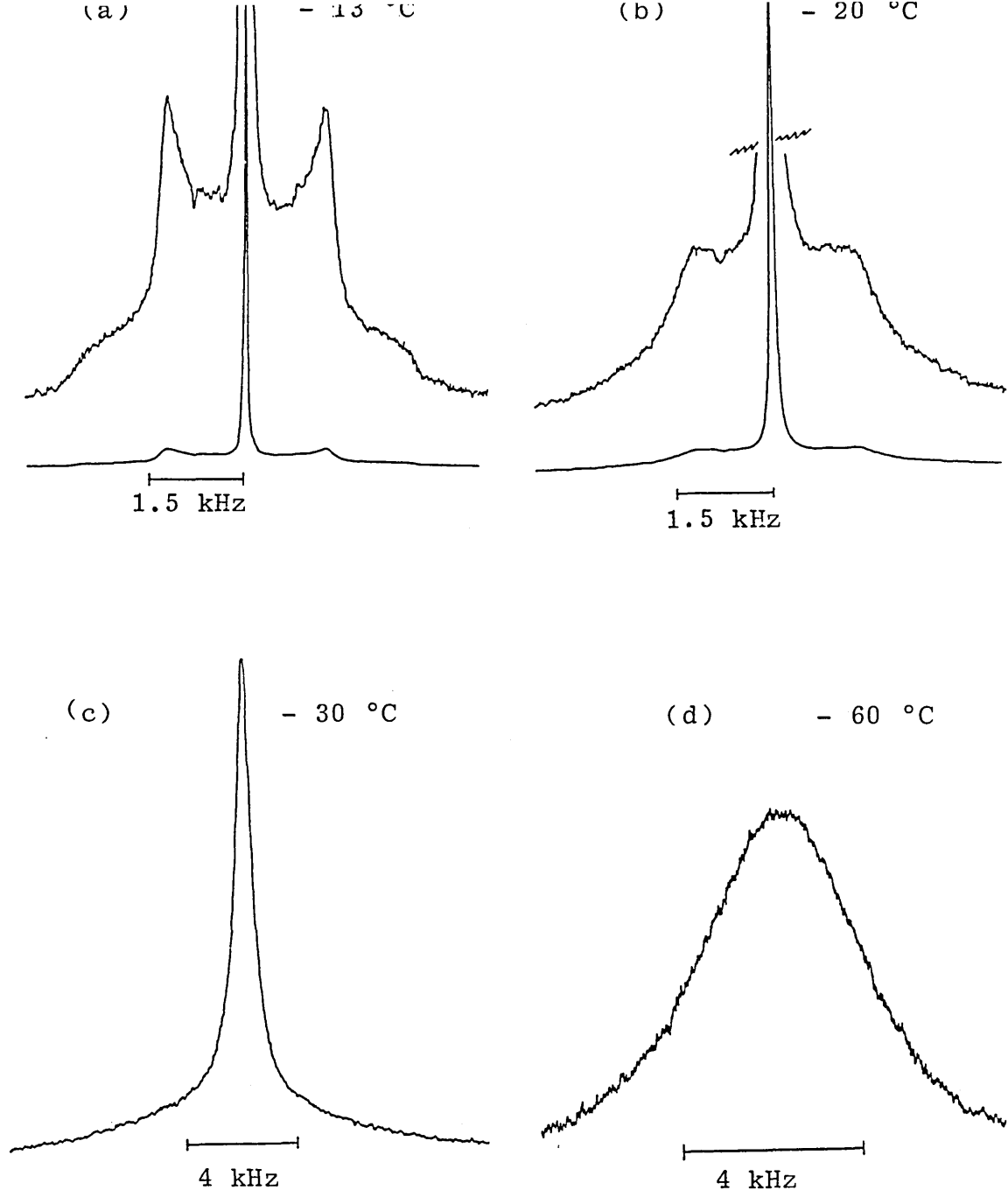


FIG. 74 : Changes in the  $^7\text{Li}$  NMR lineshape of a 50.0 % w/w lithium phenylstearate- $^2\text{H}_2\text{O}$  lamellar mesophase sample as a function of temperature below  $30\text{ }^\circ\text{C}$

may be as large as 10-15% while for larger linewidths, they are considerably less. It should also be noted that the experimental line broadening factor (Section 2.2.5.3) employed in this study had been reduced from 24.0 to 4.5 resulting in much narrower lines than those recorded in the preceding section. For the purpose of this study, however, knowledge of the absolute linewidth values was not critical.

TABLE 37 : Lithium-7 NMR counterion quadrupole splittings,  $\Delta(^7\text{Li})$ , and central resonance absorption linewidth,  $W_{\frac{1}{2}}$ , values as a function of temperature below 30 °C for a lamellar D mesophase sample (at  $X_W/X_A = 18.3$ ) in the LiPS- $^2\text{H}_2\text{O}$

T/(°C)	$\Delta(^7\text{Li})$ /(kHz)	$W_{\frac{1}{2}}$ /(kHz)
- 70	-	4.14
- 60	-	3.93
- 50	-	3.38
- 40	-	1.44
- 30	-	0.40
- 25	-	0.18
- 20	~ 1.3	0.08
- 13	1.25	0.05
- 7	1.23	0.04
0	1.22	0.03
30	1.75	0.03

The qualitative and quantitative changes observed by NMR spectroscopy appears to be in concordance with thermodynamic data obtained for a similar sample by DSC (Section 5.2.2).

As the temperature of the sample was reduced below 0 °C the NMR quadrupole splittings remained sharp and well resolved (FIG. 74a) and approximately constant in value despite the presence of a calorimetrically observed first-order transition (H5) at approximately - 2.4 °C which has been attributed to the freezing of the "free" (unbound) bilayer water. Unfortunately, attempts to record spectra at both 7 °C and 15 °C were hindered by poor temperature stability at the sample (with fluctuations of the order of  $\pm 5$  °C) resulting in broad poorly resolved satellite peaks. Estimates of  $\Delta(^7\text{Li})$  at these temperatures were of the order of 1.4 kHz, however, suggesting a gradual reduction in  $\Delta$  over this temperature range rather than on abrupt decrease at the H5 transition. The decrease in  $\Delta(^7\text{Li})$  may be attributed to a change in the order parameter of the bound counterions due to either an increase in  $\theta_{\text{DM}}$  or to an increase in the population of specifically bound (as opposed to diffusely bound) lithium ions with decreasing temperature (refer to Section 5.4.2.2).

Between - 20 °C and - 30 °C, the quadrupole splitting satellite peaks became progressively broadened and poorly resolved (FIGS 74b and 74c) reducing the peak amplitudes to values too small to be measured accurately. This is

attributed to a rapid quadrupole relaxation mechanism resulting from slower reorientations of the counterions as the temperature approached the calorimetrically observed H4 transition at approximately - 33 °C. This transition has been attributed to the combined "immobilization" of the surfactant head groups and "bound" counterions and water molecules.

Beyond this transition, rapid increases in  $W_{\frac{1}{2}}$  were observed with decreasing temperature until approximately - 60 °C where the value became relatively constant (FIG. 74d). This temperature corresponded to the calorimetrically observed H3 transition which has been attributed to a freezing-in of motion of the soap hydrocarbon chains.

The absence of a rapid and pronounced decrease in  $\Delta(^7\text{Li})$  with decreasing temperature precludes the possibility of a change in the sign of the quadrupole splitting from positive to negative as the temperature is reduced over this range (refer to Section 5.4.2.2).

## 5.5 The Equilibrium Phase Diagram

The equilibrium phase diagram constructed for the lithium phenylstearate -  $^2\text{H}_2\text{O}$  system is presented in FIG. 56 (refer to Section 5). The positions of the boundaries indicated by broken lines are tentative. The phase notations employed are:

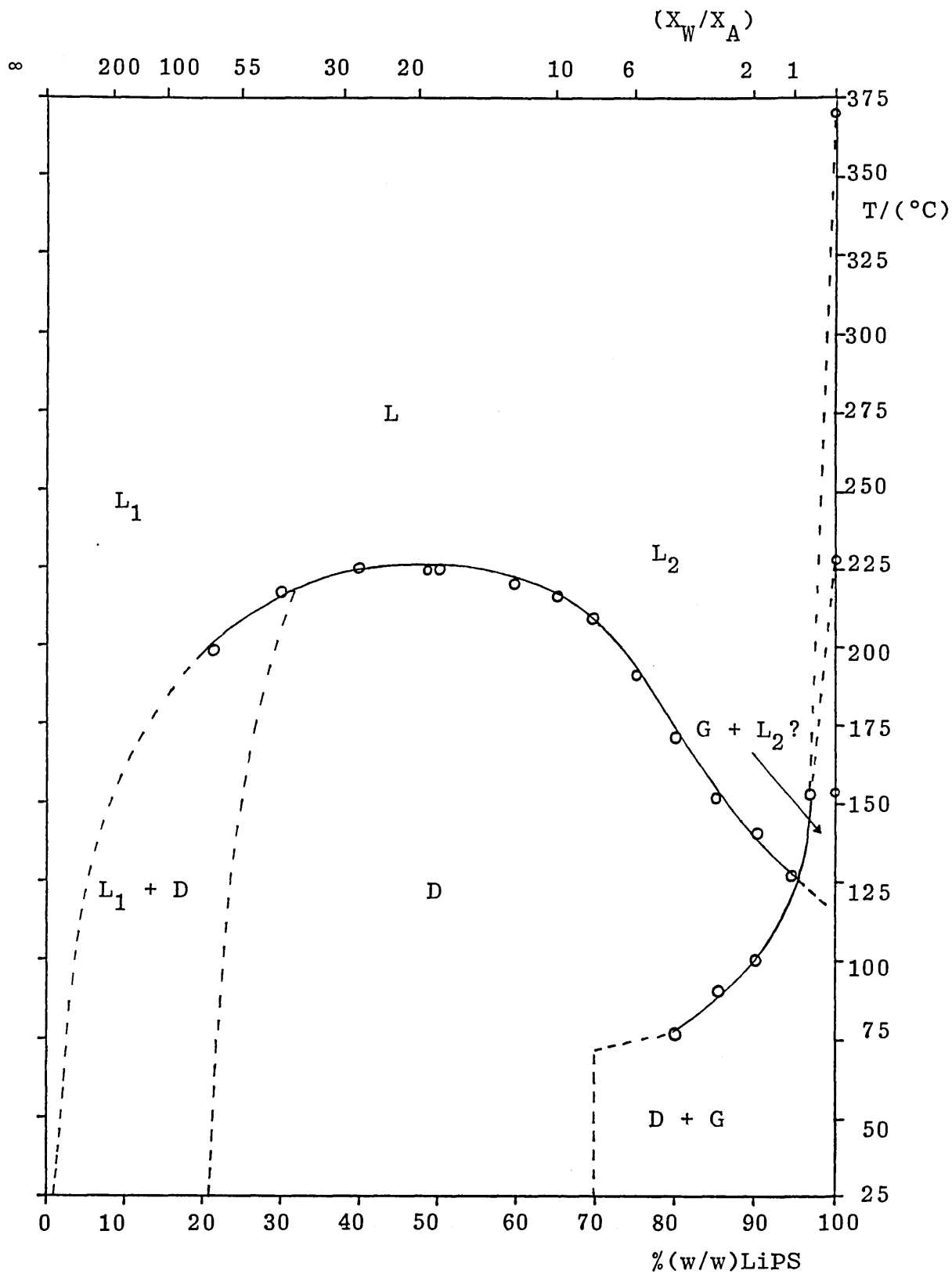


FIG. 56 : An equilibrium phase diagram for the system  
LITHIUM PHENYLSTEARATE- $2\text{H}_2\text{O}$

L ( $L_1$ ,  $L_2$ ), mobile isotropic soap solution phases,  
D, lamellar "neat" phase,  
G, "solid" LiPS

## 5.6 Discussion

In marked contrast to the crystalline fatty acid soaps of sodium, potassium, rubidium and caesium, those containing lithium are quite insoluble in water, their Krafft points being above 100 °C [316]. For example, Demarcq and Dervichian [316] have reported temperatures of 123 - 125 °C and 140 °C corresponding to the Krafft points of lithium laurate,  $\text{LiC}_{12}$ , and lithium palmitate,  $\text{LiC}_{16}$ , (refer to Section 1.3.1.3) respectively.

Murray and Hartley [152] have explained the Krafft point in aqueous soap solutions as the temperature at which the solubility of the crystalline soap, reaches the critical micelle concentration. At temperatures appreciably higher than the Krafft point, the crystalline phase cannot exist in equilibrium with micelles and mesophases may consequently form over wide temperature and composition ranges. In this connection, it is appropriate to distinguish between two types of amphiphiles; on the one hand, amphiphiles whose solubilities in water are so high that the c.m.c. of the substance is exceeded and different types of micelles are formed (typical association colloids), and on the other, amphiphiles that have a lower solubility in water but can take up water while swelling (swelling amphiphiles). In both types, water molecules are bound to the polar groups.

Whereas the molecules of the association colloids are separated from each other and dispersed in the water, in the swelling amphiphiles this dispersion is prevented by a mutual attraction or binding between the molecules or a hydrophilic-lipophilic balance strongly in the lipophilic direction. In these cases (eg the dialkyl lipids such as lecithins), mesophases, usually dispersed in an aqueous solution of surfactant monomer, form in preference to the micellar solution at low surfactant concentrations.

The main factor that determines the solubility of an ionic surfactant is the stability of the crystal [339]. The most efficient way to lower the Krafft point is consequently to chemically modify the surfactant in such a way that the packing in the crystal is perturbed [340]. The introduction of branching or unsaturation into a hydrocarbon chain will reduce the chain-melting transition of the soap, thus allowing water to penetrate the hydrophilic region of the soap structure at much lower temperatures causing a marked depression of the Krafft point. For example, whereas the Krafft point of lithium stearate,  $\text{LiC}_{18}$ , is believed to be in the region of  $\sim 150$  °C [316] that of the unsaturated oleate soap was found to be 72 °C [316].

In the extreme case of lithium phenylstearate, the complex heterogeneous composition of the "solid" phase (Section 1.2.3.1) prevents the crystallization of the soap hydrocarbon chains and the Krafft point is depressed to

a temperature below 25 °C.

It can be seen in FIG. 56 that the equilibrium phase diagram for the LiPS-<sup>2</sup>H<sub>2</sub>O system is dominated by a broad region composed of a lamellar D ("neat") mesophase at room temperature. The results of this study have indicated that a minimum amount of water is necessary to stabilize this phase at room temperature (corresponding to ~ 8-10 moles of water per mole of soap) equivalent to that required for, more or less, complete hydration of the surfactant counterion and head group. When this condition has been fulfilled, it would appear that the cross-section of the hydrated ionic head groups (~ 43 Å<sup>2</sup>) becomes comparable with the maximum cross-sectional requirement of the phenyl substituted hydrocarbon tails. The varied location of the phenyl group on the aliphatic chains no longer imposes the geometrical constraints which led to the semi-crystalline reversed hexagonal structure (SCH 1) as the arrangement of lowest free energy in the anhydrous state (Section 3.3.5.3). As the thermal energy of the system is increased, however, this requisite minimum appears to decrease, resulting in a displacement of the boundary between the D and (D + G) regions to lower water contents (see FIG. 56).

The increase in the lamellar x-ray diffraction spacings with water content has indicated a 1-d swelling behaviour. This mechanism involves no increase in the interfacial area per polar group, S, and the uptake of water can therefore continue without producing a transition to another

mesophase. Furthermore, the constancy of  $S$  ( $\sim 43 \text{ \AA}^2$ ) as the water content is increased from 35 wt % to 70 wt % implies that the additional water is intercalated between the double layers in the free state. This behaviour is characteristic of the so-called swelling amphiphiles (eg various monoglycerides, diethylene glycol monolaurate and the dialkyl sulphosuccinates, Aerosol OT and Aerosol MA [10]) and is in marked contrast to the behaviour found in binary aqueous systems primarily of ionic association colloids (sodium alkylsulphates and sulphonates, various alkylammonium salts and, more importantly, the alkali metal fatty acid soaps [10]).

For these latter systems, a non-expanding type of neat phase is formed in which the interfacial area per polar group varies with the water content. The existence of the mesophase is consequently restricted to certain maximum and minimum values of water content. For anionic association colloids of this class, this minimum amount of water has proved to be that needed for more or less complete hydration of their alkali ions, namely 2-3 moles for potassium, 5-6 for sodium and 7-8 moles for lithium soaps [10]. The water content at the boundary of the neat phase shows that the maximum amount that can be incorporated would not seem to exceed that which can be bound to the alkali counterions by ion-dipole attraction and to the carboxylate head groups by hydrogen bonds. The maximum values of  $S$  found for the neat phase of the

alkali soaps (of the order of  $40-46 \text{ \AA}^2$  [10]) are comparable with the constant value recorded throughout the neat phase region of the LiPS- $^2\text{H}_2\text{O}$  system.

The solubilization of alcohols in the initially non-expanding neat phase of the ionic association colloids, however, produces a change so that the effect of water intake on the swelling changes with progressively increasing alcohol content of the amphiphile layer to one where it is accompanied by 1-d swelling. The sudden increase, above a certain alcohol soap ratio, in the ability of the neat mesophase to incorporate water has been ascribed to the interaction between the hydroxyl groups of the alcohol and the ionized polar groups of the soap. This reduces the charge density in the boundaries of the amphiphilic layers to rather low values (of the order of 1 charge per  $72-75 \text{ \AA}^2$ ) allowing the liberation of counterions from the double layers.

This liberation of ions makes a Donnan distribution of them possible between an "inner solution" consisting of bound water and bound ions and an "outer solution" consisting of free water and ions. The binding of ions in the inner layers thus works in the same way as if the ions were separated from the outer solution by a membrane permeable to counterion and monomeric surfactant ions but not to aggregated surfactant ions. The distribution provides conditions for intake and retention of free water in the mesophase [10]. It is possible that this mechanism may be responsible for the 1-d swelling behaviour of the

lamellar neat phase formed in the Aerosol OT-water system at room temperature (Section 1.3.2.1). Here, the charge density in the interfacial layers of ionic polar groups from the beginning is rather low (about 1 charge per  $68 \text{ \AA}^2$  [341]) permitting the liberation of counterions from the double layers and thus enabling the phase to incorporate much more water than the polar groups can bind.

This may not be the case, however, for the neat phase in the LiPS- $^2\text{H}_2\text{O}$  system where the charge density in the interfacial layers is constant at about 1 charge per  $43 \text{ \AA}^2$  throughout the whole composition range of existence of the mesophase. Here the conditions for a Donnan equilibrium would probably not be established with the lithium ions being largely retained within the interfacial layer of polar groups. This suggests that, in the case of this carboxylate soap with lithium as the counterion, the bonds between the amphiphilic molecules (primarily between the polar groups by ion-ion attractions or water links between them affected by hydrogen bonds) endow the amphiphile layers with a stability that permits amounts of water to be incorporated far in excess of that which is bound to the polar groups. (A similar line of reasoning may be used to explain the high intake of water by the neat phase of non-ionic swelling amphiphiles of the monoglycerides). The intake of water by the neat phase therefore continues until the water vapour pressure increases to the value of the dilute aqueous soap solution  $L_1$ , with which it is in equilibrium.

The results of this present study have indicated that the lamellar phase observed at water contents between  $\sim 60$  wt % and  $\sim 80$  wt % (originally designated lamellar type B on the basis of polarizing microscopy observations) is merely a continuation of the 1-d swelling lamellar D phase at high water contents and that no first-order B/D phase transition exists.

The lamellar mesophase designated as type B by Ekwall et al [260] has so far not been detected in binary systems of amphiphile and water but only in ternary systems where in addition to a typical association colloid and water, there is an amphiphilic compound of the alcohol or fatty acid type [10]. The difference between the mesophases D and B has been ascribed primary to differences in the mutual orientations of the polar heads in the interfacial layers [10]. The molecules in the amphiphile layers of phase B are fairly tightly packed. In the system most carefully studied to date, sodium octanoate-decanol-water, a constant mean interfacial area per polar group (carboxyl + hydroxyl groups) of about  $25\text{--}27 \text{ \AA}^2$  has been calculated with charge densities which vary from one negative charge per  $\sim 68 \text{ \AA}^2$  to one per  $\sim 83 \text{ \AA}^2$ . The corresponding values observed in the present LiPS- $^2$ H<sub>2</sub>O system are, however, much higher and are constant throughout the whole composition range of existence of the lamellar phase.

In the binary aqueous systems containing typical swelling amphiphiles, a transition to a mesophase of the reversed

type (eg reversed hexagonal, F, or reversed cubic I<sub>2</sub>) may be observed on reducing the water content below that required to stabilize the neat phase. In the LiPS-<sup>2</sup>H<sub>2</sub>O system, however, this was found not to be the case. Probably as a direct result of the complex isomeric composition of the "solid" soap phase, a process of selective "crystallization" is believed to occur as the water content is decreased below ~ 35 wt % (ie below  $X_W/X_A \sim 9.9$ ) to give a hydrated "solid" soap phase (probably of the SCH I type; refer to Section 3.3.5.3). denoted G. This allows the lamellar D neat phase, with which it is in equilibrium, to maintain the critical minimum concentration of water necessary to stabilize this mesophase.

Further studies are necessary in order to establish the exact position of the phase boundary at the lowest water contents between the two-phase (D + G) region and the homogeneous hydrated "solid" soap phase (G). From this work it appears to occur, however, at a water content of < 4 wt %.

## CHAPTER SIX : SUMMARY OF RESULTS

6.1 The thermotropic polymorphism of lithium stearate (n-octadecanoate),  $\text{LiC}_{18}$ , has been reinvestigated using differential scanning calorimetry (DSC) and macroscopic and microscopic observations in polarized light.

In general, the results were in agreement with those reported in the literature.

It has been shown in this study, however, that a fused lamellar mesophase, having a very limited temperature range of stability ( $\sim 1$  °C) was formed immediately preceding the amorphous melt. This liquid crystal phase was previously thought not to occur for  $\text{LiC}_{18}$ .

6.2 The thermotropic phase behaviour of lithium oleate (cis-9-octadecenoate) has been investigated. A similar stepwise melting process to that of  $\text{LiC}_{18}$  was observed, although a number of the polymorphic transitions were significantly lowered in temperature. The high temperature lamellar mesophase was not formed however.

6.3 The thermotropic polymorphism of a lithium phenyl-stearate, LiPS, "solid" soap mixture (composed of 12 positional isomers) has been studied using DSC, polarizing microscopy, x-ray diffraction and  $^7\text{Li}$  NMR spectroscopy.

Unlike the lamellar crystalline structure formed by the stearate and oleate soaps, LiPS has been shown to form an unusual semi-crystalline reversed hexagonal structure,

possessing quasi-crystalline polar groups and disordered hydrocarbon chains at room temperature.

6.4 Despite its complex isomeric composition, LiPS was found to behave like a typical single-component soap, exhibiting a stepwise melting behaviour. This soap formed a high temperature reversed hexagonal mesophase at  $\sim 227$  °C preceding the amorphous melt, with a large temperature range of stability ( $\sim 144$  °C). The corresponding sodium soap was observed to behave in a similar manner.

6.5 The phase behaviour of  $\text{LiC}_{18}$  in the hydrocarbon solvents, n-hexadecane and squalane was investigated using DSC and macroscopic and microscopic observations in polarized light and equilibrium binary phase diagrams were constructed.

In each system the number and nature of the phases formed were remarkably similar with each soap-containing phase being continuous with a phase of solvent-free  $\text{LiC}_{18}$ . However, the high temperature lamellar mesophase was not detected in these solvent systems.

6.6 Whilst the results were in good agreement with those reported by Cox and co-workers for  $\text{LiC}_{18}$  in n-hexadecane [51] and several mineral oils [196], it has been shown that the high temperature "liquid crystal" phase reported by these workers for such systems is a solvent-swollen semi-crystalline ribbon-type phase.

6.7 No evidence for the existence of a liquid crystal "phase island" as postulated by Vold and Vold [195] for the  $\text{LiC}_{18}$ -n-hexadecane system was found. These marked differences in phase behaviour may be attributed to the presence of traces of water in the Volds' system.

6.8 The phase behaviour of LiPS in aromatic hydrocarbons such as benzene, toluene and 1-phenylheptane was investigated using DSC, macroscopic and microscopic observations in polarized light, x-ray diffraction and  $^7\text{Li}$  NMR spectroscopy.

An equilibrium phase diagram was constructed for the LiPS-1-phenylheptane system where the soap was found to behave as a single component.

6.9 Unlike  $\text{LiC}_{18}$ , which proved to be essentially insoluble in hydrocarbon solvents at room temperature, LiPS was found to be miscible with such aromatic hydrocarbons in all proportions at room temperature. The results of this study have shown that the highly viscous, shear-birefringent solutions formed in such solvents at low LiPS concentrations ( $\sim 1$  to 2.5 wt % LiPS), originally reported by Singleterry and co-workers [175-180], are composed of long rigid reversed rod micelles.

6.10 At higher temperatures, two distinct mesophases have been shown to form in the 1-phenylheptane system. At solvent concentrations less than  $\sim 50$  wt % 1-phenylheptane, a solvent-swollen reversed hexagonal mesophase was formed.

- 6.11 At higher solvent concentrations a novel reversed cylindrical lyotropic nematic mesophase was formed. This is believed to be the first reported case of such a mesophase.
- 6.12 The lyotropic phase behaviour of LiPS with water has been investigated using DSC, macroscopic and microscopic observations in polarized light, x-ray diffraction and NMR ( $^2\text{H}$  and  $^7\text{Li}$ ) spectroscopy and an equilibrium phase diagram constructed.
- 6.13 In marked contrast to crystalline  $\text{LiC}_{18}$  which is quite insoluble in water, its Krafft point being above  $100\text{ }^\circ\text{C}$ , LiPS was observed to form a homogenous lamellar mesophase at room temperature. The phase diagram was dominated by this single mesophase which had a broad composition and temperature range of stability.

Unlike the ionic association colloids (eg the alkali metal soaps), LiPS was found to behave like a typical 1-d swelling amphiphile (eg Aerosol OT) over the entire composition range of stability of the lamellar phase at room temperature.

- 6.14 At low water concentrations ( $< 30\text{ wt } \%$  approximately), the soap ceased to behave as a single component and selective crystallization of a number of the LiPS isomers occurred producing a two-phase region composed of hydrated "solid" soap plus the lamellar mesophase at room temperature.

## References

1. R. Perron and C. Madelmont, *Rev. Franc. Corps Gras*, 20(5), 261 (1973).
2. P. A. Winsor, in: *Liquid Crystals and Plastic Crystals*, eds. G. W. Gray and P. A. Winsor (Ellis Horwood Ltd., Chichester, U.K., 1974) Vol. 1, Chap. 5, p.199.
3. D. M. Small, in: *Handbook of Lipid Research 4, The Physical Chemistry of Lipids* (Plenum Press, London, 1986), Chap. 9.
4. P. A. Winsor, *Chem. Revs.*, 68(1), 1 (1968).
5. *Handbook of Liquid Crystals*, eds. H. Kelker and R. Hatz, (Verlag Chemie, Weinheim, 1980), Chap. 11, p. 511.
6. I. Danielsson, in; *Lyotropic Liquid Crystals*, ed. S. Friberg (Advances in Chemistry Series No. 152, American Chemical Society, Washington D.C. 1976), Chap. 2, p.13.
7. G. J. T. Tiddy, *Physics Reports*, 57(1), 1 (1980).
8. G. J. T. Tiddy and M. F. Walsh, in: *Aggregation Processes in Solution*, eds, E. Wyn-Jones and J. Gormally (Elsevier Science Publishing Co., Oxford, 1983). Chap. 7, p. 151.
9. G. J. T. Tiddy, in: *Modern Trends of Colloid Science in Chemistry and Biology*, ed. H.-F. Eicke (Birkhäuser Verlag, Basel, 1985), p. 148.
10. P. Ekwall, in: *Advances in Liquid Crystals*, ed. G.H. Brown (Academic Press, London, 1975), Chap. 1, p. 1.

11. B. Gallot and A. Skoulios, Kolloid-Z. u.Z. Polymere, 213, 143 (1966).
12. J. J. Duruz, H. J. Michels and P. Franzosini, Proc. Roy. Soc. Lond., A322, 281 (1971).
13. P. Ferloni, M. Sanesi and P. Franzosini, Z. Naturforsch, 30A, 1447 (1975).
14. H. J. Michels and A. R. Ubbelohde, J. Chem. Soc. Perkin Trans. II, 1879 (1972).
15. P. Ferloni and P. Franzosini, Gazz. Chim. Ital., 105, 391 (1975).
16. M. Sanesi, P. Ferloni, M. Zangen and P. Franzosini, Z. Naturforsch, 32A, 285 (1977).
17. M. Sanesi, P. Ferloni and P. Franzosini, Z. Naturforsch, 32A, 1173 (1977).
18. P. Ferloni, M. Zangen and P. Franzosini, Z. Naturforsch, 32A, 627 (1977).
19. B. Gallot and A. Skoulios, Kolloid-Z. u. Z. Polymere, 209, 164 (1966).
20. A. R. Ubbelohde, H. J. Michels and J. J. Duruz, Nature, 228, 50 (1970).
21. A. R. Ubbelohde, H. J. Michels and J. J. Duruz, J. Phys. E., 5, 283 (1972).

22. J. J. Duruz and A. R. Ubbelohde, Proc. Roy. Soc. Lond., A330, 1 (1972).
23. A. R. Ubbelohde, Nature, 244, 487 (1973).
24. H. J. Michels and A. R. Ubbelohde, Proc. Roy. Soc. Lond., A338, 447 (1974).
25. J. J. Duruz and A. R. Ubbelohde, Proc. Roy. Soc. Lond., A342, 39 (1975).
26. J. J. Duruz and A. R. Ubbelohde, Proc. Roy. Soc. Lond., A347, 301 (1976).
27. A. R. Ubbelohde, in: The Molten State of Matter (Wiley-Interscience, Chichester, U.K., 1978).
28. M. Wolfe, J. Bonekamp and J. Jonas, J. Chem. Phys., 70, 3993 (1979).
29. J. Bonekamp, T. Eguchi and J. Jonas, Chem. Phys. Lett., 75, 360 (1980).
30. J. Bonekamp, T. Eguchi, S. Plesko and J. Jonas, J. Chem. Phys., 79, 1203 (1983).
31. J. Bonekamp, I. Artaki, M. L. Phillips, S. Plesko and J. Jonas, J. Phys. Chem., 87, 4991 (1983).
32. S. Plesko, M. L. Phillips, R. Cassell and J. Jonas, J. Chem. Phys., 80, 5806 (1984).

33. J. Bonekamp, B. Hegemann and J. Jonas, Mol. Cryst. Liq. Cryst., 87, 13 (1982).
34. D. Vörländer, Ber. dt. Chem. Gess., 43, 3120 (1910).
35. P. Ferloni, G. Spinolo, M. Zangen and P. Franzosini, Z. Naturforsch, A32, 329 (1977).
36. E. Baum, D. Demus and H. Sackmann, Wiss. Z. Univ. Halle, 19, 37 (1970).
37. A. S. C. Lawrence, Trans. Faraday Soc., 34, 660 (1938).
38. J. W. McBain, L. H. Lazarus and A. V. Pitter, Z. Phys. Chem., 147, 87 (1930).
39. R. D. Vold, F. B. Rosevear and R. H. Ferguson, Oil and Soap, 16, 48 (1939).
40. R. D. Vold and M. J. Vold, J. Am. Chem. Soc., 61, 808 (1939).
41. R. D. Vold, J. Phys. Chem., 43, 1213 (1939).
42. J. W. McBain, R. D. Vold and M. Frick, J. Phys. Chem., 44, 1013 (1940).
43. R. D. Vold, R. Reivere and J. W. McBain, J. Am. Chem. Soc., 63, 1293 (1941).
44. J. W. McBain and W. W. Lee, Oil and Soap, 20, 17 (1943).
45. J. W. McBain and W. C. Sierichs, J. Am. Oil Chem. Soc., 25, 221 (1948).

46. M. J. Vold, J. Am. Chem. Soc., 65, 465 (1943).
47. R. D. Vold, J. Am. Chem. Soc., 63, 2915 (1941).
48. V. Busico, A. Ferraro and M. Vacatello, J. Phys. Chem., 88, 4055 (1984).
49. V. Busico, A. Ferraro and M. Vacatello, J. Chem. Phys., 84, 471 (1986).
50. A. Cingolani, G. Spinolo, M. Sanesi and P. Franzosini, Z. Naturforsch, A35, 757 (1980).
51. D. B. Cox and J. F. McGlynn, Anal. Chem., 29, 960 (1957).
52. J. L. Curat and R. Perron, Chem. Phys. Lipids, 19, 301 (1977).
53. G. Förster, G. Brezesinski, E. Gerlach, A. Mödicke and H.-D. Dörfler, Z. Phys. Chemie, Leipzig, 6, 1009 (1981).
54. P. Franzosini, M. Sanesi, A. Cingolani and P. Ferloni, Z. Naturforsch, 35A, 98 (1980).
55. C. Madelmont and R. Perron, Colloid and Polymer Sci., 254, 581 (1976).
56. P. Pacor and H. L. Spier, J. Am. Oil Chem. Soc., 45, 338 (1968).
57. G. B. Ravich and N. A. Nechitailo, Doklady Akad Nauk SSSR, 83, 117 (1952).

58. J. A. Ripmeester and B. A. Dunell, *Can. J. Chem.*, 49, 2906 (1971).
59. F. H. Stross and S. T. Abrams, *J. Am. Chem. Soc.*, 73, 2825 (1951).
60. N. Trzebowski, *Wiss. Z. Univ. Jena*, 14, 207 (1965).
61. Y. Uzu, *Yukagaku*, 24, 261 (1975).
62. R. D. Vold and M. J. Vold, *J. Phys. Chem.*, 49, 32 (1945).
63. R. D. Vold, *J. Phys. Chem.*, 49, 315 (1945).
64. R. D. Vold, *J. Phys. Colloid Chem.*, 51, 797 (1947).
65. M. J. Vold and R. D. Vold, *J. Am. Oil Chem. Soc.*, 26, 520 (1949).
66. M. J. Vold, H. Funakoshi and R. D. Vold, *J. Phys. Chem.*, 80, 1753 (1976).
67. P. Montmittonet, B. Monasse, J. M. Haudin and F. Delamare, *Materials Letts.*, 3, 98 (1985).
68. R. D. Vold, J. D. Grandine 2nd and M. J. Vold, *J. Colloid Sci.*, 3, 339 (1948).
69. M. J. Vold, G. S. Hattiangdi and R. D. Vold, *J. Colloid Sci.*, 4, 93 (1949).
70. G. S. Hattiangdi, M. J. Vold and R. D. Vold, *Ind. and Eng. Chem.*, 41, 2320 (1949).

71. S. O. Adeosun and S. J. Sime, *Thermochim. Acta*, 17, 351 (1976).
72. S. O. Adeosun, A. O. Kehinde and G. A. Odesola, *Thermochim. Acta*, 28, 133 (1979).
73. H. D. Burrows, H. A. Ellis and M. S. Akanni, *Procs. Eur. Symp. Therm. Anal.*, 1981, 2nd, 302.
74. S. Shiba, *Bull. Chem. Soc. Japan*, 34, 804 (1961).
75. S. O. Adeosun, *Can. J. Chem.*, 57, 151 (1979).
76. H. D. Burrows and H. A. Ellis, *Thermochim. Acta*, 52, 121 (1982).
77. I. K-Thege, I. Ruff, S. O. Adeosun and S. J. Sime, *Thermochim. Acta*, 24, 89 (1978).
78. S. O. Adeosun, *J. Therm. Anal.*, 14, 235 (1978).
79. D. P. Benton, P. G. Howe, R. Farnand and I. E. Puddington, *Can. J. Chem.*, 33, 1798 (1955).
80. W. Skoda, *Kolloid Z.-u. Z. Polymere*, 234, 1128 (1969).
81. M. J. Vold, M. Macomber and R. D. Vold, *J. Am. Chem. Soc.*, 63, 168 (1941).
82. D. Chapman, *J. Chem. Soc.*, 784 (1958).
83. M. Kawano, *Nippon Kagaku Zasshi*, 81, 1652 (1960).
84. M. Kawano, *Nippon Kagaku Zasshi*, 81, 1805 (1960).

85. M. Kawano, Nippon Kagaku Zasshi, 82, 12, (1961).
86. N. Trzebowski and H. Kasch, Freiburger Forschungshefte, A251, 243 (1962).
87. R. Gotoh and T. Takenaka, Nippon Kagaku Zasshi, 84, 392 (1963).
88. E. M. Kirby, M. J. Evans-Vader and M. A. Brown, J. Am. Oil Chem. Soc., 42, 437 (1965).
89. N. Trzebowski, Z. Chem., 7, 245 (1967).
90. N. Trzebowski, Z. Chem., 7, 282 (1967).
91. B. A. Dunell and W. R. Janzen, Wiss. Z. Univ. Jena, 14, 191 (1965).
92. R. F. Grant, N. Hedgecock and B. A. Dunell, Can. J. Chem. 34, 1514 (1956).
93. R. F. Grant and B. A. Dunell, Can. J. Chem., 38, 2395, (1960).
94. R. F. Grant and B. A. Dunell, Can. J. Chem., 38, 1951 (1960).
95. D. J. Shaw and B. A. Dunell, Trans. Faraday Soc., 58, 132 (1962).
96. K. D. Lawson and T. J. Flautt, J. Phys. Chem., 69, 4256, (1965).

97. K. D. Lawson and T. J. Flautt, *Molec. Crystals*, 1, 241, (1966).
98. R. F. Grant and B. A. Dunell, *Can. J. Chem.*, 39, 359 (1961).
99. M. R. Barr and B. A. Dunell, *Can. J. Chem.*, 42, 1098, (1964).
100. W. R. Janzen and B. A. Dunell, *Can. J. Chem.*, 47, 2722 (1969).
101. T. J. R. Cyr, W. R. Janzen and B. A. Dunell in: *Ordered Fluids and Liquid Crystals (Advances in Chemistry Series No 63, American Chemical Society, Washington D.C., 1967)*, p. 13.
102. T. J. Flautt and K. D. Lawson, in: *Ordered Fluids and Liquid Crystals (Advances in Chemistry Series No 63, American Chemical Society, Washington D.C. 1967)*, p. 26.
103. J. A. Ripmeester and B. A. Dunell, *Can. J. Chem.*, 49, 731 (1971).
104. K. P. van Putte, *Trans Faraday Soc.*, 66, 523 (1970).
105. K. P. van Putte, *J. Magn. Res.*, 2, 33 (1970).
106. K. P. van Putte and G. J. Egmond, *J. Magn. Res.*, 4, 236 (1971).
107. W. R. Krigbaum, J. C. Poirier and M. J. Costello, *Mol. Cryst. Liq. Cryst.*, 20, 133 (1973).

108. R. D. Vold and G. S. Hattiangdi, *Ind. and Eng. Chem.*, 41, 2311 (1949).
109. A de Bretteville Jnr. and J. W. McBain, *J. Chem. Phys.*, 11, 426 (1943).
110. H. Nordsieck, F. B. Rosevear and R. H. Ferguson, *J. Chem. Phys.*, 16, 175 (1948).
111. A. Skoulios and V. Luzzatti, *Nature*, 183, 1310 (1959).
112. A. Skoulios and V. Luzzatti, *Acta Cryst.*, 14, 278 (1961).
113. B. Gallot and A. Skoulios, *Compt. Rend. Acad. Sci.*, 260, 3033, (1965).
114. B. Gallot and A. E. Skoulios, *Acta Cryst.*, 15, 826 (1962).
115. A. Skoulios and B. Gallot, *Compt. Rend. Acad. Sci.*, 252, 142 (1961).
116. B. Gallot and A. Skoulios, *Kolloid-Z. u. Z. Polymere*, 210, 143 (1966).
117. B. Gallot and A. Skoulios, *Mol. Cryst.*, 1, 263 (1966).
118. P. Spegt and A. Skoulios, *Compt. Rend. Acad. Sci.*, 254, 4316, (1962).
119. P. Spegt and A. Skoulios, *Compt. Rend. Acad. Sci.*, 251, 2199 (1960).
120. P. A. Spegt and A. E. Skoulios, *Acta Cryst.*, 17, 198 (1964).

121. V. Luzzatti and P. A. Spegt, *Nature*, 215, 701 (1967).
122. V. Luzzatti, A. Tardieu and T. G.-Krzywicki, *Nature*, 217, 1028 (1968).
123. P. A. Spegt and A. E. Skoulios, *Acta Cryst.*, 21, 892, (1966).
124. P. A. Spegt and A. E. Skoulios, *Acta Cryst.*, 16, 301 (1963).
125. P. Spegt and A. Skoulios, *J. Chim. Phys.*, 62, 418 (1965).
126. V. Busico, P. Corradini, G. Guerra and P. Severino, *Gazz. Chim. Ital.*, 115, 17 (1985).
127. R. H. Ferguson, F. B. Rosevear and R. C. Stillman, *Ind. and Eng. Chem.*, 35, 1005 (1943).
128. M. J. Buerger, L. B. Smith, F. V. Ryer and J. E. Spike Jnr., *Proc. Nat. Acad. Sci. U.S.*, 31, 226 (1945).
129. K. W. Gardiner, M. J. Buerger and L. B. Smith, *J. Phys. Chem.*, 49, 417 (1945).
130. V. Busico, P. Cernicchiaro, P. Corradini and M. Vacatello, *J. Phys. Chem.*, 87, 1631 (1983).
131. P. Ferloni, M. Sanesi, P. L. Tonelli and P. Franzosini, *Z. Naturforsch.*, 33A, 240 (1978).
132. M. Sanesi, P. Ferloni and P. L. Tonelli, *Z. Naturforsch.*, 33A, 386 (1978).

133. J. Rogers and P. A. Winsor, 5th Int. Congr. on Surface Active Substances, Barcelona, Vol. 2, p. 933 Ediciones Unidas. Barcelona, 1969.
134. R. R. Balmbra, J. S. Clunie and J. F. Goodman, Proc. Roy. Soc., London, A285, 534 (1965).
135. R. R. Balmbra, J. S. Clunie and J. F. Goodman, Molecular Crystals, 3, 281 (1967).
136. P. A. Winsor, in: Solvent Properties of Amphiphilic Compounds (Butterworth and Co Ltd, London, 1954), pp. 65, 69, 117, 135 and 185.
137. C. R. Singleterry, J. Am. Oil Chem. Soc., 32, 446 (1955).
138. N. Pilpel, Chem. Revs., 63, 221 (1963).
139. F. M. Fowkes, in: Solvent Properties of Surfactant Solutions, ed, K. Shinoda (Surfactant Science Series, Marcel Dekker Inc. New York, 1967), Vol. 2, Chap. 3, p. 65.
140. H.-F. Eicke, in: Topics in Current Chemistry No 87 (Springer Verlag, 1980), p. 85.
141. M. J. Vold, G. S. Hattiangdi and R. D. Vold, Ind. and Eng. Chem., 41, 2539 (1949).
142. M. J. Vold and R. D. Vold, J. Inst. Pet., 38, 155 (1952).
143. E. Kissa, J. Colloid Sci., 17, 857 (1962).
144. A. E. Skoulios, Acta Cryst., 14, 419 (1961).
145. P. Spegt and A. Skoulios, J. Chim. Phys., 62, 377 (1965).

146. M. S. Akanni, H. D. Burrows, H. A. Ellis, D. N. Asongwed, H. B. Babalola and P. O. Ojo, *J. Chem. Tech. Biotechnol.*, 34A, 127 (1984).
147. S. Kaufman and C. R. Singleterry, *J. Phys. Chem.*, 62, 1257 (1958).
148. E. R. Martin and R. C. Pink, *J. Chem. Soc.*, 1750 (1948).
149. V. D. Tughan and R. C. Pink, *J. Chem. Soc.*, 1804 (1951).
150. S. M. Nelson and R. C. Pink, *J. Chem. Soc.*, 1744 (1952).
151. R. C. Little, *J. Colloid Int. Sci.*, 21, 266 (1966).
152. R. C. Murray and G. S. Hartley, *Trans Faraday Soc.*, 31, 183 (1935).
153. J. W. McBain and E. B. Working, *J. Phys. Chem.*, 51, 974 (1947).
154. V. R. Grey and A. E. Alexander, *J. Phys. Chem.*, 53, 923 (1949).
155. H. Sheffer, *Can. J. Res.*, 26B, 481 (1948).
156. P. Debye, W. A. Barber and A. P. Autrey, Summary Report to Army Chemical Centre, Edgewood Arsenal, Md. Contract DA-18-108-CML-2144.
157. W. O. Ludke, S. E. Wiberley, J. Goldenson and W. H. Bauer, *J. Phys. Chem.*, 59, 222 (1955).
158. W. H. Bauer, N. Weber and S. E. Wiberley, *J. Phys. Chem.*, 62, 106 (1958).

159. S. Friberg, *Acta Chem. Scand.*, 18, 1078 (1964).
160. B. Chu, Z-K. Zhou, Y. Georgalis and R. Xu, 6th Int. Symp. on Surfactants in Solution, New Delhi, Aug 18-22, 1986; Z. Zhou, Y. Georgalis, W. Liang, J. Li, R. Xu and B. Chu, *J. Colloid Int. Sci.*, 116, 473 (1987).
161. R. W. Mattoon and M. B. Mathews, *J. Phys. Chem.*, 17, 496 (1949).
162. M. B. Mathews and E. Hirschhorn, *J. Colloid Sci.*, 8, 86 (1952).
163. A. Kitahara, T. Kobayashi and T. Tachibana, *J. Phys. Chem.*, 66, 363 (1962).
164. H-F. Eicke and H. Christen, *J. Colloid Int. Sci.*, 46, 417 (1974).
165. H-F. Eicke and H. Christen, *Helv. Chim. Acta*, 61, 2258 (1978).
166. M. van der Waarden, *J. Colloid Sci.*, 5, 448 (1950).
167. S. Kaufman and C. R. Singleterry, *J. Colloid Sci.*, 10, 139 (1955).
168. S. Kaufman and C. R. Singleterry, *J. Colloid Sci.*, 12, 465 (1957).
169. H. Reerink, *Proc. Int. Cong. Surf. Act. 3rd, Cologne, 1960*, 1, 255, (1960).

170. F. M. Fowkes, J. Phys. Chem., 66, 1843 (1962).
171. R. C. Little and C. R. Singleterry, J. Phys. Chem., 68, 3453 (1964).
172. I. J. Heilweil, J. Colloid Sci., 19, 105 (1964).
173. H. Reerink, J. Colloid Sci., 20, 217 (1965).
174. E. I. Franses, J. Colloid Int. Sci., 101, 500 (1984).
175. L. Arkin and C. R. Singleterry, J. Colloid Sci., 4, 539 (1949).
176. C. R. Singleterry and L. A. Weinberger, J. Am. Chem. Soc., 73, 4574 (1951).
177. S. Kaufman and C. R. Singleterry, J. Colloid Sci., 7, 453, (1952).
178. J. G. Honig and C. R. Singleterry, J. Phys. Chem., 58, 201 (1954).
179. J. G. Honig and C. R. Singleterry, J. Phys. Chem., 60, 1108 (1956).
180. J. G. Honig and C. R. Singleterry, J. Phys. Chem., 60, 1114 (1956).
181. S. O. Adeosun, W. J. Sime and S. J. Sime, Thermochem. Acta, 19, 275 (1977).
182. S. S. Marsden Jnr., J. Am. Oil Chem. Soc., 26, 57 (1949).

183. D. Evans, J. F. Hutton and J. B. Matthews, J. Appl. Chem. (London), 2, 252, (1952).
184. B. W. Hotten and D. H. Birdsall, J. Colloid Sci., 7, 284, (1952).
185. H. Wochnowski and R. Freitag, Schmiertech. Tribol., 24(3), 69 (1977).
186. G. H. Smith and J. W. McBain, J. Phys. Colloid Chem., 51, 1189 (1947).
187. T. M. Doscher and R. D. Vold, J. Phys. Colloid Chem., 52, 97 (1948).
188. F. H. Stross and S. T. Abrams, J. Am. Chem. Soc., 72, 3309 (1950).
189. R. D. Vold and J. M. Philipson, J. Phys. Chem., 50, 39 (1946).
190. G. H. Smith, J. Am. Oil Chem. Soc., 24, 353 (1947).
191. A. S. C. Lawrence, J. Phys. Colloid Chem., 52, 1504 (1948).
192. T. M. Doscher and S. Davis, J. Phys. Colloid Chem., 55, 53 (1951).
193. R. D. Vold and T. D. Smith, J. Am. Chem. Soc., 73, 2006 (1951).
194. R. D. Vold and M. J. Vold, J. Phys. Colloid Chem., 52, 1424 (1948).

195. M. J. Vold and R. D. Vold, J. Colloid Sci., 5, 1 (1950).
196. D. B. Cox, J. Phys. Chem., 62, 1254 (1958).
197. M. J. Vold, Y. Uzu and R. F. Bills, NLGI Spokesman, 32(10), 362 (1969).
198. L. A. Siegel, J. Chem. Phys., 29(5), 1091 (1958).
199. R. E. Rosenfeld and S. G. Frank, J. Pharm. Sci., 62, 1194 (1973).
200. B. H. Nicolet and C. M. De Milt, J. Am. Chem. Soc., 49, 1103 (1927).
201. J. Harmon and C. S. Marvel, J. Am. Chem. Soc., 54, 2515 (1932).
202. C. D. Nenitzescu and A. Glatz, Bull. Soc. Chim. France, 218, (1961).
203. F. D. Smith, H. E. Kenney and A. J. Stirton, J. Org. Chem., 30(3), 885 (1965).
204. F. D. Smith, A. J. Stirton and C. J. Dooley, J. Am. Oil Chem. Soc., 45(11), 747 (1968).
205. F. D. Smith and A. J. Stirton, J. Am. Oil Chem. Soc., 48(4), 160 (1971).
206. P. Saul, Certificate in Advanced Analytical Chem. Project Report, Sheffield City Polytechnic, March 1985.
207. I. Kemmery, Certificate in Advanced Analytical Chem. Project Report, Sheffield City Polytechnic, April 1986.

208. M. H. Allen, BSc Hons App. Chem. Final Year Project Report, June 1986, *Sheffield City Polytechnic*.
209. E. Kissa, J. Colloid Sci., 19, 279 (1964).
210. W. C. Bigelow, E. Glass and W. A. Zisman, J. Colloid Sci., 2, 563 (1947).
211. C. L. Duval, J. Lecomte and E. Douvillé, Ann. Phys., 17, 5 (1942).
212. R. E. Kagarise, J. Phys. Chem., 59, 271 (1955).
213. T. S. McRoberts and J. H. Schulman, Proc. Roy. Soc. London, A200, 136 (1950).
214. V. Luzzati, H. Mustacchi, A. Skoulios and F. Husson, Acta Cryst., 13, 660 (1960).
215. F. Husson, H. Mustacchi and V. Luzzati, Acta Cryst., 13, 668 (1960).
216. C. Madelmont and R. Perron, Bull. Soc. Chim. France, No 12, 3259 (1973).
217. C. Madelmont and R. Perron, Bull. Soc. Chim. France, No 12, 3263 (1973).
218. C. Madelmont and R. Perron, Bull. Soc. Chim. France, No 3-4, 425 (1974).
219. C. Madelmont and R. Perron, Bull. Soc. Chim. France, No 3-4, 430 (1974).

220. C. Madelmont and R. Perron, Bull. Soc. Chim. France, No 9-10, 1795 (1974).
221. C. Madelmont and R. Perron, Bull. Soc. Chim. France, No 9-10, 1799 (1974).
222. K. Rendall, G. J. T. Tiddy and M. A. Trevethan, J. Chem. Soc., Faraday Trans I, 79, 637 (1983).
223. B. Gallot and A. Skoulios, Kolloid-Z. u. Z. Polymere, 208, 37 (1966).
224. A. E. Skoulios, Advances in Colloid and Int. Sci., 1, 79 (1967).
225. J. M. Vincent and A. E. Skoulios, Acta Cryst., 20, 432 (1966).
226. J. M. Vincent and A. E. Skoulios, Acta Cryst., 20, 441 (1966).
227. J. M. Vincent and A. E. Skoulios, Acta Cryst., 20, 447, (1966).
228. B. Mely and J. Charvolin, Chem. Phys. Lipids, 19, 43 (1977).
229. K. R. Jeffrey, T. C. Wong and A. P. Tulloch, Mol. Phys., 52, 289 (1984).
230. J. Rogers and P. A. Winsor, J. Colloid Int. Sci., 30, 247 (1969).

231. P. Ekwall, L. Mandell and K. Fontell, J. Colloid Int. Sci., 33, 215 (1970).
232. A. Khan, K. Fontell and B. Lindman, J. Colloid Int. Sci., 101, 193 (1984).
233. H. Wennerström, B. Jönsson and P. Linse, J. Chem. Phys., 76, 4665 (1982).
234. E. I. Franses, J. E. Puig, Y. Talmon, W. G. Miller, L. E. Scriven and H. T. Davis, J. Phys. Chem., 84, 1547 (1980).
235. F. D. Blum and W. G. Miller, J. Phys. Chem., 86, 1729 (1982).
236. E. I. Franses, Y. Talmon, L. E. Scriven, H. T. Davis, and W. G. Miller, J. Colloid Int. Sci., 86, 449 (1982).
237. W. G. Miller, F. D. Blum, H. T. Davis, E. I. Franses, E. W. Kaler, P. K. Kilpatrick, K. E. Nietering, J. E. Puig and L. E. Scriven, in: Surfactants in Solution, eds K. L. Mittal and B. Lindman (Plenum Press, London, 1984), Vol 1, p 175.
238. E. I. Franses and W. G. Miller, J. Colloid Int. Sci., 101, 500 (1984).
239. P. K. Kilpatrick and W. G. Miller, J. Phys. Chem., 88, 1649 (1984).

240. J. E. Puig, L. E. Scriven, H. T. Davis and W. G. Miller, in: Interfacial Phenomena in Enhanced Oil Recovery, eds. D. Wason and A. Payatakes, American Institute of Chemical Engineers, New York AIChE Symp. Series S-212, p 1 (1982).
241. E. F. Williams, N. T. Woodberry and J. K. Dixon, J. Colloid Sci., 12, 45 (1957).
242. S. V. Rudenko, K. O. Averbakh, O. K. Smirmov and S. M. Levi, Colloid J. USSR, 30, 312 (1968).
243. K. Fontell, J. Colloid Int. Sci., 44, 318 (1973).
244. R. J. M. Tausk, J. Karmiggelt, C. Oudshorn and J. Th. G. Overbeek, Biophys. Chem., 1, 175 (1974).
245. R. J. M. Tausk, J. Van Esch, J. Karmiggelt, C. Voordouw, and J. Th. G. Overbeek, Biophys. Chem., 1, 184 (1974).
246. C. Tanford, in: The Hydrophobic Effect (Wiley-Interscience, New York, 1978).
247. S. Mabrey and J. M. Sturtevant, Proc. Natl. Acad. Sci. US, 73, 3862 (1976).
248. E. I. Franses and T. J. Hart, J. Colloid Int. Sci., 94, 1 (1983).
249. M. A. Marcus, Liquid Crystals, 1, 73 (1986).
250. N. Boden and M. C. Holmes, Chem. Phys. Letts., 109, 76, (1984).

251. K. Radley, Mol. Cryst. Liq. Cryst., 102, 199 (1984).
252. K. Radley and A. S. Tracey, Mol. Cryst. Liq. Cryst. Letts., 1, 95 (1985).
253. P. J. Photinos and A. Saupe, J. Chem. Phys., 84, 517 (1986).
254. B. J. Forrest and L. W. Reeves, Chem. Revs., 81, 1 (1981).
255. A. J. Stirton, B. B. Schaeffer, A. A. Stawitzke, J. K. Weil and W. C. Ault, J. Am. Oil Chem. Soc., 25, 365 (1948).
256. D. D. Perrin, W. L. F. Armarego and D. R. Perrin, in: Purification of Laboratory Chemicals (Pergamon Press Ltd, 2nd Edition, 1980).
257. N. H. Hartshorne, in: The Microscopy of Liquid Crystals (Microscope Publications Ltd, London, 1974).
258. F. B. Rosevear, J. Am. Oil Chem. Soc., 31, 628 (1954).
259. F. B. Rosevear, J. Soc. Cosmetic Chem., 19, 581 (1968).
260. L. Mandell and P. Ekwall, Acta Polytech. Scand., Chap. 74, (1968), Part I, p. 1.
261. A. S. C. Lawrence, in: Surface Activity and Detergency, ed. K. Durham (Macmillan, London, 1961), p. 158.
262. R. D. McElhaney, Chem. Phys. Lipids, 30, 229 (1982).

263. K. Fontell, in: Liquid Crystals and Plastic Crystals  
eds. G. W. Gray and P. A. Winsor (Ellis Horwood Ltd,  
Chichester, UK, 1974) Vol. 2, Chap. 4, p. 80.
264. V. Luzzatti, in: Biological Membranes, Physical Fact and  
Function, ed. D. Chapman (Academic Press, London, 1968),  
Chap. 3, p. 71.
265. V. Luzzatti and F. Husson, J. Cell Biol., 12, 207 (1962).
266. V. Luzzatti and A. Tardieu, Ann. Rev. Phys. Chem., 25,  
79 (1974).
267. F. Husson and V. Luzzatti, J. Phys. Chem., 68, 3504 (1964).
268. J. A. Lake, Acta Cryst., 23, 191 (1967).
269. A. Johansson and B. Lindman, in: Liquid Crystals and  
Plastic Crystals, eds. G. W. Gray and P. A. Winsor (Ellis  
Horwood Ltd, Chichester, England, 1974), Vol. 2, Chap. 8,  
p. 192.
270. G. Lindblom, B. Lindman and G. J. T. Tiddy, J. Am. Chem.  
Soc., 100, 2299 (1978).
271. H. Wennerström, G. Lindblom and B. Lindman, Chem. Scripta,  
6, 97 (1974).
272. E. Everiss, G. J. T. Tiddy and B. A. Wheeler, J. Chem.  
Soc. Faraday Trans. I, 72, 1747 (1976).
273. J. Rosenholm and B. Lindman, J. Colloid Int. Sci., 57,  
362 (1976).

274. I. D. Leigh, M. P. McDonald, R. M. Wood, G. J. T. Tiddy, and M. A. Trevethan, *J. Chem. Soc. Faraday Trans. I.*, 77, 2867, (1981).
275. G. J. T. Tiddy, M. Walsh and E. W-Jones, *J. Chem. Soc. Faraday Trans I*, 78, 389 (1982).
276. A. Khan, K. Fontell and B. Lindman, in: *Surfactants in Solution*, eds. K. L. Mittal and B. Lindman (Plenum Press, New York, 1984), Vol. 1, p. 193.
277. Reference 269, p. 213.
278. N.-O. Persson and B. Lindman, *J. Phys. Chem.*, 79, 1410 (1975).
279. G. Lindblom, N.-O. Persson and G. Arvidson, in: Reference 6, Chap. 9, p. 121.
280. B. Lindman, G. Lindblom, H. Wennerström and H. Gustavsson, in: *Micellization, Solubilization and Microemulsions*, ed. K. L. Mittal (Plenum Press, New York, 1977), Vol. 1, p. 195.
281. G. J. T. Tiddy, G. Lindblom and B. Lindman, *J. Chem. Soc., Faraday Trans. I*, 74, 1290 (1978).
282. H. Wennerström, B. Lindman, G. Lindblom and G. J. T. Tiddy, *J. Chem. Soc. Faraday Trans. I*, 75, 663 (1979).
283. O. Söderman, S. Engström and H. Wennerström, *J. Colloid Int. Sci.*, 78, 110 (1980).

284. B. Lindman, G. Lindblom, H. Wennerström, N.-O. Persson, H. Gustavsson and A. Khan, in: *Magnetic Resonance in Colloid and Interface Science*, eds. J. P. Fraissard and H. A. Resing (D. Reidel Pub. Co., 1980), Vol. 61, p. 307.
285. N. Boden and S. A. Jones, in: *NMR of Liquid Crystals*, ed. J. W. Emsley (D. Reidel Pub. Co., 1985), NATO ASI Series C, Vol. 141, p. 473.
286. O. Söderman, *Nucl. Mag. Reson.*, 14, 350 (1985).
287. M. H. Cohen and F. Reif, in: *Solid State Physics*, eds. F. Seitz and D. Turnbull (Academic Press, New York, 1957), Vol. 5, p. 321.
288. *CRC Handbook of Chemistry and Physics*, ed. R. C. Weast, (CRC Press, Ohio, USA, 1975-1976), 5th Edition.
289. P. A. Thiessen and E. Ehrlich, *Z. Physik Chem.*, A165, 453 (1933).
290. S. Abrahamsson and I. R. -Nahringbauer, *Acta Cryst.*, 15, 1261 (1962).
291. T. R. Lomer, *Acta Cryst.*, 5, 11 (1952).
292. J. H. Dumbleton and T. R. Lomer, *Acta Cryst.*, 19, 301 (1965).
293. G. Zerbi, R. Magni, M. Gussoni, K. Holland Moritz, A. Bigotto and S. Dirlikov, *J. Chem. Phys.*, 75, 3175 (1981).

294. M. Maroncelli, S. P. Qi, H. L. Strauss and R. G. Snyder, J. Am. Chem. Soc., 104, 6237 (1982).
295. M. Maroncelli, H. L. Strauss and R. G. Snyder, J. Chem. Phys., 82, 2811 (1985).
296. D. Chapman, in: The Structure of Lipids, (Methuen and Co. Ltd., London, 1965), Chap. 8, p. 239-240.
297. G. Strobl, B. Ewen, E. W. Fischer and W. Piesczek, J. Chem. Phys., 61, 5257 (1974).
298. K. Fontell, Mol. Cryst. Liq. Cryst., 63, 59 (1981).
299. R. C. Mehrotra, in: Metal Carboxylates, eds. R. C. Mehrotra and R. Bohra (Academic Press, New York, 1983).
300. E. S. Lutton, Oil and Soap, 23, 265 (1946).
301. J. D. Lee, in: A New Concise Inorganic Chemistry, (Van Nostrand Reinhold Co., England, 1977), Chap. 4, p. 129.
302. G. W. Ossman and A. A. Silvidi, J. Chem. Phys., 54, 979 (1971).
303. T. K. Halstead, J. Chem. Phys., 53, 3427 (1970).
304. G. W. Ossman, A. A. Silvidi and J. W. McGrath, J. Chem. Phys., 52, 509 (1970).
305. F. Wolf, D. Kline and H. S. Story, J. Chem. Phys., 53, 3538 (1970).
306. E. von Sydow, Acta Cryst., 8, 557 (1955).

307. A. Streitwieser Jnr. and C. H. Heathcock, in: Introduction to Organic Chemistry (Macmillan Pub. Co. Inc. New York, 1976), Chap. 4, p. 55.
308. B. Wunderlich, in: Proceedings from the 7th Int. Conf. on Therm. Anal., ed. B. Miller (Wiley, Chichester UK, 1982), Vol. 2, p. 1084.
309. B. Wunderlich and J. Grebowicz, Polym. Mater. Sci. Eng., 50, 114 (1984).
310. M. Boidart, A. Hochapfel and M. Laurent, Mol. Cryst. Liq. Cryst., 154, 61 (1988).
311. A. Saupe, Il Nuovo Cimento, 3, 16 (1984).
312. O. Glatter, in: Small-Angle X-ray Scattering, eds. O. Glatter and O. Kratky (Academic Press, London, 1982), Chap. 5, p. 189.
313. W. Philippoff, J. Colloid Sci., 5, 169 (1950).
314. M. Doi and S. Edwards, J. Chem. Soc., Faraday Trans II, 74, 918 (1978).
315. N. Boden, K. Radley and M. C. Holmes, Mol. Phys., 42, 493 (1981).
316. M. Démarcq and D. Dervichian, Bull. Soc. Chim. France, 12, 939 (1945).
317. J. H. Hildebrand and R. L. Scott, in: The Solubility of Nonelectrolytes, 3rd Ed. (Reinhold Pub. Corp. New York, 1950).

318. W. D. Bascom, S. Kaufman and C. R. Singleterry, U.S. Naval Research Laboratories Report 5422, 1960.
319. H. Hoffmann, H. Rehage, W. Schörr and H. Thurn, in: *Surfactants in Solution*, eds. K. L. Mittal and B. Lindman (Plenum Press, New York, 1984), Vol. 1, p. 425.
320. H. Z. Cummins, in: *Photon Correlation and Light Beating Spectroscopy*, Eds. H. Z. Cummins and E. R. Pike (Plenum Press, New York, 1974), p. 285.
321. J. B. Hayter and J. Penfold, *J. Phys. Chem.*, 88, 4589, (1984).
322. H. Hoffmann, J. Kalus and H. Thurn, *Ber. Bunsen-Ges. Phys. Chem.*, 87, 1120 (1983).
323. H.-F. Eicke and J. Rehak, *Helv. Chim. Acta*, 59, 2883, (1976).
324. M. Wang, J. K. Thomas and T. Nowak, *J. Am. Chem. Soc.*, 99, 4730 (1977).
325. K. Fontell, L. Mandell, H. Lehtinen and P. Ekwall, *Acta Polytech. Scand.*, Chap. 74 (1968), Part III, p. 1.
326. D. Chapman, R. M. Williams and B. D. Ladbrooke, *Chem. Phys. Lipids*, 1, 445 (1967).
327. Y. K. Levine, J. M. Birdsall, A. G. Lee and J. C. Metcalfe, *Biochem.*, 11, 1416 (1972).

328. J. H. Davis, *Biophys. J.*, 27, 339 (1979).
329. K. Rendall and G. J. T. Tiddy, *J. Chem. Soc., Faraday Trans I.*, 80, 3339 (1984).
330. M. Kléman, C. Colliex and M. Veyssie, *Adv. Chem. Ser.* No. 152, 71 (1976).
331. T. Klason and U. Henriksson in: *Surfactants in Solution*, eds. K. L. Mittal and B. Lindman, (Plenum Press, New York, 1984), Vol. 1, p. 93.
332. C. Deverell, in: *Progress in NMR Spectroscopy* (Pergamon Press, Oxford, 1969), Vol. IV, p. 268.
333. P. Waldstein, S. W. Rabideau and J. A. Jackson, *J. Chem. Phys.*, 41, 3407 (1964).
334. A. D. Buckingham and K. A. McLauchlan, in: *Progress in Nuclear Magnetic Resonance Spectroscopy*, eds. J. W. Emsley, J. Feeney and L. H. Sutcliffe (Pergamon Press, Oxford, 1967). Vol. 2, Chap 2, p. 63.
335. N.-O. Persson and A. Johansson, *Acta Chem. Scand.*, 25, 2118 (1971).
336. K. Czarniecki et al, *J. Colloid Int. Sci.*, 92, 358 (1983).
337. G. Lindblom, H. Wennerström, B. Lindman, A. C. S. Symposium Series, 34, 372 (1976).
338. G. Lindblom, B. Lindman and G. J. T. Tiddy, *Acta Chem. Scand.*, 29A, 876 (1975).

339. B. Jönsson, P-G. Nilsson, B. Lindman, L. Guldbrand and H. Wennerström, in: Surfactants in Solution, eds. K. L. Mittal and B. Lindman (Plenum Press, New York, 1984), Vol. 1, p. 3.
340. E. Hutchinson and K. Shinoda, in: Solvent Properties of Surfactant Solutions, ed. K. Shinoda (Surfactant Science Series, Marcel Dekker Inc., New York, 1967), Vol. 2, Chap. 1, p. 1.
341. P. Ekwall, Adv. Liq. Crystals, 1, 1 (1975). (= Ref. 10).

## Lecture Courses Attended

Department of Chemistry,  
Sheffield University.

- (i) Diffraction Methods (Dr Bailey)
- (ii) Applications of NMR (Drs Mann and Taylor)
- (iii) Liquid Crystals (Dr Dunmur)

## Conferences Attended

- (i) Magnetic Resonance Spectroscopy of Liquid Crystal and Biological Membranes (British Radiofrequency Spectroscopy Group, The University of Leeds, April 1983).
- (ii) The British Liquid Crystal Group Second Meeting (The University of Aberystwyth, September 1983).
- (iii) The 10th International Liquid Crystal Conference (The University of York, July 1984).
- (iv) The British Liquid Crystal Group Third Meeting (Royal Holloway College, University of London, January 1985).